Emulsion Templated Porous Polymers as Scaffolds for 3D Hepatocyte Culture

HAYWARD, ADAM,SIMON

School of Biological and Biomedical Sciences

&

Department of Chemistry

Emulsion Templated Porous Polymers as Scaffolds for 3D Hepatocyte Culture

Adam Simon Hayward

A thesis submitted for the degree of Doctor of Philosophy

2014

Thesis Publications

Hayward, A. S.; Sano, N.; Przyborski, S. A.; Cameron, N. R., Acrylic-Acid-Functionalized PolyHIPE Scaffolds for Use in 3D Cell Culture. *Macromolecular Rapid Communications* **2013,** 34, 1844-1849.

Hayward, A. S.; Eissa, A. M.; Maltman, D. J.; Sano, N.; Przyborski, S. A.; Cameron, N. R., Galactose-Functionalized PolyHIPE Scaffolds for Use in Routine Three Dimensional Culture of Mammalian Hepatocytes. *Biomacromolecules* **2013,** 14, 4271-4277.

Godoy, P.; Hewitt, N. J.; Albrecht, U.; Andersen, M. E.; Ansari, N.; **Hayward, A**.; *et al.*, Recent advances in 2D and 3D in vitro systems using primary hepatocytes, alternative hepatocyte sources and non-parenchymal liver cells and their use in investigating mechanisms of hepatotoxicity, cell signaling and ADME. *Arch. Toxicol.* **2013,** 87, 1315-1530.

Hayward, A. S.; Przyborski, S. A.; Cameron, N. R., Biointerfaces Between Cells and Substrates in Three Dimensions (3D). In *Biointerfaces: Where Material Meets Biology***,** RSC Publishing: 2014; *In press.*

Thesis Presentations (Oral)

RSC Biomaterials Group 7th Annual Meeting, Sheffield, UK, 2013.

IUPAC 10th International Conference on Advanced Polymers via Macromolecular Engineering, Durham, UK, 2013.

Abstract

Hepatocytes are the main functional cells of the liver and are used extensively *in vitro* for predicting *in vivo* drug toxicity profiles. However, the predictive accuracy of *in vitro* hepatocyte models depends on the physiological relevance of the artificial growth environment. Conventional *in vitro* hepatocyte models have employed monolayer cultures on two-dimensional (2D) substrates, forcing cells into a flattened morphology that is far removed from the *in vivo* scenario. Unsurprisingly, 2D cultures often show significant deviations from native liver genotype and phenotype and so are unable to accurately predict drug toxicity. Accordingly, it is hypothesised that approximating the native liver three-dimensional (3D) tissue architecture *in vitro* will help to preserve genotype and phenotype and so improve predictive accuracy.

In this study, emulsion templated porous polymers were investigated as scaffolds for 3D hepatocyte culture. In particular, porous polystyrene scaffolds were explored due to their high porosity, reproducibility and suitable mechanical strength properties. Hepatocytes were cultured on polystyrene scaffolds under a range of culture conditions and were found to approximate native liver density and architecture. The morphology of hepatocytes in scaffolds was representative of *in vivo*, unlike the flattened morphology of 2D cultures. Crucial ultrastructural features involved in drug detoxification such as bile canaliculi were also present in scaffold cultures, but almost absent from 2D cultures. Importantly, these representative structural features translated into functional and genetic improvements *in vitro*. Hepatocytes in scaffolds displayed increased albumin synthesis, a key marker of hepatocyte function. Hepatic cell lines also showed increased resistance to drug toxicity compared to 2D cultures. Hepatic drug metabolising genotype was also increased to more physiologically relevant levels in scaffolds compared to 2D cultures.

In addition, emulsion templated polystyrene scaffolds were also made more biochemically relevant by surface functionalising with galactose, a ligand known to selectively bind to hepatocytes *in vivo* via the asialoglycoprotein receptor (ASGP-R). Scaffold morphology was maintained with the incorporation of galactose, allowing cells to approximate native liver tissue architecture. Moreover, the pendent galactose ligands were found to be accessible to hepatocytes adhering onto the scaffold.

In summary, this thesis has shown that emulsion templated porous polymers can offer a more physiologically relevant growth environment for hepatocytes *in vitro*. This could have a profound effect on improving drug toxicity predictions and so reducing the dependence on animal testing.

Acknowledgements

I would like to acknowledge the Engineering and Physical Sciences Research Council (EPSRC), the Chemistry Innovation Knowledge Transfer Network (CIKTN) and Reinnervate Ltd for funding this thesis.

I would also like to thank the following people:

My supervisors Professor Stefan Przyborski and Professor Neil Cameron for all their kind support and guidance over the three years.

Dan Maltman, Frederique Tholozan, Ross Carnachan, Bridie Murray and David Johnson for all their technical advice and training. Christine Richardson, Helen Grindly and Helen Riggs for their support in electron microscopy. Naoko Sano for her expertise at Nexus and David Apperley from the Durham NMR service.

All members, past and present of the two research groups, for making my studentship an enjoyable and memorable experience. A special thanks to Paul Thornton, Dan Tams, Matt Didsbury and Andy Henderson for their friendship.

To Mum, Paul, Dad, Maurissa, Jamie and Kent for their endless love and support throughout my life. Without their encouragement I would not have had the courage to leave my career to pursue a Ph.D.

Finally, to Charlene who has stood by me throughout and put up with the frustrations, late nights and even writing-up on holiday. I am so grateful to you.

This thesis is dedicated to Gill Leonard and Rene Hayward.

Declaration

The work described herein was carried out in the School of Biological and Biomedical Sciences, or the Department of Chemistry, University of Durham, between October 2010 and February 2014. All of the work is my own, except where specifically stated otherwise. No part has previously been submitted for a degree at this or any other university.

Statement of Copyright

Table of Contents

List of Abbreviations

2D	Two-Dimensional
3D	Three-Dimensional
Aa	Acrylic Acid
ABC	Adenosine Triphosphate Binding Cassette (Protein)
AIBN	Azobisisobutyronitrile
APAP	Acetaminophen
ASGP-R	Asialoglycoprotein Receptor
ATR-FTIR	Attenuated Total Reflection Fourier Transform Infra Red
BC	Bile Canaliculi
BCRP	Breast Cancer Resistance Protein
BD	Interlobular Bile Duct
BEC	Biliary Epithelial Cell
BPO	Benzoyl Peroxide
BSEP	Bile Salt Export Pump
CM	Cell Membrane
CoH	Canals of Herring
CV	Central Vein
CYP	Cytochrome P450
D	Desmosomes
DMEM	Dulbecco's Modified Eagle's Medium
DMSO	Dimethyl Sulfoxide
dsDNA	Double Stranded Deoxyribonucleic Acid
DVB	Divinylbenzene
ECM	Extracellular Matrix
EHA	2-Ethylhexyl Acrylate
ELISA	Enzyme-linked Immunosorbent Assay
FMO	Flavin-containing Monooxygenase
GLY	Glycogen
GST	Glutathione S-transferase
HA	Hepatic Artery
H&E	Haematoxylin and Eosin Staining (Histology)
HepG2	Human Hepatocellular Carcinoma Cell Line
HIPE	High Internal Phase Emulsion

HLB	Hydrophilic Lipophilic Balance
HPC	Hepatic Progenitor Cell
HPLC	High Performance Liquid Chromatography
HSC	Hepatic Stellate Cell
KC	Kupffer Cell
KPS	Potassium Persulfate
LD	Lipid Storing Droplets
LSEC	Liver Sinusoidal Endothelial Cell
MDR1	Multi-Drug Resistance Protein 1
MEM	Minimum Essential Medium
MRP2	Multi-Drug Resistance Protein 2
MRP3	Multi-Drug Resistance Protein 3
MRP4	Multi-Drug Resistance Protein 4
Mt	Mitochondria
MTT	Thiazolyl Blue Tetrazolium Bromide
MV	Microvilli
NAT	N-Acetyltransferase
NU	Nucleus
O/W	Oil in Water Emulsion
OAT	Organic Anion Transporter
OATP	Organic Anion Transport Polypeptide
OCT	Organic Cationic Transporter
PBS	Phosphate-Buffered Saline Solution
PCL	Polycaprolactone
PFPA	Pentafluorophenyl Acrylate
PolyHIPE	Polymerised High Internal Phase Emulsion
PV	Portal Vein
RER	Rough Endoplasmic Reticulum
RNA	Ribonucleic Acid
RT-PCR	Real-Time Quantitative Polymerase Chain Reaction
SC	Scaffold
SEM	Scanning Electron Microscopy
SER	Smooth Endoplasmic Reticulum
SoD	Space of Disse
ssNMR	Solid State Nuclear Magnetic Resonance

STY	Styrene
SULT	Sulfotransferase
TBO	Toluidine Blue O
TEM	Transmission Electron Microscopy
TJ	Tight Junction
UGT	Uridine Diphosphate Glucuronosyl Transferase
UV	Ultraviolet
W/O	Water in Oil Emulsion
XPS	X-ray Photoelectron Spectroscopy
Za	Zonula Adherens
Zo	Zonula Occludens

Chapter 1: Literature Review

1.1 Hepatocytes *In Vivo*

In order to re-create the native liver environment *in vitro* it is first necessary to understand the anatomy and physiology experienced by hepatocytes *in vivo*. This first section therefore briefly introduces the liver and then focuses on the structural organisation of hepatocytes within the liver. A description of hepatocyte drug metabolism physiology is also described in relation to structural organisation.

1.1.1 The Liver

The liver is the largest internal organ and gland in the human body and is essential for survival. It is estimated to perform over 500 functions and plays a crucial role in digestion, metabolism, immunity, nutrient storage, protein synthesis and xenobiotic metabolism[1].

1.1.1.1 Gross Liver Anatomy

The liver is a soft reddish-brown organ that is surrounded by a collagenous capsule. It is approximately triangular in shape and normally weighs around 1.5 kg in humans[2]. It is located in the upper right-hand side of the abdominal cavity, just below the diaphragm and to the right of the stomach. It is normally divided into two lobes when viewing the parietal surface; a large right lobe and a smaller left lobe. However when viewing the visceral surface, the liver is typically divided into four lobes; right, left, quadrate and caudate lobes. The liver receives its blood supply from two major blood vessels; the hepatic portal vein and the hepatic artery. The hepatic portal vein carries venous blood from the stomach, intestines, pancreas and spleen and therefore contains nutrient-rich/oxygen-poor blood from the digestive system. The hepatic artery stems from the celiac artery (a descendent of the aorta) and thus supplies more nutrient-poor/oxygen-rich blood into the liver. Blood exits the liver via the hepatic veins into the inferior vena cava to re-join the circulation system.

1.1.1.2 *General Liver Physiology*

The liver has many functions. It produces bile that aids the emulsification and digestion of fats. It metabolises glucose into the macromolecule glycogen for energy storage. Similarly it converts glycogen back into glucose as a timely energy release. It stores essential vitamins and minerals. It removes various bacteria, fungi and parasites from the blood stream to play a pivotal role in immunity. It synthesises and regulates blood plasma proteins. It detoxifies ammonia into urea. The liver is also the principle organ concerned with drug/xenobiotic metabolism and detoxification (see section 1.1.3). Uniquely, the liver is also the only organ in the human body to

possess a regenerative capacity, and is able to reconstruct its entire mass from just 25 % of the original tissue.

1.1.2 Hepatocyte Cells

Hepatocytes are the main functional cells of the liver and constitute approximately 80 % of total human liver volume[3]. They perform most functions commonly associated with the liver, including xenobiotic metabolism, plasma protein synthesis, ammonia detoxification, glycogen storage and bile secretion[4]. Structurally, hepatocytes are part of a complex three-dimensional (3D) architecture that is highly vascularised by blood sinusoids. The repeating structural unit of this 3D architecture is known as the liver lobule[3] (see Figure 1.1). Thousands of lobules make up a single lobe of the liver. When viewed under cross section, lobules are hexagonal in shape. At the centre of each lobule is the central vein, which serves as the drainage point for the vascularised blood network. At the corners of each hexagonal lobule are the portal triads, containing a branch of the portal vein, hepatic artery and an interlobular bile duct. Approximately 80 % of the lobule blood supply enters via the portal vein, with the remainder entering via the hepatic artery to provide a more oxygen-rich top-up. Hepatocytes in the lobule are organised into 3D plates or cords that run parallel to the sinusoids. A constant biochemical exchange occurs between hepatocytes and the blood flowing through the sinusoids towards the central vein. A biliary network running counter to the sinusoidal blood flow towards the interlobular bile duct further complicates the 3D architecture of the liver lobule.

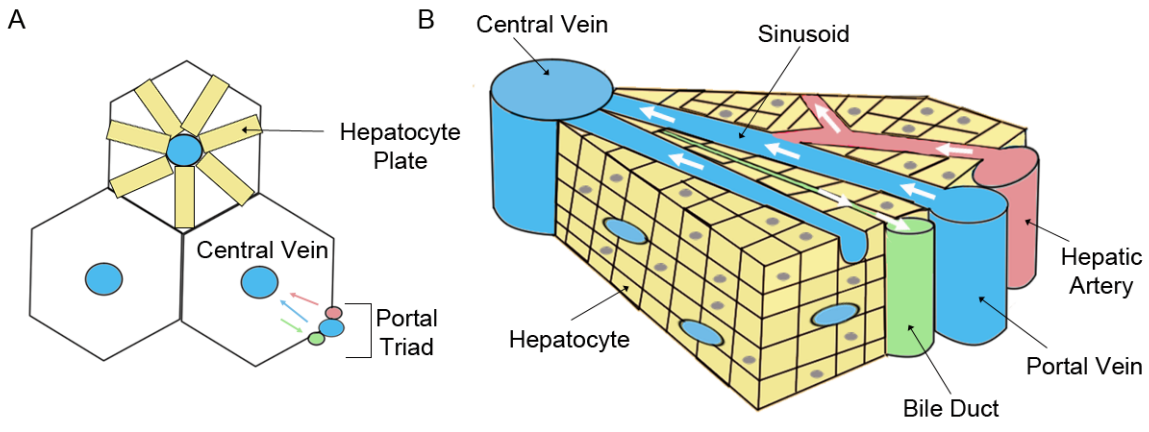

Figure 1.1 Illustration of the liver lobule. (A): Each lobule is hexagonal in shape with the central vein in the middle and the portal triads at the corners. Hepatocyte plates radiate from the centre out to the edges of the hexagon. (B): The lobule architecture is 3D with hepatocyte plates being highly vascularised by blood sinusoids carrying blood from the portal vein and hepatic artery towards the central vein. A biliary network running counter to the sinusoidal flow towards the interlobular bile duct is also present.

The actual shape of hepatocytes within the 3D plates is cuboidal (see Figure 1.2). Each hepatocyte is multi-polarised carrying at least two sinusoidal (baso-lateral) and two canalicular (apical) membrane domains[5]. The sinusoidal domains protrude surface microvilli into the sinusoidal lumen for endogenous and exogenous uptake and exchange with the blood sinusoids. The canaliculi domains contain small intercellular channels between adjacent hepatocytes known as the bile canaliculi. These channels wrap around the hepatocytes and join with other bile canaliculi at the Canals of Herring to form an extensive tubular network within the 3D plate architecture. This network terminates at the interlobular bile duct of the portal triad before moving on towards the gall bladder and common bile duct. The primary role of these bile canaliculi is to provide a transport network for the bile secreted by hepatocytes to eventually reach the gut to emulsify lipids. Indeed, various transporter proteins reside at the canalicular membrane and are involved in pumping bile acids into the bile canaliculi[6]. However, bile canaliculi and the associated transporter proteins also play a crucial role in the elimination of many xenobiotic substances metabolised in the liver (see section 1.1.3)[7].

Intercellular adhesions and cell junctions (cell-cell contact) within the 3D hepatocyte plate are believed to be crucial for maintaining normal hepatocyte structure and function. For example, gap junctions between hepatocytes have been shown to be important in controlling hepatocyte growth mechanisms[8, 9] and inducing drug metabolising enzymes[10]. Moreover, bile canaliculi formation relies on the presence of effective cell-adhesion junctions involving desmosomes, adherens and occludens[11]. Similar adhesion complexes are also required for microvilli formation at the sinusoidal domain. Hepatocytes within the 3D plate also anchor and interact with a surrounding extracellular matrix (ECM). Within the liver, this ECM is found in the liver capsule, the portal triads and in the small gap between hepatocytes and the sinusoids known as the *Space of Disse.* The hepatic ECM contains various glycoproteins, collagens, proteoglycans and glycosaminoglycans, as well as various hormones, growth factors and cytokines[12]. Interactions between hepatocytes and the ECM (integrin complexes) have been shown to regulate a range of hepatocyte processes, including albumin synthesis, drug metabolism capacity, proliferation and differentiation[13-17]. Indeed, ECM composition and stiffness are key controllers of hepatocyte phenotype, with harder, stiff ECM components favouring proliferation over differentiation[18]. Furthermore, ECM disruptions are closely associated with liver fibrosis and cirrhosis, emphasising the importance of the ECM in maintaining normal liver function[19, 20].

There are also other non-parenchymal liver cells that have influence on hepatocyte physiology with the 3D lobule. Liver sinusoidal endothelial cells (LSECs) line the walls of the sinusoids and so

significantly influence the exposure of hepatocytes to various substances[21]. These cells also secrete various cytokines into the ECM and have been shown to possess some drug biotransformation capacity[22]. Hepatic stellate cells (storing vitamin A) are present in the *Space of Disse* and are involved in the secretion of growth factors, cytokines and ECM components[23]. They also have been linked to many other roles including stem cell behaviour in liver regeneration as well as immunoregulation[24, 25]. Kupffer cells (macrophages) are present in the sinusoidal lumen and are involved in scavenging various pathogens and particulates from the blood stream[26]. These cells are also capable of regulating the viability and function of hepatocytes by producing various cytokines[27]. All of these non-parenchymal cells can influence hepatocyte behaviour.

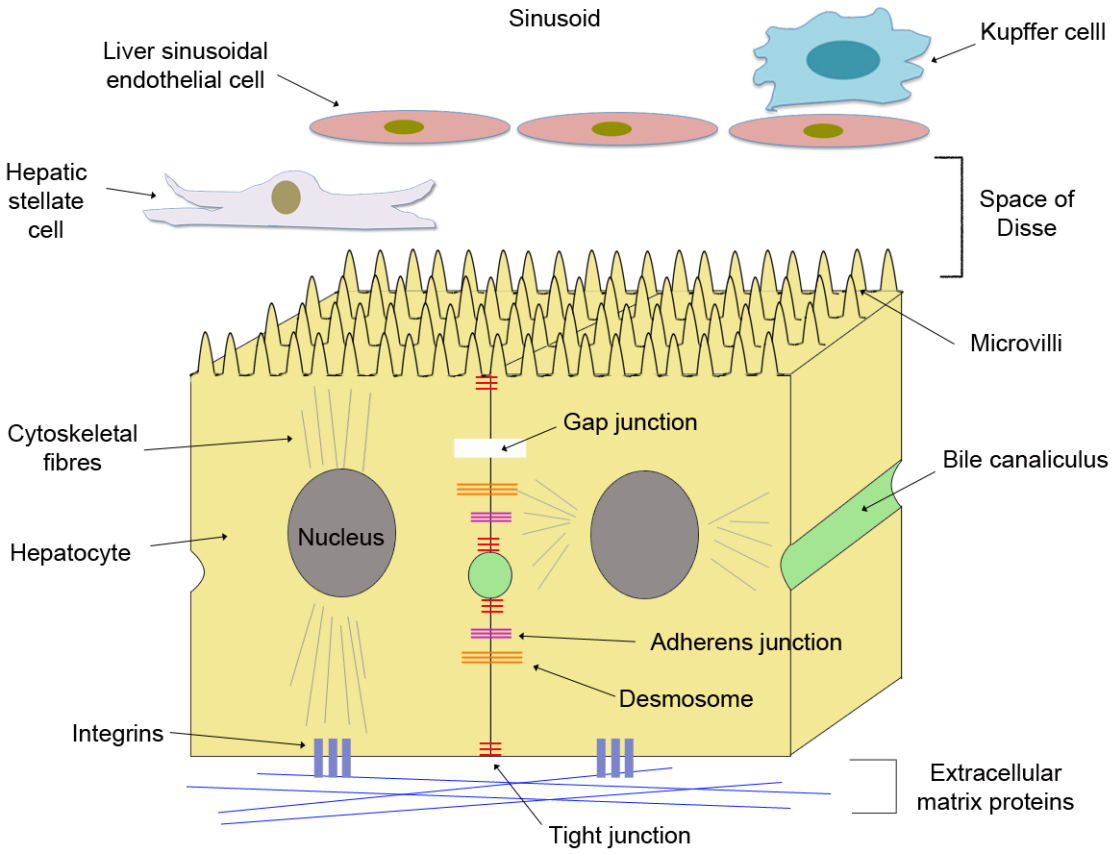

Figure 1.2 Illustration of the cuboidal shape of hepatocytes within the 3D plate. Hepatocytes protrude microvilli into the sinusoidal domain for exchange with the LSECs. Cell adhesions and gap junctions form between adjacent hepatocytes for crucial communication and formation of bile canaliculi. Hepatocytes also anchor their cytoskeleton to ECM proteins via integrins. Hepatic stellate cells and Kupffer cells are nearby providing important biochemical cues that regulate normal hepatocyte behaviour.

Significant metabolic heterogeneity exists along the 3D hepatocyte plate, forming the basis for the liver's functional repeating unit known as the liver acinus (see Figure 1.3). The acinus spans an approximately elliptical shape over two adjacent lobules with the line of symmetry passing

through the joining portal triads. As blood travels through the sinusoids towards the central vein, the oxygen and nutrient content of the blood is diminished and so a biochemical gradient is set up along the hepatocyte plate. Hepatocyte gene expression and function therefore differ along the plate depending on their location[28, 29]; zone 1 (periportal); zone 2 (midlobular); zone 3 (pericentral). Zone 1, which is closest to the portal triad and therefore has the richest oxygen supply, is predominantly immature hepatocytes involved in glycogen synthesis, oxidation and ureogenesis. Zone 3, which is furthest from the portal triad and thus has the poorest oxygen content, mainly contains fully differentiated hepatocytes involved in xenobiotic metabolism. Zone 2 contains a mixture of hepatocytes that are maturing parenchyma and therefore displays a mixture of different functions. Hepatic progenitor cells (bi-potential stem cells) supply the liver with these maturing hepatocytes as well as cholangiocytes (biliary epithelial cells, BEC) and reside in a small compartment within the Canals of Herring[30, 31].

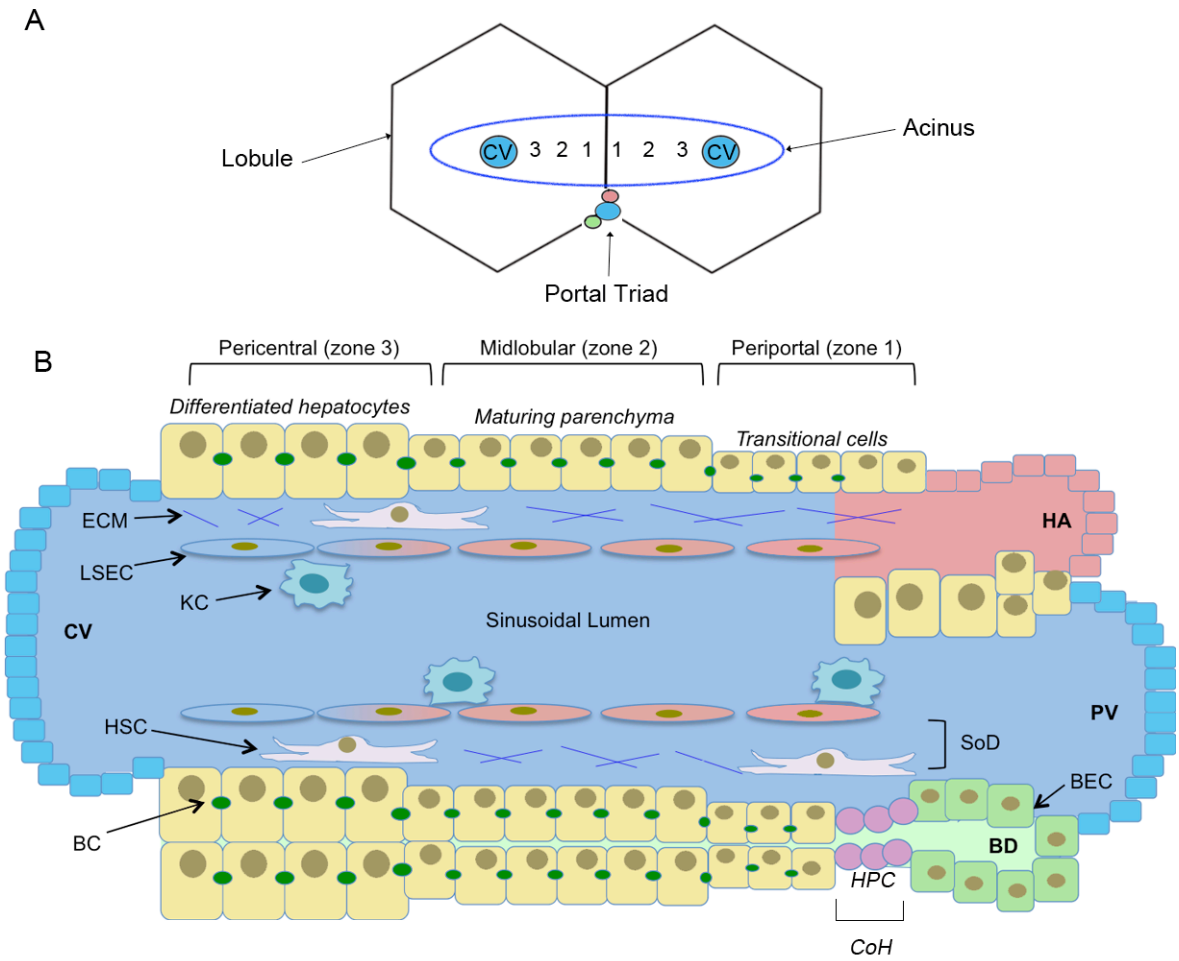

Figure 1.3 Illustration of the liver acinus. (A): The liver acinus spans two adjacent lobules in an elliptical shape with the portal triad providing the line of symmetry. Hepatocytes within the acinus receive a different quality of blood supply depending on their location. (B): Maturing hepatocytes along the acinus. Hepatocytes closest to the portal triad are less differentiated compared to those close to the central vein. Hepatic progenitor cells (HPC) are found in the Canals of Herring (CoH) that can progress onto either a hepatocyte or biliary epithelial cell (BEC) lineage. LSEC = liver endothelial sinusoidal cell. SoD = Space of Disse. HSC = hepatic stellate cell. KC = Kupffer cell. HA = hepatic artery. PV = portal vein. BD = interlobular bile duct. BC = bile canaliculi. ECM = extracellular matrix. CV = central vein.

In summary, hepatocyte anatomy and physiology *in vivo* is highly complex. As well as being 3D in shape (cuboidal), hepatocytes belong to an intricate 3D lobule architecture that dictates function. They are multi-polarised and rely on crucial cell—cell and cell-ECM contact for regulating normal behaviour. Other non-parenchymal liver cells such as LSECs, HSCs and Kupffer cells all interact with hepatocytes to influence hepatic function. Moreover, a biochemical gradient exists along the 3D acinus that influences hepatocyte differentiation and function, with only the most mature (differentiated) hepatocytes being involved in drug metabolism.

1.1.3 Role of Hepatocytes in Drug Metabolism

One of the key functional responsibilities of differentiated hepatocytes is the metabolism of xenobiotic substances such as drugs, making them crucial *in vitro* laboratory tools in drug discovery[32, 33]. Hepatic drug metabolism can usually be separated into two chemical reaction phases; phase I and phase II. However there are also many important transporter proteins involved in the uptake and elimination process (see Figure 1.4)[34].

Drugs present in the blood stream enter the liver lobule where they are first absorbed by hepatocytes. Most drugs require transporter proteins present at the sinusoidal interface to mediate uptake into hepatocytes. The organic anion transport polypeptides (OATPs) and organic anion transporters (OATs) are involved in the uptake of most hydrophobic drugs[35, 36]. Conversely organic cation transporters (OCTs) are usually involved in the uptake of small hydrophilic drugs[37].

Several transporter proteins are involved in the elimination of the drug and/or drug metabolites from inside the hepatocyte. These proteins typically belong to the adenosine triphosphate (ATP) binding cassette (ABC) superfamily, which provide a pump-efflux mechanism upon ATP binding[38]. For example, the multidrug resistance proteins MDR1 or P-glycoprotein (ABCB1) and MRP2 (ABCC2) are localised in the bile canaliculi membrane alongside the bile salt export pump (BSEP). Similarly the breast cancer resistance protein (BCRP, ABCG2) is also located at this canaliculi membrane[39]. These transporter proteins pump drugs and drug metabolites into bile to then re-enter the digestive system to be secreted as faeces[38]. Other transporter proteins are also located at the sinusoidal domain; MRP3 (ABCC3) and MRP4 (ABCC4). These proteins control the elimination of drugs and drug metabolites back into the sinusoidal bloodstream to enter the kidneys for renal excretion[40, 41]. Whilst all of these proteins play a crucial role in drug elimination, they can also be problematic in facilitating drug resistance by too eagerly eliminating the drug from the body[42].

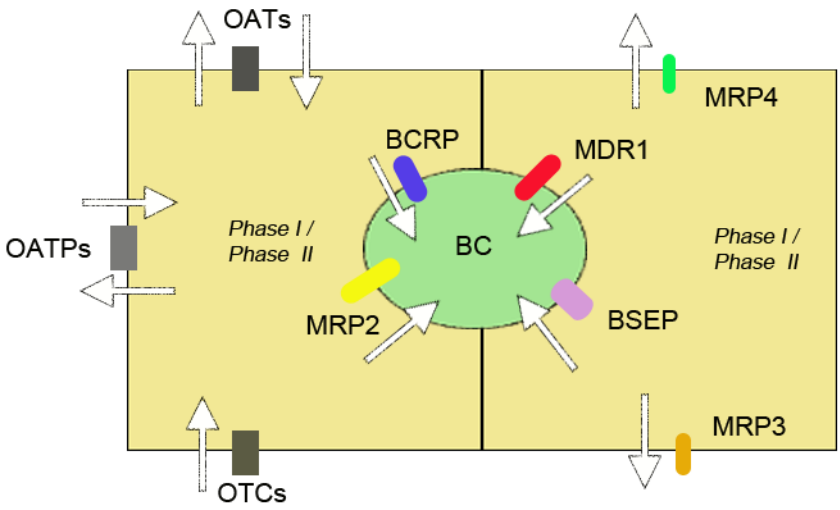

Figure 1.4 Illustration of the different hepatocyte transporter proteins involved in drug metabolism. Drugs enter the hepatocyte from the blood via organic anion transporter polypeptides (OATPs), organic anion transports (OATs) and organic cation transporters (OCTs). Drugs can then undergo phase I and phase II metabolism (or remain in the parent form). Drugs and/or drug metabolites are expelled from hepatocytes back into the sinusoids via the multidrug resistance protein 3 (MRP3) and multidrug resistance protein 4 (MRP4). Alternatively they are pumped into the bile via the multidrug resistance protein 1 (MDR1), multidrug resistance protein 2 (MRP2) and the breast cancer resistance protein (BCRP). These proteins reside at the bile canaliculi domain alongside the bile salt export pump (BSEP).

Phase I metabolism usually involves the cytochrome P450 (CYP) enzyme superfamily, which are predominantly, but not exclusively, found in the endoplasmic reticulum of hepatocytes[43]. Most common drugs are metabolised by the CYP1, CYP2 and CYP3 families, with the CYP3A4 isoform being one of the most common enzymes involved in drug metabolism[44]. Some typical drug substrates for different CYP isoforms are shown in Table 1-1.

Table 1-1 Typical Drugs Metabolised by Hepatocyte CYP Enzyme Isoforms.

CYP Isoform	Drug
CYP1A1	Theophylline
CYP1A2	Caffeine, paracetamol, tacrine, theophylline
CYP2A6	Methoxyflurane
CYP2C8	Taxol
CYP2C9	Ibuprofen, phenytoin, tolbutamide, warfarin
CYP2C19	Omeprazole
CYP2D6	Clozapine, codeine, debrisoquine, metoprolol
CYP2E1	Alcohol, enflurane, halothane
CYP3A4/5	Ciclosporin, losartan, nifedipine, terenadine

Table adapted from Rang, H.P. *et al*., *Pharmacology*, 5th Edn, Churchill Livingstone, p108

CYP enzymes perform a range of chemical reactions, however the most common is to hydroxlyate the drug to increase polarity[45]. They are heme-thiolate proteins and are monooxygenases. Flavin-containing monooxygenases (FMO) are another family of phase I enzymes that catalyse oxidation of drugs at nucleophilic nitrogen, sulphur and phosphorus[46].

Phase II metabolism usually involves a conjugation reaction to render the drug more polar, more acidic and more water-soluble to then allow for effective renal elimination from the body. A common phase II reaction involves the addition of glucuronic acid to an active functional group present on the drug. The enzymes responsible for this specific type of conjugation are the uridine diphosphate glucuronosyl transferases[47] (UGTs), which are a family of enzymes also located in the smooth endoplasmic reticulum of hepatocytes. Other conjugation mechanisms include the addition of sulfate groups (by sulfotransferases, SULTs), acetyl groups (by N-acetyltransferases, NATs) and glutathione groups (by glutathione S-transferases, GSTs). Figure 1.5 illustrates an example reaction scheme for a drug undergoing phase I and phase II metabolism inside a hepatocyte.

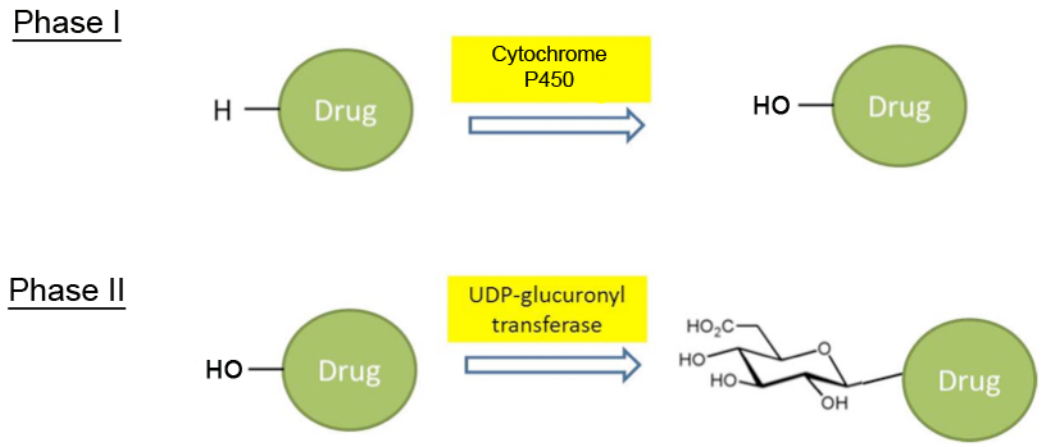

Figure 1.5 Illustration showing example phase I and phase II metabolising reactions performed by hepatocytes. Phase I shows the CYP mediated hydroxylation of a drug to render it more polar. Phase II shows the conjugation of glucuronic acid to the substrate to allow for effective renal elimination from the body.

In summary, hepatocytes are the principal cells involved in drug metabolism. Crucially, the uptake and elimination of drugs by various hepatic membrane proteins relies on the presence of key ultrastructural features such as bile canaliculi and sinusoidal domains. Failing to replicate these ultrastructural features *in vitro* is expected to significantly alter the drug uptake and elimination process and so lead to a poor predictive accuracy of a drug's true toxicity profile.

1.2 *In Vitro* Hepatocyte Culture

The previous section described the *in vivo* growth environment experienced by hepatocytes in the liver. This section introduces the concept of *in vitro* hepatocyte culture, starting with a general background to animal cell culture and then focusing on *in vitro* drug toxicity models.

1.2.1 General Principles of Animal Cell Culture: 2D *versus* 3D

Animal cell or tissue culture refers to the growth and maintenance of animal cells in an artificial environment. The technique dates back as early as 1885, when the German zoologist Wilhelm Roux first cultured portions of the medullary plate of an embryonic chicken for several days on a flat glass plate. The technique was then further developed by scientists such as Ross Granville Harrison and Julius Richard Petri, credited with the Petri dish, to form the basis of modern day cell culture. Today the technique typically employs disposable polystyrene Petri dishes and welled-plates as the artificial growth substrate. Cell culture is now a routine and often high-throughput tool for progressing our understanding of cell biology, cancer, stem cell research and drug metabolism.

Culturing animal cells on a flat two-dimensional (2D) surface such as a Petri dish has proved extremely practical. Cells can be easily monitored on a daily basis using standard bright field microscopes. Most cells can be easily extracted for subsequent analysis and/or passaging. Polystyrene is also inexpensive. However, there are several key disadvantages with 2D culture that has severely limited the physiological relevance and predictive accuracy of the method. Firstly is that 2D monolayer culture forces cells to stretch out across the plastic into a severely flattened morphology that lacks structural organisation. This is far removed from the complex three-dimensional (3D) environment found *in vivo*. Crucially, alterations in cell morphology and structural organisation from their native state are known to significantly impact cell genotype and phenotype[48, 49]. For example, cell shape can influence stem cell fate[50]. Cell shape can influence apoptosis[51]. Cell geometry can dictate cell polarisation and the formation of specialised structural features such as those in epithelial[52]. Importantly these specific structural arrangements can influence cell function, as demonstrated by Bissell *et. al.* for breast epithelial function[53]. Similarly tissue morphogenesis and tumorigenesis are also highly influenced by the spatial geometry of the surrounding architecture[54]. Unsurprisingly, failing to mimic these important geometric components has limited 2D cultures to more primitive studies of structure-function relationships.

Another disadvantage of 2D culture is that most of the cell surface is in contact with the plastic substrate, restricting cell-cell contact to the edges of the cells (see Figure 1.6). Conversely, cells *in vivo* rely on frequent juxtacrine, autocrine and paracrine signalling for normal tissue homeostasis and function. Indeed a constant interplay between neighbouring cells and the surrounding ECM

helps cells to stay in tune with their surroundings and adapt to external stimuli accordingly. The minimal cell-cell contact possible in 2D culture deprives cells of these vital communications, making them more vulnerable to changes in their surroundings.

A third disadvantage of 2D culture is that the absence of 3D tissue organisation fails to recreate important biochemical gradients found *in vivo*. Cells in 2D are uniformly exposed to a fluctuating media quality, unlike *in vivo* where cells receive a steady state biochemical gradient dependent on their location in the vascularised tissue. Overall the combination of distorted cell geometry, poor cell-cell contact and a lack of biochemical gradients significantly contribute to harsh deviations in cell differentiation, gene expression and function during 2D culture compared to *in vivo*[55]. For example, cell lines used heavily in 2D *in vitro* models are often over-adherent and over-proliferative compared to their native counterparts[56].

Recognising the limitations of 2D culture there is now a strong demand for materials that can offer a 3D interface for cell growth[57-59]. By adding the third dimension to the growth substrate, it is hypothesised that cells can approximate their native 3D architecture and organisation *in vitro.* This in turn is hypothesised to encourage cell-cell contact and so preserve crucial cellular communication. The formation of 3D tissue structures is also hypothesised to replicate important biochemical gradients found *in vivo.* In essence, 3D cultures are expected to preserve native structure-function relationships and thus provide more accurate models of *in vivo* behaviour[60].

One of the earliest reports to demonstrate the importance of re-creating the 3D microenvironment for predictive function *in vitro* was that from Bissell *et al.,* where they showed a more *in vivo* like phenotype could be achieved for breast cancer cells when growing in 3D[61]. The same group also produced a seminal paper showing how gene expression of mammary epithelial cells is profoundly influenced by the 3D microenvironment[62]. From there the field of 3D cell growth exploded; 3D cell growth is now being used to direct stem cell fate by mimicking niche architectures found *in vivo*[63, 64]. 3D cell growth is being used to approximate the complex tumour microenvironment to better understand the mechanisms behind cancer and tumorigenesis[54, 65]. 3D cell growth is opening up exciting opportunities for tissue engineering and regenerative medicine, where 3D constructs grown *in vitro* or *ex vivo* can later be implanted into the body for organ repair[66, 67]. However, significant work still needs to be done in transitioning these learnings into successful and clinically relevant 3D products for commercial use[68].

1.2.2 Conventional 2D Hepatocyte Culture in Drug Discovery

Hepatocyte cell culture forms a crucial part of *in vitro* drug toxicity screening by providing a model of native liver xenobiotic metabolism[32, 33]. Traditionally, multi-welled-plates have been used as the artificial growth environment for most *in vitro* drug toxicity studies, offering only 2D interface for

hepatocyte attachment and growth. Whilst this approach has offered a high-throughput model of drug toxicity, it is now regarded as highly unrealistic compared to the complex 3D scenario found in native liver[58, 59]. The 2D environment forces hepatocytes into a flattened morphology, as shown in Figure 1.6. This then restricts the formation of gap junctions and adhesion junctions and therefore inhibits the maintenance of polarised membranes presenting sinusoidal and bile canaliculi domains. Moreover, important biochemical gradients present in the liver acinus are almost impossible to replicate along a flat 2D surface. Unsurprisingly, most hepatocytes isolated from *in vivo* rapidly lose their differentiated phenotype in 2D culture, with drug metabolising capacity one of the first functions to be lost[69]. The result is a poor predictive capacity of a drug's biotransformation properties and so a much higher risk of failure later in the drug development process. A significant dependence on animal testing is therefore required due to the poor predictive accuracy of 2D hepatocyte models.

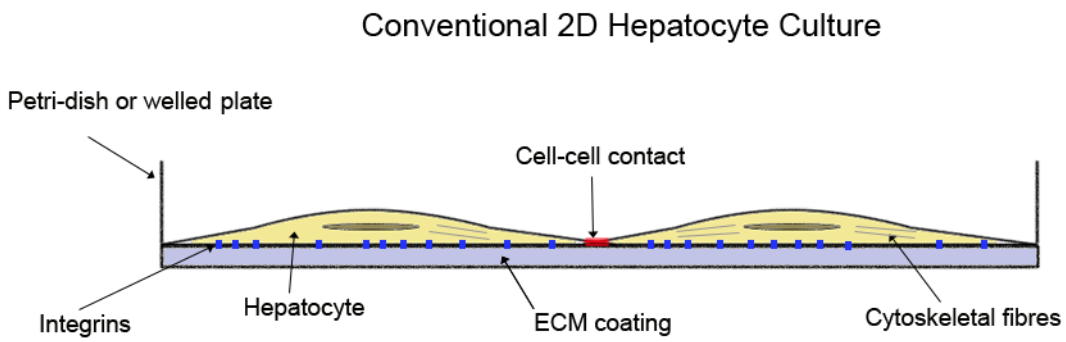

Figure 1.6 Illustration of hepatocytes cultured on a conventional 2D plastic substrate. Cells spread out across the plastic creating a severely flattened morphology. A large portion of the cell is in contact with the substrate whereas only a small portion is able to interact with adjacent cells. This limits the opportunity for cell-cell adhesion and communication and limits polarisation towards bile canaliculi and sinusoidal domains.

1.2.3 The Concept of 3D Hepatocyte Culture in Drug Discovery

Huge emphasis is now placed on developing predictive *in vitro* hepatocyte models to better screen out unsuitable drug candidates as early as possible, reducing the risk of failure at the animal and clinical stages of the drug development process[70-72]. However, in order to successfully achieve this, the artificial growth environment used for *in vitro* pharmaceutical testing needs to be physiologically relevant to that of the native liver[73, 74].

The development of 3D hepatocyte models *in vitro* is now regarded a key part of improving the predictive accuracy of drug toxicity screening and are therefore gaining significant attention[32, 75]. However, many of these models are still in developmental phase and are not yet commercialised

or even suitable for routine application. Moreover, a thorough understanding of hepatocyte behaviour in these 3D models is yet to be determined. The following section discusses in turn the key developments in 3D cell models for drug discovery applications.

1.3 Technology Developments to Enable 3D *In Vitro* Hepatocyte Culture

There are now a variety of different materials that can offer a 3D microenvironment for hepatocyte growth, evident by the substantial academic and patent literature recently published[32, 57, 75]. The materials can be broadly divided into those originating from natural (biological) tissue and those derived synthetically. Natural based materials such as protein gels or polysaccharide scaffolds offer attractive biocompatibility properties. They can also even mimic certain aspects of the native ECM that influences cell function. However, for routine *in vitro* toxicology studies, natural based materials have several limitations. Batch to batch variability inherent of biological material can lead poor experimental reproducibility. Biodegradability can cause issues with long term laboratory experiments and storage. There is also the issue of sourcing sufficient biological material for extensive drug screening studies. Consequently synthetic materials (often polymers) have been developed to provide 3D scaffolds for a range of applications, including tissue engineering, regenerative medicine and of course routine *in vitro* hepatocyte growth for drug toxicity studies. A brief summary of each technology category is shown in Table 1-2, followed by a more detailed discussion in the text.

Table 1-2 Summary of the Different Technologies Available for 3D Cell Growth

Technology	Advantages for Routine Use	Disadvantages for Routine Use
Sandwiching with ECM proteins	- Can mimic biochemical aspects of native ECM - Simple to use	- Not strictly 3D cell growth (3D monolayer) - Degradable - Variable consistency
Spheroid/Aggregate Culture	- Simple to use	- Not extensive 3D growth throughout - Poor mass transfer into centre of aggregate
Hydrogels	- Can mimic mechanical and biochemical aspects of native ECM - Extensive 3D growth throughout the gel - Commercially available	- Poor mass transfer - Degradable - Variable consistency (natural based hydrogels) - Additional preparation steps (gelation)
Electrospun scaffolds	- Versatile range of polymers can be electrospun - Commercially available - High porosity	- 3D growth restricted to the nodes of the fibres - Poor mechanical properties for routine use
Scaffolds from Rapid Prototyping	- Excellent reproducibility	- Synthetic surface chemistry - Expensive machinery required - 3D growth restricted to individual compartments
Porous Polymers from Fibre Bonding	- High porosity - Mechanically strong	- Synthetic surface chemistry - Risk of residual toxic solvents/salts -Poor reproducibility - Not extensive 3D growth throughout
Porous Polymers from Solvent casting / Particle Leaching		
Porous Polymers from Gas-Foaming		
Porous Polymers from Phase Separation		
Porous Polymers from Emulsion Freeze Drying		
Porous Polymers from Emulsion Templating	- High porosity - Excellent reproducibility - Mechanically strong	- Synthetic surface chemistry

1.3.1 Sandwiching with Extracellular Matrix Proteins

1.3.1.1 *Overview*

ECM proteins such as collagen, laminin or fibronectin have long been used to coat Petri dishes and welled-plates to improve the physiological relevance of the 2D interface and thus promote hepatocyte adhesion and function. Taking this further, researchers found that applying a second layer of ECM protein directly above the monolayer, to create a sandwich of protein/cell/protein, was beneficial for hepatocyte growth (see Figure 1.7)[76, 77]. In this configuration, cell-matrix adhesion from above and below reduces cytoskeletal flattening and maintains cell-cell contact between adjacent hepatocytes. Although not a definitive 3D organisation, sandwich systems have been shown to promote a polygonal hepatocyte morphology for extended culture periods[78]. Results have shown that sandwich cultures with matrix proteins can lead to prolonged hepatocyte viability[76], extended cytochrome P450 activity[79] and increased cell polarisation towards more advanced bile canaliculi networks[80]. Consequently this approach is a popular method of culturing hepatocyte cells, particularly to monitor hepatobiliary mechanisms *in vitro*[81].

1.3.1.2 *Advantages*

ECM components can mimic certain biochemical aspects of the native ECM. Sandwich cultures are also easy to set up and are useful for the study of hepatobiliary mechanisms.

1.3.1.3 *Disadvantages*

Growth is essentially a 3D monolayer rather than an extensive 3D organisation. Cell-cell contact is therefore still limited and not strictly 3D. Biodegradability of the ECM proteins raises issues for long term experiments and storage. Once more, ECM components derived from natural sources are inherently variable with unknown impurities.

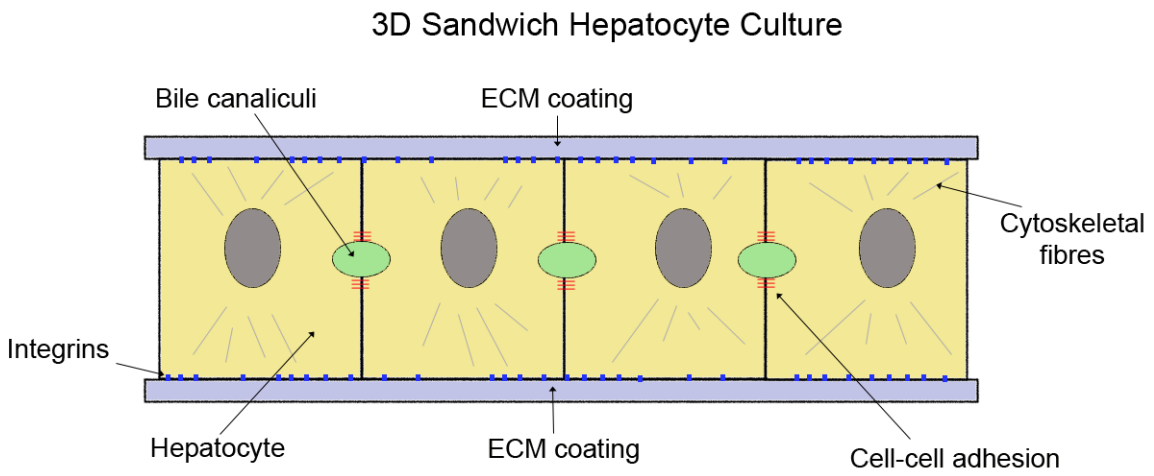

Figure 1.7 Illustration of hepatocytes in sandwich culture. An ECM protein coating above and below encourages cells to adopt an upright morphology that preserves cell-cell contact. This allows for cell adhesions that retain polarisation and thus the formation of bile canaliculi.

1.3.2 Spheroidal Aggregate Cultures

1.3.2.1 *Overview*

Plating cells onto non-adhesive surfaces will often encourage the formation of 3D spheroid/aggregate cultures, whereby cells secrete their own ECM to keep the aggregate intact[82, 83]. Within this configuration, cells cluster together rather than adhering to the substrate to establish important cell-cell contacts relevant to the native 3D architecture (Figure 1.8). Some of the first reports by Bissell *et al.* demonstrating the influence of the 3D microenvironment employed aggregate cultures[62]. Indeed, hepatocytes in spheroid culture display a more differentiated functional behaviour and gene expression compared to 2D[84-86]. They also show prolonged (3-4 weeks) viability and hepatic function[87, 88]. Rainbow trout hepatocytes also show a much closer gene expression profile to *in vivo* when cultured in aggregates compared to 2D[89].

1.3.2.2 Advantages

Spheroids/aggregates are very easy to set up and do not require any specialist equipment. Moreover, the formation of an aggregate culture relies on the secretion of ECM components to keep the aggregate intact, which can serve to mimic native cell-ECM interactions. Aggregate cultures also enable the formation of biochemical gradients to be set up, with those on the outside of the aggregate experiencing a different quality of culture media to those in the middle.

1.3.2.3 *Disadvantages*

3D cell growth is limited to individual spheroids and so an extensive 3D organisation cannot usually be achieved. Aggregates are also non-vascularised which can lead to mass transfer issues for those cells in the centre of the aggregate.

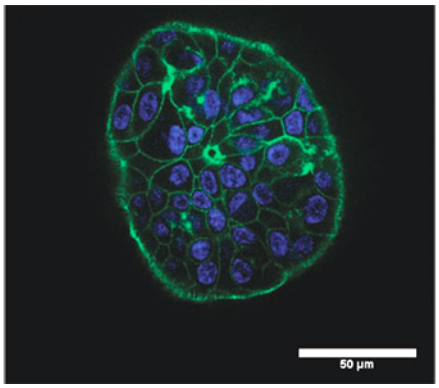

Figure 1.8 Primary human hepatocytes in spheroid formation after 2 weeks culture. Confocal fluorescence microscopy was used to obtain the image; Green staining = F-actin; Blue staining = DAPI. Cells are aggregated together in a 3D formation. Image taken from Alves *et al.*, Hepatology **2012**, 55, 1227-1236.

1.3.3 Hydrogels

1.3.3.1 *Overview*

Hydrogels derived from natural or synthetic polymers can be used to immobilise cells within a 3D gel matrix that mimics certain physical, mechanical and/or biochemical aspects of the native ECM. Their soft nature and often bio-based composition makes them attractive materials for tissue engineering and regenerative medicine applications[90, 91]. Within the gel, cells aggregate into 3D structures that promote cell contact and interaction across multiple surfaces (see Figure 1.9). Some of the early pioneering 3D cell culture experiments involving hydrogels were performed by Bissell *et al.*, demonstrating significant differences in breast cancer growth compared to 2D cultures[61, 92]. Their work employed a commercial hydrogel known as Matrigel™ (*BD Biosciences*), based on a cocktail of different ECM proteins obtained from a mouse sarcoma[93, 94]. Since then, Matrigel™ has been used extensively as a technology for *in vitro* 3D cell growth[95]. For hepatocytes, Matrigel™ has been shown to prolong aspects of hepatocyte function beyond those observed in collagen sandwich cultures[96]. Hepatocytes in Matrigel™ also adopt a more native structure with appropriate polarisation[97]. Other hydrogel-based materials have also been applied to 3D cell culture. For example, the hyaluronate based Extracel™ (*glycosan biosystems*) has been shown to prolong *in vitro* hepatocyte cytochrome P450 activity for up to 17 days[98]. PuraMatrix™ (*3-D Matrix*) is another commercially available peptide hydrogel that has been shown to induce

the differentiation of putative rat liver progenitor cells into mature hepatocyte-like cells exhibiting up-regulated albumin and cytochrome p450 activity[99].

1.3.3.2 *Advantages*

Hydrogels are a popular technology choice for many researchers as they can replicate native cell-cell and cell-ECM biochemical and physical interactions. They are particularly attractive for soft tissue growth, especially as the surrounding matrix stiffness in known to be a contributing factor to cell phenotype[100]. Synthetic hydrogels that facilitate cell invasion *in vivo* are also showing extremely promising results for tissue regeneration applications[101]. They also enable extensive 3D growth about the gel and are commercially available.

1.3.3.3 *Disadvantages*

Mass-transfer issues have long been a concern for hydrogels, in that the diffusion of nutrients and waste through the gel may be too slow to accommodate dense 3D structures. Natural based hydrogels such as Matrigel™ are inherently variable and also biodegradable, although synthetic hydrogels help to address this issue. Another limitation is gel formation. Many hydrogels require some form of external switch to gel, such as a change in temperature, pH or exposure to UV radiation. Hence if cells are dispersed into the material prior to gelation, which is common practice, care needs to be taken to ensure that the gelation process does not have any detrimental effect on cell viability. Gelation also adds additional preparation steps and decreases the high throughput suitability.

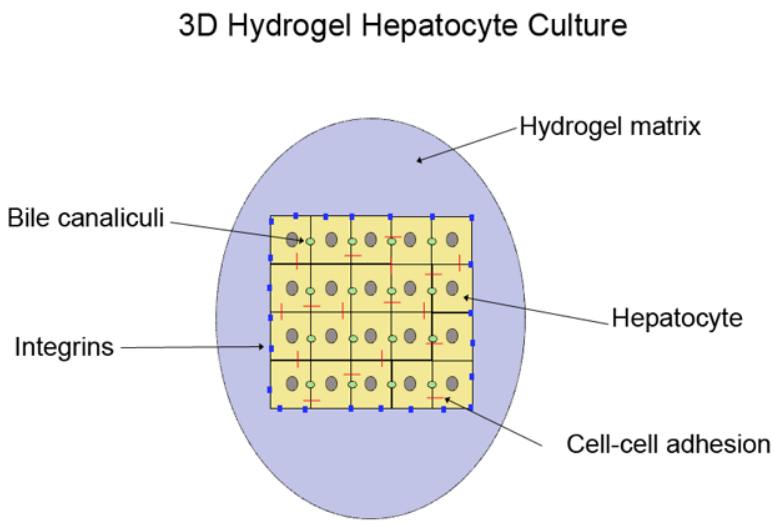

Figure 1.9 Illustration of hepatocytes growing in a 3D hydrogel. The gel encapsulates the cells in a 3D organisation encouraging cell-cell contact and therefore maintenance of cell polarisation and bile canaliculi. ECM hydrogels such as Matrigel™ can also mimic cell-ECM interactions found *in vivo*. They are also soft and so mimic certain mechanical aspects of the native ECM.

1.3.4 Electrospun Scaffolds.

1.3.4.1 *Overview*

Electrospinning is a technique that converts polymeric liquids (natural or synthetic) into micro- or nano-scale fibres creating a 3D mesh topography. The technique is hugely versatile enabling a range of different fibrous compositions and architectures with different diameters and porosities to be formed. As a result the technique has attracted significant attention for 3D cell growth applications, with cells being able to migrate into the mesh structure and grow in a 3D manner[102]. Figure 1.10 is an illustration of how 3D polymer fibres provide a scaffold for 3D hepatocyte growth and Figure 1.11 is an actual example of cells growing in an electrospun scaffold, taken from *The Electrospinning Company* (UK). A comprehensive study by MacNeil *et al.* was one of the first reports to demonstrate the suitability of electrospun scaffolds for 3D cell culture[103]. They showed that these scaffolds encouraged 3D cell migration and 3D aggregate formation within the material, which in turn translated into a more physiologically accurate response to cytotoxic agents compared to 2D cell culture[104].

Hepatocytes cultured on synthetic electrospun fibres have also been shown to become engulfed by the fibrous structure to form 3D aggregates with increased cell-cell contacts[105]. Such scaffolds have been shown to enhance liver specific functions such as albumin synthesis, urea synthesis and cytochrome P450 activity[106]. Electrospun scaffolds have also been used to direct stem cells into a differentiated hepatocyte lineage[107].

1.3.4.2 *Advantages*

Electrospun scaffolds are cheap to produce once the initial electrospinning equipment has been purchased. A versatile range of polymers can be electrospun, offering excellent choice on chemical composition. Developments in aligned electrospun fibres are also showing great promise for neural tissue engineering[108]. Furthermore, electrospun materials are now available as commercial scaffolds for 3D cell growth (Mimetix™, *The Electrospinning Company*).

1.3.4.3 *Disadvantages*

Cell growth is generally restricted to the nodes where fibres overlap, as large holes separating individual fibres can prevent extensive organisation. Consequently 3D growth tends to be as individual pockets dispersed throughout the material, and very rarely will high cell densities be packed into the structure. The mechanical properties of electrospun scaffolds are also quite poor, significantly reducing their suitability for routine *in vitro* applications.

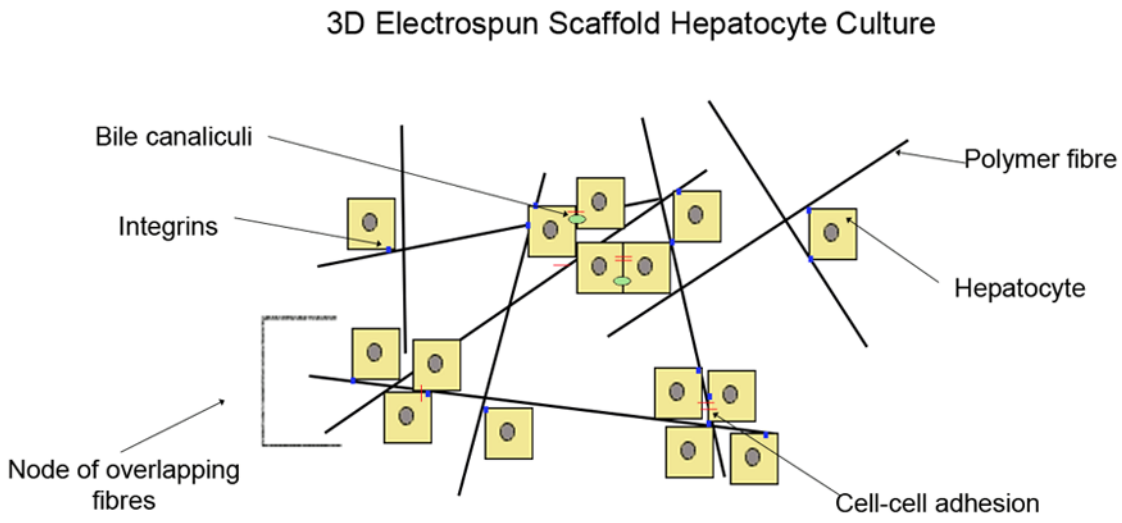

Figure 1.10 Illustration of hepatocytes growing in a 3D electrospun scaffold. Polymer fibres create a 3D mesh structure allowing 3D cell growth at the nodes of overlapping fibres. These pockets of 3D cell growth enable localised 3D cell-cell contacts, however extensive 3D growth is challenging as cells can fall through the areas where fibres do not overlap.

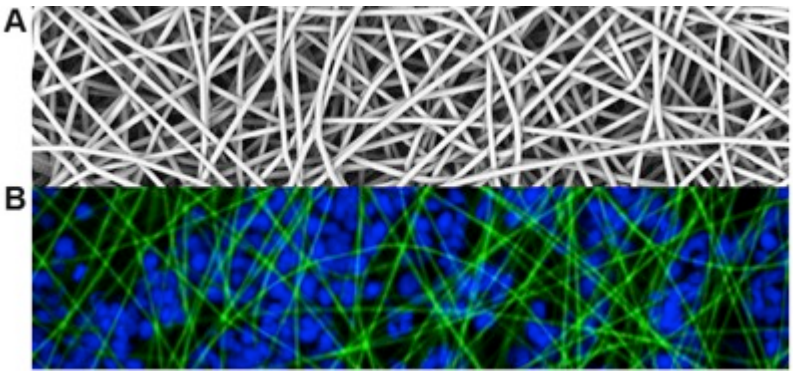

Figure 1.11 Micrographs of 3D cell culture in electrospun scaffolds. (A): scanning electron micrograph of an electrospun scaffold. (B): Confocal fluorescence microscopy of MCF7 breast cancer cells (TO-PRO®-3, blue) growing in the Mimetix® electrospun scaffold (Rhodamine 6G, green) after 4 days. Images taken from E. Heister, *Electrospinning Company, UK* (www.electrospinning.co.uk).

1.3.5 Rapid Prototyping

1.3.5.1 *Overview*

The development of 3D printing, selective laser sintering (SLS) and other rapid prototyping techniques has opened up new opportunities for a range of versatile 3D interfaces which are suitable for 3D cell growth[109], particularly for hard tissues such as bone[110]. Here digital prototypes are used to construct 3D structures of a material one layer at a time. The resulting hard scaffolds can be engineered to mimic the native elasticity and mechanical properties of bone tissue[111]. Typically the materials offer small 3D compartments for cell growth as printing extensive interconnected networks is challenging (see Figure 1.12 and Figure 1.13). As the materials are digitally designed, there is excellent control over morphology and porosity (material reproducibility).

1.3.5.2 *Advantages*

Excellent scaffold reproducibility as the materials as digitally designed. High porosities are obtainable. The scaffolds also offer physiologically relevant mechanical properties for bone and cartilage tissue engineering, although this is less suitable for hepatocytes.

1.3.5.3 *Disadvantages*

The materials are very expensive to produce and require specialist equipment. 3D cell growth is also restricted to individual compartments, preventing extensive 3D cell growth. Often cells can fall out of the materials if the voids are too large.

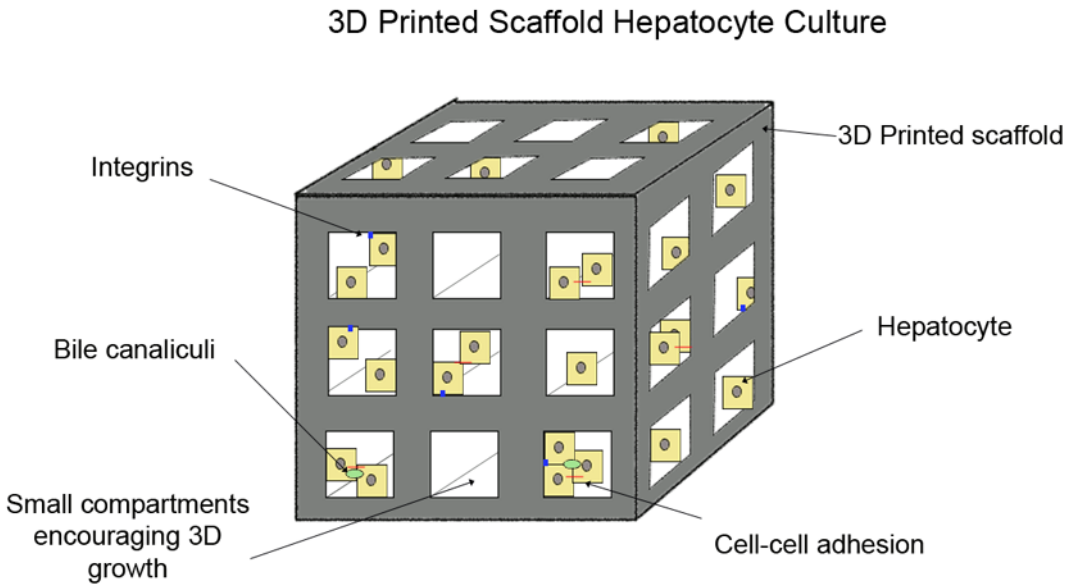

Figure 1.12 Illustration of hepatocytes growing on a 3D printed scaffold. Small separate 3D compartments encourage 3D growth, preventing extensive 3D organisation.

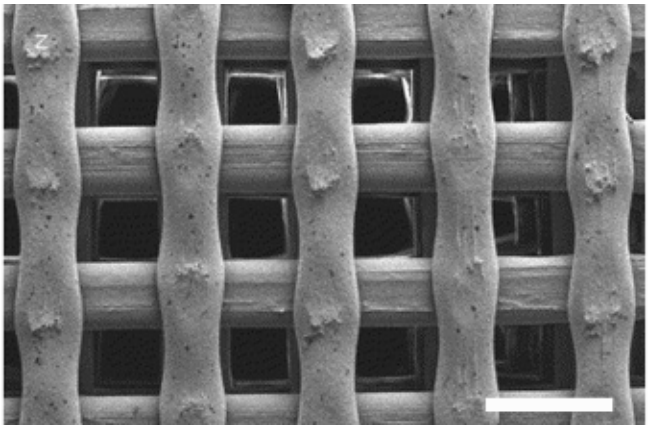

Figure 1.13 Micrograph of a rapid prototyped scaffold used in 3D cell culture. Image taken from Yeong *et al.*, Trends in Biotechnology **2004**, 22, 643-652. Scale bar = 1 mm.

1.3.6 Porous Polymers from Fibre Bonding

1.3.6.1 *Overview*

With a versatile range of morphologies and fabrication techniques available, porous polymers are attractive materials as substrates for 3D cell growth[112]. Some of the first porous polymers to be used as 3D scaffolds were based on polylactic acid (PLA), polyglycolic acid (PGA) and polylactic-co-glycolic acid (PLGA) for tissue engineering applications. These materials were first prepared using a technique known as fibre bonding[113, 114]. With this method, a PLA-solvent solution is cast over PGA fibres to create a composite that is then heated to bond the fibres at the nodes of intersection. The resulting materials are highly porous (80 %) and display void diameters up to

500 μm. Hepatocytes cultured on these materials remained viable for 1 week and also showed encouraging signs of 3D organisation[115].

1.3.6.2 *Advantages*

The materials display high porosities (typically 80 %). They also have suitable mechanical properties for routine laboratory use.

1.3.6.3 *Disadvantages*

Residual solvents from fabrication can be toxic to cells. Consequently, extensive and prolonged vacuum drying steps are required during processing. Synthetic polymers often display an inappropriate surface chemistry for optimal cell growth.

1.3.7 Porous Polymers from Solvent Casting / Particle Leaching

1.3.7.1 *Overview*

An alternative fabrication method of porous polymers is to use a technique known as solvent casting/particulate leaching[115, 116]. Here a polymer-solvent solution is cast over a mold containing porogen particles such as crystalline salts. After solvent evaporation the polymer-salt composite is washed to dissolve the salt, leaving a porous structure behind. 3D hepatocytes have been cultured on these materials and then successfully transplanted into laboratory rats[117]. Hepatocytes also remained viable on these materials for up to 14 days, although a gradual reduction in albumin synthesis and liver-specific gene expression was observed[118].

1.3.7.2 *Advantages*

The materials display high porosities (typically 80 %). They also have suitable mechanical properties for routine laboratory use.

1.3.7.3 *Disadvantages*

Residual salts left in the matrix can affect cell growth. Consequently, extensive washing steps are required to fully remove the salts. Salt crystal size cannot be strictly controlled and so void diameter can be variable. Synthetic polymers often display an inappropriate surface chemistry for optimal cell growth.

1.3.8 Porous Polymers from Gas Foaming

1.3.8.1 *Overview*

Gas foaming is another fabrication method of porous polymers used for 3D cell culture applications[119, 120]. Here solid polymer discs are prepared using compression molding. The discs are then exposed to high-pressure gas (e.g. CO_2) for several hours/days to render porosities of approximately 90 % and void sizes of up to 100 μm. This technique has also been combined with elements of particle leaching, employing both salt and gas as porogens. Rat hepatocytes cultured on these materials maintained viability for up to 1 week[121].

1.3.8.2 *Advantages*

The materials display high porosities (typically 90 %). They also have suitable mechanical properties for routine laboratory use.

1.3.8.3 *Disadvantages*

Gas bubbles can coalesce and so void diameter can be variable. Synthetic polymers often display an inappropriate surface chemistry for optimal cell growth.

1.3.9 Porous Polymers from Phase Separation

1.3.9.1 Overview

Phase separation is another approach to fabricating porous polymers[122-125]. Here the polymer is dissolved in a solvent solution that then cooled below the melting point of the solvent. The mixture is then vacuum dried to remove the solvent via sublimation and leave a porous polymer. With this method porosities of up to 90 % and void diameter of 100 μm have been reported[124].

1.3.9.2 *Advantages*

The materials display high porosities (typically 90 %). They also have suitable mechanical properties for routine laboratory use.

1.3.9.3 *Disadvantages*

Residual organic solvents can be toxic to cells. Synthetic polymers often display an inappropriate surface chemistry for optimal cell growth.

1.3.10 Porous Polymers from Emulsion Freeze Drying

1.3.10.1 *Overview*

Emulsion freeze drying is another common approach to porous polymers[126]. Here an emulsion is created with the polymer as the external phase and a solvent as the internal phase. The emulsion is frozen and then slowly dried to allow the solvent to sublime and thus leaving a porous structure behind. Scaffolds with high porosities (90 %) and voids of ca. 30 μm are formed which have been used to support 3D hepatocyte growth for up to 2 weeks[127].

A similar freeze drying technique has also been applied to alginate gels to create porous alginate sponges with voids in the region of 70 to 300 μm[128]. Hepatocytes cultured on these materials form 3D spheroid structures that displayed enhanced albumin and urea function over conventional 2D cultures[129]. Moreover, new-born hepatocytes cultured on alginate sponges displayed signs of terminal differentiation towards mature hepatocytes with drug metabolising capacity[130]. These alginate sponges are now commercially available as AlgiMatrix™ (*Life Technologies)* and are being employed for routine *in vitro* cancer cell studies[131].

1.3.10.2 *Advantages*

The materials display high porosities (typically 90 %). They also have suitable mechanical properties for routine laboratory use.

1.3.10.3 *Disadvantages*

Residual solvents can be toxic to cells. For alginate sponges, 3D cell growth is restricted to the individual voids rather than extensively throughout the structure.

In summary, this section has described a range of different technologies that can be used to re-create aspects of the native liver microenvironment *in vitro*. However, there are significant disadvantages associated with many of these technologies. Naturally derived technologies (ECM sandwiches or hydrogels) are often unsuitable for routine *in vitro* use due to biodegradability and batch to batch variability. Similarly many synthetic technologies (electrospun scaffolds or porous polymers derived from chemical processing) are either poorly controlled or contain residual solvents that may be toxic to cells. Porous polymers derived from emulsion templating aims to address some of these issues.

1.4 Porous Polymers from Emulsion Templating

Emulsion templating uses emulsion internal phase droplets to template voids into a material polymerising in the emulsion external phase. The method was first employed in the 1960's as an emulsion based polymerisation tool[132], but was then extensively developed by Unilever in the 1980's and by Sherrington/Cameron in the 1990's as a method of creating highly porous polymers[133, 134]. Typically, an internal droplet phase is slowly added to a monomeric external (continuous) phase under mixing to create an emulsion (see Figure 1.14). When the volume fraction of the emulsion internal phase occupies greater than 74.05 % of the total emulsion volume these emulsions are termed high internal phase emulsions (HIPEs) (74.05 % represents the packing limit of uniform non-deformable spheres). The external phase of the HIPE is then cured around the internal droplets to produce a polymer (or polyHIPE) containing voids in the structure where the droplets had once been. Once more, during this polymerisation process, the thin external phase film separating each internal phase droplet from its neighbours is believed to contract and rupture to create interconnecting holes within the material voids[135]. The resulting polymer is therefore an interconnected network of voids producing a highly permeable material with a porosity of around 90 % (see Figure 1.15). Usually the materials are prepared in monolithic form, however a variety of other physical forms have been reported including polyHIPE beads[136] and even 3D laser patterned polyHIPEs[137].

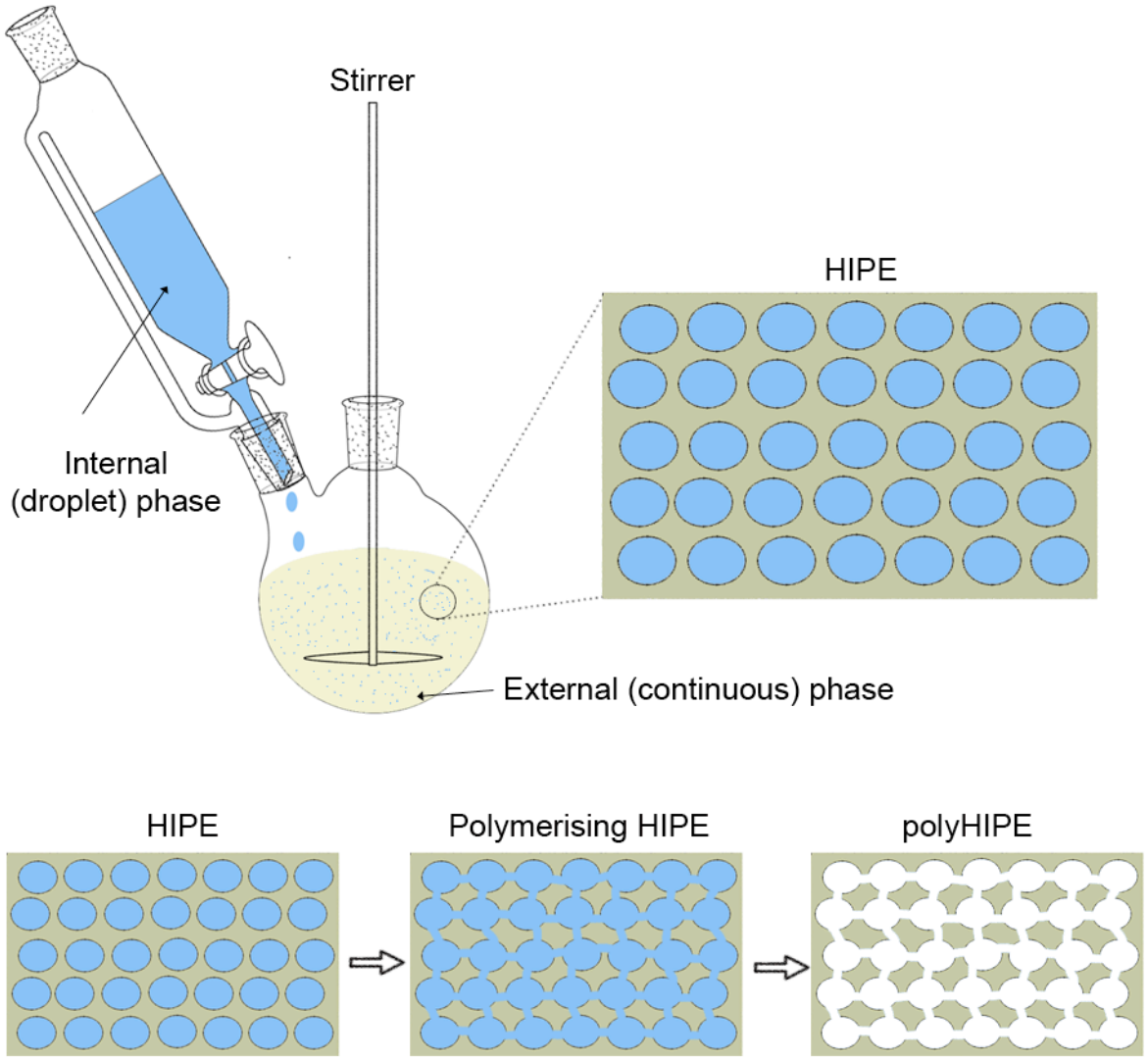

Figure 1.14 Illustration showing the preparation of a polyHIPE using emulsion templating. An emulsion internal droplet phase is slowly added to an emulsion external phase under mixing to create a HIPE, where the volume fraction of the internal phase is at least 74.05 %. The internal phase droplets in the HIPE are then used to template voids. During the polymerisation process the thin continuous phase film is believed to rupture around the voids creating small interconnecting windows between each void in the polyHIPE.

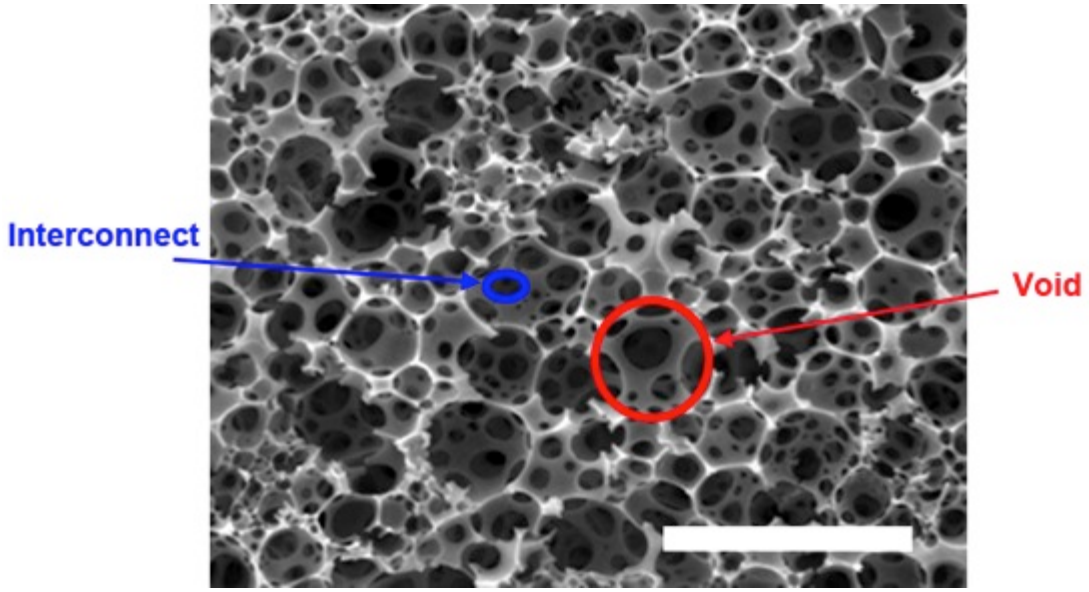

Figure 1.15 Typical polyHIPE morphology observed through scanning electron microscopy (SEM). Polymer voids are present that have been templated from the internal phase. These voids are also interconnected with small windows to render a highly porous material. The image was obtained from results of this thesis using a styrene based HIPE formulation. Scale bar = 100 μm.

PolyHIPEs can be produced using either water-in-oil (w/o) or oil-in-water (o/w) emulsions[138]. Generally w/o emulsions are more popular for polyHIPE synthesis as the emulsions are more easily stabilised. Often a non-ionic surfactant with a low hydrophilic-lipophilic balance (HLB) such as Span80™ is employed for w/o emulsions. Span80™ is insoluble in the water droplet phase and so inhibits emulsion phase separation. Electrolytes such as calcium chloride ($CaCl_2$) are also sometimes used in the fabrication process of these materials to promote emulsion stabilisation by improving surfactant packing at the interface[139]. A variety of different polymerisation initiators can be employed, including potassium persulfate (KPS), azobisisobutyronitrile (AIBN) and benzoyl peroxide (BPO). The potential to create a variety of different emulsions has therefore resulted in a broad range of functional polyHIPEs derived from a variety of functional monomers[140, 141].

Importantly, the structure of polyHIPEs can be tailored by manipulating the initial HIPE properties prior to curing[142]. For instance, methods to destabilise the emulsion such as increasing temperature or reducing surfactant concentration can give rise to mechanisms such as Ostwald ripening and droplet coalescence that serve to increase droplet diameter and ultimately increase final void size. As a result, careful determination and selection of surfactant, initiator, process conditions, phase compositions and the use of additives are all possible variables to help control HIPE properties and thus tailor the final polyHIPE structure. This morphological control is seen as

a key advantage over other fabrication methods of porous polymers as it allows for a homogeneous and reproducible scaffold structure.

Emulsion templated porous polymers are suitable for 3D scaffold applications for several reasons. Their high porosity facilitates effective nutrient and waste transfer to the cells. They possess a controllable, uniform morphology that can potentially allow for extensive homogeneous 3D cell organisation. They also offer suitable mechanical strength properties when fabricated with a chemical cross-linker. This supports the weight of large cell numbers and also allows sectioning of the polyHIPE monolith into thin membranes for use in 3D cell culture applications. Several groups have therefore successfully applied polyHIPEs for 3D scaffold applications and demonstrated more appropriate cell growth behaviour compared to conventional monolayer cultures. For example, Akay *et al*. and Cosgriff-Hernandez *et al.* have reported promising results in developing 3D bone growth within polyHIPEs[143-145]. Barbetta *et al*. have developed biocompatible polyHIPEs based on gelatin and applied these to 3D neural cell growth[146, 147]. Similarly Silverstein *et al.* have reported biocompatible and biodegradable polyHIPEs based on polycaprolactone (PCL) that offer promising applications in tissue engineering[148, 149]. Furthermore, Cameron/Przyborski *et al.* previously reported the suitability of polystyrene based polyHIPEs as replacements for conventional 2D plastic-ware with a range of cell types[150-153]. These materials are particularly attractive for routine *in vitro* use as they are essentially just a more appropriate geometric version of the typical polystyrene plates used in cell culture for decades. They are also inert and chemically stable and so are suitable for routine laboratory use and storage. Indeed, the commercial versions of these materials (Alvetex®Scaffold and Alvetex®Strata by *Reinnervate*)[154] are already being adopted by other research groups as more appropriate tools for *in vitro* cell culture[155-158].

Despite the encouraging results of emulsion templated porous polymers (polyHIPEs) as scaffolds for 3D cell growth, very few reports have investigated the materials for 3D hepatocyte growth in the context of drug discovery tools. Przyborski *et al*. showed that a hepatocyte derived cell line (HepG2) displays a different functional response to methotrexate compared to conventional 2D cultures[151]. They also showed enhanced viability and basal albumin synthesis compared to 2D[150]. Marshall *et al.* also observed a different functional response of primary rat hepatocytes to acetaminophen (APAP) compared to 2D, with hepatocytes in 3D being more sensitive to the toxic intermediate produced during APAP metabolism[159]. Barbetta *et al*. applied gelatin based polyHIPEs for 3D hepatocyte growth as a preliminary study, but did not provide a functional assessment of the cells behaviour[146, 147]. Whilst these are all encouraging results, a more in depth

study regarding the suitability of emulsion templated porous polymers as scaffolds for 3D hepatocyte culture is required if the materials are to be widely adopted in routine drug toxicity studies. For example, how well the scaffolds can approximate native liver architecture under different culture conditions is unknown. The impact of the scaffold microenvironment on hepatocyte structure, function and gene expression is also broadly unknown. Finally, no reports have addressed the biochemical relevance of synthetic emulsion templated scaffolds for hepatocyte culture. This study therefore aims to address some of these unknowns.

1.5 Summary

This literature review has covered the following key concepts to introduce this project:

- Improving the predictive accuracy of *in vitro* hepatocyte models requires technologies that can re-create elements of the native liver environment *in vitro*.

- Hepatocytes in their native liver environment are part of a complex 3D architecture that is crucial for normal cell function. They adopt a specific 3D shape, experience extensive cell-cell contact, are multi-polarised and constantly pick up biochemical cues from their surroundings to regulate normal behaviour.

- Accordingly, maintaining appropriate cell shape and cell-cell contact *in vitro* is important in developing physiologically relevant *in vitro* hepatocyte models. Unfortunately, conventional 2D hepatocyte models force an unrealistic cell shape with limited cell-cell contacts, thus promoting a phenotype that is far removed from the *in vivo* scenario. Unsurprisingly, 2D hepatocyte models are not very predictive of a drug's toxicity profile.

- Technologies that enable 3D hepatocyte growth *in vitro* are hypothesised to improve the physiological relevance of hepatocyte culture models and thus provide more predictive in *vitro* drug toxicity tools.

- A range of different technologies are available for 3D hepatocyte culture, each with their own advantages and disadvantages. These include ECM sandwich cultures, spheroid cultures, hydrogels, electrospun scaffolds, rapid prototype scaffolds and porous polymers derived from different fabrication methods.

- Emulsion templated porous polymers are an attractive choice for *in vitro* 3D hepatocyte growth over other technologies due to their high porosity, controllable morphology and suitable mechanical strength properties.

- A comprehensive understanding of 3D hepatocyte growth in emulsion templated porous polymers is yet to be determined. Achieving this could result in more representative hepatocyte culture phenotypes and thus more predictive *in vitro* toxicity tools.

1.6 Project Aims

The overall aim of this project is to develop a more physiologically relevant *in vitro* hepatocyte model using emulsion templated porous polystyrene scaffolds. This could have applications for more predictive *in vitro* drug toxicity tools. Importantly the model should be suitable for routine application, offering compatibility with existing laboratory plastic ware (inserts/welled plates), excellent reproducibility and suitability with analytical methods.

The overall aim is separated into three sub-aims that correspond to the three results chapters.

- Understand, develop and optimise hepatocyte growth in emulsion templated polystyrene scaffolds. This will include exploring different culture conditions and optimisations such as protein coatings and 3D media perfusion to re-create native liver tissue architecture *in vitro*.

- Compare structure, function and gene expression of hepatocytes in emulsion templated polystyrene scaffolds with those in monolayer culture and *in vivo*.

- Functionalise the surface chemistry of emulsion templated polystyrene scaffolds to improve the biochemical relevance of the materials for hepatocytes. This will include developing novel emulsion templated scaffolds that carry desirable physical characteristics whilst being easily functionalisable with appropriate biochemical residues that mimic native cell-ECM interactions.

Chapter 2: Materials and Methods

2.1 Biological Procedures

2.1.1 Cell Culture

All cells were cultured in a humidified atmosphere of 5 % CO_2 in air at 37 ^{o}C inside a Sanyo CO_2 incubator. Cells were maintained using aseptic techniques in a class II biological safety cabinet (Esco Airstream®) operating under class I procedures.

2.1.1.1 2D HepG2 Cell Culture

HepG2 cells (ATCC®, HB-8065™) with passage numbers between 4 and 30 were used for all experiments throughout this study. Cells were brought up from frozen and pre-cultured on standard T75 tissue-culture flasks (Nunc™). Minimum Essential Medium Eagle's (MEM) (Sigma, 500mL) supplemented with 50 mL fetal bovine serum (FBS) (Gibco), 5 mL of 2 mM L-Glutamine (Lonza) and 1.1 mL penicillin/streptomycin solution (100 active units each) (Gibco) was used as the thawing, seeding and culture media for all 2D and 3D HepG2 culture. Media was changed every 2-3 days. Cells were passaged at 90 % confluence into fresh T75 flasks by 5 minutes treatment with 0.25 % Trypsin-EDTA solution (Sigma).

Assessments of HepG2 structure and function were performed in 12-well plates (Greiner Bio-One) with or without circular glass coverslips at the bottom. Wells were pre-coated with either rat-tail collagen I (BD Biosciences, 534236), or bovine fibronectin (Sigma F1141). For collagen I coatings, 500 μL of a 50 μg/mL collagen I solution in 0.02M acetic acid was added to the each well/coverslip for 1 hour. For fibronectin coatings, 500 μL of a 1 mg/mL fibronectin solution in phosphate buffered saline solution (PBS) was added to each well/coverslip for 1 hour. After the 1 hour period the coating solutions were removed and the wells/coverslips washed extensively in PBS before seeding cells.

Pre-cultured HepG2 cells were extracted from T75 flasks and counted using a haemocytometer and Trypan Blue staining (Gibco). A cell suspension of 0.1 x 10^5 cells in 500 μL media was prepared. Each well/coverslip then received 500 μL of this cell suspension (1 x 10^5 viable cells) and the cells were left to adhere overnight in the incubator. Media was then made up to 4 mL and changed every 2-3 days throughout the 2D culture period.

2.1.1.2 3D HepG2 Culture

Various scaffolds were used for 3D HepG2 culture throughout the study; Alvetex®Scaffold (Reinnervate), Alvetex®Strata (Reinnervate), prototype Strata materials and the poly[26PFPA-SDE(AIBN)] material developed in Chapter 5 (see Chapter 5 for details of this material). In all

cases, 15 mm scaffold membranes were first rendered hydrophilic by treatment with 1 mL 70 % ethanol followed by extensive PBS washing.

HepG2 cells were always seeded onto scaffolds at a density of 5 x 10^5 cells in MEM. For Alvetex®Scaffold and poly[26PFPA-SDE(AIBN)], cells were seeded via 100 μL MEM per scaffold. For Alvetex®Strata and prototype Strata materials, cells were seeded via 25 μL MEM per scaffold. All scaffolds were left for 2 hours in the incubator before topping up with media. Final culture media volumes for each scaffold presentation/format (see Chapter 3 for scaffold format details) are shown in Table 2-1. As with 2D cultures, media were changed every 2-3 days.

Table 2-1 Volume of Culture Media Used for Each 3D Scaffold Presentation

Insert/ Petri-dish/ Submerged*	Insert/ 6-well plate/ submerged	Insert/ 6-well plate/ contact	Insert/ 12-well plate/ submerged	Insert/ 12-well plate/ contact	24-well plate
70 mL	8 mL	4 mL	4 mL	2 mL	1 mL

*Note that 3 scaffold inserts are housed in 1 Petri dish.

2.1.1.3 2D Upcyte® Cell Culture

Cryopreserved Upcyte® human hepatocytes (Medicyte, 422A-03-UH0-C00W-0037) were kindly donated by Dr. Nicola Hewitt at Medicyte. These cells were not pre-cultured in 2D but seeded directly onto collagen I coated 12-well plates with/without glass coverslips for structural and functional assessments. Note that the 2D collagen I coatings were prepared as described above in section 2.1.1.1.

Three separate media compositions were employed for 2D and 3D Upcyte® culture; Upcyte® Thawing Media; Upcyte® Seeding Media; Upcyte® Culture Media. Upcyte® Thawing Media was kindly donated by Medicyte (UH0-MT0-0100). Upcyte® Seeding Media consisted of Upcyte® High Performance Media (UH0-ME0-K500, 500 mL) supplemented with 10 % FBS, 5 mL Upcyte® Supplement A (20130207) and 1.1 mL penicillin/streptomycin solution (100 active units each). Upcyte® Culture Media consisted of Upcyte® High Performance Media (500 mL) supplemented with 5 mL Upcyte® Supplement A and 1.1 mL penicillin/streptomycin solution (100 active units each).

Upcyte® cells were brought up from frozen and transferred into 45 mL Upcyte® Thawing Media. Cells were then re-suspended in 10 mL Upcyte® Seeding Media and counted using a haemocytometer and Trypan Blue staining. Cells were then again re-suspended in Upcyte® Seeding Media to obtain 1 x 10^5 cells in 500 μL. 500 μL of this cell suspension (1 x 10^5 viable cells) was added to each collagen I coated well/glass coverslip and left to adhere overnight in the

incubator. The following day media was changed to 4 mL of Upcyte® Culture Media. Media was changed every 2-3 days.

2.1.1.4 3D Upcyte® Culture

Upcyte® cells were brought up from frozen and seeded directly onto ethanol-wetted scaffolds (5 x 10^5 cells in 100 μL) using Upcyte® Seeding Media. Cells were left for 2 hours in the incubator before replacing the Upcyte® Seeding Media with an appropriate volume of Upcyte® Culture Media, depending on the scaffold presentation employed (see Table 2-1). Media was changed every 2-3 days. Note that for the Upcyte® adhesion experiments involving the poly[13Aa-SDE(AIBN)] scaffold (see Chapter 5) only a small 48-well plate scaffold presentation was employed due to material restrictions. Here Upcyte® cells were seeded at 4 x 10^4 cells in 500 μL in Upcyte® Seeding Media and left to adhere for 2 hours before washing with PBS to determine cell attachment.

2.1.1.5 2D Primary Rat Hepatocyte Cell Culture

Male Sprague-Dawley pooled cryopreserved primary rat hepatocytes (Grade P) were obtained from Biopredic International (HEP134029). These cells were not pre-cultured in 2D but seeded directly onto collagen I coated 12-well plates with/without glass coverslips for structural and functional assessments. Note that the 2D collagen I coatings were prepared as described above in section 2.1.1.1.

Similar to Upcyte® culture, three separate media were employed for 2D and 3D primary rat culture; Rat Thawing Media; Rat Seeding Media; Rat Culture Media. Biopredic International kindly donated Rat Thawing Media (MIL261). Rat Seeding Media consisted of Williams E Media (GIBCO, 500 mL) supplemented with 10 % FBS, 5 mL L-glutamine, 4 μg/mL bovine insulin (Sigma) and 1.1 mL penicillin/streptomycin solution (100 active units each). Rat Culture Media consisted of Williams E Media (500 mL) supplemented with 5 mL L-glutamine, 4 μg/mL bovine insulin, 50 μM hydrocortisone (Sigma) and 1.1 mL penicillin/streptomycin solution (100 active units each).

Rat cells were brought up from frozen and transferred into 30 mL Rat Thawing Media. Cells were then re-suspended in 3 mL Rat Seeding Media and counted using a haemocytometer and Trypan Blue staining. Cells were then again re-suspended in Rat Seeding Media to obtain 1 x 10^5 cells in 500 μL. 500 μL of this cell suspension (1 x 10^5 viable cells) was added to each collagen I coated well/glass coverslip and left to adhere overnight in the incubator. The following day media was changed to 4 mL of Rat Culture Media. Media was changed every 2-3 days.

2.1.1.6 3D Primary Rat Hepatocyte Culture

Rat cells were brought up from frozen and seeded directly onto ethanol-wetted scaffolds in Rat Seeding Media; 5 x 10^5 cells in 100 μL for growth assessments with Alvetex®Scaffold and 5 x 10^5 cells in 25 μL for growth assessments with Alvetex®Strata. Cells were left for 2 hours in the incubator before replacing the Rat Seeding Media with an appropriate volume of Rat Culture Media, depending on the scaffold presentation employed (see Table 2-1). Media was changed every 2-3 days. Note that only 2 x 10^4 cells added via 100 μL was employed for the rat albumin assessments using the GAL-poly[26PFPA-SDE(AIBN)] scaffold and the corresponding control scaffolds described in Chapter 5.

2.1.2 Coating Scaffolds with Extracellular Matrix Proteins

Scaffolds were first rendered hydrophilic by treatment with 70 % ethanol followed by extensive washing in PBS. Collagen I solutions were prepared in 0.02M acetic acid. Fibronectin solutions were prepared in PBS. 200 μL of the appropriate protein solution (see Chapter 3) was added to the pre-wetted scaffolds and incubated for 1 hour at room temperature. Extensive washing in PBS was then performed. Protein deposition onto the scaffolds was checked by a 1 hour incubation in a 1 mL solution of Coomassie Brilliant Blue G-245 (BioRad). Scaffolds were then de-stained in a solution of 15 % methanol and 10 % acetic acid and photographed for residual blue dye uptake.

2.1.3 Media Perfusion Using the Reinnervate Perfusion Plate

2.1.3.1 Materials

Table 2-2 shows the required materials for media perfusion with the Reinnervate Perfusion Plate.

Table 2-2 Materials Required for the Set-Up of the Reinnervate Perfusion Plate

Item	Supplier	Details/Product Code
Reinnervate Perfusion Plate	Reinnervate	N/A
Multi-channel cassette pump	Watson Marlow	Multichannel Cassette 205S/CA. Product code: 020.3704.00A
Silicone tubing	Sigma	T1664-25FT (1.6 mm ID)
Larger silicone tubing	Sigma	T1914-25FT (2.4 mm ID)
Luer locks	Value Plastics	MTLL004-6005 (for 1.6 mm ID tubing)
Larger luer locks	Value Plastics	MTLL007-1 (for 2.4 mm ID tubing)
Tube-to-tube connectors	Value Plastics	AA-J1A (1.6 mm)
Larger tube-to-tube connectors	Value Plastics	DD-1 (for 2.4 mm ID tubing)
0.22 μm sterile filter	Millipore	SLGP033RS
6-well plates (for lids)	Greiner Bio-One	657160
Empty 1 mL pipette tip box	Starlab	Empty (racked) 1 mL tip box

The Reinnervate Perfusion Plate is shown in Figure 2.1. The plate is based on a modified conventional 6-well plate format. It consists of an in-port, out-port, two levelling/sampling reservoirs and four interconnected wells/chambers (Figure 2.1A). Each plate therefore has the capacity to house up to four scaffold inserts, one in each chamber. Luer locks and silicone tubing are attached to the ports to transfer media in and out of the plate (Figure 2.1B). Media is pumped from a bottle to the in-port, levels in the levelling reservoir and then circulates around the four chambers. Media is then pumped out from the out-port back to the media bottle. 1.6 mm internal diameter (ID) tubing luer locks and silicone tubing are used for media entering the plate. 2.4 mm ID tubing luer locks and silicone tubing are used for media leaving the plate. The larger tubing on the out-port helps to prevent media build-up within the plate. A standard 6-well plate lid is used as the lid (Figure 2.1C). Complete media circulation therefore requires two pump heads per plate; one pumping media into the plate and the other pumping media out of the plate.

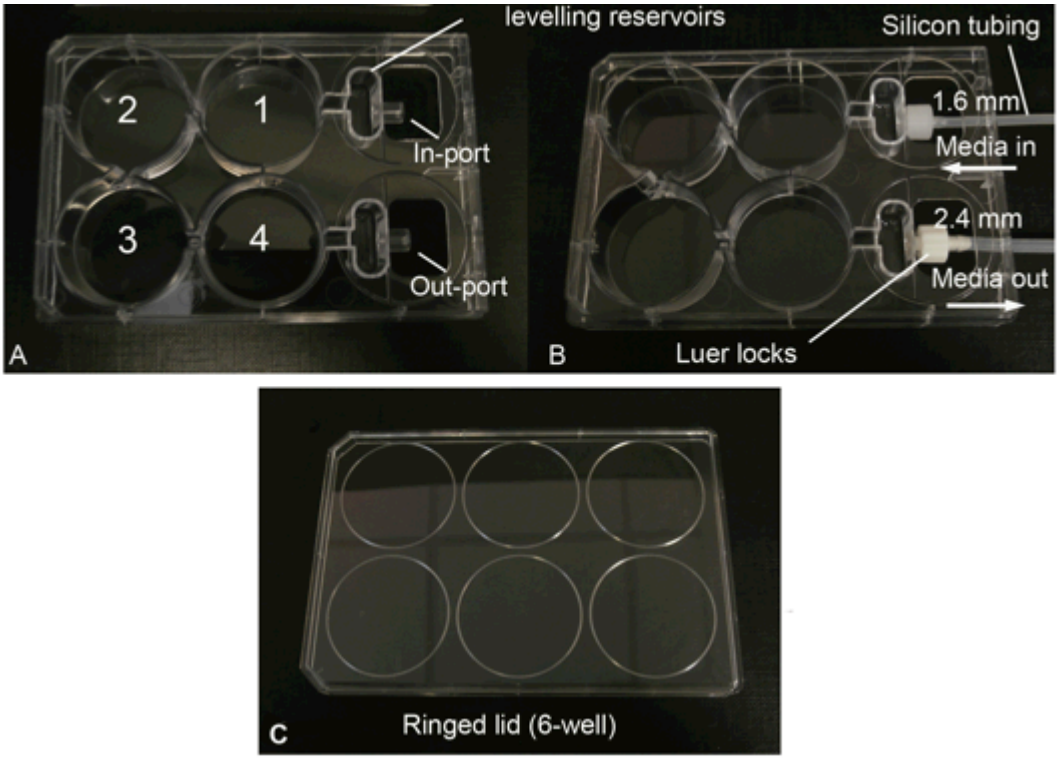

Figure 2.1 Photographs of the Reinnervate Perfusion Plate. (A): Plate design based on a modified 6-well plate format but with an in-port, out-port and media levelling reservoirs. (B): Luer locks and silicone tubing are attached to the ports to transfer media. 1.6 mm internal diameter (ID) tubing and luer locks are applied for media entering the plate but 2.4 mm ID tubing and luer locks are used for media leaving the plate. (C): A standard 6-well plate lid with rings is employed.

A Watson-Marlow Multichannel Cassette Pump (205S/CA) with 4 pump-head channels was used to pump media to and from the Reinnervate Perfusion Plate (Figure 2.2A). Four pump-head channels therefore allowed for two media circuits simultaneously (i.e. two Reinnervate Perfusion Plates). For each pump channel, silicone tubing connecting the media bottle and plate was placed over the pump rollers (Figure 2.2B). A pump channel cassette was used to clamp the tubing in place. The rolling action of the pump over the silicone tubing created the desired pumping. **IMPORTANT**: The pump rolling action sometimes caused the silicone tubing to be pulled in the direction the rollers were moving, creating unwanted tension and/or tubing slippage. It was then important to place a tube-to-tube straight connector in the tubing (i.e. creating a joint) just before the tubing entered the pump so that slippage was prevented.

Media flow was altered via the pump rotations-per-minute (RPM) button on the pump keypad. RPM was set to 2 and the media direction clockwise (CW). This ensured a media flow rate of 200 μL/min.

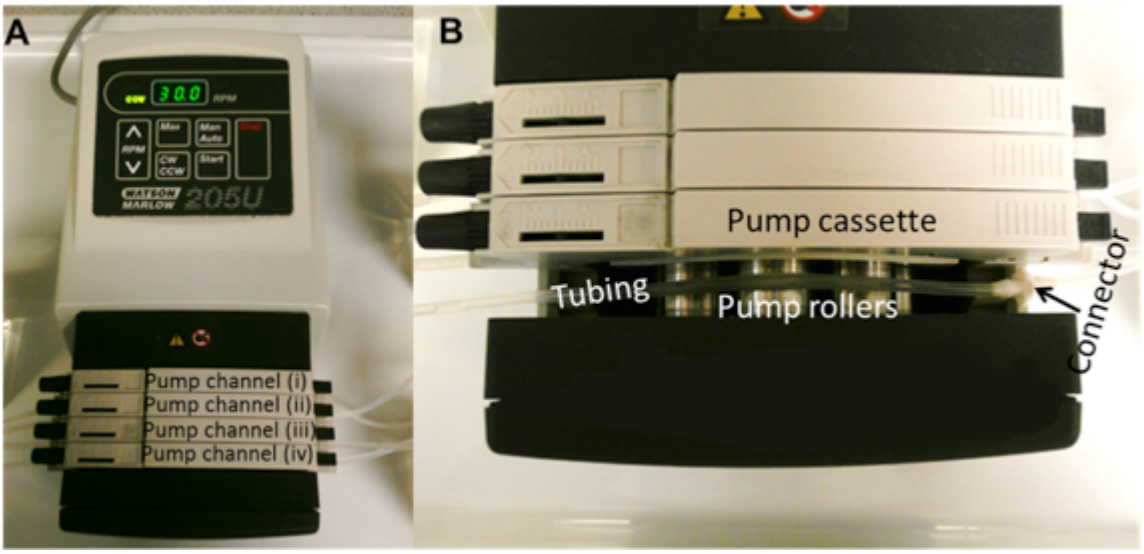

Figure 2.2 A Watson Marlow multi-channel cassette pump used for pumping media to and from the Reinnervate Perfusion Plate (pump model 205S/CA). (A): The pump has 4 channels and therefore allowed 2 media circuits (2 Reinnervate Perfusion Plates simultaneously). (B): Tubing was placed over the pump rollers and a pump channel cassette was used to secure it in place. Note that a joint in the tubing was made with a tube-to-tube straight connector to prevent tubing slipping whilst the rollers were moving.

The media reservoir was housed in a 125 mL bottle. Three small holes (ca. 1 mm diameter) were drilled into the plastic cap of the media bottle (Figure 2.3). One hole was used for silicone tubing transferring media to the plate. Another hole was used for silicone tubing transferring media from the plate. A third hole was used as an air vent, with tubing connected to a 0.22 µm sterile filter to prevent bottle deformation under pressure changes.

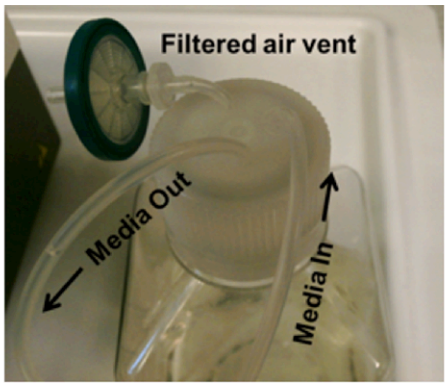

Figure 2.3 Photograph of the cap of the media bottle used as the media reservoir for the perfusion set-up. Three holes were drilled into the cap; One for media in; One for Media Out; One for an air vent.

Figure 2.4 shows the final perfusion set-up for a single circuit. All equipment was assembled on top of an incubator shelf to allow easy access to and from the incubator. Plates were placed on

top of an upside-down empty pipette tip box so that the tubing height remained approximately level with the pump-head channels. IMPORTANT: As the pump rollers are uni-directional it means that each pump head pumps media in the same direction. In order to ensure that media was pumped to the plate and then back out in the opposite direction, the media-in tubing had to be looped around the pump to ensure media always travelled in the correct direction. This tubing carrying media in to the plate was approximately 60 cm in length. The tubing carrying media out from plate was approximately 35 cm in length. This ensured that media in tubing had the furthest distance to travel and thus avoided issues with media building up within the plate.

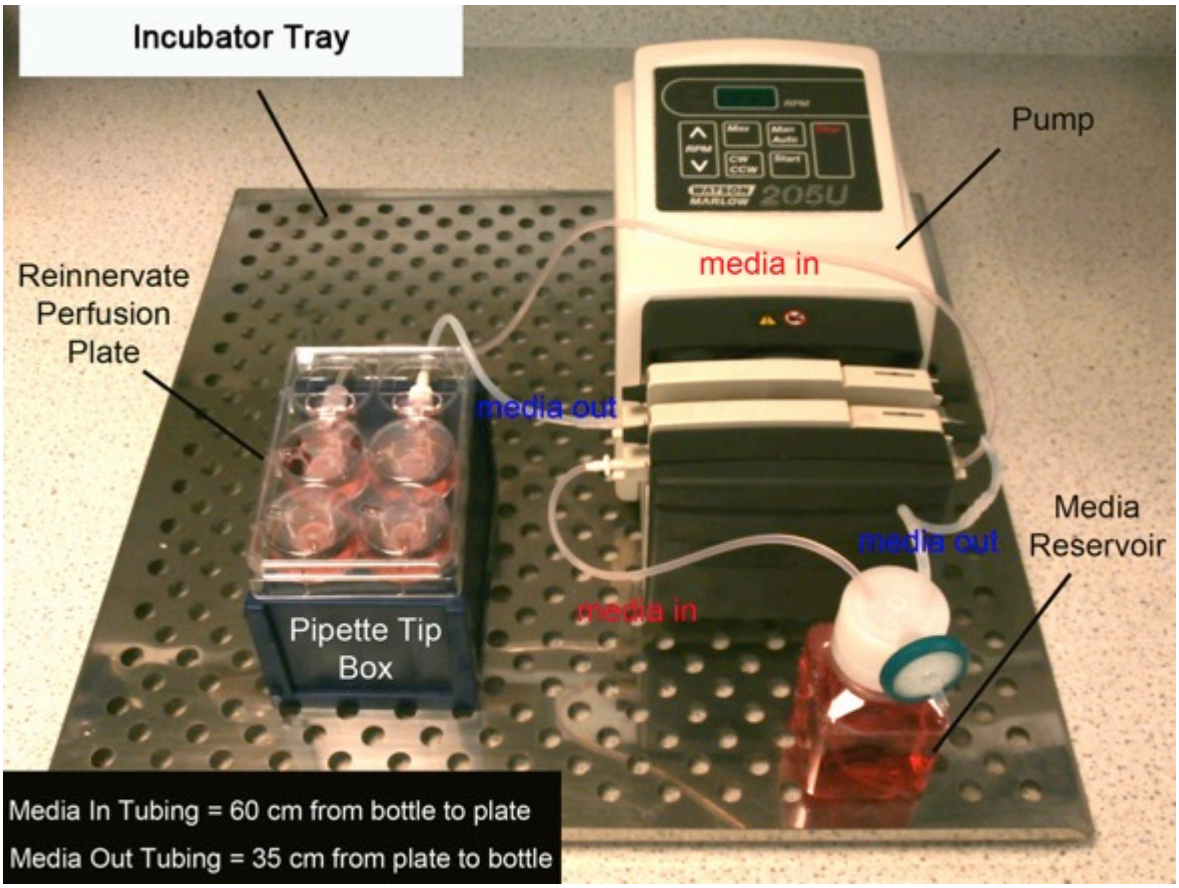

Figure 2.4 Final set-up for 3D media perfusion using the Reinnervate Perfusion Plate. Example is a circuit for a single plate. All equipment was assembled on an incubator tray. The plate was raised on top of an upside-down empty pipette tip box. Tubing carrying media in looped across the pump (total 60 cm in length) to ensure a correct uni-directional flow of media.

2.1.3.2 Method for Perfusion with the Reinnervate Perfusion Plate

Scaffolds in inserts in 6-well plates (see Chapter 3) were ethanol wetted and washed extensively in PBS. Hepatocytes were seeded at 5 x 10^4 in 100 μL seeding media and left for 2 hours in the incubator. Seeding media was then made to 8 mL and the scaffolds left overnight in the 6-well plates for cultures to establish (static media conditions). Scaffold inserts were then placed in the

Reinnervate Perfusion Plate. 130 mL of culture media was added to the media bottle and the media perfusion was applied (200 μL/min). Experiments were performed for up to 7 days without changing the media. Static cultures involving scaffolds in inserts in 12-well plates (4 mL media) were used as controls with the media changed every 2 days.

2.1.4 Histology

2.1.4.1 Haematoxylin and Eosin (H&E) Staining of Scaffolds

Haematoxylin stains cell nuclei purple and Eosin stains the cytoplasm pink. After the desired cell culture period, scaffolds were removed from inserts and/or plates (see Chapter 3) and gently dipped in PBS before transferring into a fresh 12-well plate. Cells on the scaffolds were then fixed by treatment with 2 mL of either Bouin's fixative or 4 % paraformaldehyde overnight at 4 ^{o}C. Scaffolds were then washed 3 x 5 minutes in PBS with gentle agitation. Scaffolds were then slowly dehydrated through a series of ethanol gradients (15 minutes each); 30 %, 50 %, 70 %, 80 %, 90 %, 95 % and 100 %. Scaffold discs were then cut into 2 halves (to produce two semi-circles) and then carefully placed into a 10 mL glass vial containing 5 mL Histo-Clear (National Diagnostics). Scaffolds were left for 15 minutes in Histo-Clear before an additional 5 mL of melted paraffin wax was added using a Leica EG1120 wax dispenser (to create a 50:50 mixture of Histo-Clear to paraffin wax). Scaffolds were incubated in this mixture for 30 minutes in a 60 ^{o}C oven. Following that the mixture was replaced with 10 mL paraffin wax. Scaffolds were then incubated in the wax for 1 hour at 60 ^{o}C. After this time the scaffold semi-circles were embedded vertically in an embedding cassette (Simport, Histosette I) and plastic mould (CellPath, Dispomould) and left to set overnight.

Sectioning of wax blocks into a hot water bath was performed using a Leica RM2125RT Microtome. 10 μm sections were employed for all H&E staining with HepG2 cells, Upcyte® cells and primary rat hepatocytes. The sections were then mounted on glass slides and left to dry overnight. The H&E staining protocol involved de-waxing the slides in Histoclear for 5 minutes then hydrating through 100 % ethanol (2 minutes), 95 % ethanol (1 minute), 70 % ethanol (1 minute) and distilled H_2O (1 minute). Nuclei were stained using Mayer's Haematoxylin (Sigma) for 5 minutes prior to being washed in distilled H_2O for 30 seconds. Nuclei were blued in alkaline ethanol (30 mL ammonia in 970 mL 70 % ethanol) for 30 seconds. Slides were dehydrated through 70 % and 95 % ethanol for 30 seconds each and the cytoplasm was stained pink using Eosin Y (5 g in 1 L of 70 % ethanol) for 45 seconds. Sections were quickly dipped in 95 % ethanol and then twice in 100 % ethanol before clearing in Histo-Clear. Slides were mounted in DPX mountant and cover-slipped.

2.1.4.2 H&E Staining of Human Liver Tissue

Commercial pre-sectioned (5 μm), paraffin embedded histological slides of human liver tissue were obtained from abcam (ab4348). These were H&E stained following the H&E staining protocol described above.

2.1.4.3 H&E Staining of 2D Cultures

Although not strictly a histology process, cells cultured on collagen I coated 12-well plates were processed for H&E staining to provide a direct comparison with scaffold and *in vivo* histology images. Samples were fixed in 4 % paraformaldehyde for 1 hour and washed excessively in PBS. Nuclei were stained using Mayer's Haematoxylin for 5 minutes prior to being washed in distilled H_2O for 30 seconds. Nuclei were blued in alkaline ethanol (30 mL ammonia in 970 mL 70 % ethanol) for 30 seconds. Samples were then dehydrated through 70 % and 95 % ethanol for 30 seconds each and the cytoplasm was stained pink using Eosin Y (5 g in 1 L of 70 % ethanol) for 45 seconds. Samples were quickly dipped in 95 % ethanol and then twice in 100 % ethanol and then imaged directly.

2.1.4.4 Toluidine Blue Staining

Resin-embedded 1 μm sections prepared from transmission electron microscopy (TEM) processing (see section 2.1.5.1) were placed on a glass slide and dried on a hotplate. Slides were then dipped in a Toluidine Blue O (Sigma) staining solution for 30 seconds and rinsed extensively in distilled water. Slides were mounted in DPX mountant and cover-slipped.

2.1.5 Imaging

2.1.5.1 Transmission Electron Microscopy (TEM)

Cell culture samples were first fixed in a fixative solution of 0.1 M sodium cacodylate buffer containing 4 % paraformaldehyde and 5 % glutaldehyde for 1 hour. Mouse liver samples were kindly donated by Eleanor Knight at Durham University and were obtained from adult male nude (nu/nu) mice in accordance with guidelines and permission granted by the Home Office, UK. Liver tissue was immediately cut into small pieces (ca. 1 mm^3) after surgical extraction and fixed in 4 % paraformaldehyde overnight at 4 ^{o}C. All fixed samples (cell culture and liver tissue) were then washed in 0.1 M sodium cacodylate buffer before being treated with 1 % osmium tetroxide for 1 hour. Samples were again washed in 0.1 M sodium cacodylate buffer and then slowly dehydrated through a series of ethanol gradients (3 x 5 minutes each); 50 %, 70 %, 95 % and 100 %. Samples were then infiltrated with mixtures of ethanol: LR white (Agar Scientific, Medium grade) for 30

minutes each; 2:1, 1:1, 1:2. Samples were then left in resin overnight before being embedded into polypropylene capsules (Agar Scientific). Capsules were then placed in a 37 ^{o}C oven overnight to set. For 2D cultures, the glass coverslips were embedded horizontally on top of the capsule. Once set, the coverslip was removed from the capsule by exposure to liquid nitrogen vapour, leaving the 2D cells behind in the resin. Resins were removed from the capsules and then sectioned using a Leica Reichert Ultracut S microtome using a glass knife and water boat. 1 μm sections were taken for Toluidine Blue staining. Sections of ca. 50 – 80 nm were placed onto copper grids (150 mesh) and stained with 1 % uranyl acetate followed by lead citrate (10 minutes each with excessive water washing in between). Samples were imaged using a Hitachi H-7600 TEM. Images were processed using Adobe Photoshop CS5.

2.1.5.2 Scanning Electron Microscopy (SEM) for Biological Analysis

Samples were first fixed in a fixative solution of 0.1 M sodium cacodylate buffer containing 4 % paraformaldehyde and 5 % glutaldehyde for 1 hour. Samples were then washed in 0.1 M sodium cacodylate buffer before being treated with 1 % osmium tetroxide for 1 hour. Samples were again washed in 0.1 M sodium cacodylate buffer and then slowly dehydrated through a series of ethanol gradients (3 x 5 minutes each); 50 %, 70 %, 95 % and 100 %. Samples were then passed through a critical point dryer (Bal-tec CPD 030) to dry the samples. Two SEM machines were used for biological analysis; Hitachi S-5200 and Phillips XL30 ESEM. For the Hitachi, samples were first mounted on silicon wafer chips using double sided sticky tape and then platinum coated using a Cressington 328 coating system before imaging. Images were taken at 10 kV. For the Phillips XL30 ESEM, samples were first mounted on carbon fibre pads pre-adhered to aluminium stubs and then gold coated using an Edwards Pirani 501 sputter coater before imaging. Images were taken between 10 kV and 30 kV. Images were processed using Adobe Photoshop CS5.

2.1.5.3 Bright-field Light Microscopy

Histology slides and 2D cell cultures were imaged using a Leica DM500 light microscope. Images were processed using Adobe Photoshop CS5. All images were processed in the exactly the same manner. Image brightness was enhanced +15 and image contrast was enhanced +50. Cell diameters in the XY plane were obtained from light microscopy images using ImageJ™ analysis as a digital measuring tool.

2.1.5.4 Confocal Immunofluorescence

Samples were first fixed in 4 % paraformaldehyde overnight at 4 ^{o}C. Samples were then washed extensively in PBS and then permeabilised by treatment with 0.1 % Triton X-100 solution for 15

minutes. Note that Ki-67 immunofluorescence (see Chapter 3) was performed on wax-embedded samples that had to be first de-paraffinised and heat-treated in citrate buffer before permeabilisation. Samples were then exposed to a blocking buffer of 1 % normal goat serum and 0.1 % Tween 20 in PBS for 30 minutes. Samples were then exposed to the specific primary antibody overnight at 4 ^{o}C (see Table 2-3). A control (no primary antibody) was included alongside each primary antibody.

Table 2-3 Primary and Secondary Antibodies used in Confocal Immunofluorescence

Antibody	Supplier	Description	Code	Dilution (in blocking buffer)
ZO1	Life Technologies	Rabbit Polyclonal	402200	1 in 100
MDR1	abcam	Mouse Monoclonal	ab3366	1 in 100
MRP2	abcam	Mouse Monoclonal	ab3373	1 in 100
Phalloidin	Cytoskeleton Inc.	Acti-Stain Fluorescent 488	PHDG1	1 in 143*
Ki-67	Leica	Mouse Monoclonal	NCL-L-Ki67-MM1	1 in 100
Fibronectin	Sigma	Mouse Monoclonal	F7387	1 in 300
Collagen I	Sigma	Mouse Monoclonal	C2456	1 in 2000
2^{o} Mouse	Life Technologies	Alexa Fluor 488 Goat Anti-Mouse IgG	A-11001	1 in 600
2^{o} Rabbit	Life Technologies	Alexa Fluor 488 Goat Anti-Rabbit IgG	A-11008	1 in 600

*Dilution of a 14 µM Phalloidin stock solution in blocking buffer.

Samples were then washed extensively in blocking buffer. Samples were then incubated in the dark for 1 hour with secondary antibody at a dilution of 1:600 in blocking buffer. DAPI (Hoechst 33342) was also included at 1:1000 as a nuclei counterstain. Note that Phalloidin was supplied pre-coupled to a green fluorescent dye (proprietary to Cytoskeleton Inc.) and so there was no need for incubation with a secondary antibody. Samples were then washed extensively in blocking buffer and then mounted in Vectashield (VectorLabs). Coverslips were sealed with nail varnish and samples imaged with 2 days. A Zeiss Axiovert 200M confocal microscope was used for imaging. Images were processed using Adobe Photoshop CS5.

2.1.6 Functional Assays

2.1.6.1 MTT Metabolic Assay

The MTT assay exposes cells to Thiazolyl Blue Tetrazolium Bromide (MTT, Sigma) to which they metabolise and convert into an insoluble blue formazan product. The amount of formazan produced is therefore a simple indicator of a population's total metabolic activity. An MTT

solution of 1 mg/mL in phenol-red free Dulbecco's Modified Eagle's Medium (DMEM, Sigma) was prepared. This was then passed through a 0.22 μm sterile filter and warmed to 37 ^{o}C. Scaffolds were removed from inserts/plates and transferred into a fresh 12-well plate. 2D cultures were analysed directly in the welled plate. A short PBS wash of the cell cultures was applied to remove residual culture media. 1 mL of the MTT solution was added to each well and then the plates were incubated for 1 hour in the dark in an incubator. After this period, the excess MTT reagent was aspirated from the wells and 1 mL of acidified isopropyl alcohol (IPA) was added to dissolve the blue formazan product (1 μL hydrochloric acid in 1 mL IPA). 200 μL aliquots of the blue IPA solutions were then transferred into a 96-well plate and the absorbance measured at 570 nm using a BioTek ELx800 plate reader.

2.1.6.2 Albumin Assay

Secreted albumin present in the culture media was assessed using a commercial enzyme-linked immunosorbent assay (ELISA). Primary rat culture media samples were assessed using a rat ELISA (AssayPro, ERA3201-1). Human HepG2 culture media samples were assessed using a human ELISA (AssayPro, EA3201-1). The exact manufacturers protocol was followed. In brief, aliquots of the media samples were taken and diluted in the assay diluent as per the protocol recommendations. Albumin standards were prepared in parallel using known rat or human albumin concentrations. Samples and standards were then transferred into immunosorbent plate and incubated in the assay reagents. Plates were then read at 450 nm using a BioTek ELx800 plate reader. A standard curve was used to correlate absorbance with albumin quantity in culture samples.

2.1.6.3 Urea Assay

Secreted urea present in the culture media was assessed using commercial colorimetric urea assay (BioAssay Systems, DIUR-500). The exact manufacturers protocol was followed. In brief, aliquots of the media samples were taken and diluted in the assay diluent as per the protocol recommendations. Urea standards were prepared in parallel using known urea concentrations. Samples and standards were then transferred into a 96-well plate and incubated with the assay reagent for 40 minutes. Plates were then read at 540 nm using a BioTek ELx800 plate reader. A standard curve was used to correlate absorbance with urea quantity in culture samples.

2.1.6.4 Quant-iT™ PicoGreen®

A commercial Quant-iT™ PicoGreen® assay (Life Technologies, P7589) was used to quantify double-stranded DNA (dsDNA) in the hepatocyte cultures and thus provide an indication of cell number. Cultures were first treated with a standard lysis buffer. Lysate solutions and scaffolds

were then transferred into an eppendorf tube and homogenised with a 20-gauge needle. Scaffold cultures were also subject to additional vortexing and centrifugation steps to ensure all cellular material was extracted from the scaffold into the lysate. Note that standards of known HepG2 cell numbers (from haemocytometer counting) were lysed and homogenised alongside the culture samples. Aliquots of the lysates were then incubated with the Quant-iT™ PicoGreen® reagent as per the assay protocol. The fluorescence intensity was measured at 540 nm was measured using a BioTek Synergy H4 plate reader (excitation at 460 nm). A standard curve was used to correlate fluorescence intensity with cell/DNA number in culture samples.

2.1.6.5 Flow Cytometry

The commercial Guava Nexin® assay (Millipore 4500-0450) was used for flow cytometric analysis of hepatocytes. Cells on scaffolds were extracted by 15 minutes treatment in Trypsin-EDTA solution followed by gentle scraping with a cell scraper. The cells were then re-suspended in fresh culture media and then treated with the Guava Nexin® reagent as per the assay protocol. A Guava EasyCyte™ Plus flow cytometer was used for the experiment. Data was analysed using Cytosoft flow cytometric analysis software (Millipore). Thresholds for hepatocyte apoptosis were set using a control apoptotic population pre-treated with 2 μM staurosporine (Sigma). Thresholds for hepatocyte necrosis were set using a control necrotic population pre-exposed to heat treatment (58 ^{o}C for 20 minutes).

2.1.6.6 Glucose Measurements

Media glucose was measured directly from the culture media sample using the GlucCell™ glucose monitoring system (CESCO BioProducts)[160]. Cultures were first gently swirled to distribute the media and then a 50 μL aliquot was taken and vortexed. A fresh glucose test strip was inserted into the GlucCell™ meter. A 2 μL sample of the 50 μL media aliquot was then gently loaded into the side of the test strip as per the manufacturer protocol. Glucose concentrations displayed on the GlucCell™ meter were then recorded. Fresh media pre-warmed to 37 ^{o}C were also analysed to provide a benchmark for initial glucose concentration.

2.1.6.7 Bio-Rad® Assay for Protein Quantification

The Bio-Rad® Protein Assay Dye (Bio-Rad, 500-0006) was used to determine total protein content in cell cultures. Cultures were first treated with a standard lysis buffer. Lysate solutions and scaffolds were then transferred into an eppendorf tube and homogenised with a 20-gauge needle. Scaffold cultures were also subject to additional vortexing and centrifugation steps to ensure all cellular material was extracted from the scaffold into the lysate. Lysates were then

centrifuged at 10,000 rpm and then heated on a heating block at 95 ^{o}C for 3 minutes. Standards of known concentrations of bovine serum albumin (Sigma) were then prepared. Samples and standards were then incubated in Bio-Rad® Protein Assay Dye and the absorbance measured at 600 nm using a BioTek ELx800 plate reader. A standard curve was used to correlate absorbance with protein quantity in culture samples

2.1.6.8 Drug Exposure Studies

Acetaminophen (APAP, Sigma) and Gemfibrozil (Sigma) were pre-dissolved in culture media without using DMSO. Rifampicin (Sigma) was pre-dissolved in pure Dimethyl Sulfoxide (DMSO, Sigma) and then added to culture media to produce a final concentration of 20 μM rifampicin. A DMSO control was therefore used in conjunction with all rifampicin studies.

2.1.6.9 CYP3A4 Activity

The testosterone assay was used to determine CYP3A4 activity by exposing hepatocytes to testosterone and then measuring the metabolite 6-β-OH-testosterone by high performance liquid chromatography analysis (HPLC). Scaffolds were removed from inserts and placed in a fresh 12-well plate. Samples were then washed in PBS supplemented with 1 mM $CaCl_2$. Samples were then incubated in PBS supplemented with 1 mM $CaCl_2$ and 250 μM testosterone (Sigma) for 1 hour in an incubator. The supernatants were then transferred into an eppendorf tube and sent to Medicyte for HPLC analysis. A standard curve using known 6-β-OH-testosterone concentrations was used to correlate HPLC peak-area-ratio with CYP3A4 activity in cell culture samples.

2.1.7 Real Time Quantitative Polymerase Chain Reaction

Cells cultured on 2D and on scaffolds were first treated with RLT Lysis Buffer (Qiagen) and then homogenised using a 20-gauge needle and 1 mL syringe. A commercial RNA spin-column extraction kit and procedure was then followed to isolate the RNA (Qiagen, RNeasy® Mini Kit, 74106). DNAse digestion using a commercial DNAse digestion kit (Qiagen, DNAse set, 79254) was performed as part of this RNA isolation. Quantity and quality of isolated RNA was checked using a Nanodrop Spectrophotometer (NanoDrop® ND-1000). Reverse transcription using a commercial complementary DNA (cDNA) reverse transcription kit (Applied Biosystems, 4368814) and a thermal cycler (Biometra) was then performed to convert RNA into cDNA. All cDNA was then stored at -20 ^{o}C in preparation for analysis.

TaqMan® gene expression assays were used in all real time quantitative polymerase chain reaction (RT-PCR) analysis. Table 2-4 shows the different genes that were assessed. All gene

expression assays were quantified against the housekeeping GAPDH gene. Experiments were performed on an Applied Biosystems 7500 Fast RT-PCR machine and analysed using the 7500 Fast System software.

Table 2-4 TaqMan® Gene Expression Assays used in RT-PCR Analysis

Gene	Supplier	Code
CYP1A2	Life Technologies	Hs00167927_m1
CYP2E1	Life Technologies	Hs00559368_m1
CYP3A4	Life Technologies	Hs00604506_m1
GSTP1	Life Technologies	Hs02512067_s1
UGT1A1	Life Technologies	Hs02511055_s1
ABCB1	Life Technologies	Hs00184500_m1
ABCC2	Life Technologies	Hs00166123_m1
GAPDH (reference gene)	Applied Biosystems	4352934-1001030

2.2 Procedures For Materials Chemistry

For simplification reasons, all chemical sources/suppliers are noted in brackets in the text.

2.2.1 Synthesis of Galactose-Functionalised Emulsion Templated Polystyrene Scaffolds

This study employed a two-step strategy towards the fabrication of galactose-functionalised emulsion templated polystyrene scaffolds. The first step involved the incorporation of ester or acid functionality into the scaffold surface. This was achieved via the addition of a new functional co-monomer (ester-containing or acid-containing) into the pre-polymerised HIPE. The second step then involved a post-polymerisation modification reaction to attach galactose onto the new functional scaffold.

2.2.1.1 General Procedure for Synthesising Emulsion-Templated Polystyrene Scaffolds

The preparation of emulsion-templated polystyrene scaffolds for 3D cell culture applications has already been well documented[143, 152, 153]. Briefly, an oil phase consisting of the monomers styrene (60 wt.% of total monomers) (STY, Sigma), divinylbenzene (10 wt.% of total monomers) (DVB, Sigma, Technical Grade 80%), 2-ethylhexyl acrylate (30 wt.% of total monomers) (EHA, Sigma) and the surfactant Span80™ (Sigma) were placed in a 250 mL 3-necked round bottom flask and stirred continually at 350 rpm using a PTFE paddle connected to an overhead stirrer. To this organic phase, deionised water containing 1 % potassium persulfate (KPS, Sigma) was slowly added at room temperature via a dropping funnel. Stirring continued for an additional 2 minutes after the last water droplet to form a HIPE. The HIPE was then transferred into a 50 mL Falcon Tube and placed in a 60 ^{o}C oven for 24 hours to thermally polymerise. After this period, the polymers (polyHIPEs) were removed from the falcon tube and washed in acetone for 24 hours using soxhlet recirculation. The materials were then left to air dry overnight in a fume hood.

2.2.1.2 Synthesis of Pentafluorophenyl Acrylate (PFPA)

Pentafluorophenyl acrylate (PFPA) was kindly donated by Dr. Ahmed Eissa at Durham University. Figure 2.5 shows the reaction scheme he used for the synthesis.

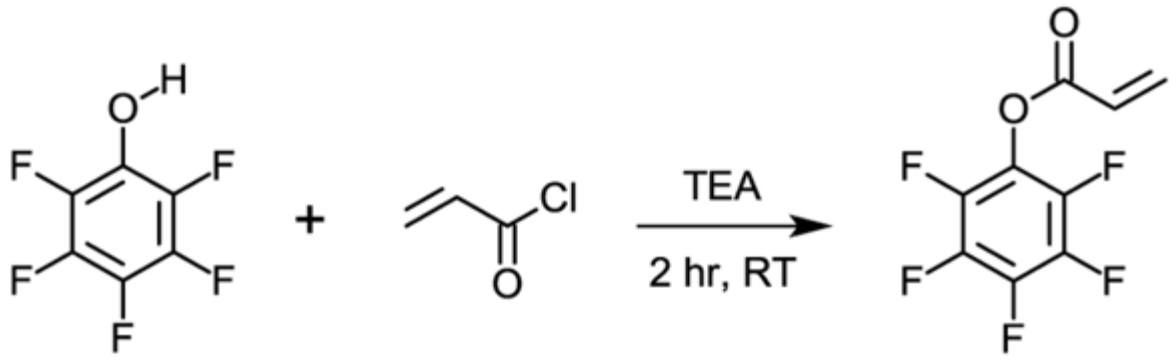

Figure 2.5 Reaction scheme for the synthesis of PFPA from pentafluorophenol.

In a two-neck round bottomed flask, 1 g (5.43 mmol) of pentafluorophenol (Sigma) and 0.66 g (6.52 mmol) of triethylamine (TEA) (Sigma) were dissolved in 10 mL of dry diethyl ether, and 0.59 g (6.52 mmol) of acryloyl chloride (Sigma) was added drop-wise through a funnel under cooling with an ice bath. After stirring for an additional 2 h at ambient temperature, the precipitated salt was removed by filtration. After evaporation of the solvent, the residue was filtered again and purified with column chromatography (column material: silica gel; solvent: petroleum ether).
0.8 g (74 %) of a colourless liquid was obtained. The pure PFPA was stored at -7 °C.
Characterisation data of the PFPA are shown in Figure 2.6, Figure 2.7 and Figure 2.8.

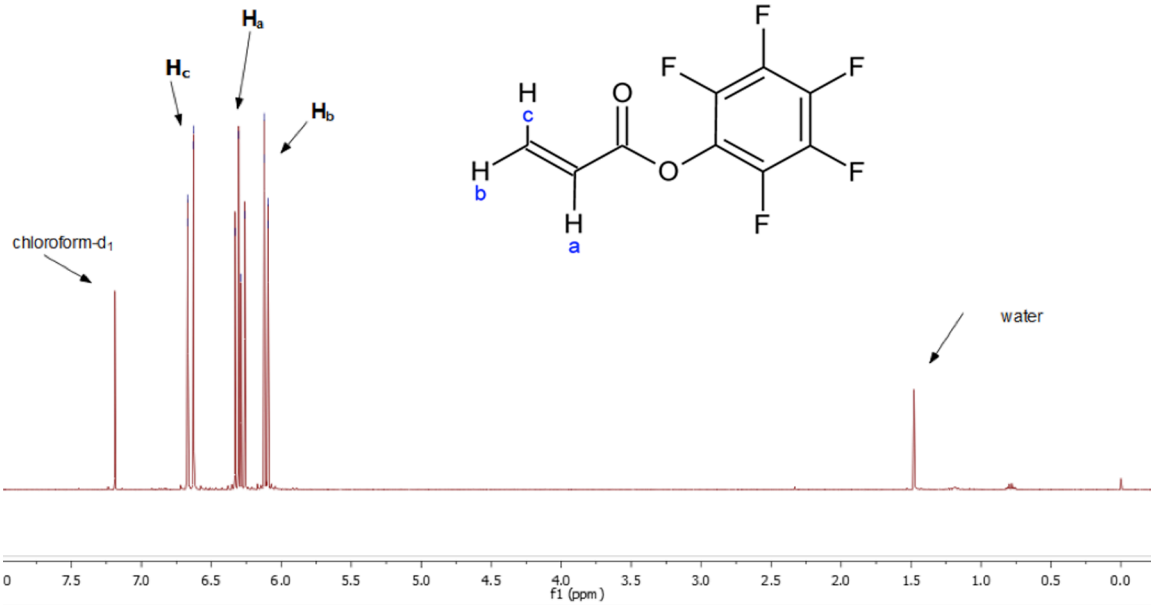

Figure 2.6 ^{1}H NMR spectrum of PFPA. The molecular structure is shown to aid with peak assignments.

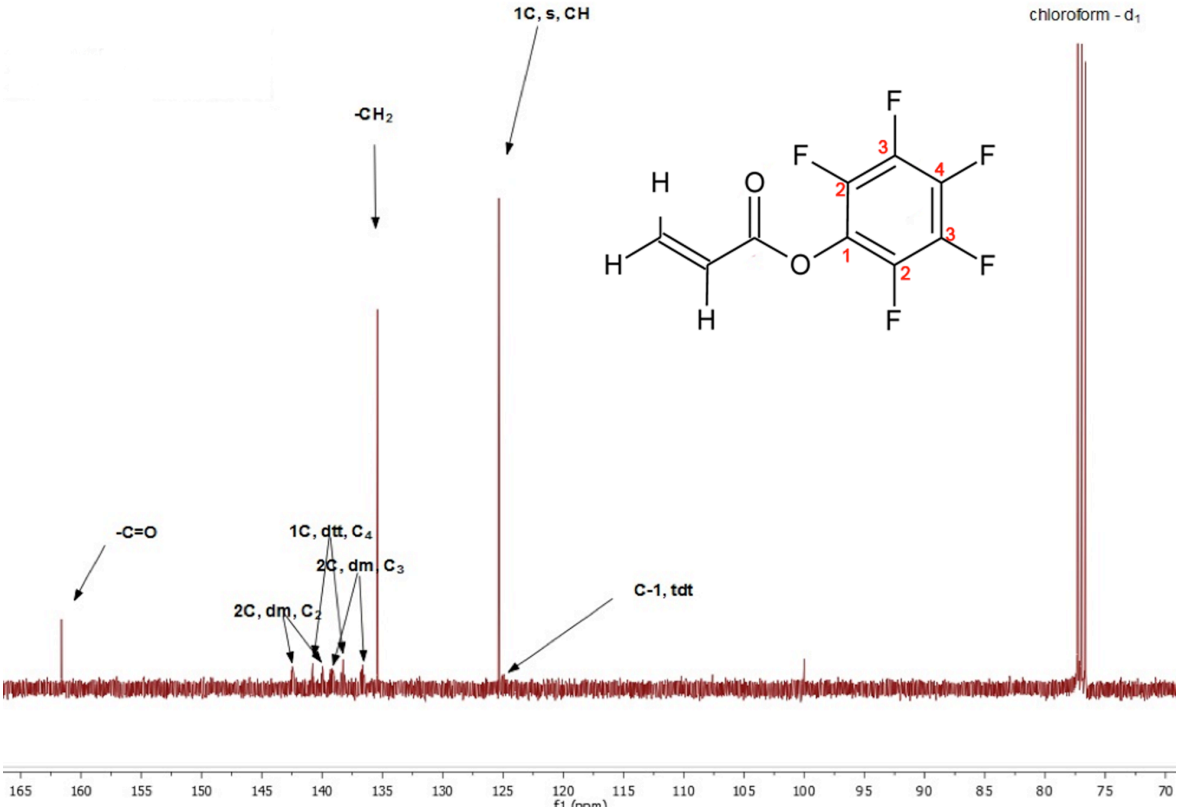

Figure 2.7 ^{13}C NMR spectrum of PFPA. The molecular structure is shown to aid with peak assignments.

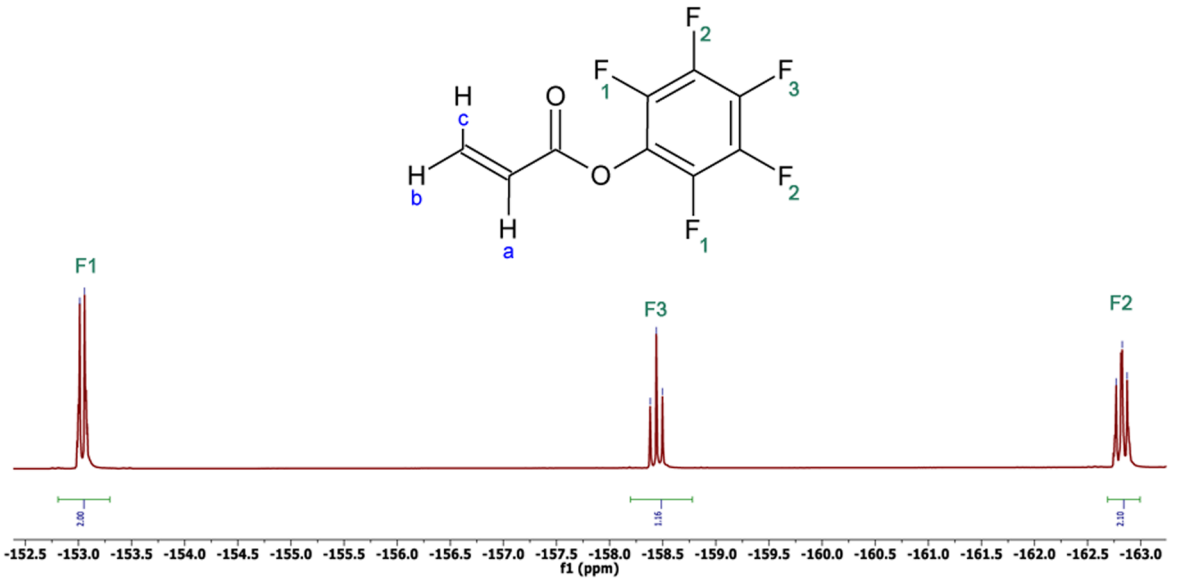

Figure 2.8 ^{19}F NMR spectrum of PFPA. The molecular structure is shown to aid with peak assignments.

2.2.1.3 Preparation of Ester-Containing Polystyrene Scaffolds

The exact procedure described in section 2.2.1.1 was followed, but with two exceptions. Firstly, PFPA was included as an additional functional (ester-containing) co-monomer and was added to the monomeric oil phase prior to water addition. Secondly, KPS was absent from the water phase and 0.3 wt.% (of total emulsion) azobisisobutyronitrile (AIBN, Acros Organics) was dissolved in the oil phase prior to water addition. AIBN was first recrystallized from methanol before use.

2.2.1.4 Preparation of Acid-Containing Polystyrene Scaffolds

The exact procedure described in section 2.2.1.1 was followed, but with two exceptions. Firstly, acrylic acid (Aa, Sigma) was included as an additional functional (acid-containing) co-monomer and was added to the aqueous phase prior to HIPE formation. Secondly is that some formulations were polymerised with AIBN as the polymerisation initiator rather than KPS.

2.2.1.5 Synthesis of Aminoethyl Glycosides

2'-aminoethyl-β-D-galactopyranoside and 2'-aminoethyl-β-D-glucopyranoside were kindly donated by Dr. Ahmed Eissa at Durham University. The synthetic route to obtaining these materials is shown in Figure 2.9. Note this example is for 2'-aminoethyl-β-D-glucopyranoside, but the same principles apply for the synthesis of 2'-aminoethyl-β-D-galactopyranoside.

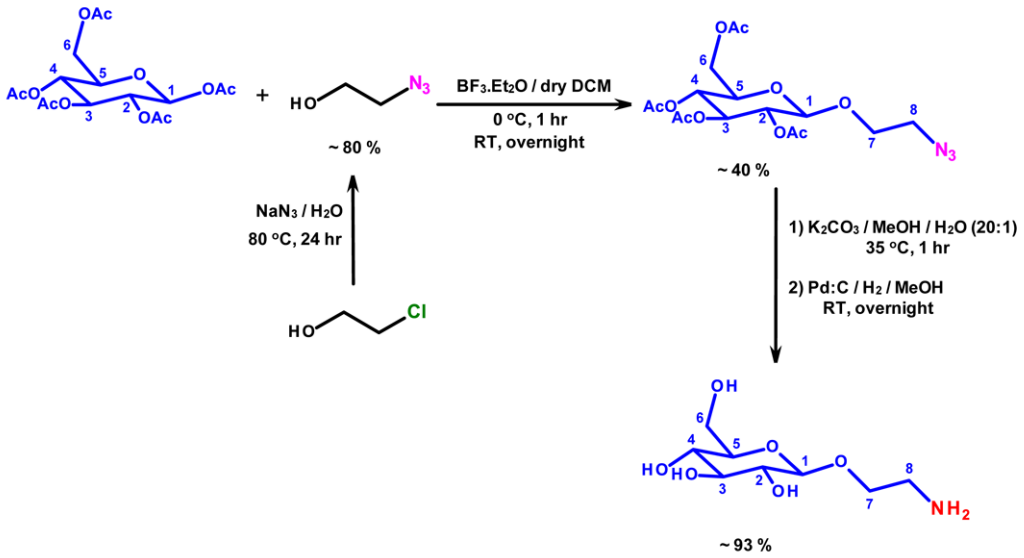

Figure 2.9 Synthetic route to obtaining 2'-aminoethyl-β-D-glucopyranoside employed by Dr. Ahmed Eissa at Durham University. Note the same principles apply for obtaining 2'-aminoethyl-β-D-galactopyranoside.

Characterisation data for 2'-aminoethyl-β-D-galactopyranoside and 2'-aminoethyl-β-D-glucopyranoside was also supplied by Dr. Ahmed Eissa. Data for 2'-aminoethyl-β-D-

glucopyranoside is shown in Figure 2.10, Figure 2.11, Figure 2.12 and Figure 2.13. Data for 2'-aminoethyl-β-D-galactopyranoside was consistent with expected spectra (not shown for simplicity).

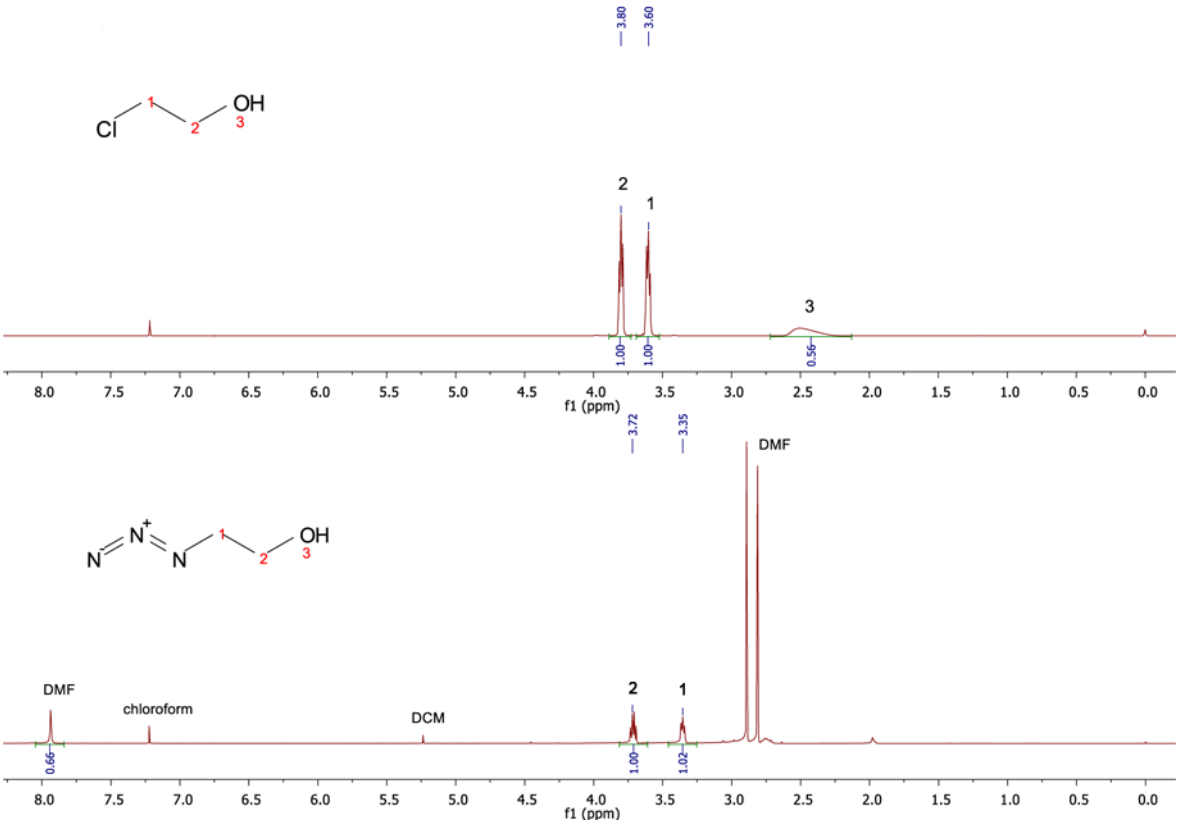

Figure 2.10 ^{1}H NMR spectra for the synthesis of 2-azidoethanol from 2-chloroethanol. Molecular structures are shown to aid with peak assignments.

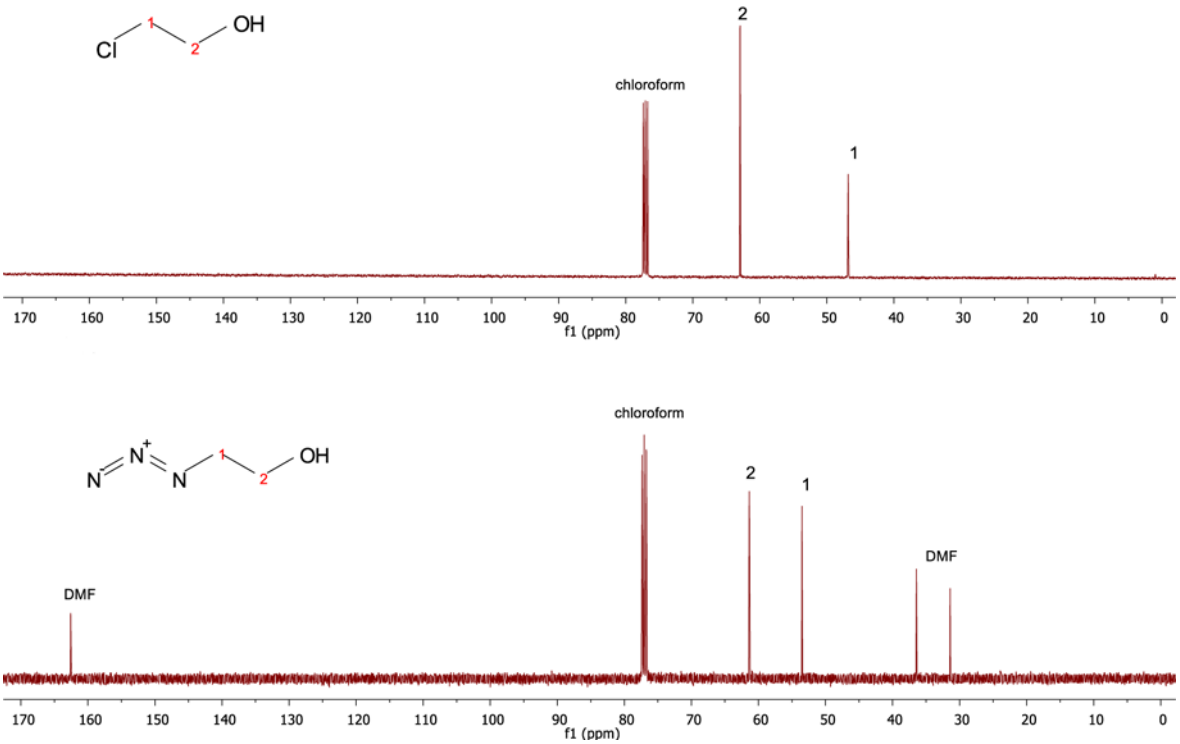

Figure 2.11 ^{13}C NMR spectra for the synthesis of 2-azidoethanol from 2-chloroethanol. Molecular structures are shown to aid with peak assignments.

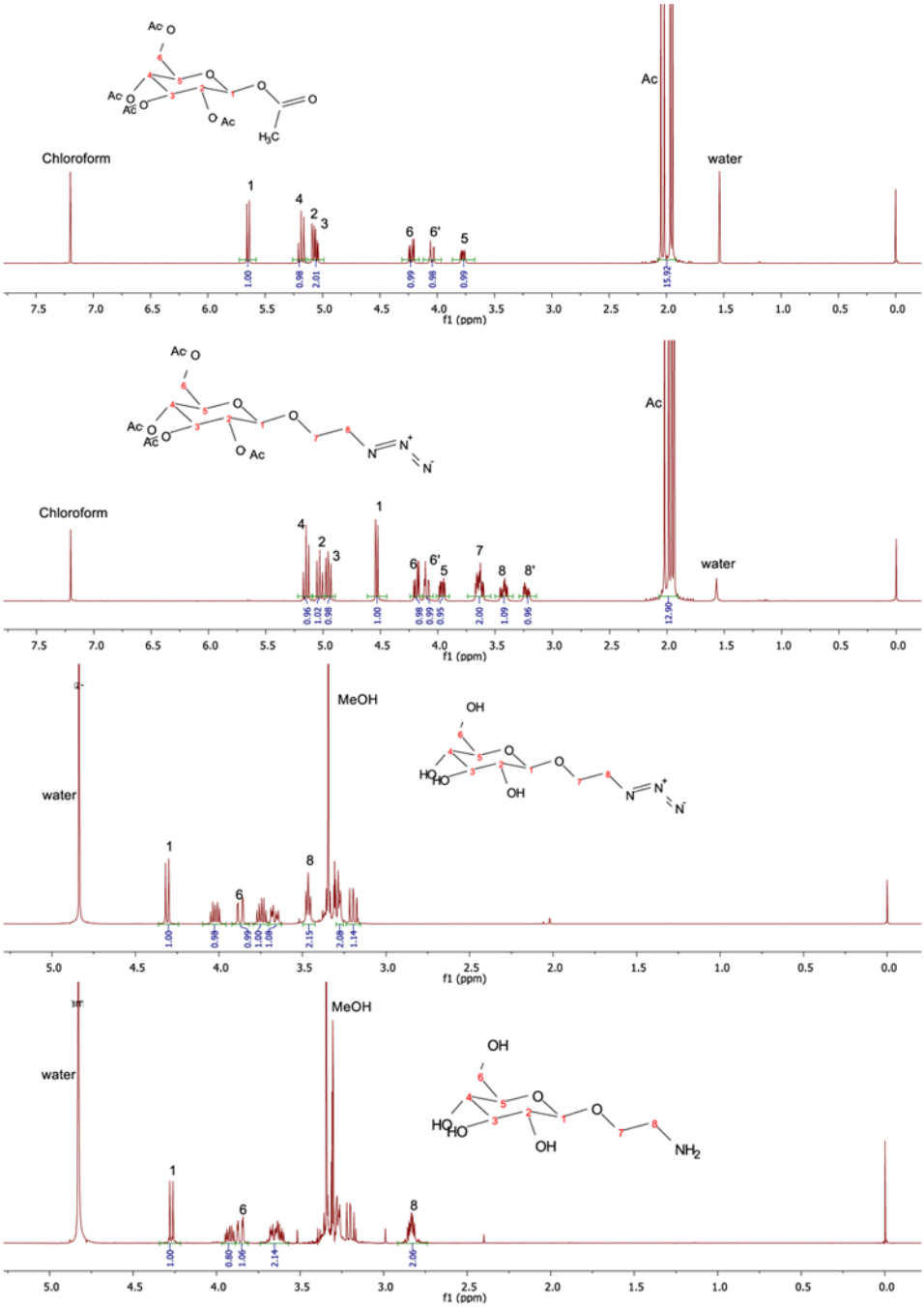

Figure 2.12 ^{1}H NMR spectra for the synthesis of 2′-aminoethyl-β-D-glucopyranoside from glucose pentaacetate and 2-azidoethanol. Molecular structures are shown to aid with peak assignments.

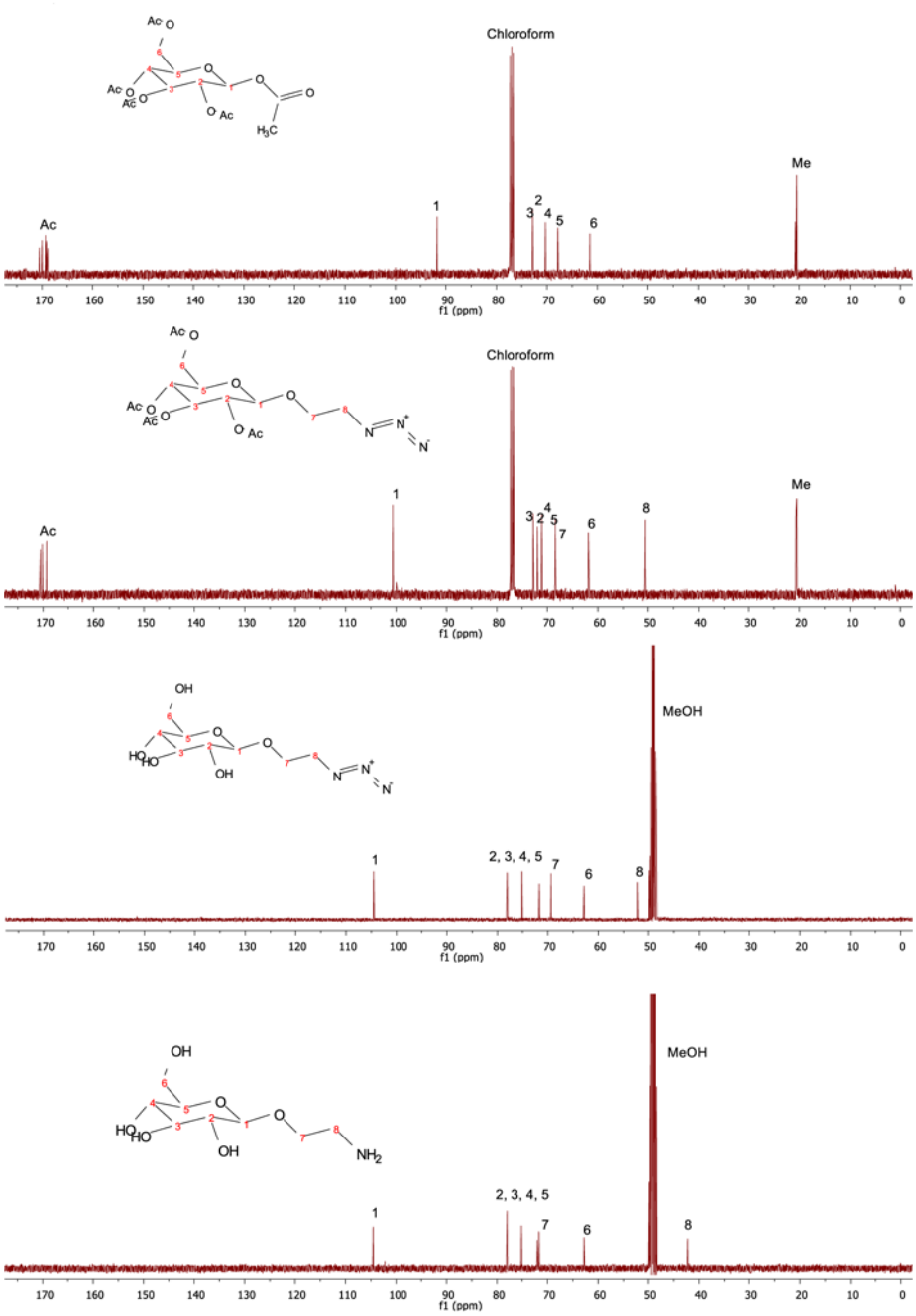

Figure 2.13 ^{13}C NMR spectra for the synthesis of 2′-aminoethyl-β-D-glucopyranoside from glucose pentaacetate and 2-azidoethanol. Molecular structures are shown to aid with peak assignments.

2.2.1.6 Attaching Galactose and Glucose to Ester-Containing Polystyrene Scaffolds

Ester-containing polystyrene scaffold monoliths were first sectioned into 200 µm membranes using a Leica VT1000S vibrotome and then cut into circles of 15 mm diameter using a metal bore-cutter. Six scaffold discs were then placed in a glass vial containing 12 mL dimethylformamide (DMF) and 60 mg of either 2′-aminoethyl-β-D-galactopyranoside or 2′-aminoethyl-β-D-glucopyranoside. The glass vials were then placed in a shaker oven at 40 °C for 48 hours with the

shaker operating at 150 rpm. After this period samples were then slowly re-hydrated though a series of MilliQ water-DMF gradients so as not to collapse the scaffold structure during de-swelling. The scaffolds were then washed in MilliQ water and then left to dry before analysis.

2.2.2 Scanning Electron Microscopy

Scanning electron microscopy (SEM) was employed in the characterisation of emulsion templated polystyrene scaffolds. Analysis was performed on a Phillips XL30 ESEM operating in SEM mode between 10 kV and 25 kV. Samples were first mounted on carbon fibre pads pre-adhered to aluminium stubs and then gold coated using an Edwards Pirani 501 sputter coater before imaging. ImageJ™ software was used to measure void diameters on each micrograph.

2.2.3 Mercury Intrusion Porosimetry

Mercury intrusion porosimetry was employed in the characterisation of emulsion templated polystyrene scaffolds. A Micromeritics AutoPore IV using penetrometers with a stem volume of 1.836 mL and a bulb volume of 5 mL was employed. Analysis was performed from 0.5 psi to 1600 psi.

2.2.4 Attenuated Total Reflection Fourier Transform Infra Red Spectroscopy

Attenuated Total Reflection Fourier Transform Infra Red (ATR-FTIR) spectroscopy was employed in the characterisation of functional emulsion templated polystyrene scaffolds. Spectra were recorded on a Perkin Elmer 1600 Series FTIR spectrometer fitted with a Golden Gate™ ATR element. Solid samples were pressed using a spatula before being placed on the crystal. Spectra were evaluated with Omnic version 7.3.

2.2.5 Solid State Nuclear Magnetic Resonance Spectroscopy

Solid State Nuclear Magnetic Resonance (ssNMR) ^{13}C and ^{19}F spectroscopy were employed in the characterisation of functional emulsion templated polystyrene scaffolds. ^{13}C ssNMR spectra were recorded on a Varian VNMRS 400 spectrometer at a frequency of 100.56 MHz using direct excitation with proton decoupling. Spectra were obtained with total sideband suppression (TOSS). ^{19}F ssNMR spectra were recorded on a Varian Unity Inova 300 spectrometer at a frequency of 282.10 MHz, using direct polarisation and no decoupling. Spectra were evaluated with MestReNova version 8.1.1-11591.

2.2.6 X-Ray Photoelectron Spectroscopy

X-Ray Photoelectron Spectroscopy (XPS) was used in the surface-characterisation of functional emulsion templated polystyrene scaffolds. Analysis was performed at the National EPSRC XPS User's Service (NEXUS) at Newcastle University. A K-Alpha instrument equipped with monochromated AlKa source (Thermo Scientific) was used. A pass energy of 40 eV and a step size of 0.1 eV was used for high resolution spectra of the elements of interest. Spectra were analysed using Casa XPS licensed at Newcastle University.

2.2.7 Toluidine Blue O Staining

Toluidine Blue O (TBO) staining was employed in the characterisation of functional emulsion templated polystyrene scaffolds. The stain was prepared by dissolving 0.002 g of the stain in 20 mL of water. Scaffolds were then submerged in the staining solution for 2 minutes. Scaffolds were then washed in water to remove excess blue staining solution and a photograph taken.

2.2.8 Acid-Base Back Titration

Acid-base back titrations were employed in the characterisation of functional emulsion templated polystyrene scaffolds. Scaffolds (0.6 g) were ground into a powder using a mortar and pestle and then mixed with 0.2 M NaOH solution for 24 hours. This solution was then filtered and then titrated against 0.2 M HCl using a pH meter (Hanna instruments).

2.2.9 Scaffold Wettability By Water

Scaffold wettability by water was employed in the characterisation of functional emulsion templated polystyrene scaffolds. Similar sized scaffold samples (20 mm x 20 mm x 20 mm) were first immersed in deionised water for 5 seconds. After removing from the water solution, a small water droplet was then reapplied to the scaffolds and a photograph immediately taken to capture if the water beads had soaked into the scaffolds.

Chapter 3: Hepatocyte Growth in Emulsion Templated Polystyrene Scaffolds Under Different Culture Conditions

3.1 Introduction

3.1.1 Overview

As discussed in Chapter 1, there is now significant demand for technologies that can approximate native 3D hepatocyte growth *in vitro*[57, 58, 75]. Emulsion templated porous polymers are an attractive technology choice to achieve this due to their high porosity, open-cell morphology and suitable mechanical properties[161]. Indeed, several groups have already demonstrated the suitability of these materials for 3D hepatocyte growth[147, 151, 159], as well as for a range of other cell types including osteoblasts[143, 144], neurons[146] and keratinocytes[155]. In particular, polystyrene scaffolds derived from emulsion templating are showing great promise as potential replacements for conventional 2D laboratory polystyrene[150, 152, 153, 159]. These materials are chemically stable and inexpensive to produce. They also possess a highly reproducible morphology, achieved by controlling the initial emulsion characteristics prior to polymerisation[142]. Moreover, these materials are now commercially available (Alvetex®Scaffold and Alvetex®Strata by *Reinnervate*[154]) and are already being employed by several research groups as more suitable substrates for routine laboratory-based molecular and cancer biology studies[156, 162, 163].

Developing and optimising 3D hepatocyte growth in polystyrene scaffolds is now an important next step if the materials are to be widely adopted by the research community as drug discovery tools. As part of this, a more comprehensive understanding of hepatocyte growth behaviour in the scaffold microenvironment needs to be determined. Similarly, the impact of different scaffold presentations and culture conditions also needs to be investigated. Moreover, important optimisations previously employed to enhance 2D cultures have yet to be translated into polystyrene scaffolds, such as the use of ECM coatings and media perfusion. Developments also need to be made in extracting intact hepatocytes from these scaffolds for subsequent 3D-3D passaging and/or analysis, an important aspect for some *in vitro* experiments. This study therefore set out to address some of these unknowns using commercial Alvetex®Scaffold and Alvetex®Strata.

3.1.2 Alvetex®Scaffold and Alvetex®Strata.

Alvetex®Scaffold is an emulsion templated polystyrene scaffold with an average void diameter of ca. 42 μm. The material originally stems from research by Przyborski *et al.* and Cameron *et al.* but has since been modified and commercialised by *Reinnervate* for routine laboratory use[164, 165]. Alvetex®Strata is also an emulsion templated polystyrene scaffold with the same chemical composition as Alvetex®Scaffold, but with an average void diameter of ca. 12 μm. This material

was initially developed in conjunction with early results from this study, using prototype materials supplied by the Cameron group at Durham University (Dr. D. W. Johnson) and the *Reinnervate* development team (Mr. Simon Padbury). A full structural characterisation of Alvetex®Scaffold and Alvetex®Strata is described in the results section of this Chapter.

3.1.3 Anticipated Hepatocyte Growth on Alvetex®Scaffold and Alvetex®Strata

Prior to this study, hepatocytes had not been grown on the final commercial Alvetex®Scaffold or Alvetex®Strata materials. However, it was hypothesised that the scaffolds would create a more physiologically relevant (3D) growth profile for hepatocytes compared to conventional 2D culture, consistent with preliminary reports in the literature using similar scaffolds[147, 151]. The anticipated growth profiles for hepatocytes in 2D, Alvetex®Scaffold and Alvetex®Strata is illustrated in Figure 3.1. With 2D culture, hepatocytes were expected to flatten into a distorted morphology with limited opportunity for cell-cell contact, far removed from the complex 3D liver architecture described in Chapter 1[76, 166]. For Alvetex®Scaffold, hepatocytes were expected to enter the scaffold and grow within the 3D microenvironment. The topology of the scaffold was expected to keep cells in their native 3D morphology, which in turn would increase cell-cell contact. For Alvetex®Strata, a different 3D growth profile was hypothesised. The smaller void diameter was expected to prevent hepatocytes from entering the scaffold but actually encourage growth on top in a ''scaffold-free'' manner. The highly uneven surface topography was expected to inhibit cell flattening during initial seeding and so preserve the natural 3D morphology of the cells. This in turn should encourage cells to build up on top of one another to closely approximate native liver density and organisation.

Hepatocyte growth on top of Alvetex®Strata was expected to offer two distinct advantages; Firstly cells would have maximum opportunity for cell-cell contact due to the ''scaffold-free'' growth environment; Secondly 3D cell growth on top of the scaffold was expected to offer new opportunities to extract cells for subsequent 3D-3D passaging and/or analysis (see Figure 3.2).

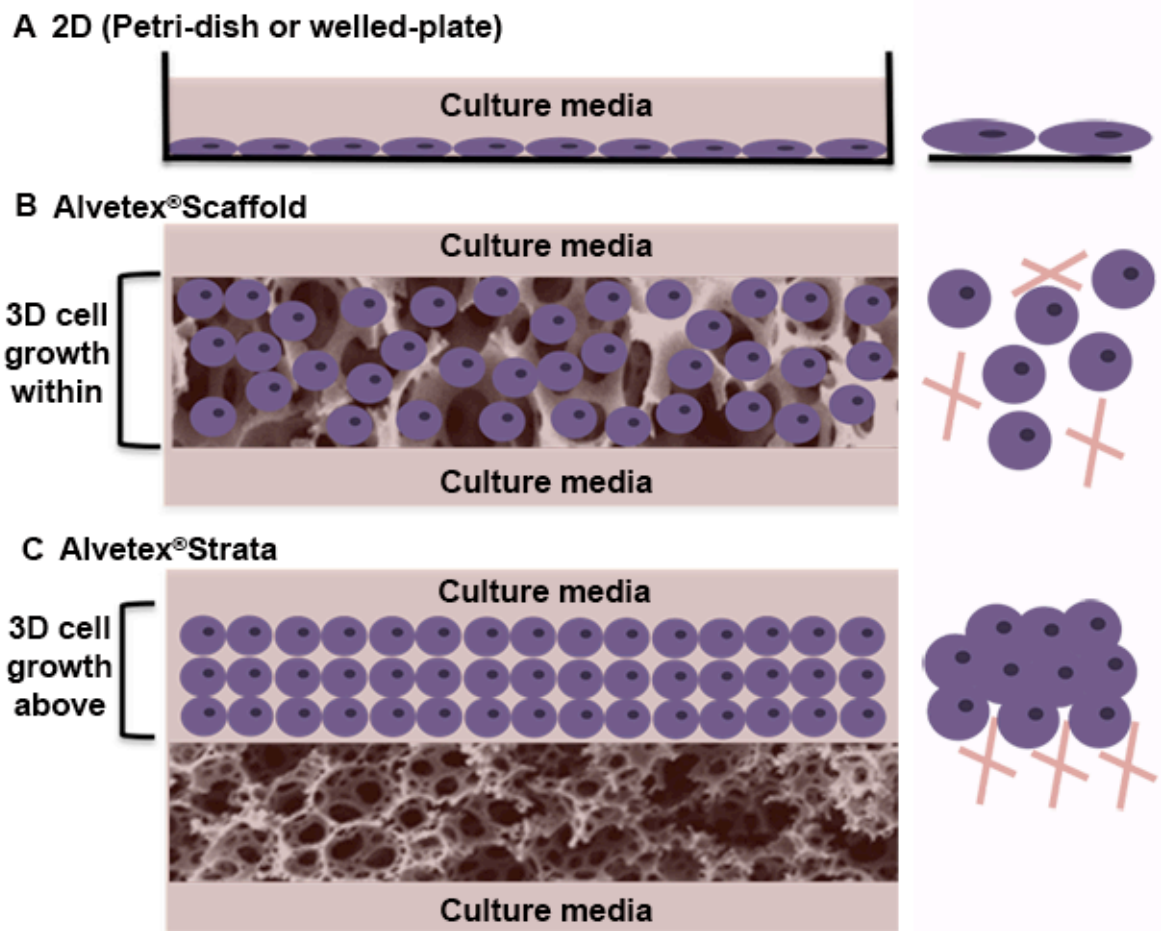

Figure 3.1 Illustration showing the anticipated growth profiles of hepatocytes in 2D, Alvetex®Scaffold and Alvetex®Strata. (A): 2D hepatocytes flattening across the flat surface (B): Alvetex®Scaffold accommodating hepatocytes within the scaffold, encouraging a more native (round) morphology and increased opportunity for cell-cell contact. (C): Alvetex®Strata encouraging hepatocytes to grow on top of the scaffold. This ''scaffold-free'' growth profile encourages maximal cell contact and cell extraction opportunities.

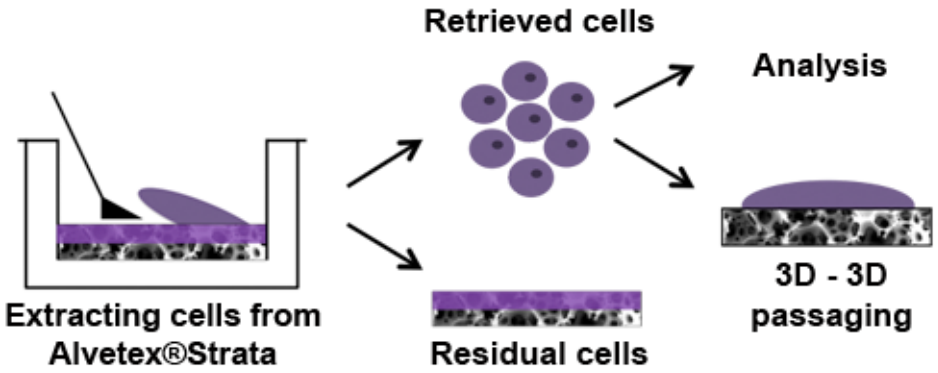

Figure 3.2 Illustration of extracting hepatocytes from Alvetex®Strata. Growing hepatocytes on top of the scaffold rather than within was anticipated to enable maximal cell contact as well as cell retrieval opportunities for subsequent 3D-3D passaging or analysis.

3.1.4 Scaffold Presentation and Culture Conditions

It was expected that scaffold presentation and culture conditions would influence hepatocyte growth within the scaffold, with some scenarios favouring a more physiologically relevant growth profile than others.

Alvetex®Scaffold and Alvetex®Strata are supplied by *Reinnervate* as sterile 200 μm thick membranes, 15 mm in diameter. These membranes can be placed in inserts or clipped to a 24 welled-plate, allowing different scaffold presentations to be investigated (see Figure 3.3). Inserts can create systems similar to Transwell® cultures inside a Petri dish, 6-well plate or 12-well plate. Media can be applied to the insert to either fully submerge the scaffold or merely contact the scaffold membrane from underneath. Fully submerged scaffold inserts were expected to offer cells maximum nutrient supply as media could access the cells from above and below the insert. Conversely, contact scaffold inserts (media underneath and so creating air-liquid interface cultures) were expected to promote native tissue density and organisation due to increased surface tension holding cells together and the absence of a turbulent media supply. This presentation was anticipated to be particularly important for Alvetex®Strata, where hepatocytes growing on top of the scaffold were expected to be more susceptible to being washed away and lost from the insert during media changes.

A naming protocol for the insert formats was developed for simplicity: insert/(insert housing)/(media supply). For example, culturing hepatocytes using an insert housed in 6-well plate and submerged with media would be defined as: insert/6-well plate/submerged.

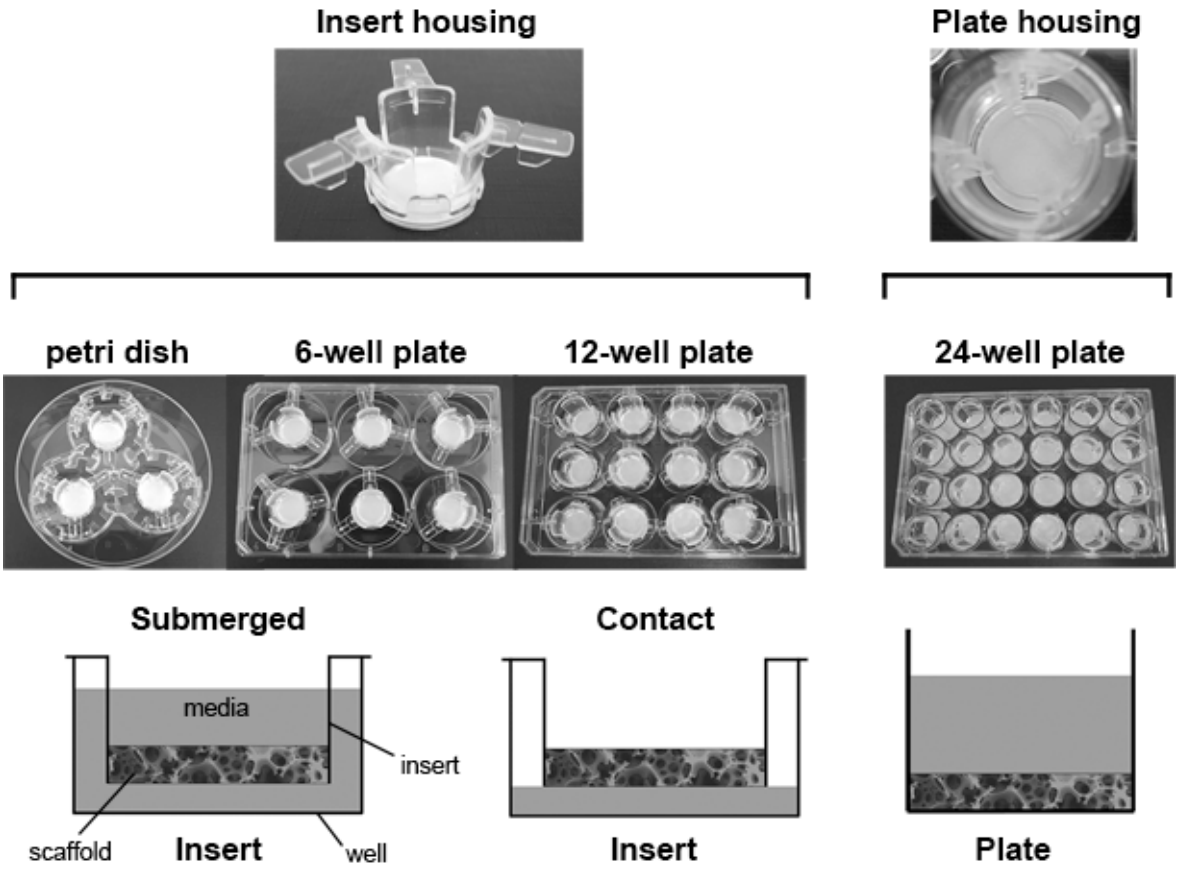

Figure 3.3 Scaffold presentations using inserts or a 24 welled-plate. The 200 μm thick scaffold membranes (15 mm in diameter) can be housed in either an insert or secured to the bottom of a 24-well plate using a plastic clip. Inserts can be placed in a Petri dish, 6-well plate or 12-well plate. The insert housings enable the scaffolds to be either fully submerged in culture media, or just contacted by media from underneath to create air-liquid interface cultures.

3.1.5 The Use of Extracellular Matrix Proteins in Hepatocyte Culture

The use of ECM components in general cell culture is now well established[167]. Most cells generally will not directly adhere to synthetic *in vitro* substrates such as polystyrene, but rely on extracellular glycoproteins to enable cell attachment[168]. These glycoproteins, such as fibronectin, are present in the serum component of the culture media or are secreted by the cells themselves. Moreover, basement membrane proteins such as collagen also facilitate cell adhesion and growth *in vitro*, mainly via a glycoprotein-mediated mechanism. *In vivo*, the hepatic ECM is composed of various collagens, fibronectin, laminin and heparin/heparin-sulfate proteoglycans[12, 15, 169]. This matrix plays a critical role in the maintenance of normal hepatic structure and function[14]. As a result, the application of such components for *in vitro* hepatocyte culture has been shown to enhance cell adhesion, survival and function (see discussion section of this Chapter). Coating

emulsion templated polystyrene scaffolds with ECM components was therefore hypothesised to improve the physiological relevance of these materials and thus was investigated in this study.

3.1.6 The Use of Media Perfusion in Hepatocyte Culture

Conventional hepatocyte cultures employ a static media supply that results in an on going fluctuation of media quality during the culture period. In between media changes nutrients and oxygen concentration are gradually depleted. Spent media and cellular waste can also build up. This is in stark contrast to the native liver environment, where hepatocytes experience a constant replenishing blood flow that transports nutrients and waste to and from the cells. Unsurprisingly, the employment of perfused media supply *in vitro* has been shown to be beneficial for hepatocyte culture. Gebhardt *et al.* demonstrated improved viability and metabolic activity using a 2D media perfusion system[170, 171]. Vinci *et al.* reported increased expression for several hepatic detoxification genes when employing perfused sandwich cultures[172]. Guzzardi *et al*. demonstrated enhanced HepG2 function using the commercial *Quasi-Vivo®* perfusion system (*Kirkstall*) in conjunction with endothelial cell co-culture[173]. Recent work is also now turning to advanced microfluidic and biochip systems that offer small-scale high throughput media perfusions[174]. Recognising these advancements, this study attempted to develop a 3D perfusion model using Alvetex®Scaffold.

3.1.7 Sources of Hepatocytes for *In Vitro* Use

A broad range of hepatocyte sources are available for *in vitro* experimentation, summarised recently by two comprehensive review articles[32, 175]. Freshly isolated primary hepatocytes direct from liver tissue are generally regarded as the current 'gold standard' for mimicking native liver function in the laboratory[33]. These cells are obtained by collagenase digestion of liver tissue followed by multiple density-gradient centrifugations. If placed in appropriate culture conditions immediately after isolation, the cells display the majority of native hepatic functions, including albumin synthesis, urea synthesis, cytochrome P450 activity and evidence of drug transporter proteins[176]. However there are several limitations with using these cells for routine *in vitro* studies; First is that terminally differentiated hepatocytes have almost no proliferative capacity, which currently restricts primary culture to short-term studies (typically days); Second is availability: To obtain freshly isolated hepatocytes researchers either need close access to hospital surgeries or animal houses. Furthermore, tissue from animal houses is not always appropriate due to reported inter-species differences in *in vitro* hepatocyte function[177, 178]; Third issue is reproducibility: Differences between donors can often vary significantly making

experimental results more difficult to interpret. To help overcome two of these challenges (availability and reproducibility), cryopreserved primary hepatocytes have been developed by commercial vendors such as *Life Technologies* and *Biopredic International*. These hepatocytes display many of the functions of freshly isolated hepatocytes, but can be stored at low temperatures (-140 ^{o}C) for future use and transport[179-181]. Furthermore, multiple vials of hepatocytes from the same donor can be purchased to improve experimental reproducibility. This study employed cryopreserved primary rat hepatocytes (*Biopredic*) as one of the hepatocyte sources for culture on Alvetex®Scaffold and Alvetex®Strata.

Immortalised hepatocyte-derived cell lines such as HepG2, C3A, HepaRG and Fa2N-4 are another common source of hepatocyte material used for *in vitro* studies[182]. Typically these cells possess a potentially limitless growth capacity making them easy and inexpensive to handle. However these cells often carry mutations that produce phenotypes different to native tissue, especially with regards to drug metabolism capacity. Probably the most popular and well-characterised cell line is the HepG2 cell line (*ATCC®*, HB-8065™). This cell line derives from a human hepatocellular carcinoma, but still displays several hepatocyte functions including plasma protein synthesis[183], bile acid secretion[184] and expression of receptors such as the asialoglycoprotein receptor (ASGP-R)[185]. However, the transcription levels and protein activity levels of most drug metabolising enzymes are significantly lower compared to primary hepatocytes and so HepG2 cells are not used extensively for drug toxicity screening[186, 187]. Nonetheless, this study still employed HepG2 cells as a readily available hepatocyte source, particularly for exploring the growth profile on Alvetex®Scaffold and Alvetex®Strata under numerous culture conditions.

The third source of hepatocyte material used in this study was the recently commercialised cryopreserved Upcyte® hepatocyte cell strain (*Medicyte*)[188]. These cells originated as primary human hepatocytes from a single donor, but have been transduced with proliferative genes to enable a small proliferation capacity (2-5 population doublings). The cells display many of the features of primary human hepatocytes, including albumin synthesis, urea synthesis, glycogen storage and an almost normal phase I and II drug metabolising capacity. These cells were therefore employed as a third hepatocyte source in this study.

3.2 Aims and Objectives

The overall aim of this Chapter was to explore the growth of hepatocytes in emulsion templated polystyrene scaffolds to understand if native liver density and architecture could be approximated using these materials. This included an assessment of different culture conditions, scaffold presentations, scaffold coatings and media perfusion to identify the most physiologically relevant growth profiles.

The main objectives were to:

- Assess 2D growth characteristics of HepG2 cells, Upcyte® cells and primary rat hepatocytes prior to growing on 3D scaffolds and compare with *in vivo*.
- Fully characterise Alvetex®Scaffold and Alvetex®Strata.
- Explore hepatocyte growth in Alvetex®Scaffold and Alvetex®Strata using different scaffold presentations.
- Investigate ECM protein coatings to optimise hepatocyte growth in the 3D scaffold microenvironment.
- Investigate media perfusion to optimise hepatocyte growth in the 3D scaffold microenvironment.
- Attempt to extract intact hepatocytes from the scaffold microenvironment for subsequent 3D-3D passaging and analysis.

3.3 Results

3.3.1 Hepatocyte Growth in 2D

Prior to culturing hepatocytes on Alvetex®Scaffold and Alvetex®Strata it was first necessary to understand the growth characteristics of these cells in conventional 2D culture. Collagen I coated (50 μg/mL) conventional 12-well cell culture plates were used for this experiment. Figure 3.4 shows HepG2 cells and Upcyte® cells growing on the 2D plastic, taken 24 hours after seeding and staining using H&E. Cells appear healthy and have flattened out across the plastic to form a monolayer. The severity of Upcyte® flattening is shown in Figure 3.5, which displays a cross-sectional image of several Upcyte® cells cultured in 2D and stained with TBO. ImageJ™ measurements of these 2D Upcyte® cells show that the average cell height is 2.8 μm ± 0.3 μm (n=20), even though the average cell diameter is 56.1 μm ± 3.1 μm (n=20).

Figure 3.6 shows the growth of primary rat hepatocytes on 2D plastic (24 hours culture) in comparison to native human liver tissue taken from *in vivo* (both H&E stained). The primary rat cells have also formed a 2D monolayer with most of the cells appearing healthy. However some notable signs of cell death are observed, indicated by the dark condensed nuclei lacking a cytoplasm (white arrows in Figure 3.6C). Cells in the human liver tissue are very densely packed, with almost the entire field of view being filled with cells. Furthermore, this high cell density enables extensive cell-cell contact in multiple directions. Consequently, achieving high cell density with opportunity for multiple surface interactions should be a target for *in vitro* hepatocyte growth.

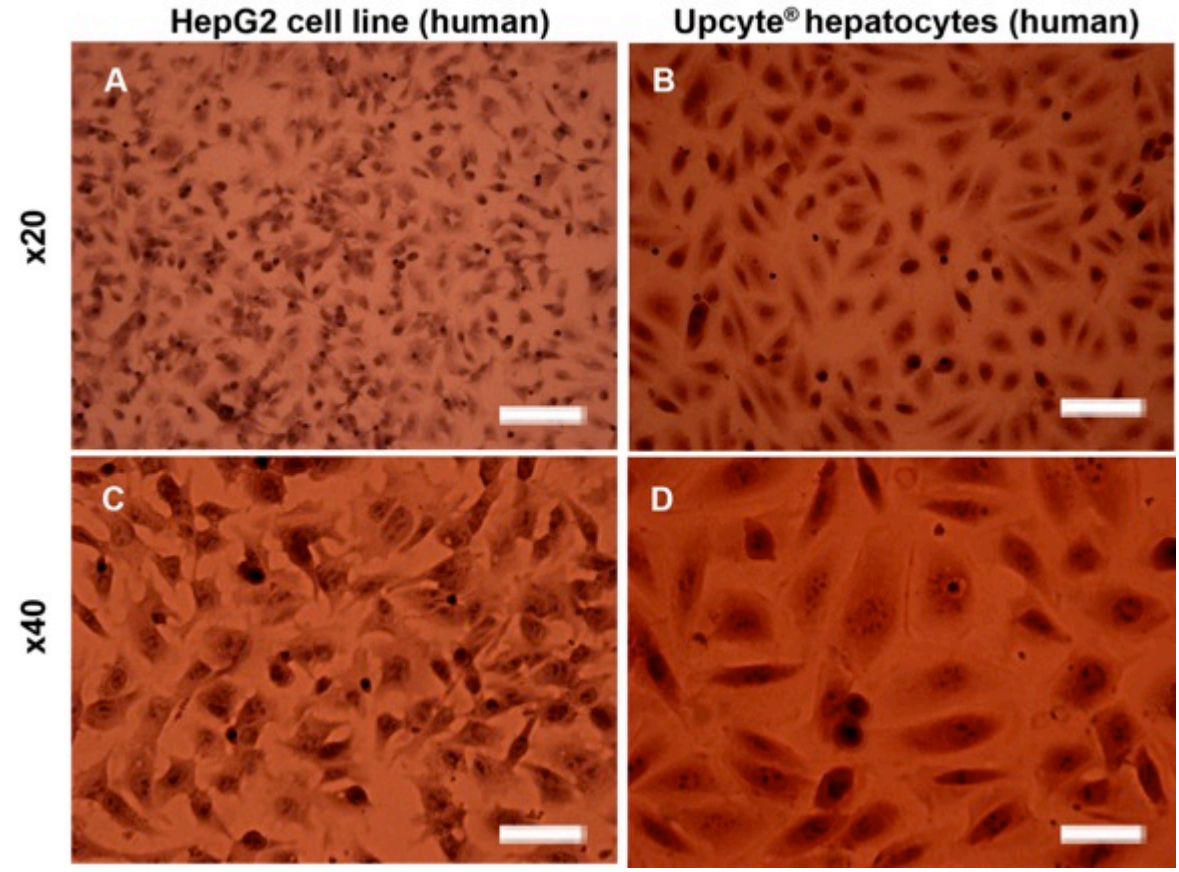

Figure 3.4 Growth of HepG2 cells and Upcyte® cells on 2D plastic. (A,C): HepG2 cells. (B,D): Upcyte® cells. Most cells appear healthy and have flattened out across the plastic creating a monolayer. Images represent H&E staining of fixed cells 24 hours after seeding. Scale bars: A,B = 100 μm, C,D = 50 μm.

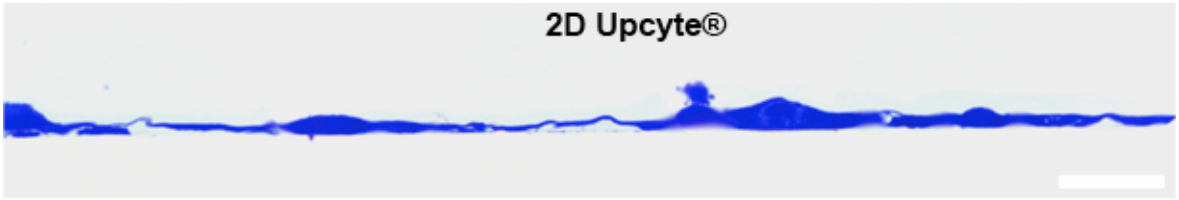

Figure 3.5 Cross-sectional image of Upcyte® hepatocytes cultured in 2D and stained using TBO. A severely flattened morphology is observed consistent with the H&E images. Cell height is 2.8 μm ± 0.3 μm, compared to 56.1 μm ± 3.1 μm for cell diameter. Scale bar = 20 μm.

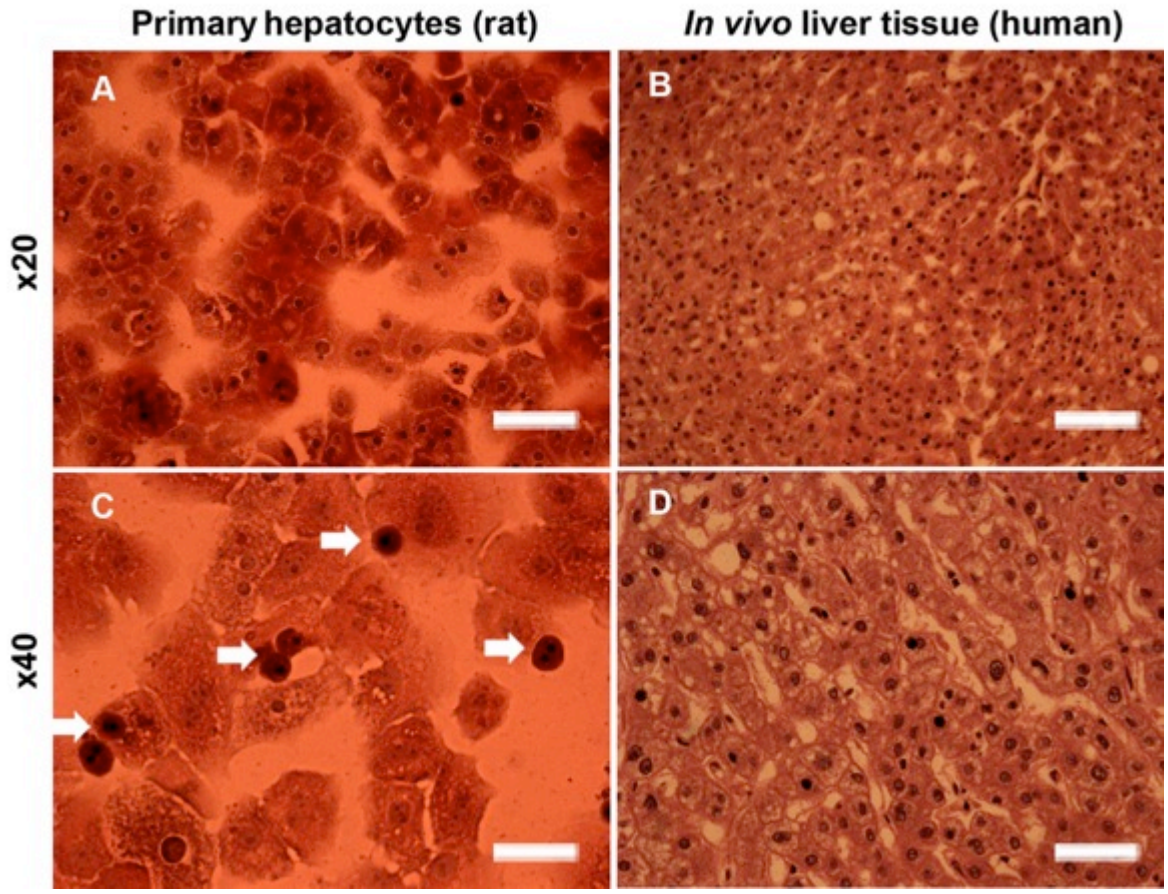

Figure 3.6 Growth of primary rat hepatocytes on 2D plastic compared to native *in vivo* liver tissue. (A,C): Primary rat cells (*Biopredic International*) after 24 hours culture. (B,D): *In vivo* (human) liver tissue (*abcam®* ab4348). The primary rat cells also spread out across the plastic towards a monolayer, similar to HepG2 and Upcyte® cells. Most of the primary rat cells appear viable, although some signs of cell necrosis are present (white arrows in C indicate condensed nuclei lacking a cytoplasm). Conversely no signs of cell necrosis are apparent in the *in vivo* tissue. Scale bars: A,B = 100 μm, C,D = 50 μm.

ImageJ™ measurements of all H&E images in Figure 3.4 and Figure 3.6 were employed to estimate the average cell diameter (greatest width) of 2D HepG2, Upcyte® and primary rat hepatocytes in comparison to *in vivo* hepatocytes (see Figure 3.7 and Table 3-1). The average cell diameter for 2D *in vitro* hepatocytes is significantly greater compared to *in vivo* hepatocytes; HepG2: 40.0 ± 2.9 μm (n=20); Upcyte®: 56.1 ± 3.1 μm (n=20); Primary rat: 49.0 ± 1.8 μm (n=20); *In vivo* 18.5 ± 1.0 μm (n=20). These data strongly support the spreading out of hepatocytes across 2D plastic to create cell architectures that are very different from cells in the native liver scenario.

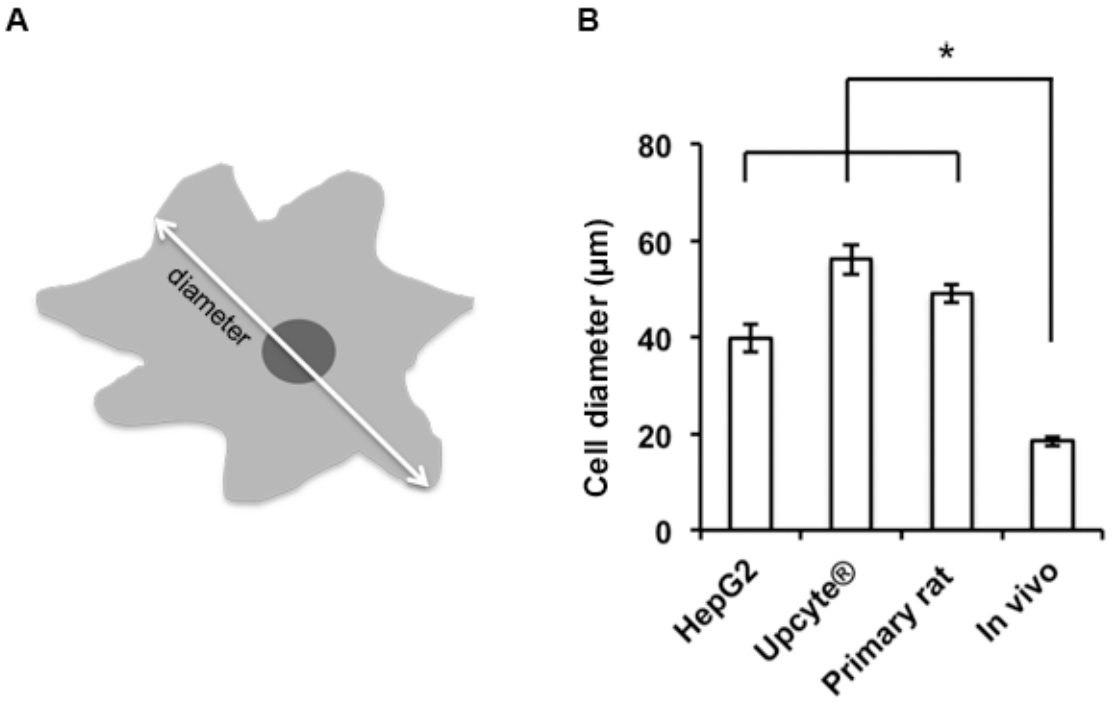

Figure 3.7 Quantifying cell diameter of 2D HepG2 cells, Upcyte® cells and primary rat hepatocytes in comparison to *in vivo* hepatocytes by ImageJ™ analysis of H&E images. (A): Illustration of cell diameter employed in the ImageJ™ analysis. (B): Average cell diameter plot. A significantly greater cell diameter is observed for all 2D *in vitro* hepatocytes compared to *in vivo* hepatocytes (*denotes $p<0.005$ according to the *Student's t-test*). Data represent mean ± s.e.m (n=20).

Table 3-1 Average Cell Diameter of 2D Hepatocytes Compared to *In vivo* hepatocytes by ImageJ™ Analysis of H&E images

Cell diameter (µm)			
2D HepG2	**2D Upcyte®**	**2D Primary Rat**	***In Vivo***
40.0 ± 2.9	56.1 ± 3.1	49.0 ± 1.8	18.5 ± 1.0

The MTT assay measures the cellular metabolism of a tetrazolium dye into a blue formazan product that is subsequently quantified by the absorbance intensity at 570 nm. 2D cell metabolic activity was measured using the MTT assay for each hepatocyte source across a period of 7 days (Figure 3.8). HepG2 cells are the most metabolically active (being tumour-derived) and show a steady increase in MTT absorbance throughout the culture period, consistent with their proliferative nature. Upcyte® cells are less active compared to HepG2 cells, which is to be expected as they originate from a primary hepatocyte source. They show a slight decreasing trend in MTT absorbance as the culture period progresses, however cells are still metabolically active after 7 days. Primary rat hepatocytes are the least viable in 2D. Even after 3 days the MTT

absorbance is much lower compared to HepG2 cells and Upcyte® cells. After 5 days the cells are almost completely metabolically inactive.

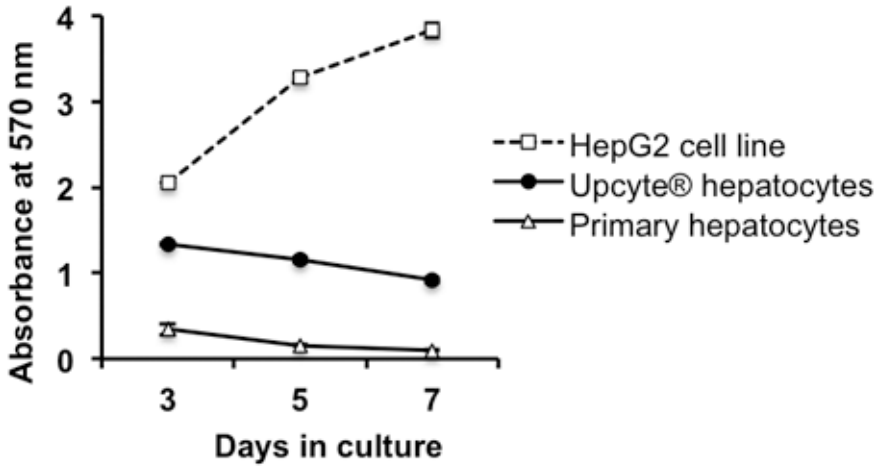

Figure 3.8 Metabolic activity of 2D hepatocytes by the MTT assay. HepG2 cells show an increase in absorbance across the culture period unlike Upcyte® cells and primary rat hepatocytes. Data represent mean ± s.e.m (n=2).

In summary, this results section has shown that all three *in vitro* hepatocyte sources adhere to 2D collagen I coated plastic and grow in a monolayer. They adopt a flattened structure that is greatly removed from that of cells in the liver *in vivo.* HepG2 cells are proliferative in 2D, whereas Upcyte® cells and primary rat hepatocytes have limited or no proliferative capacity in 2D.

3.3.2 Characterisation of Alvetex®Scaffold and Alvetex®Strata

Alvetex®Scaffold and Alvetex®Strata were supplied as thin circular membranes, 15 mm in diameter, from *Reinnervate*. Characterisation of these membranes was performed using scanning electron microscopy (SEM) and mercury intrusion porosimetry to confirm morphology and porosity. The SEM micrographs in Figure 3.9 show that both membranes are approximately 200 μm in thickness. The morphology of each membrane is highly open-cell, with clearly defined voids (red circles) and interconnecting windows (blue circles). Both membranes also appear reasonably homogenous with regards to their void and interconnect diameter distribution. As expected, Alvetex®Scaffold displays noticeably larger voids and interconnects compared to Alvetex®Strata.

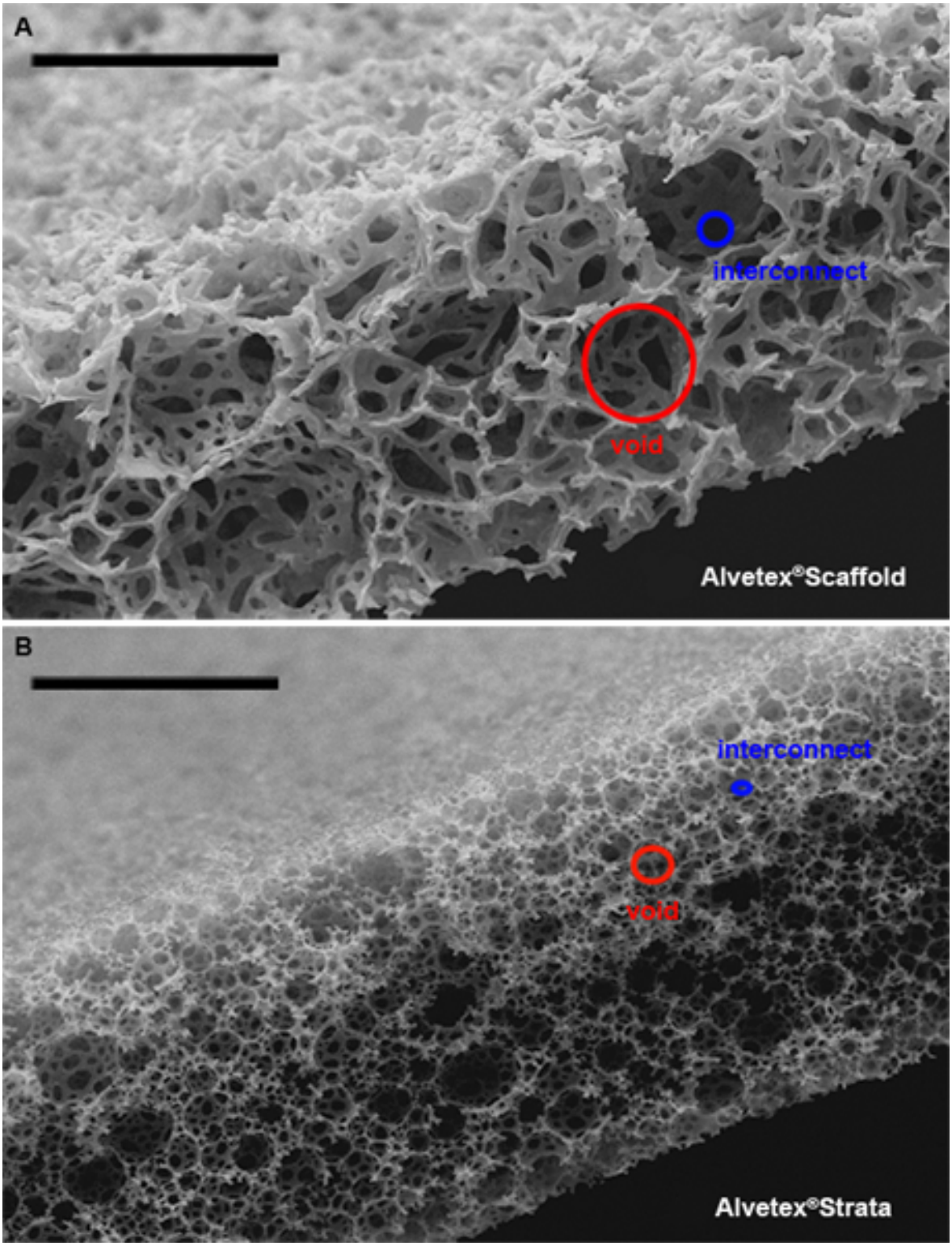

Figure 3.9 Morphology of Alvetex®Scaffold and Alvetex®Strata by SEM. (A): Alvetex®Scaffold. (B): Alvetex®Strata. Each membrane is approximately 200 μm thick. Both materials display a highly open-cell morphology with clearly defined voids (red circles) and interconnecting windows (blue circles). A larger void and interconnect diameter can be seen for Alvetex®Scaffold compared to Alvetex®Strata. Scale bars = 100 μm.

Void diameters were quantified by ImageJ™ analysis of SEM micrographs (Figure 3.10A). Alvetex®Scaffold displays an average void diameter of 42.0 μm ± 1.6 μm (n=65), compared to 11.7 μm ± 0.6 μm (n=65) for Alvetex®Strata. Interconnect diameters were estimated using mercury intrusion porosimetry (Figure 3.10B). Alvetex®Scaffold displays an average interconnect diameter of ca. 15 μm, compared to ca. 5 μm for Alvetex®Strata (n=1).

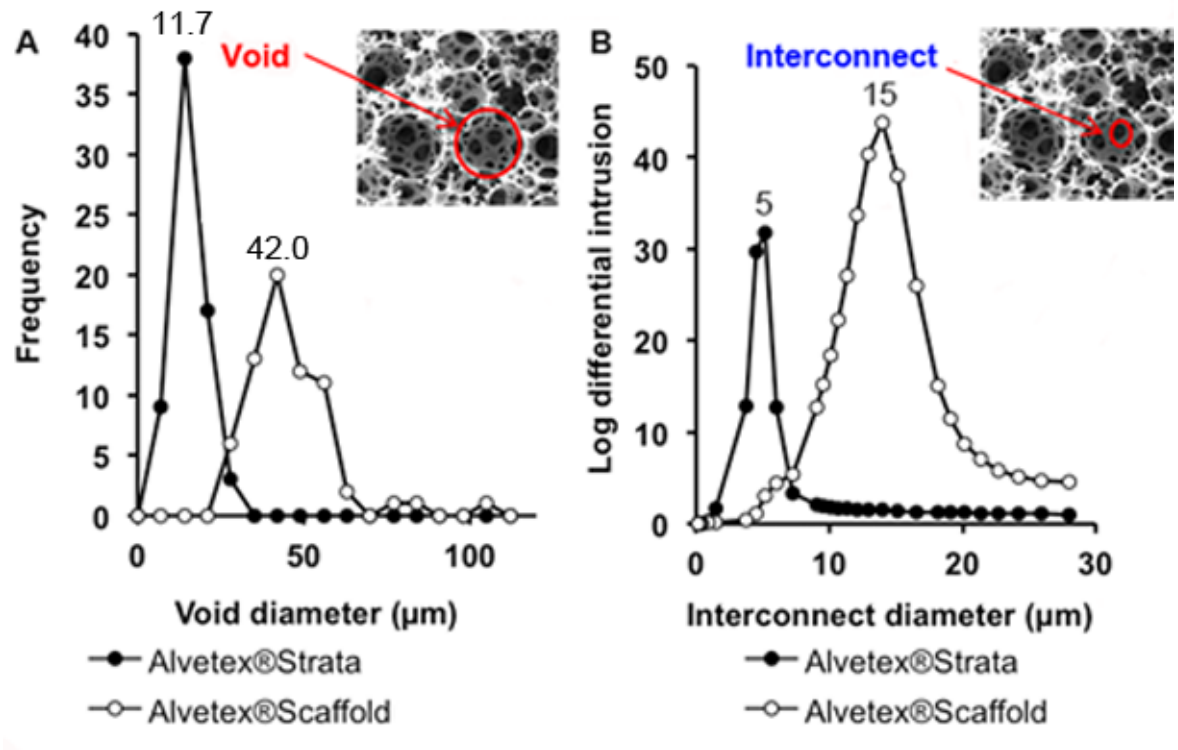

Figure 3.10 Quantifying void and interconnect diameters for Alvetex®Scaffold and Alvetex®Strata. White points = Alvetex®Scaffold. Black points = Alvetex®Strata. (A): Void diameter distribution determined by ImageJ™ analysis of SEM micrographs (n=67). (B): Interconnect diameter distribution determined by mercury intrusion porosimetry (n=1). A larger average void and interconnect diameter is observed for Alvetex®Scaffold compared to Alvetex®Strata.

Table 3-2 summarises the physical characteristics of Alvetex®Scaffold and Alvetex®Strata. The porosity of Alvetex®Scaffold, determined by mercury intrusion porosimetry, was found to be ca. 93 %, compared to ca. 90 % for Alvetex®Strata (n=1). Both of these values are highly suitable for 3D cell culture applications.

Table 3-2 Summary of Alvetex®Scaffold and Alvetex®Strata Physical Characteristics

	Average void diameter (μm)	Average interconnect diameter (μm)	Porosity (%)
Alvetex®Scaffold	42.0 ± 1.6	15	93
Alvetex®Strata	11.7 ± 0.6	5	90

In summary, this results section has characterised the different 3D scaffold microenvironments of Alevex®Scaffold and Alvetex®Strata. Whilst the porosities of the scaffolds are similar, the average void and interconnect diameter is much greater for Alvetex®Scaffold. This is consistent with the anticipated growth of hepatocytes within Alvetex®Scaffold, compared to on top for Alvetex®Strata.

3.3.3 Hepatocyte Growth on Alvetex®Scaffold

HepG2 cells were chosen for preliminary growth assessments with Alvetex®Scaffold as they are more robust and less valuable compared to Upcyte® cells and primary rat hepatocytes.

The first experiment using HepG2 cells and Alvetex®Scaffold employed the insert/Petri-dish/submerged format. This was chosen for the large culture media capacity (70 mL) and thus was expected to be the most beneficial for encouraging hepatocyte growth and viability in the scaffold microenvironment. Prior to seeding the HepG2 cells, Alvetex®Scaffold was first rendered hydrophilic by treatment with 70 % ethanol followed by extensive washing in phosphate-buffered saline (PBS) solution. This was required before every cell culture experiment and so should be assumed common practice from this point. A cell suspension of 0.5 million cells in 100 μL of Minimum Essential Medium (MEM) was then applied to the wet membranes and cells were left to adhere for 2 hours at 37 ^{o}C and 5 % CO_2. Following this adhesion period, 70 mL of culture media was added to the Petri dish housing x3 scaffold inserts. Cell growth was assessed at days 2, 7 and 14. Culture media was changed every 3 days.

Figure 3.11A shows that after 2 days culture there is an abundance of cells near the top portion of the material, suggesting successful adhesion. As the culture period progresses onto 7 and 14 days, cells gradually proliferate and migrate into the material (Figure 3.11B,C). Certainly by day 7, the growth profile of the HepG2 cells is fairly homogeneous, with an approximately equal cell density and penetration distance across the majority of the membrane diameter. Figure 3.11D,E are higher magnification images of cells cultured after 14 days. Cells appear closely packed with plenty of opportunity for cell-cell interaction. Cells also appear healthy with no signs of necrosis, suggesting that the scaffold is a suitable growth environment for prolonged culture periods. Importantly, unlike the 2D scenario, cells are not unnecessarily stretched; with individual cell

diameters being less spread out and more 3D in structure like that of the *in vivo* scenario. This is quantified in Figure 3.12 and Table 3-3, showing 3D HepG2 cell diameter to be much closer to *in vivo* hepatocytes compared to 2D (3D HepG2: 13.6 ± 0.6 μm; *In vivo* 18.5 ± 1.0 μm, n=20).

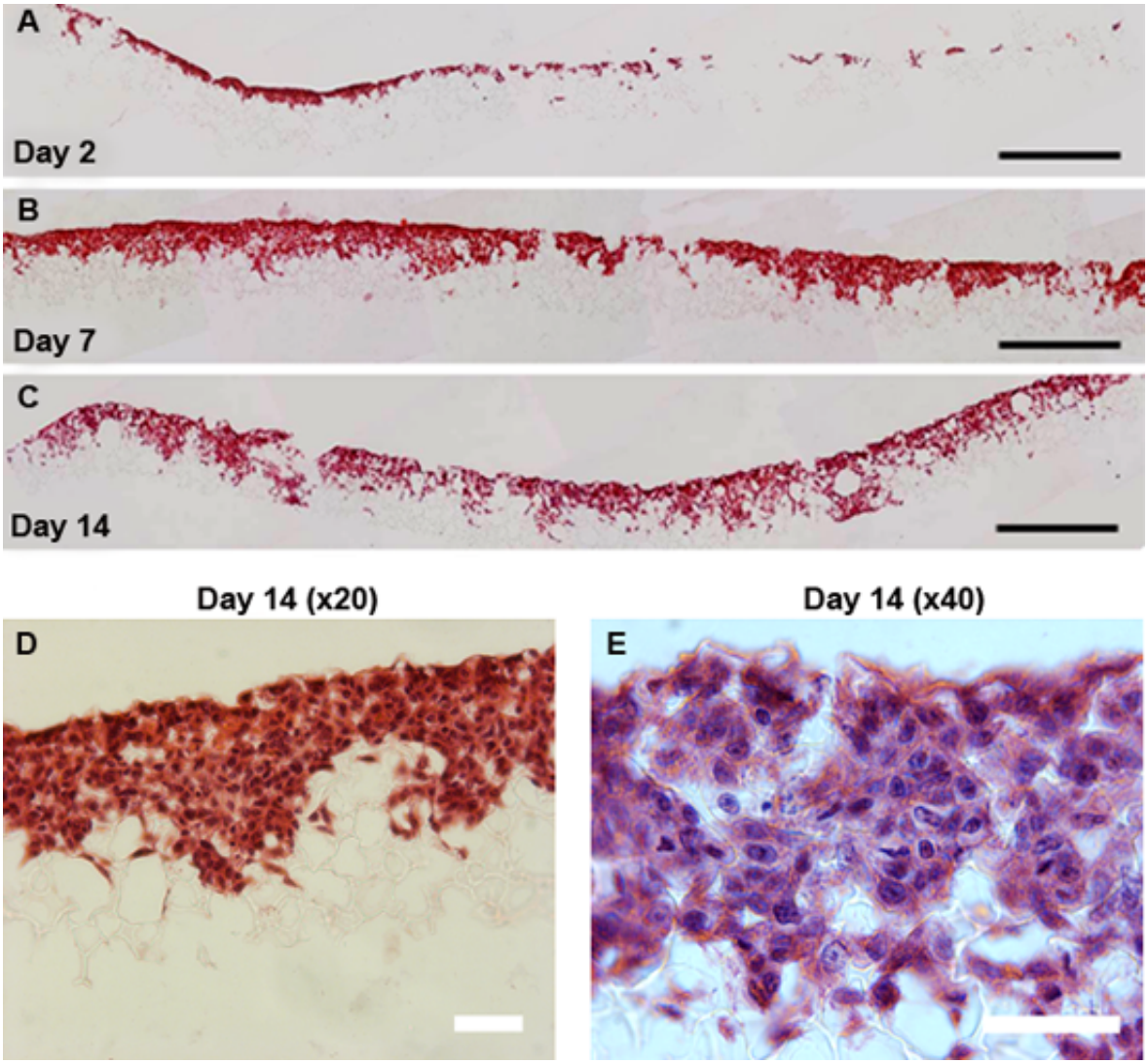

Figure 3.11 Growth of HepG2 cells in Alvetex®Scaffold by H&E staining. (A-C): Low magnification montage images at 2, 7 and 14 days. Cells appear to adhere to the scaffold and migrate into the scaffold as the culture period progresses. Scale bars = 400 μm. (D,E): High magnification images after 14 days culture showing cells are healthy with no signs of necrosis. Scale bars = 50 μm.

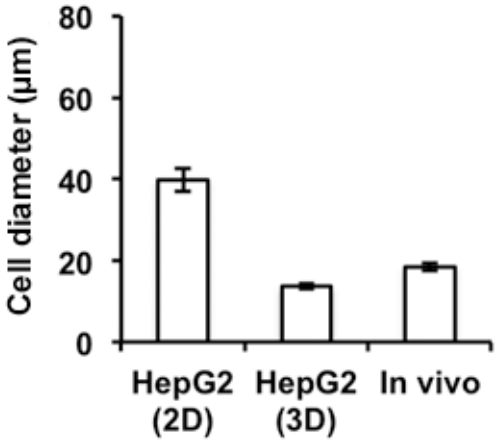

Figure 3.12 Quantifying cell diameter of 3D HepG2 cells in comparison to 2D and *in vivo* cells by ImageJ™ analysis of H&E images. A similar cell diameter is observed between 3D HepG2 cells in Alvetex®Scaffold and those *in vivo.* On the contrary 2D HepG2 cells have a larger cell diameter. Data represent mean ± s.e.m (n=20).

Table 3-3 Average Cell Diameter of 3D HepG2 Cells and 2D HepG2 Cells Compared to *In vivo* by ImageJ™ Analysis of H&E images

Cell diameter (µm)		
2D HepG2	**3D HepG2 (Alvetex®Scaffold)**	***In Vivo***
40.0 ± 2.9	13.6 ± 0.6	18.5 ± 1.0

Figure 3.13 quantifies the metabolic activity of HepG2 cells in Alvetex®Scaffold throughout the culture period using the MTT assay. An increase in MTT absorbance is observed as the culture period progresses, suggesting that the 3D scaffold microenvironment also supports proliferation of HepG2 cells in a similar manner to 2D.

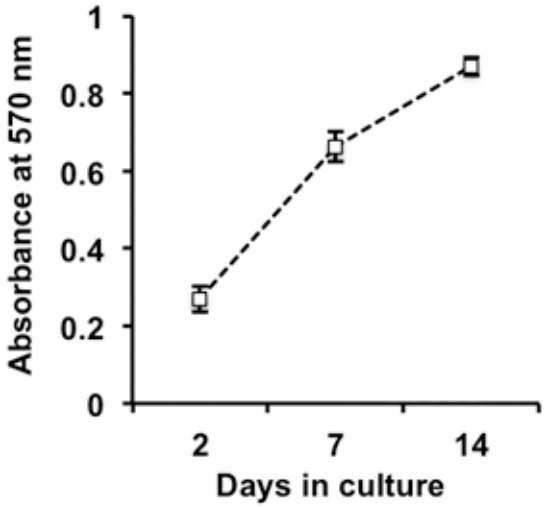

Figure 3.13 Metabolic activity (MTT assay) across the culture period for 3D HepG2 cells in Alvetex®Scaffold. Data represent mean ± s.e.m (n=3).

The above results show that HepG2 cells successfully adhere, migrate and proliferate in Alvetex®Scaffold during a 14 day culture period using the insert/Petri-dish/submerged format. Furthermore cells appear healthy and to be adopting a structure close to that of *in vivo* hepatocytes. However, the Petri-dish format may not be ideally suited for all cell culture applications. The large volumes of culture media required for each dish (70 mL) can be expensive if using specialised media. Similarly the sharing of media between three scaffold inserts may be problematic for certain media-based assays. Consequently, offering alternative, more high-throughput formats of the scaffold could be beneficial. HepG2 growth was therefore assessed using Alvetex®Scaffold in the insert/6-well plate/submerged format, which employs only 8 mL of culture media per scaffold insert.

Figure 3.14 shows the growth profile of HepG2 cells in the insert/6-well plate/submerged format after 14 days culture. HepG2 cells in the 6-well plate appear healthy with no signs of cell death (Figure 3.14A), similar to that of the Petri dish (Figure 3.14B). A small decrease in cell penetration (ca. 40 % vs. 55 %) and density can be seen for the 6-well plate compared to the Petri-dish, suggesting that volume and/or sharing of media supply enhances HepG2 migration and proliferation in the scaffold. The metabolic activity of the cells (Figure 3.14C), determined by the MTT assay, is very similar between the two formats.

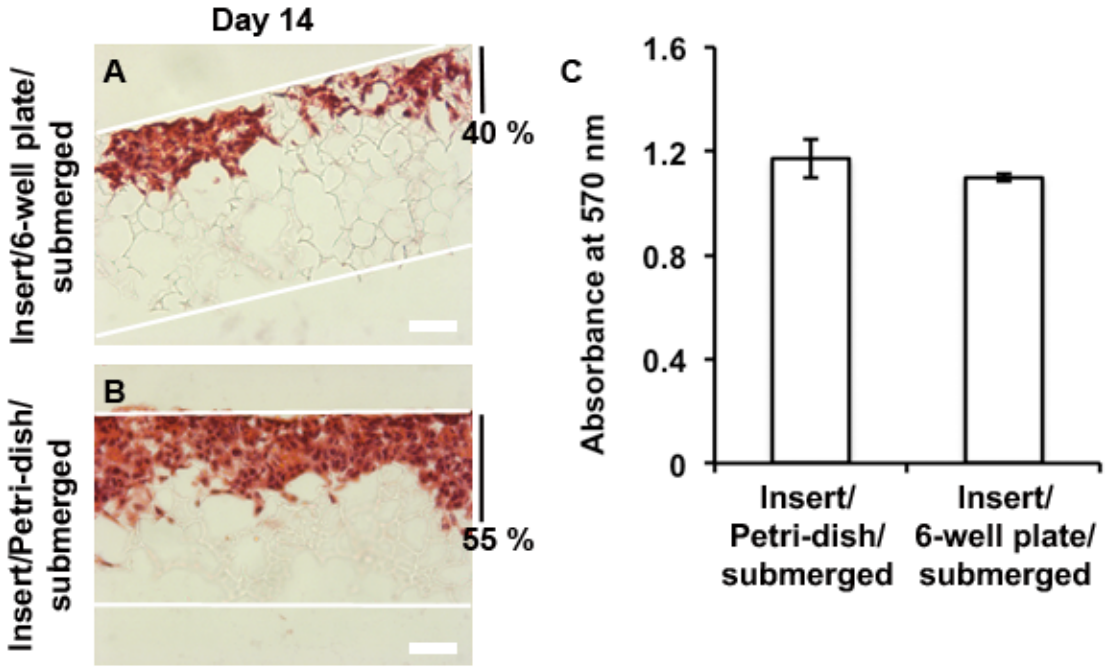

Figure 3.14 HepG2 growth in Alvetex®Scaffold after 14 days using an insert/6-well plate/submerged format compared to insert/Petri-dish/submerged format. (A,B): H&E staining showing a slight decrease in HepG2 penetration (ca. 40 % vs. 55 %) for the 6-well plate compared to the Petri-dish. Scale bars = 50 μm. (C): MTT assay showing a similar absorbance between the two formats. Data represents mean ± s.e.m (n=3).

Additional scaffold presentations employing even smaller volumes of culture media were then investigated, namely; (1) insert/12-well plate/submerged (4mL), (2) insert/12-well plate/contact (2 mL) and (3) 24-well plate (1 mL). Figure 3.15 shows the growth of HepG2 cells under each of these culture conditions after 2, 7 and 14 days culture. All insert formats show a gradual increase in cell penetration into the membrane as the culture period progresses, consistent with the above experiments. Cells in the insert/12-well plate/submerged format appear healthy with no signs of necrosis (Figure 3.15B,J,F), suggesting that as little as 4 mL of media (changed every 2-3 days) is sufficient to support extensive 3D HepG2 growth. However, a slightly lower penetration and cell density is observed for the insert/12-well plate/submerged format compared to that of the insert/Petri-dish/submerged format (see Figure 3.17). It can therefore be assumed that the large volume of media offered by the Petri dish is not critical for healthy 3D HepG2 growth, but does offer an environment for increased proliferation and migration that may be more suited to 3D cell migration and invasion models.

Surprisingly, a noticeably higher cell density was observed for the insert/12-well plate/contact format compared to the other insert formats after 14 days (see Figure 3.15K and Figure 3.17B),

even though this format only employs 2 mL of media from underneath the insert. Cells in this format appear very tightly packed with extensive opportunity for cell-cell contact, approximating native liver tissue density. This growth profile may be explained by surface tension at the air-liquid interface that serves to pull cells together. Alternatively, reduced cell loss from turbulent media changes may also contribute. However, possible cell necrosis is observed after 7 and 14 days culture using this scaffold presentation, seen by the condensed nuclei and increased eosinophilia near the top portion of the membrane (see white arrows in Figure 3.15G,K and the higher magnification image of Figure 3.16). It is likely this is due to restricted media supply, with those cells close to the media supply restricting nutrients and oxygen from reaching those cells growing above.

Unlike the insert formats, the 24-well plate format does not appear to encourage a gradual increase in cell penetration, with cells remaining in the top 20 - 40 % of the membrane even after 7 and 14 days (Figure 3.15H,L). Indeed, growth in this format does not effectively approximate native liver growth after 7 days due to the low cell density and poor migration. This behaviour may be explained by the absence of culture media entering from underneath the membrane, therefore offering cells no incentive to migrate downwards and fill out the scaffold.

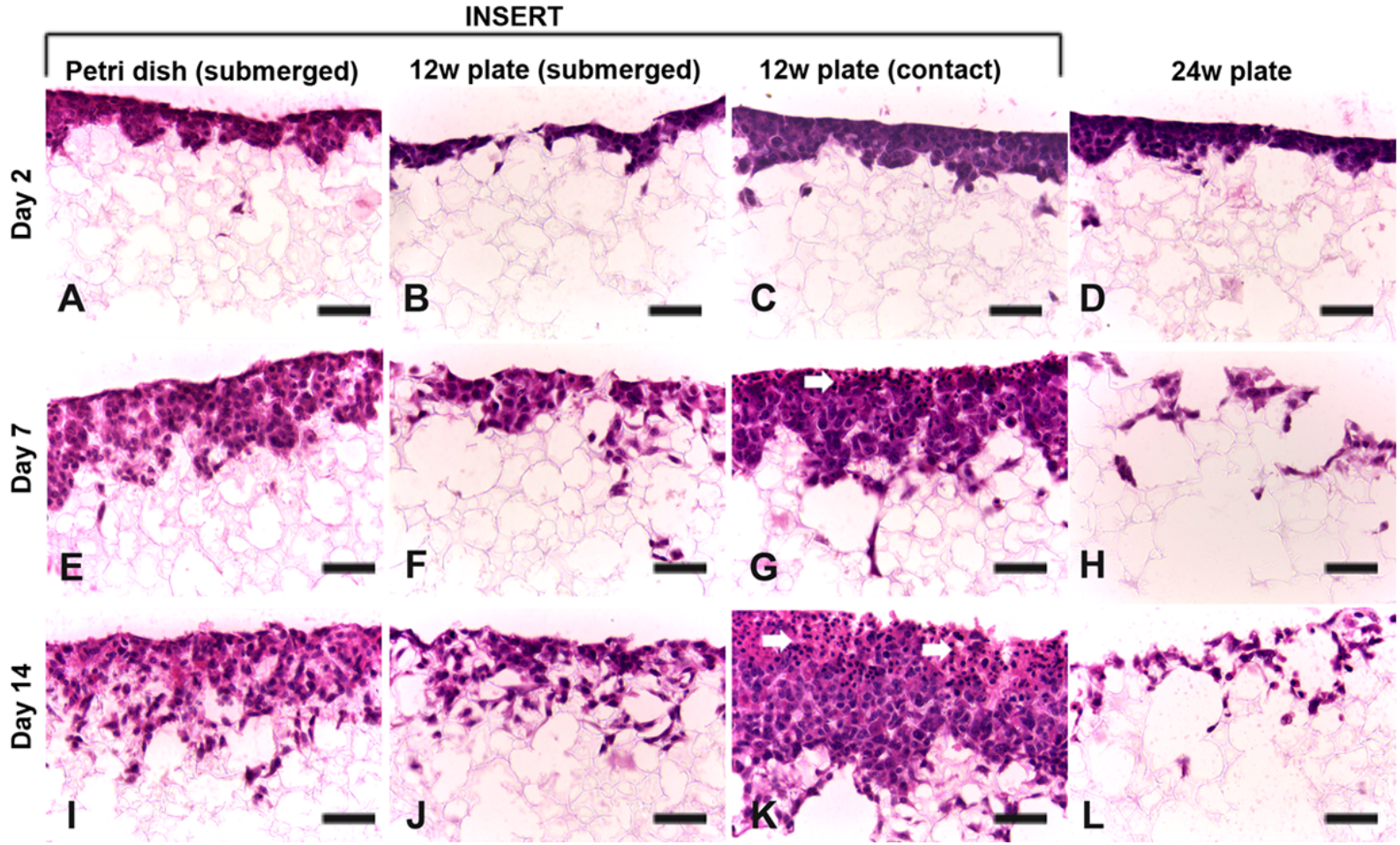

Figure 3.15 HepG2 growth in different Alvetex®Scaffold product presentations after 2, 7 and 14 days culture by H&E staining. A general increase in cell penetration and cell density is observed for all insert cultures but not for the 24-well plate format. The insert/12-well plate/contact format encourages particularly high cell densities but at the expense of possible cell necrosis (white arrows in G,K). Scale bars = 50 μm.

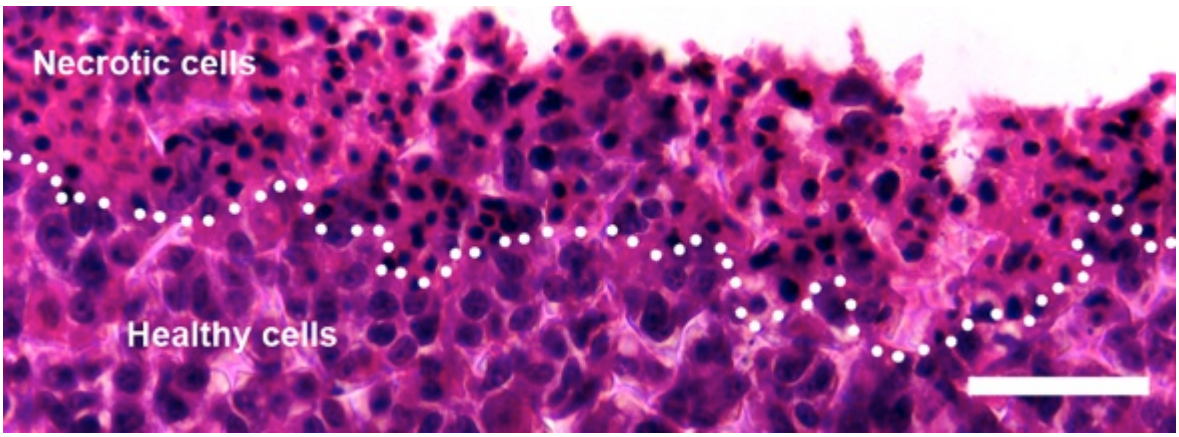

Figure 3.16 HepG2 necrosis in Alvetex®Scaffold using the insert/12well plate/contact format after 14 days culture. Possible necrotic cells close to the air-liquid interface (above the white dotted line) are observed, evident by the condensed nuclei and increased eosinophilia of these cells. Scale bar = 50 μm.

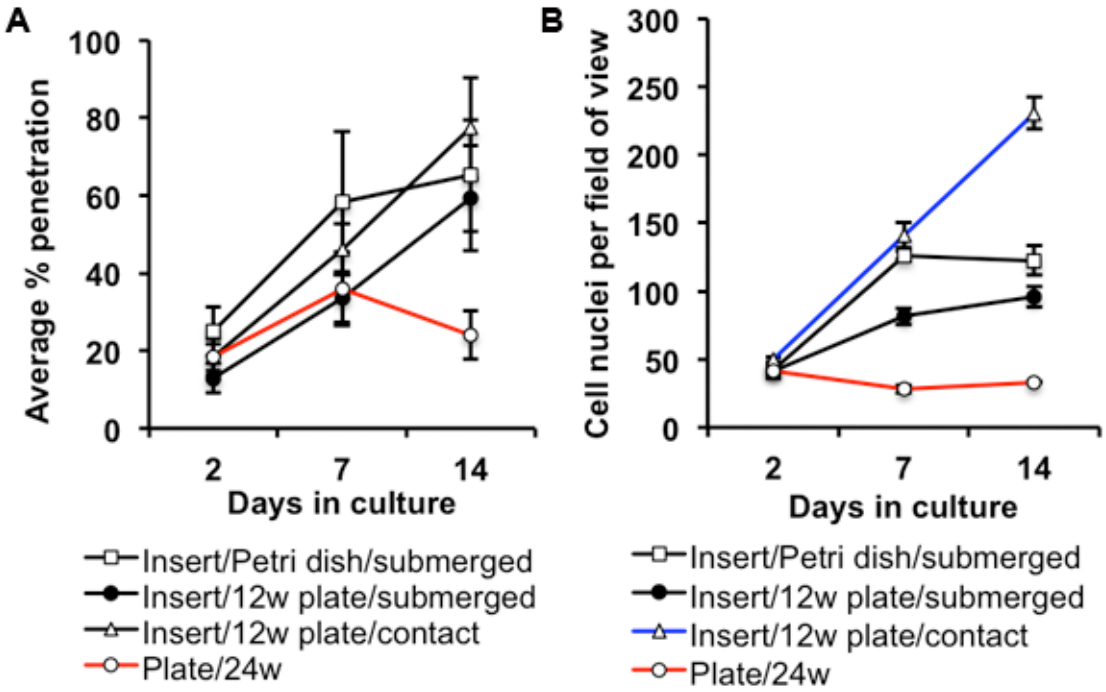

Figure 3.17 Quantification of HepG2 penetration and density obtained from measurements of H&E images in Figure 3.15. (A): HepG2 penetration showing that insert cultures support penetration into the scaffold whereas 24-well plate cultures do not. (B): HepG2 density (nuclei per field of view) showing the insert/12-well plate/contact culture has the highest cell density after 14 days. The 24-well plate format has the lowest cell density out of all the formats and does not effectively approximate *in vivo* density. Data represents mean ± s.e.m (n=15).

Having successfully grown HepG2 cells on Alvetex®Scaffold, Upcyte® cells were then assessed. The insert/6-well plate/submerged format was chosen for this experiment. Cells were thawed

from frozen and then seeded onto Alvetex®Scaffold at a density of 0.5 million cells in 100 μL. Cells were left for 2 hours to adhere and then 8 mL of Upcyte® Culture Media was added. Cells were cultured for up to 21 days and the growth profile assessed.

Figure 3.18 shows the histological analysis of Upcyte® hepatocytes growing on Alvetex®Scaffold. Most cells appeared healthy after 3 and 7 days culture, suggesting that the scaffold microenvironment is suitable for Upcyte® adhesion and survival. However after 14 days culture, a few necrotic cells were observed (black arrow in Figure 3.18C). This may be expected given the limited proliferation capacity of these cells observed after 7 days culture in 2D. Additional histological analysis was performed using thin (1 μm) sections and TBO staining. The image in Figure 3.18D shows a higher magnification image of the cells after 7 days culture. The majority of cells appear healthy, with only a small number of necrotic cells being observed (white arrows in Figure 3.18D). Encouragingly, the cells are adopting several polygonal shapes that offer opportunity for multi-directional communication with other cells.

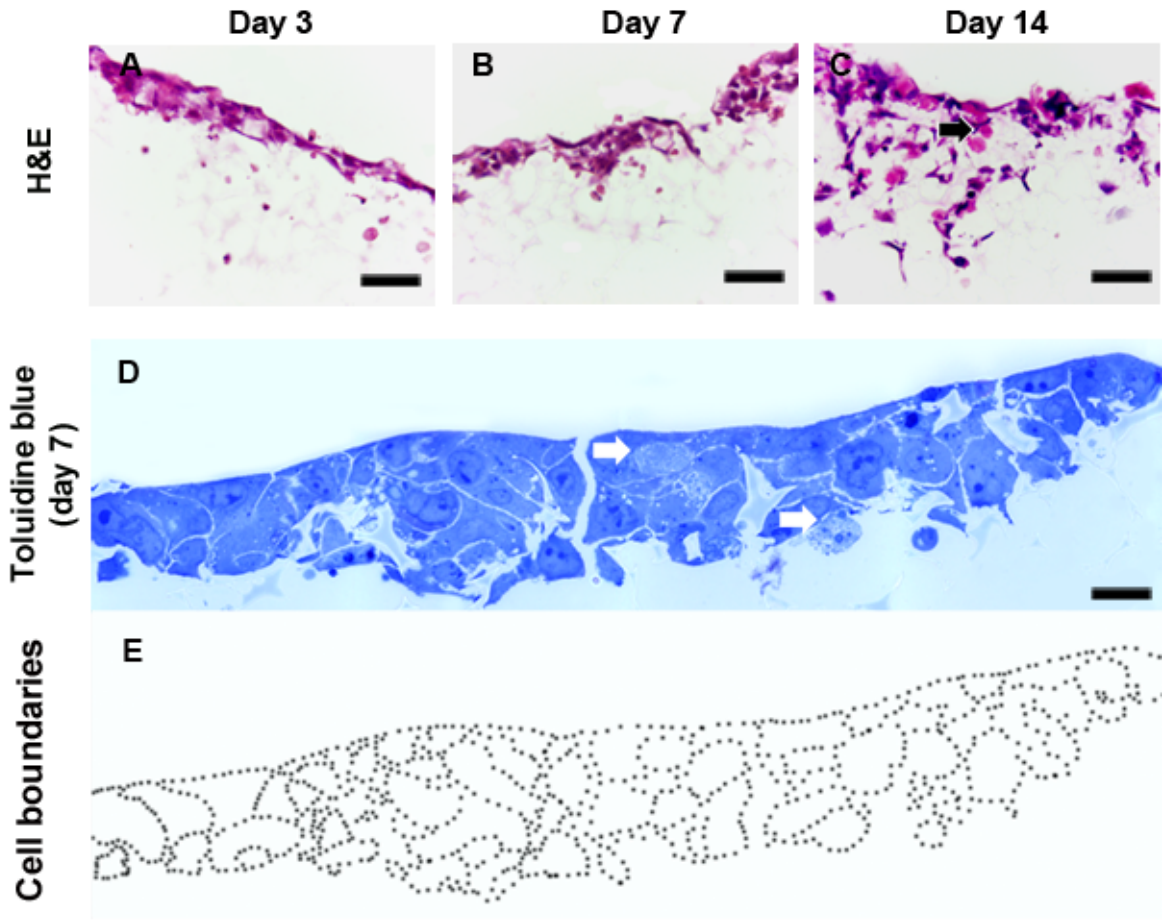

Figure 3.18 Growth of Upcyte® hepatocytes in Alvetex®Scaffold by histological analysis. (A-C): H&E images showing that most cells appear healthy after 3 and 7 days, however after 14 days several necrotic cells appear (black arrow in C indicates three necrotic cells). Scale bars = 50 μm. (D): Higher magnification montage of 1 μm sections stained with Toluidine Blue O (7 days culture). Most cells appear healthy with only the occasional necrotic cell present (white arrows). Scale bar = 20 μm. (E): Outline of cell boundaries showing the polygonal cell shapes adopted by the cells in the 3D microenvironment.

Quantification of Upcyte® cell diameter from ImageJ™ analysis of H&E images is shown in Figure 3.19 and Table 3-4. The 3D cells were found to have a morphology that is very close to *in vivo* cells, unlike 2D Upcyte® cells.

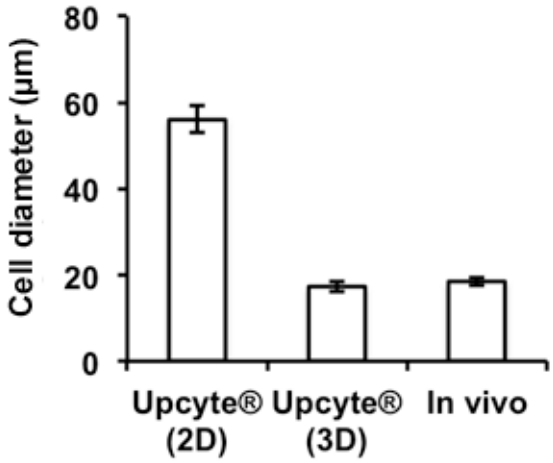

Figure 3.19 Quantifying cell diameter of 3D Upcyte® cells in comparison to 2D and *in vivo* cells by ImageJ™ analysis of H&E images. A similar cell diameter is observed between 3D Upcyte® cells in Alvetex®Scaffold and those *in vivo.* Data represent mean ± s.e.m (n=20).

Table 3-4 Average Cell Diameter of 2D Upcyte® and 3D Upcyte® Compared to *In vivo* by ImageJ™ Analysis of H&E images

Cell diameter (µm)		
2D Upcyte®	**3D Upcyte® (Alvetex®Scaffold)**	***In Vivo***
56.1 ± 3.1	17.3 ± 1.2	18.5 ± 1.0

Upcyte® metabolic activity in Alvetex®Scaffold throughout the culture is shown in Figure 3.20. Interestingly, total cell metabolic activity remains reasonably constant throughout the culture period, even after 21 days. This suggests that the scaffold microenvironment can support some proliferation of Upcyte® cells, even though older cells will inevitably die during the culture period.

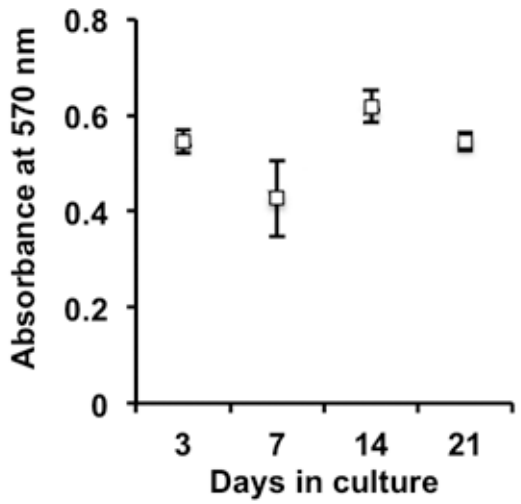

Figure 3.20 Metabolic activity (MTT assay) across the culture period for 3D Upcyte® cells in Alvetex®Scaffold. A reasonably constant metabolic activity is observed throughout the culture period suggesting that the scaffold can support some cell proliferation. Data represent mean ± s.e.m (n=2).

Primary rat hepatocytes were then seeded onto Alvetex®Scaffold and cultured using the insert/12-well plate/submerged and insert/12-well plate/contact formats for 2 days. This short culture period was chosen due to the short survival observed in 2D culture (Figure 3.8). Figure 3.21 shows all cells to be healthy and viable after this short period. Interestingly the insert/12-well plate/contact format encouraged a growth profile of closely packed cells, approximating native human liver tissue density observed in section 3.3.1 (Figure 3.21A), whereas the submerged format did not (Figure 3.21B). Quantification of 3D primary rat hepatocyte diameter from ImageJ™ analysis of H&E images is shown in Figure 3.21C and Table 3-5. The 3D cells were found to have a morphology that is very close to *in vivo* cells, unlike 2D primary cells.

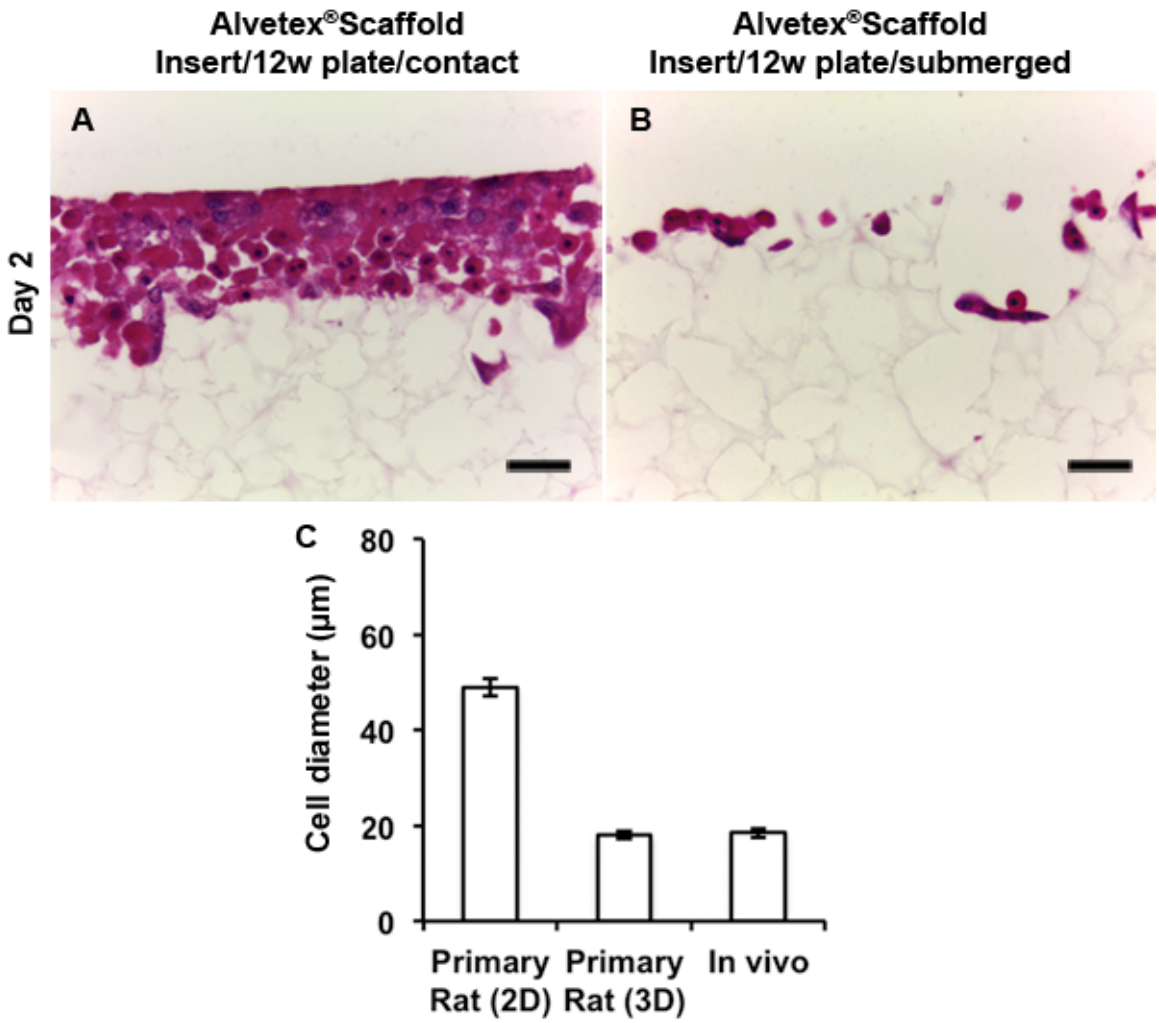

Figure 3.21 Growth of primary rat hepatocytes in Alvetex®Scaffold. (A,B): H&E images after 2 days culture showing most cells are viable. The insert/12-well plate/contact appears more effective at encouraging native tissue density and organisation. Scale bars = 50 µm. (C): Quantification of 3D cell diameter in comparison to 2D and *in vivo* cells by ImageJ™ analysis of H&E images. A similar cell diameter is observed between 3D cells in Alvetex®Scaffold and those *in vivo.* Data represent mean ± s.e.m (n=20).

Table 3-5 Average Cell Diameter of 2D Primary Rat Cells and 3D Primary Rat Cells Compared to *In vivo* by ImageJ™ Analysis of H&E images

Cell diameter (µm)		
2D Rat	**3D Rat (Alvetex®Scaffold)**	***In Vivo***
49.0 ± 1.8	18.0 ± 0.8	18.5 ± 1.0

In summary, this results section has shown that HepG2 cells, Upcyte® hepatocytes and primary rat hepatocytes can all grow and survive within the 3D scaffold microenvironment and approximate *in vivo* cell shape. The insert presentation seems to encourage HepG2 proliferation and migration into the material to promote a 3D tissue type organisation. The 24-well plate

format supports healthy cell growth, but does not effectively encourage migration and proliferation of HepG2 cells. Interestingly, contact insert cultures encourage cells to grow in a tightly packed manner that approximates native human liver tissue density observed in Figure 3.6.

3.3.4 Hepatocyte Growth on Alvetex®Strata

Unlike Alvetex®Scaffold, at the start of this thesis Alvetex®Strata had not been developed by *Reinnervate*. Indeed the initial cell culture experiments that led to the commercial (quality-controlled) development of Alvetex®Strata came from this study using prototype materials supplied by the Cameron group at Durham University (courtesy of Dr. D. W. Johnson) or the *Reinnervate* development team (courtesy of Mr. S. Padbury). These prototypes were therefore used in preliminary HepG2 growth experiments until the commercial material became available.

The first experiment involved culturing HepG2 cells on a prototype material using the insert/6-well plate/contact format. The contact format was chosen to prevent those cells growing on top of the membrane from being washed away during turbulent media changes. As with Alvetex®Scaffold, the material had to be first rendered hydrophilic with 70 % ethanol and PBS washing before seeding cells. Cells were then seeded at a density of 0.5 million cells in 25 μL of MEM. This low seeding volume of 25 μL (compared to 100 μL for Alvetex®Scaffold) was chosen in an attempt to aggregate cells as quickly as possible and thus prevent cells from penetrating into the material. Cells were left to adhere for 2 hours at 37 ^{o}C and 5 % CO_2 before 4 mL of MEM was added from underneath to contact the membrane.

Figure 3.22 shows the growth profile of HepG2 cells cultured for up to 14 days on Alvetex®Strata using the insert/6-well plate/contact format. Cells grow on top of the membrane in a thick tissue-like structure, closely resembling *in vivo* liver tissue density. The cells are densely packed with significant opportunity for cell-cell interaction. As the culture period progresses the average thickness of the tissue structure increases from 47 ± 3.5 μm (day 2) to 109 ± 3.6 μm (day 7) to 180.0 ± 3.8 μm (day 14) (n=10 at each time point), as shown in Figure 3.23. However, signs of necrosis are present at day 7 and day 14, evident by the increased eosinophilia and condensed nuclei (Figure 3.24). These necrotic cells are near the top portion of the tissue structure, furthest from the media supply and closest to the air-liquid interface. The white dotted lines in Figure 3.24 show the distinct interface between healthy and necrotic cells. As with contact cultures using Alvetex®Scaffold, it is expected that restricted media supply is the cause of this cell necrosis.

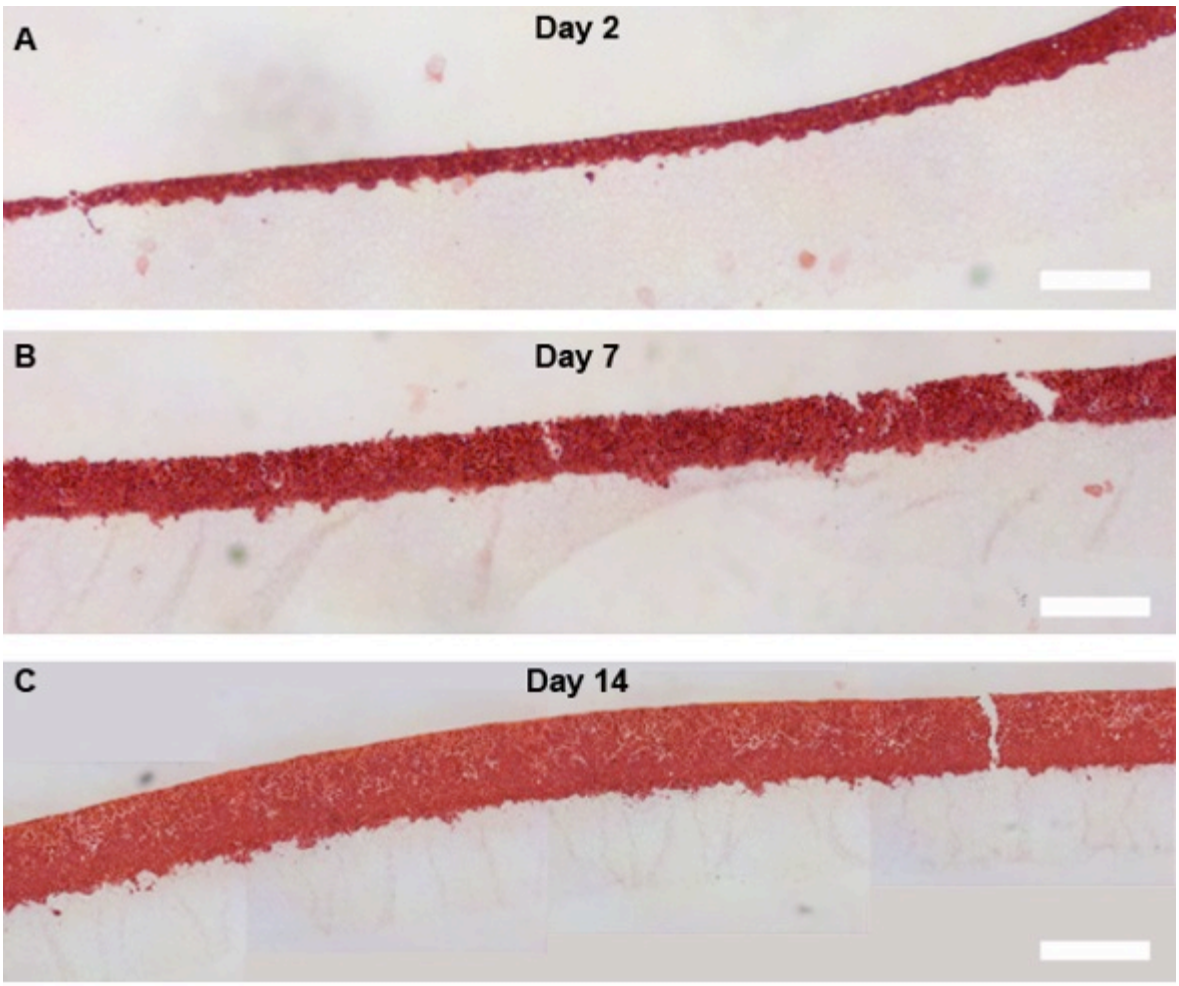

Figure 3.22 Growth of HepG2 cells on Alvetex®Strata using the insert/6-well plate/contact format. (A-C): Montage images showing HepG2 cells growing on top of the material forming a tissue-type structure. The thickness of the tissue increases as the culture period progresses. Scale bars = 200 μm.

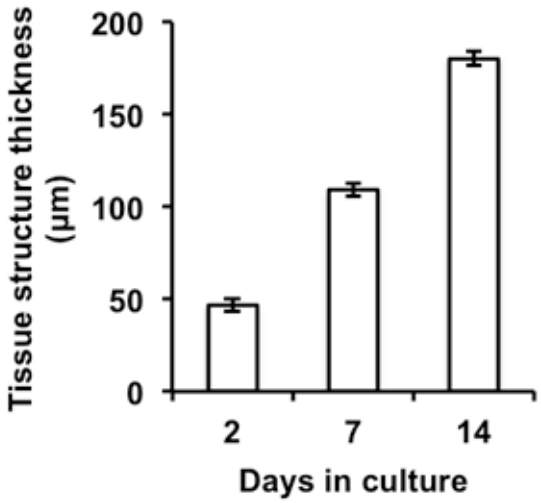

Figure 3.23 HepG2 tissue structure thickness on top of Alvetex®Strata measured from H&E images using the insert/12-well plate/contact format. Data represent mean ± s.e.m (n=10).

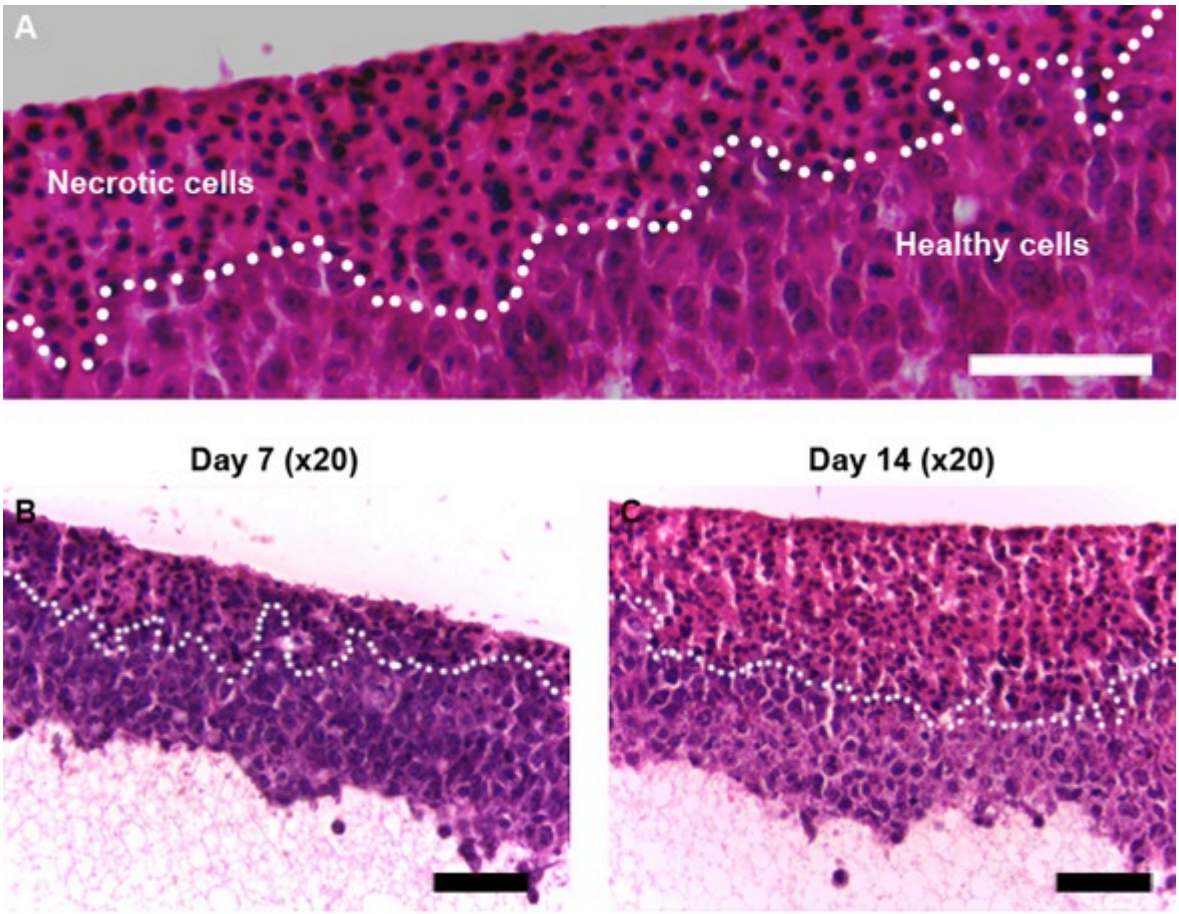

Figure 3.24 HepG2 necrosis in Alvetex®Strata using the insert/12well plate/contact format. (A): Necrotic cells closest to the air-liquid interface are observed by the condensed nuclei and increased eosinophilia (data represents 14 days). (B,C): Day 7 and day 14 cultures at lower magnification showing signs of cell necrosis. The white dotted line represents an interface between healthy and necrotic cells. Scale bar = 50 μm.

To confirm that the cells near the top portion of the membrane are non-proliferative (therefore potentially dying), immunofluorescence staining for Ki-67 (proliferation marker) was employed. It was hypothesised that those cells that appear necrotic in the H&E images would not be proliferating and would also show condensed nuclei via DAPI, or Hoechst 33342 (*Life Technologies*) counterstaining. HepG2 cells were therefore cultured for 2, 7 and 14 days on prototype Alvetex®Strata and then processed for Ki-67 immunofluorescence staining. AlexaFluor® 488 (*Life Technologies*) was used as the secondary antibody for the Ki-67 antibody.

Figure 3.25 shows the Ki-67 immunofluorescence data. At 2 days culture (average tissue thickness of 47 ± 3.5 μm) all nuclei appear normal and there is positive Ki-67 staining throughout the tissue structure (Figure 3.25D). The staining at day 7 is very similar (average tissue thickness of 109 ± 3.6 μm, although this particular sample used for staining has a greater tissue thickness than the

average; believed to be due a slanted sample mounting during histological processing). Encouragingly, positive Ki-67 staining is observed throughout the majority of the tissue at day 7 (Figure 3.25E). However, a significant change is observed at day 14 (Figure 3.25F). Nuclei near the top portion of the tissue are very condensed, further supporting that these are necrotic. The Ki-67 staining is also restricted to the bottom portion of the tissue, supporting the hypothesis that those cells near the air-liquid interface are necrotic.

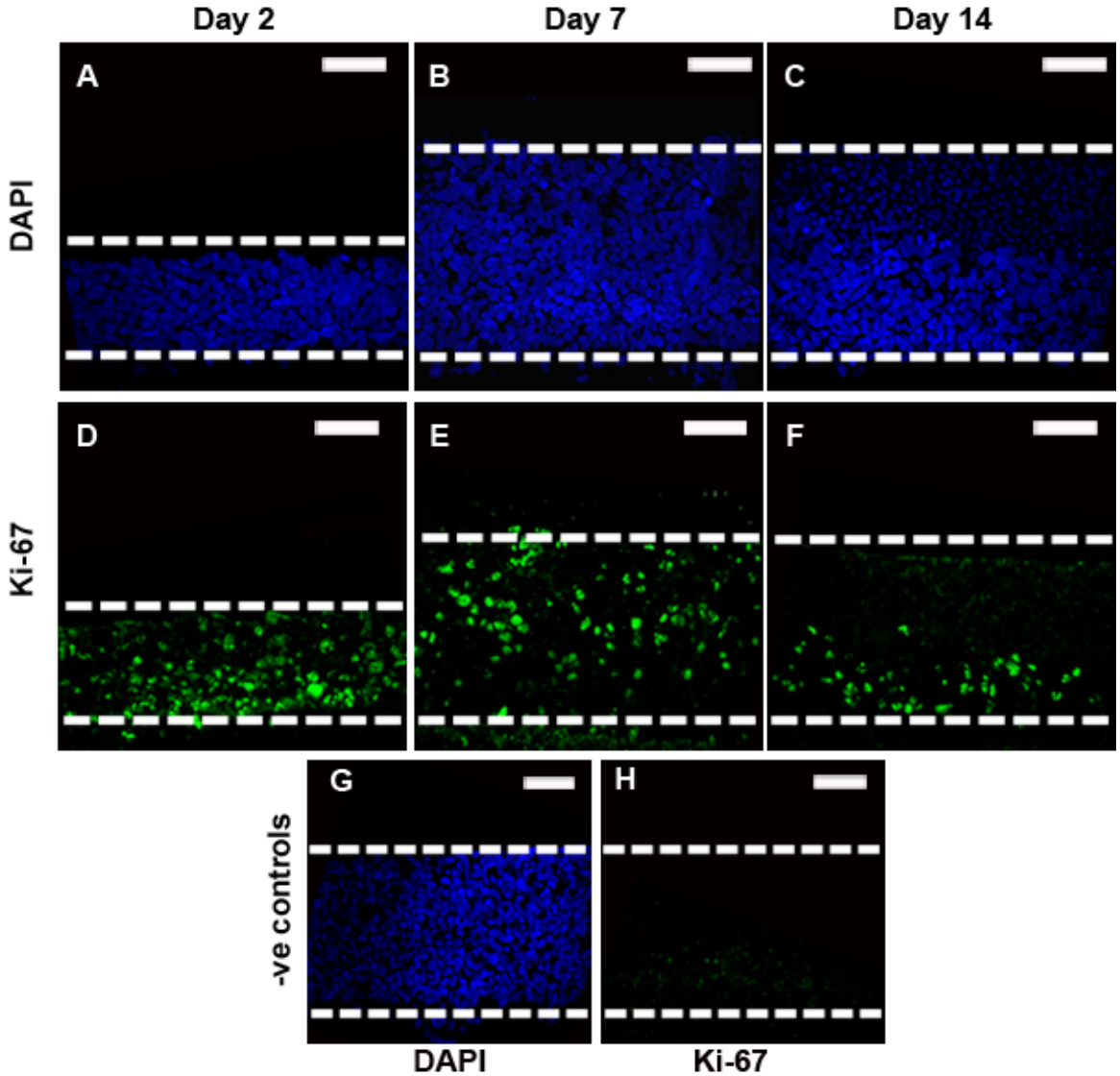

Figure 3.25 Ki-67 expression in HepG2 cells growing on top of Alvetex®Strata. (A-C): DAPI counterstaining of HepG2 nuclei. (D-F): Ki-67 staining where positive green dots correspond to proliferating nuclei. (G-H) Negative controls. At day 2 (A,D) and day 7 (B,E) proliferating cells appear throughout the tissue structure. However at day 14 (C, F), proliferating cells are restricted to the bottom portion of the tissue that is closest to the media supply. Smaller, condensed nuclei are observed in the top portion of image C which further supports cell necrosis of cells close to the air-liquid interface. Scale bars = 50 μm.

The formation of a thick hepatocyte tissue structure on the top of Alvetex®Strata that resembles native liver growth could be highly beneficial for enhancing cell-cell contact and thus cellular function *in vitro*. However, for longer-term cultures necrotic cells near the top portion of the tissue are undesirable. In an attempt to reduce cell necrosis near the top portion of the tissue, two strategies were employed. Firstly, the thickness of Alvetex®Strata was reduced from 200 μm to 150 μm, 100 μm or 60 μm to potentially increase the amount of media reaching the cells. Secondly, submerged cultures were employed. Submerged insert cultures were expected to produce healthy cell growth (based on previous results with Alvetex®Scaffold), although were also expected to reduce dense-tissue formation due to loss of surface tension and/or increased turbulent media changes. The outcomes of these two strategies to reduce cell necrosis will now be discussed.

The *Reinnervate* development team provided prototype Alvetex®Strata sectioned into membranes of thickness 150 μm, 100 μm and 60 μm. HepG2 cells were then cultured on these materials for 7 and 14 days using the insert/6-well plate/contact format and assessed for cell necrosis.

Figure 3.26 show that all cultures, including those on thin 60 μm membranes, display signs of necrosis after 7 and 14 days. Similar to 200 μm membranes, necrotic cells are restricted to the top portion of the tissue, furthest away from the culture media. These data suggest that reducing Alvetex®Strata membrane thickness has little effect on preventing cell necrosis. Once more, the thinner membranes were more difficult to process for histology compared to the 200 μm membranes (increased fragility). Consequently a decision was made to keep the membrane thickness at 200 μm.

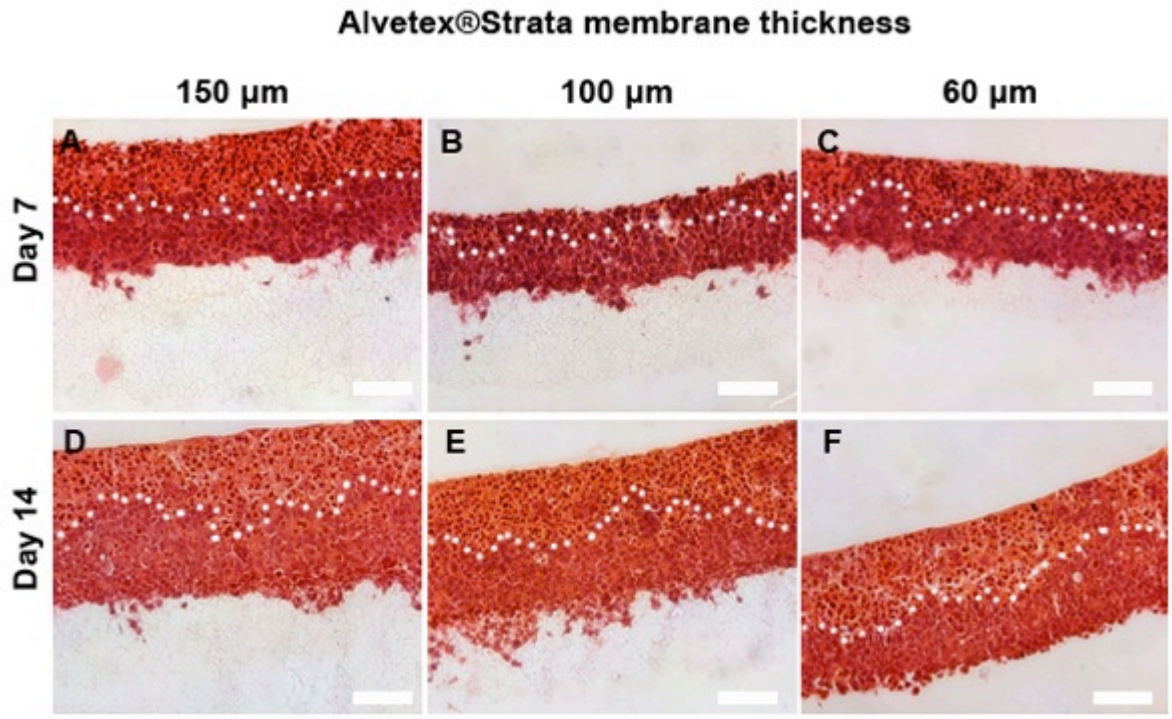

Figure 3.26 Effect of Alvetex®Strata membrane thickness on HepG2 necrosis. (A-C): H&E staining after 7 days culture. (D-F): H&E staining after 14 days culture. All cultures show signs of necrosis in the top portion of the tissue (above white dotted lines), suggesting that reduced membrane thickness has little effect on reducing cell necrosis. Scale bars = 50 µm.

The second strategy to reduce cell necrosis on Alvetex®Strata was to employ an insert/6-well plate/submerged format. It was hypothesised that supplying culture media from above and below the membrane would prolong the survival of healthy cells growing in the tissue structure. Figure 3.27 shows the growth profile after 2, 7 and 14 days culture. All cells appear healthy with no signs of necrosis, even after 14 days culture. However, unlike the contact cultures, very few cells are present on top of the material. The only cells that remain are those that have penetrated into the top portion of the material, giving a growth profile similar to Alvetex®Scaffold. Quantification of tissue thickness and cell density between the contact and submerged cultures are shown in Figure 3.28. A significantly smaller ($p<0.005$) tissue thickness is observed for the submerged format that is amplified as the culture period progresses. The number of cell nuclei per field of view is also smaller for the submerged culture, which again is amplified as the culture period progresses.

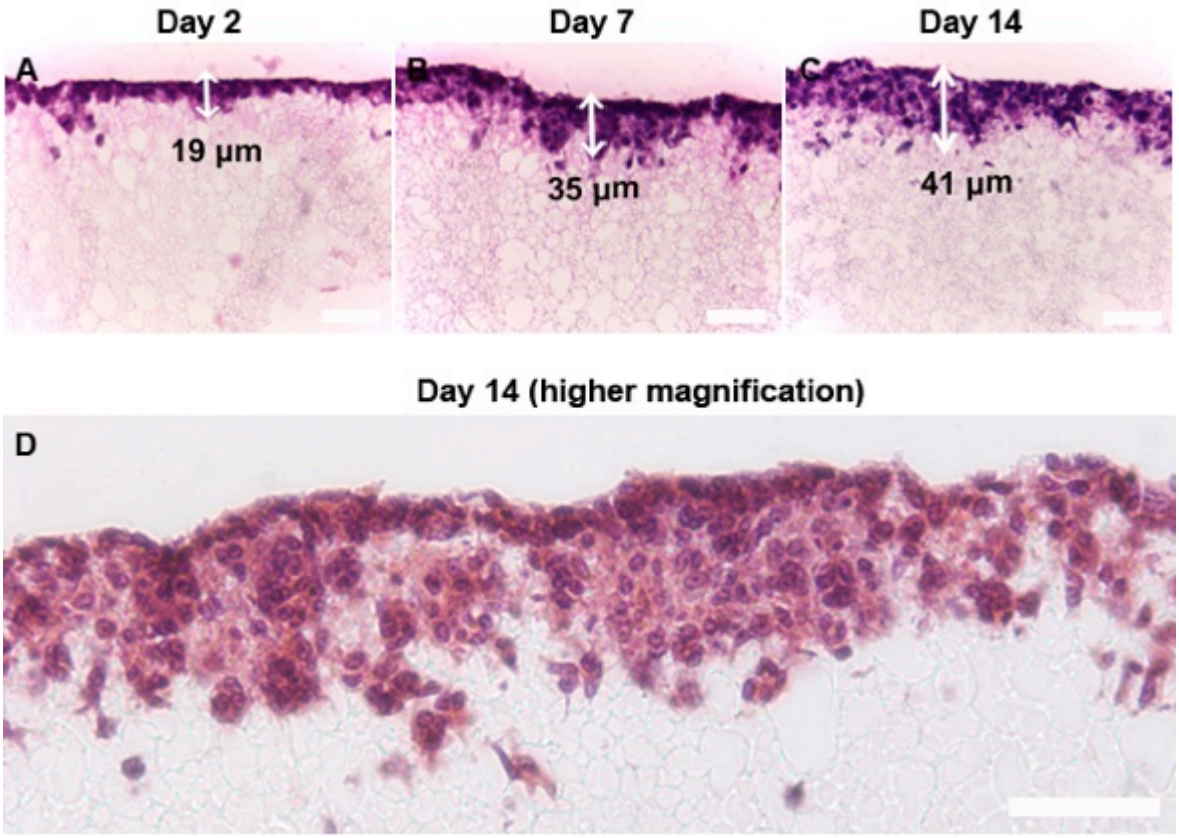

Figure 3.27 Growth of HepG2 cells on Alvetex®Strata using the insert/6-well plate/submerged format. (A-C): H&E images after 2, 7 and 14 days culture. Unlike contact cultures, very few cells are growing on top of the membrane. (D): Higher magnification H&E image after 14 days culture. All cells appear healthy but very little growth on top of the scaffold is occurring. Scale bars = 50 µm.

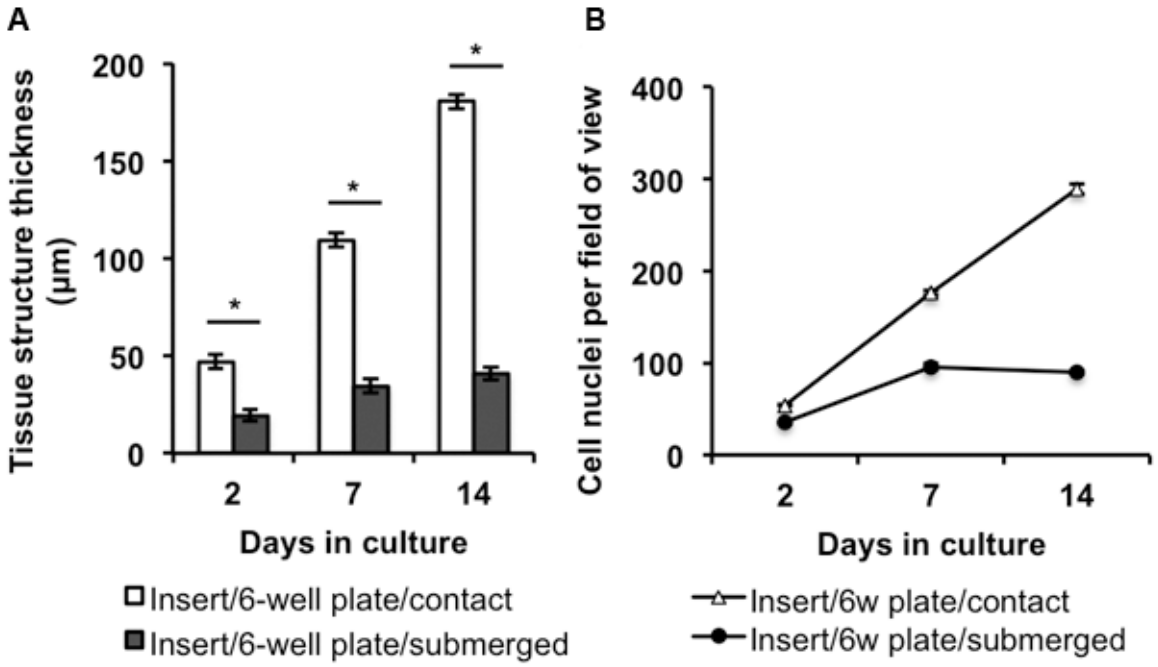

Figure 3.28 Quantification of HepG2 growth profiles using submerged and contact cultures on Alvetex®Strata. (A): Tissue structure thickness showing that contact cultures enable much thicker cell growth on top of the scaffold. Data represent mean ± s.e.m (n=10). *Denotes $p<0.005$ according to the *Student's t-test.* (B): Cell nuclei per field of view showing a much greater cell density for contact cultures. Data represent mean ± s.e.m (n=5).

To help understand the difference in tissue structure thickness and cell density between submerged cultures and contact cultures, the bottom of the 6-well plates housing the scaffold inserts were analysed for residual/lost cells after a media change. Figure 3.29 shows the Neutral Red (Sigma) staining of the plates used to house submerged and contact scaffold inserts. The submerged format shows an abundance of cells on the bottom of the 6-well plate, suggesting that the media change has washed cells from the Alvetex®Strata insert. Conversely no cells were found on the bottom of the 6-well plate for the contact format. This indicates that submerged media changes contribute to cell loss, which may be due to media turbulence or lack of surface tension that serves to keep cells in a more robust organisation. Note that both inserts were placed in fresh, clean 6-well plate prior to the media change.

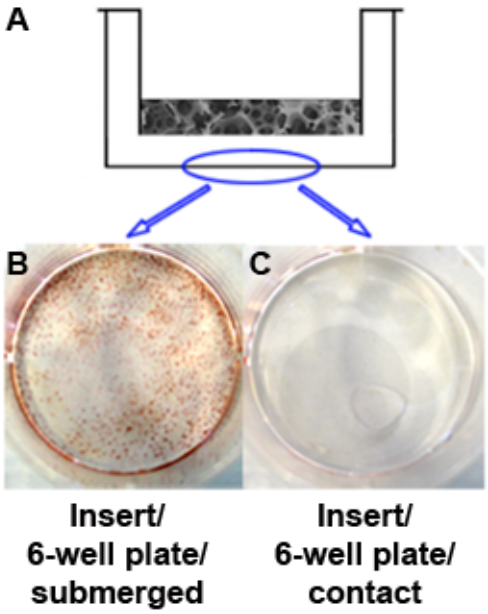

Figure 3.29 Residual HepG2 cells found on the bottom of a 6-well plate after culture on Alvetex®Strata using insert/6-well plate/submerged and insert/6-well plate/contact formats. (A): Illustration showing what is being assessed (blue circle is bottom of the 6-well plate). (B,C): Neutral red staining of HepG2 cells on the bottom of the 6-well plate. More cells are found for the submerged cultures (B) compared to contact cultures (C), suggesting more cells are being washed off the insert in submerged cultures during media changes.

Primary rat hepatocytes were also cultured on Alvetex®Strata and the growth profile assessed after 2 days, as shown in Figure 3.30. All cells appear healthy and are growing on top of the membrane in a similar manner to HepG2.

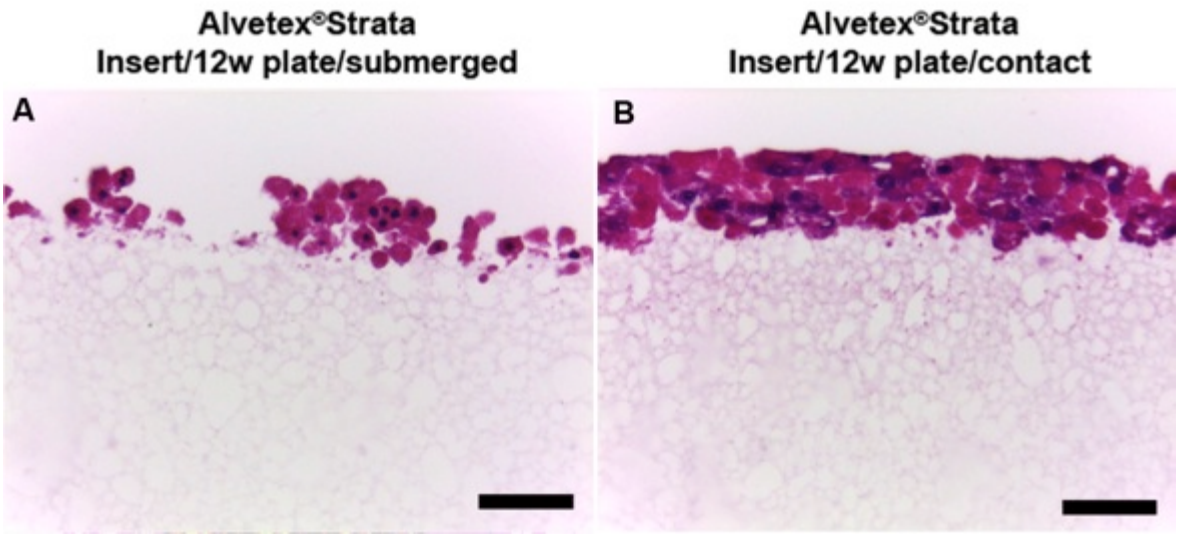

Figure 3.30 Growth of primary rat hepatocytes on Alvetex®Strata after 2 days culture. (A,B): H&E images showing cells are viable. The insert/12-well plate/contact appears much more effective at preserving cell density and organisation. Scale bars = 50 μm.

In summary, this section has shown that Alvetex®Strata can enable dense *in vivo* type hepatocyte growth on top of the membrane, providing that a contact media supply method is employed. However, after 7 and 14 days culture, cells in the top portion of the tissue display signs of necrosis (furthest from media and closest to the air-liquid interface), which is undesirable. Prior to this cells appear healthy and so this culture method could offer a viable short-term 3D *in vitro* model with extensive opportunity for cell-cell contact. Reducing the thickness of the membrane does not reduce this necrosis at the air-liquid interface. Unfortunately submerged cultures do not encourage thick tissue structures on top of the membrane.

3.3.5 Optimising the Scaffold Microenvironment with Protein Coatings

It was hypothesised that coating the scaffold surface with proteins found in the hepatic ECM would provide a more physiologically relevant microenvironment for hepatocyte growth. The two most abundant hepatic ECM proteins are fibronectin and collagen I. Consequently, Alvetex®Scaffold was coated with these proteins and then assessed for residual protein.

Alvetex®Scaffold was first rendered hydrophilic and washed extensively in PBS. After removal of excess PBS, 200 μL of protein solution was applied to the membrane and left for 1 hour. Different concentrations of protein solutions were applied, from 1000 μg/mL to 50 μg/mL. After 1 hour the membranes were re-washed in PBS and then assessed for residual protein via (1) blue staining with Coomassie Brilliant Blue G-250 (*Bio-Rad)*, (2) SEM imaging and (3) confocal immunofluorescence staining using antibodies for fibronectin and collagen I. Figure 3.31 shows the Coomassie Brilliant Blue G-250 staining across the fibronectin and collagen I concentration range. Membranes coated with fibronectin show a gradual increase in blue staining as the coating concentration is increased, suggesting an increase in deposition of the protein with increasing coating concentration. Conversely membranes coated with collagen I show overall weaker staining and only a slight increase in deposition with increasing coating concentration. This suggests that less collagen I is deposited onto the membrane compared to fibronectin, and that higher coating concentrations do not necessarily increase protein deposition.

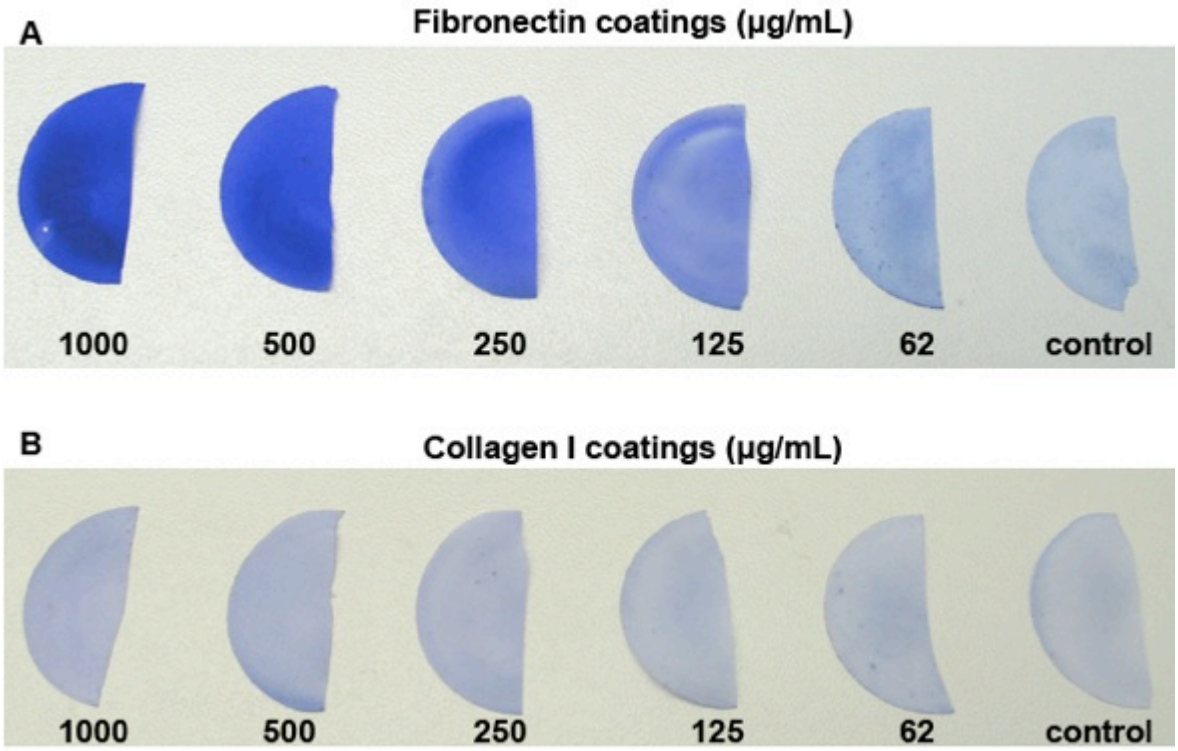

Figure 3.31 Coomassie Brilliant Blue G-250 detection of residual fibronectin and collagen I on Alvetex®Scaffold after applying a coating solution. (A): Fibronectin coatings showing a gradual increase in blue staining (protein deposition) with increasing coating concentration. (B): Collagen I coatings showing much weaker staining and less of an increase in staining with increasing coating concentration. All membranes were treated with Coomassie Brilliant Blue G-250 for 1 hour and then left in de-stain solution overnight before taking images.

SEM analysis of the coated scaffolds is shown in Figure 3.32. Thin films appear to span the voids of the membrane at fibronectin coating concentrations of 1000 µg/mL and 500 µg/mL that are absent in the uncoated control. With 1000 µg/mL, this film is mainly intact, however with 500 µg/mL the film has multiple tears and holes (white arrows in Figure 3.32B). Only small spindle structures appear to be present with a fibronectin coating concentration of 250 µg/mL. These data are consistent with the Coomassie Brilliant Blue G-250 staining for fibronectin, in that higher coating concentrations lead to increased protein deposition on the material. Collagen I coatings do not produce film or spindle structures, but leave small granule-type deposits on the scaffold walls that are absent on the uncoated control (white arrows in Figure 3.32D,E). A similar amount of these deposits were found for coating concentrations of 1000 µg/mL and 50 µg/mL. This is also consistent with the Coomassie Brilliant Blue G-250 staining for collagen I, in that higher coating concentrations do not appear to lead to increased protein deposition on the material.

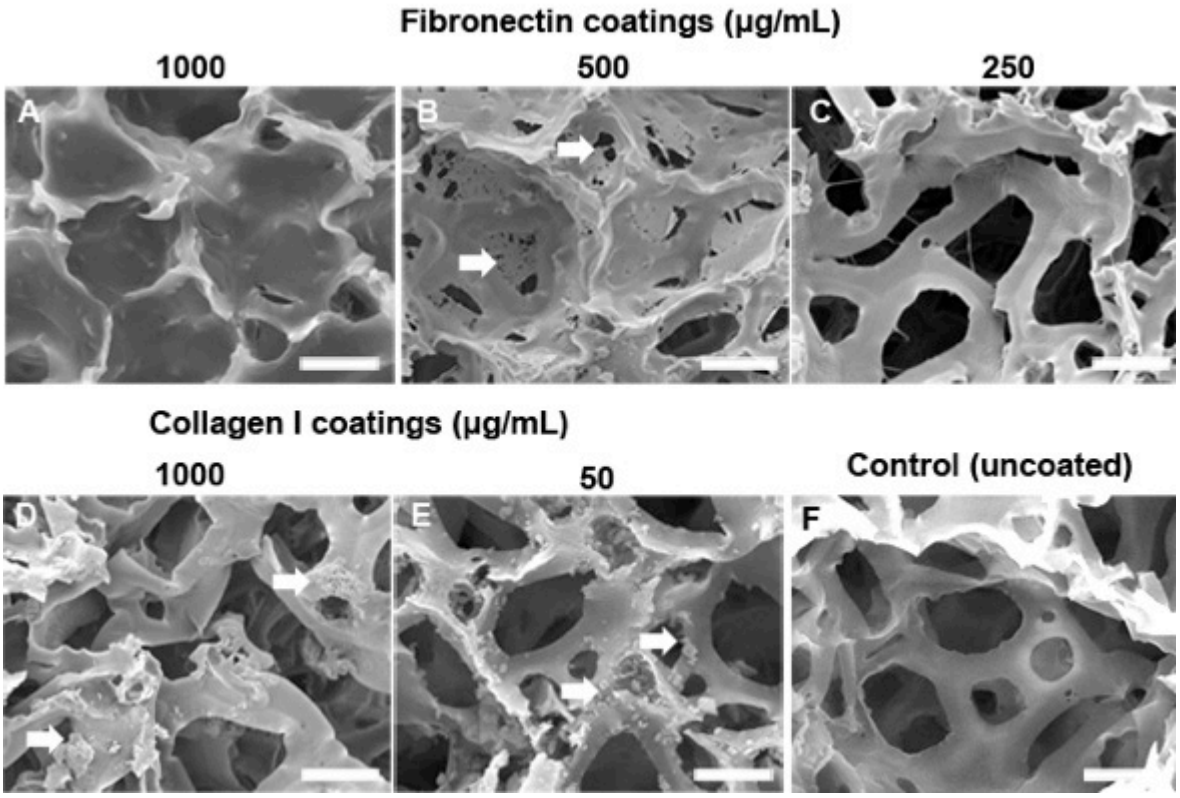

Figure 3.32 SEM analysis of deposited fibronectin and collagen I on Alvetex®Scaffold after applying a coating solution. (A-C): Fibronectin deposition gradually decreases with lower concentrations of coating solution. Higher concentrations show film-like structures whereas lower concentrations show spindle-like structures. (D-E): Collagen I deposition appears similar for the different coating concentrations tested (1000 µg/mL and 50 µg/mL). (F): Uncoated scaffold control. Scale bars = 20 µm.

Final confirmation of deposited fibronectin and collagen I was performed using confocal immunofluorescence. Membranes were coated either with 1000 µg/mL fibronectin, 500 µg/mL fibronectin or 50 µg/mL collagen I and then processed for immunofluorescence using antibodies for fibronectin (Sigma) and collagen I (Sigma). AlexaFluor® 488 (*Life Technologies*) was used as the secondary antibody. Figure 3.33 shows the confocal microscopy images after immunofluorescence processing. A green film (positive staining) can be seen for fibronectin coating concentrations of 1000 µg/mL and 500 µg/mL that are not present on the negative control, confirming that fibronectin has deposited. Note that for fibronectin immunofluorescence Nile Red (Sigma) was used as a hydrophobic dye to stain the scaffold red so that the fibronectin films could be more easily distinguished. A more sporadic positive green staining pattern is observed for collagen I immunofluorescence, consistent with the SEM data. Whilst no film or spindle structures are observed, the data confirms collagen I deposition on the walls of the material.

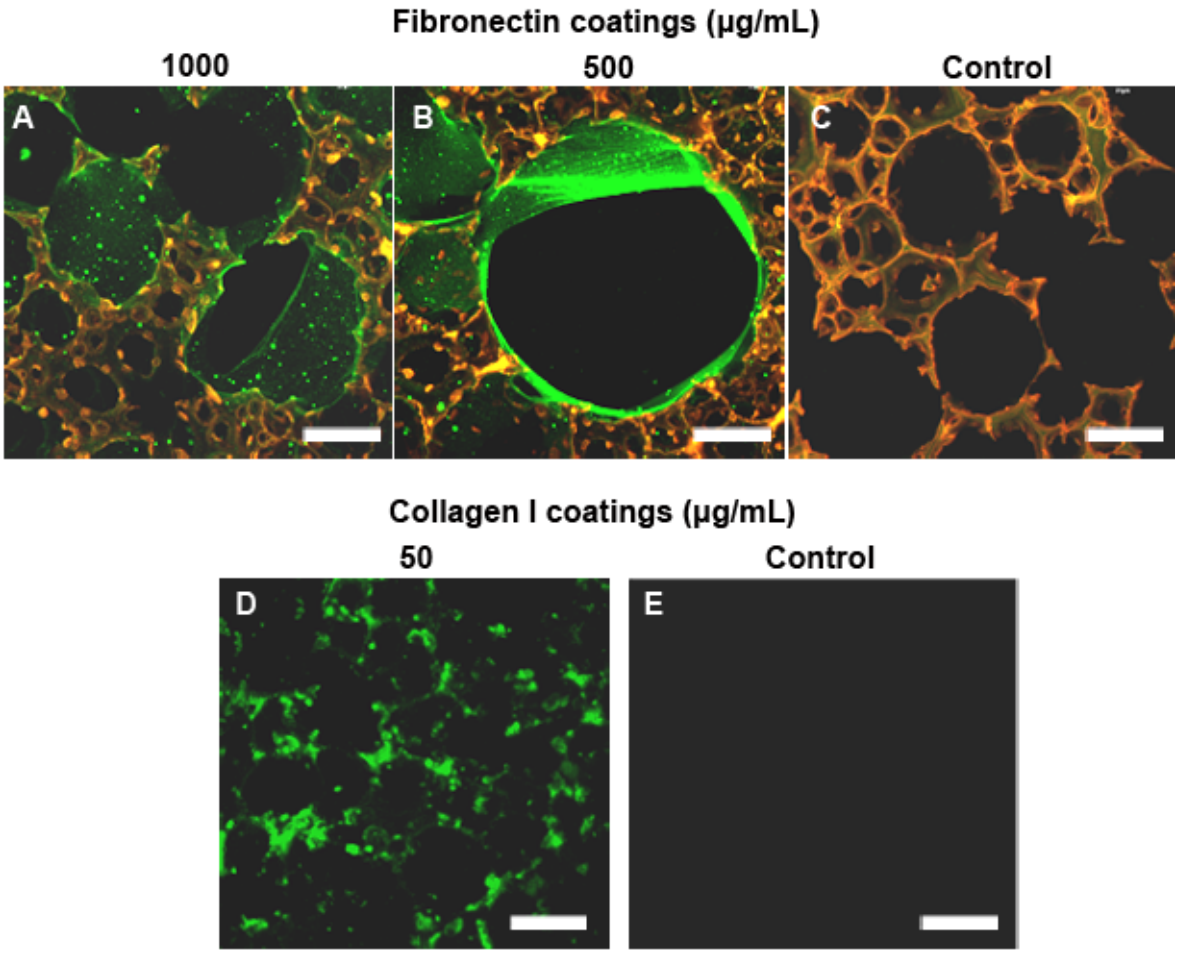

Figure 3.33 Confocal immunofluorescence analysis of deposited fibronectin and collagen I on Alvetex®Scaffold after applying a coating solution. (A-C): Fibronectin deposition observed by the positive green film-like structures which are absent on the negative control. Nile Red was used as a hydrophobic dye to stain the scaffold red so that the film structures could be more easily distinguished. Scale bars = 20 µm. (D-E): Collagen I deposition observed by the patchy green staining. Scale bars = 50 µm. All images are merged optical z-stacks of ca. 20 µm.

In summary, this section has shown that Alvetex®Scaffold can be coated with fibronectin or collagen I, potentially increasing the biochemical relevance of the material. Fibronectin coatings appear to leave film or spindle structures that span the voids of the scaffold, whereas collagen I coatings appear to leave deposited granular structures on the walls of the scaffold. Increasing the concentration of fibronectin seems to increase the amount of deposited fibronectin. Conversely, little difference in collagen I deposition is observed between high (1000 µg/mL) and low (50 µg/mL) coating concentrations.

Having demonstrated that Alvetex®Scaffold can be coated with fibronectin or collagen I, it was then necessary to assess the impact on hepatocyte growth. A fibronectin coating concentration of 1000 µg/mL was chosen, as this was believed to deposit the maximum amount of fibronectin onto

the scaffold. Conversely only a 50 μg/mL collagen I coating concentration was employed, given that very little difference in collagen I deposition was observed for higher coating concentrations. The coatings were applied to four Alvetex®Scaffold product formats, namely: (1) insert/Petri-dish/submerged, (2) insert/12-well plate/submerged, (3) insert/12-well plate/contact and (4) 24-well plate. HepG2 cells were cultured for 2, 7 and 14 days and cell penetration and cell density assessed.

Figure 3.34 shows the impact of fibronectin and collagen I coatings on HepG2 growth using the insert/Petri-dish/submerged format. All cells appear healthy with no signs of necrosis, confirming that the deposited proteins do not hinder cell survival. At day 2, HepG2 cells have penetrated much further into the collagen I scaffold compared to the fibronectin and uncoated scaffolds. Only a slight increase in cell penetration can be observed for the fibronectin scaffold compared to the uncoated. At day 7, HepG2 cells have already penetrated all the way through the collagen I scaffold, unlike the fibronectin and uncoated scaffolds. These data strongly suggest collagen I enhances HepG2 migration throughout the material. At day 14, HepG2 cells in the fibronectin scaffold appear to have penetrated further than the uncoated scaffold, but still less than those cells in the collagen I scaffold.

Figure 3.35 shows the impact of fibronectin and collagen I coatings on HepG2 growth using the insert/12-well plate/submerged format. An almost identical penetration profile is observed to that of the insert/Petri-dish/submerged format. All HepG2 cells appear healthy and penetrate furthest into collagen I coated scaffolds, followed by fibronectin and then finally the uncoated control.

Figure 3.36 shows the impact of fibronectin and collagen I coatings on HepG2 growth using the insert/12-well plate/contact format. As with the submerged insert cultures, collagen I seems to drive the furthest penetration, however the effect is much lower for these contact cultures. It is hypothesised that collagen I may not be necessary to drive penetration in this case as cells will already want to move downwards towards the media supply entering from underneath. Unfortunately a significant amount of cell necrosis is again observed after 14 days culture for those cells growing furthest from the media supply, indicated by the white circles.

Figure 3.37 shows the impact of fibronectin and collagen I coatings on HepG2 growth using the 24-well plate format. Unlike the submerged insert cultures, collagen I only drives a very small increase in cell penetration. It is expected that the lack of media entering from underneath the membrane still hinders cells from penetrating downwards, even in the presence of an ECM coating.

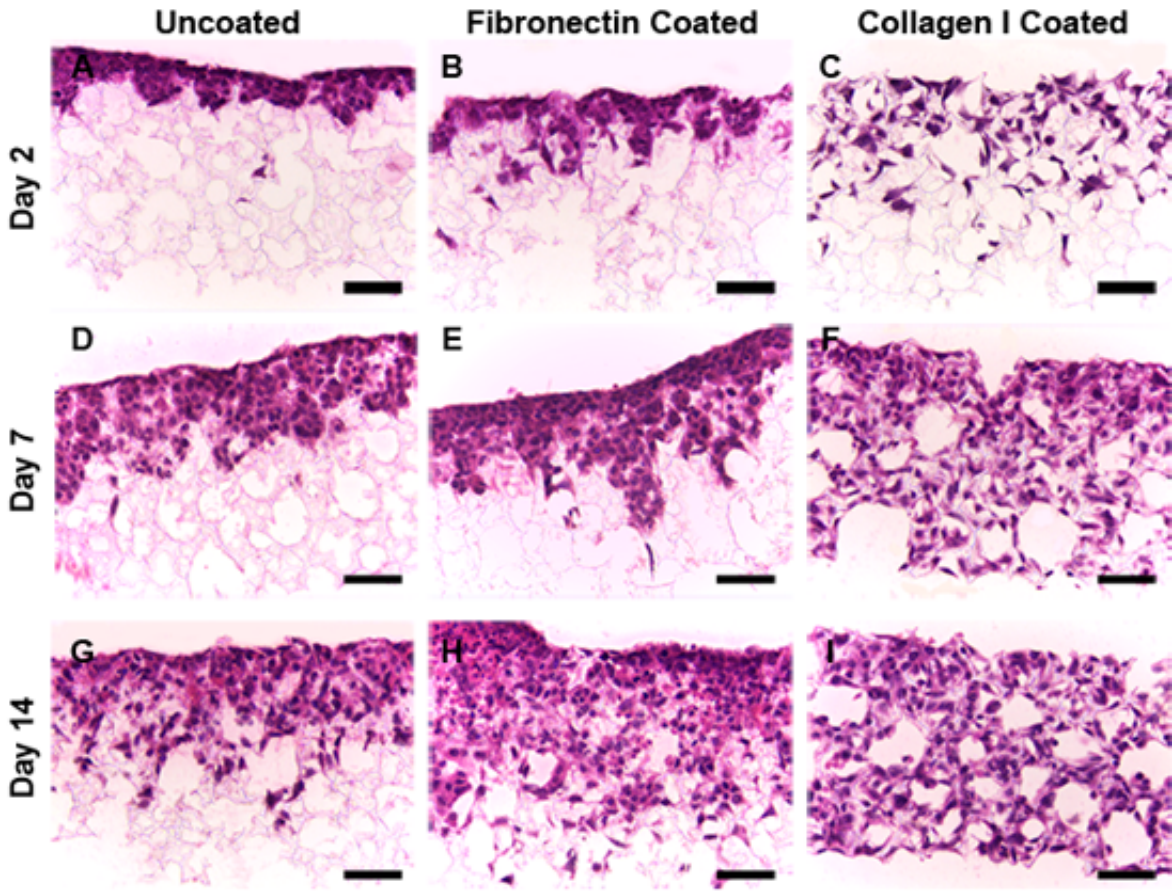

Figure 3.34 H&E staining of HepG2 growth in Alvetex®Scaffold coated with either fibronectin or collagen I using the insert/Petri-dish/submerged format. (A-C): Day 2. (D-F): Day 7. (G-I): Day 14. Scaffolds were either left uncoated (A,D,G), coated with fibronectin (B,E,H) or coated with collagen I (C,F,I). All cells appear healthy with no signs of necrosis. Cells appear to have migrated furthest into the collagen I coated scaffold, followed by fibronectin and the finally the uncoated scaffold. Scale bars = 50 μm.

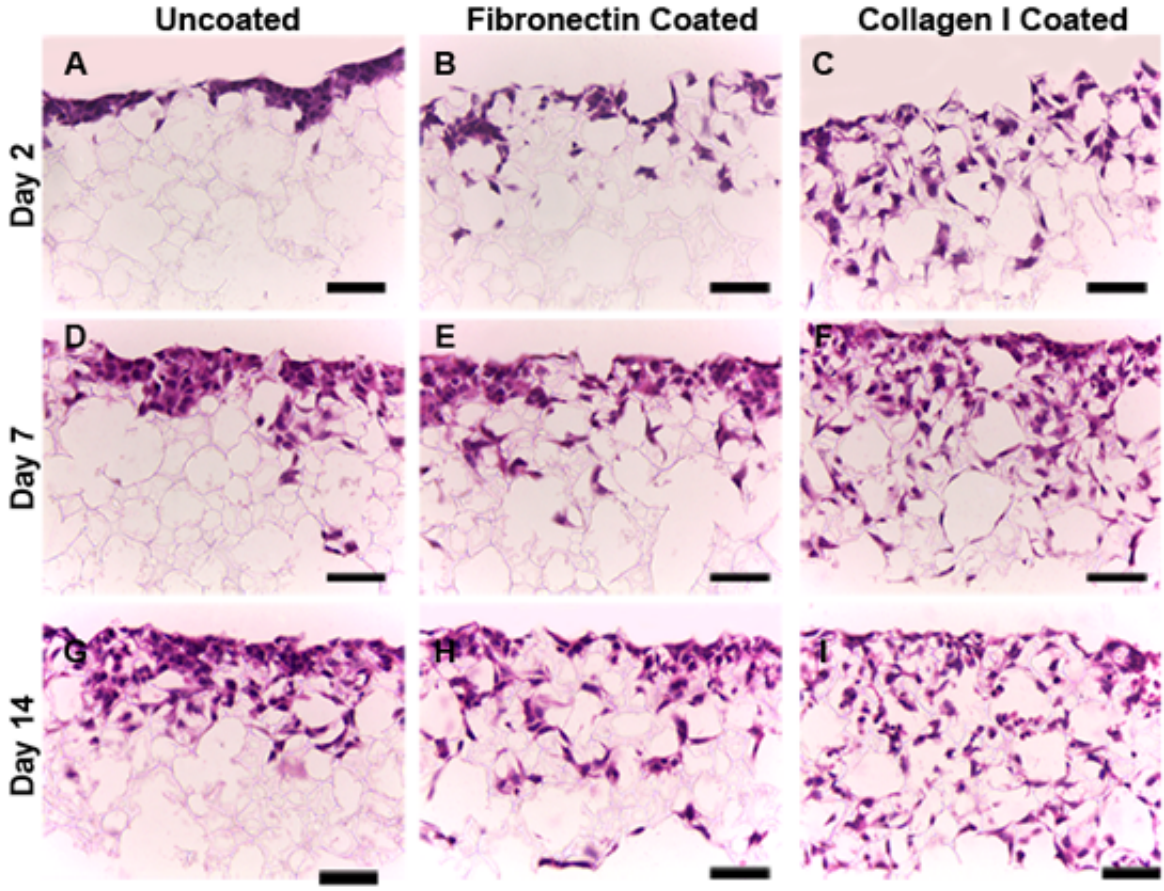

Figure 3.35 H&E staining of HepG2 growth in Alvetex®Scaffold coated with either fibronectin or collagen I using the insert/12-well plate/submerged format. (A-C): Day 2. (D-F): Day 7. (G-I): Day 14. Scaffolds were either left uncoated (A,D,G), coated with fibronectin (B,E,H) or coated with collagen I (C,F,I). All cells appear healthy with no signs of necrosis. Cells appear to have migrated furthest into the collagen I coated scaffold, followed by fibronectin and the finally the uncoated scaffold. Scale bars = 50 μm.

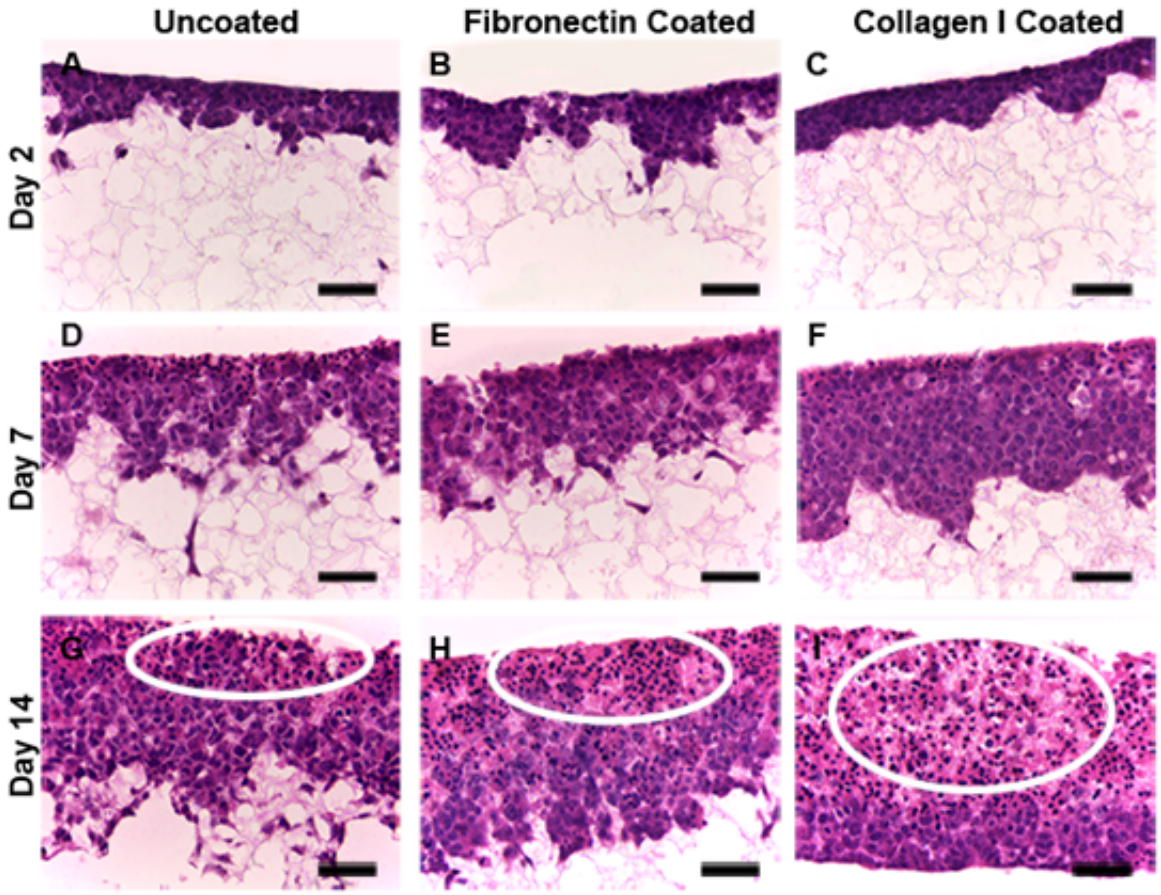

Figure 3.36 H&E staining of HepG2 growth in Alvetex®Scaffold coated with either fibronectin or collagen I using the insert/12-well plate/contact format. (A-C): Day 2. (D-F): Day 7. (G-I); Day 14. Scaffolds were either left uncoated (A,D,G), coated with fibronectin (B,E,H) or coated with collagen I (C,F,I). Collagen I seems to be the most effective at driving penetration into the material, however the effect is less than for submerged cultures. A significant amount of cell necrosis appears after 14 days culture, particularly for the collagen I scaffold, indicated by the white circles. Scale bars = 50 μm.

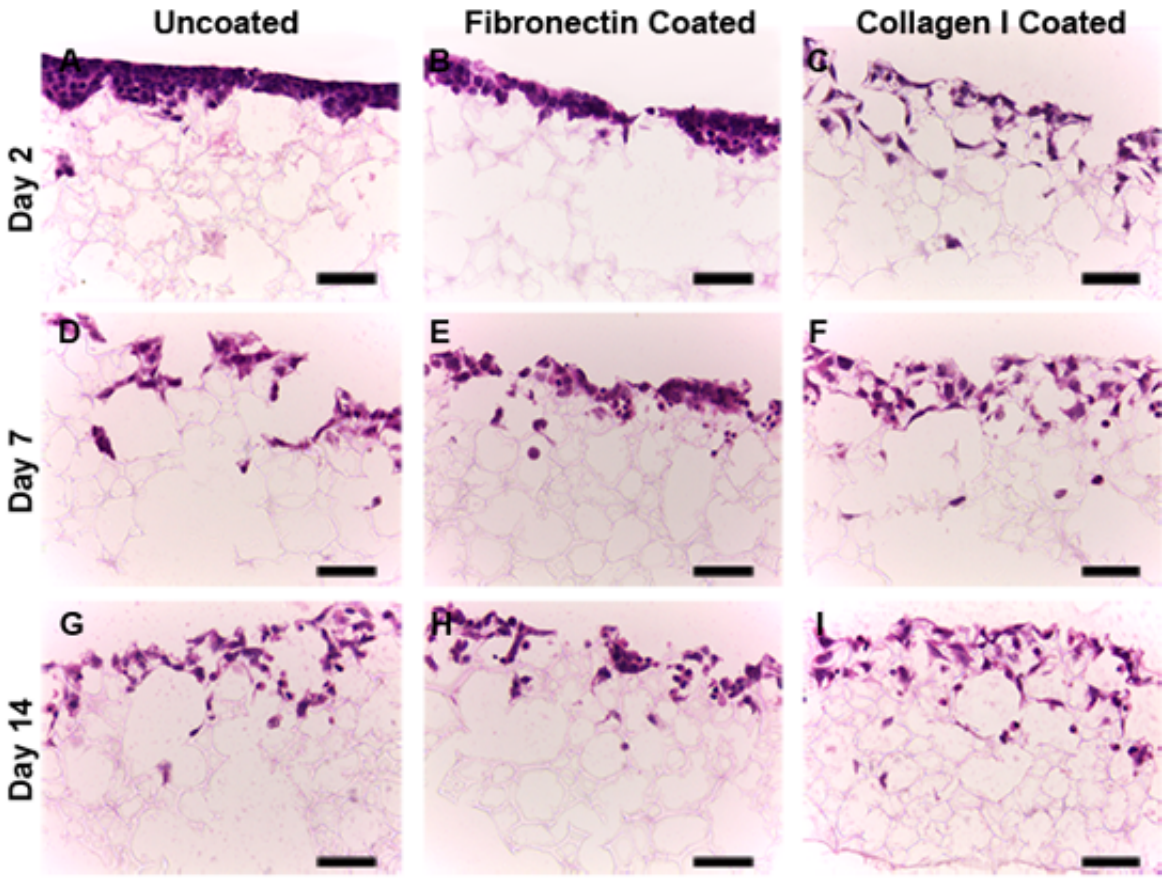

Figure 3.37 H&E staining of HepG2 growth in Alvetex®Scaffold coated with either fibronectin or collagen I using 24-well plate format. (A-C): Day 2. (D-F): Day 7. (G-I): Day 14. Scaffolds were either left uncoated (A,D,G), coated with fibronectin (B,E,H) or coated with collagen I (C,F,I). Collagen I seems to encourage a slight increase in cell penetration, but much less than for insert (submerged) cultures. Scale bars = 50 μm.

Figure 3.38 quantifies the cell penetration observed from the H&E images for each of the four product formats coated with fibronectin or collagen I. Fibronectin seems to have only a small effect on cell penetration across all formats. Conversely collagen I clearly increases cell penetration, particularly for insert/submerged cultures. For insert/contact cultures, collagen I still has an effect, however it is much lower compared to the submerged cultures, probably because media attraction from underneath the membrane is already a dominant factor in promoting cell migration. Collagen I also helped to increase penetration with the 24-well plate format, although the overall penetration remained much lower compared to the insert cultures.

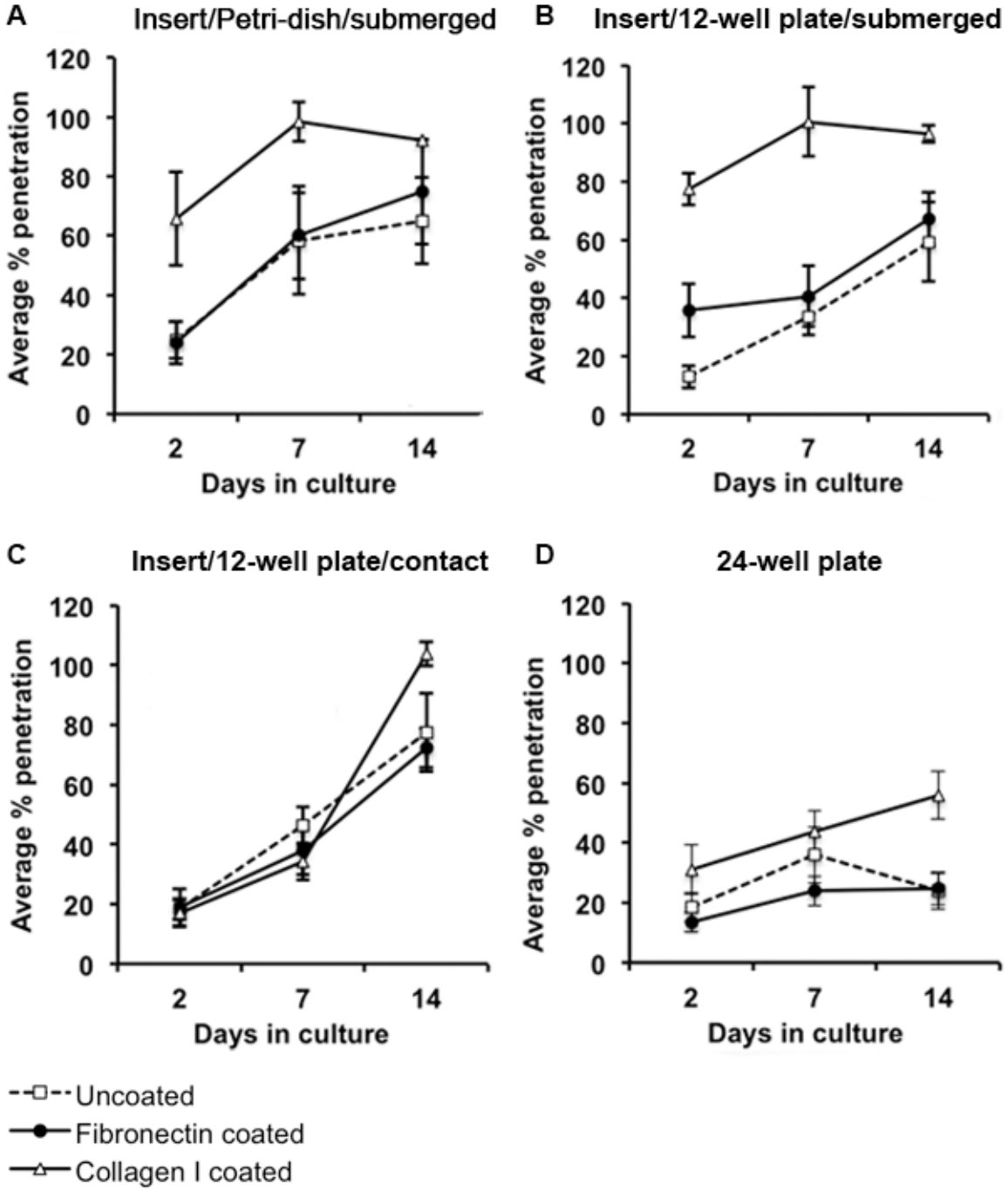

Figure 3.38 Quantification of HepG2 penetration into fibronectin or collagen I coated Alvetex®Scafffold using different product formats. (A): insert/Petri-dish/submerged. (B): insert/12-well plate/submerged. (C): insert/12-well plate/contact. (D): 24-well plate. Collagen I seems to be the most effective at driving cell penetration, followed by fibronectin. Data represent mean ± s.e.m (n=15).

The similarity in cell penetration between fibronectin coated scaffolds and uncoated scaffolds was surprising given that a significant amount of fibronectin was expected to be on the scaffold. As a result, total cell metabolic activity and total dsDNA were compared between fibronectin and

uncoated scaffolds to further probe if fibronectin coatings offered any advantage for cells growing on Alvetex®Scafffold.

Figure 3.39 shows the total HepG2 metabolic activity for cells cultured on a fibronectin coated scaffold (1000 μg/mL) compared to an uncoated scaffold, using the insert/Petri-dish/submerged format. A significant increase ($p<0.005$) was observed after 2 days culture for the coated scaffold, suggesting that fibronectin increases HepG2 adhesion onto the scaffold and/or promotes increased cellular activity. However, as the culture period progresses onto 7 and 14 days, no difference in total metabolic activity is observed. To help understand if the difference at day 2 can be attributed to increased cell adhesion or increased cellular activity, total cell number was quantified. This was achieved by measuring dsDNA content using the Quant-iT™ PicoGreen® reagent (*Life Technologies*). Firstly, a series of known HepG2 cell numbers were prepared in 2D pre-culture. These known cell numbers were then treated with the Quant-iT™ PicoGreen® reagent to measure dsDNA content and thus create a calibration curve of fluorescence intensity *versus* cell number (Figure 3.40A). A good correlation between cell number and fluorescence intensity was observed (R^2 = 0.987). Following this, HepG2 cells cultured on either uncoated Alvetex®Scaffold or fibronectin coated Alvetex®Scaffold were then lysed and homogenised to extract dsDNA and then treated with the Quant-iT™ PicoGreen® reagent. Fluorescence intensities were then converted into cell numbers using the calibration curve. Figure 3.40B shows no difference in cell number between the two scaffolds, suggesting that fibronectin does not enhance adhesion onto the material. These data are consistent with the previous H&E images, where no noticeable differences in cell density were observed.

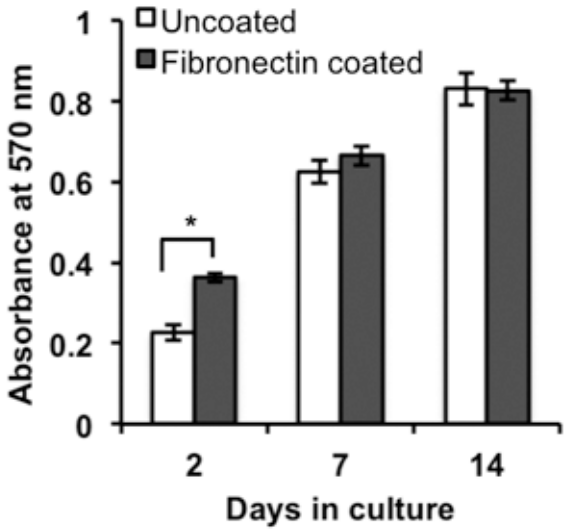

Figure 3.39 Impact of fibronectin coated Alvetex®Scaffold on HepG2 total metabolic activity. A significant increase is observed after 2 days culture, however no difference is observed after 7 and 14 days culture. Data obtained using the MTT assay. Data represent mean ± s.e.m (n= 7). * denotes $p<0.005$ as determined by the *Student's t-test.*

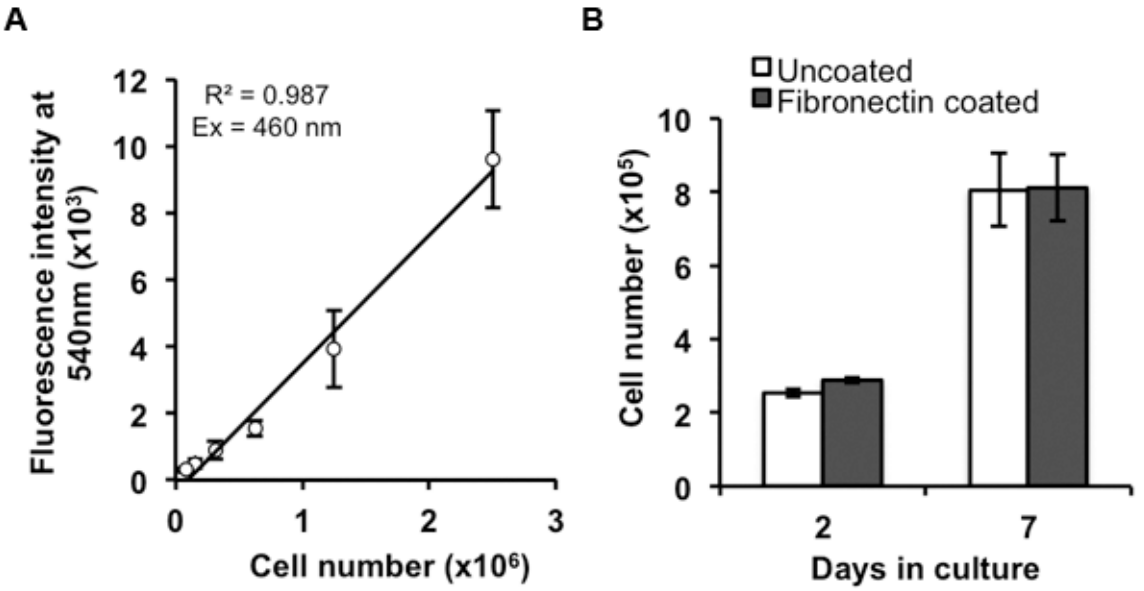

Figure 3.40 Analysis of total cell number from HepG2 dsDNA obtained from culture on uncoated and fibronectin coated Alvetex®Scaffolds. The Quant-iT™ PicoGreen® reagent was used to correlate dsDNA (fluorescence) with cell number. (A): Cell number – fluorescence calibration curve. (B): Cell number showing no significant differences. Data represent mean ± s.e.m (n=3).

In summary, this section has shown that coating Alvetex®Scaffold with 50 μg/mL collagen I solution helps to drive HepG2 migration into the material for insert/submerged cultures which could potentially lead to more extensive 3D tissue constructs throughout the scaffold. Conversely for insert/contact cultures and the 24-well plate, a collagen I coating only slightly improves HepG2 migration into the material. Coating Alvetex®Scaffold with 1000 μg/mL fibronectin has very little impact on HepG2 migration or adhesion. However, a fibronectin coating may help to increase the initial metabolic activity of the cells during the early stages of the culture period.

3.3.6 Optimising the Scaffold Microenvironment with Media Perfusion

A media perfusion model was developed in collaboration with *Reinnervate* for 3D culture using scaffold inserts. The media perfusion was set up as shown in Figure 3.41. Alvetex®Scaffold was used in an insert format so that media could perfuse above and below the scaffold. A *Watson Marlow* multichannel cassette pump was used to pump media from a reservoir stock through a specifically designed plate housing the inserts. The plate was designed by *Reinnervate* and was based on a modified 6-well plate, using a standard 6-well plate ringed-lid. However, in place of two of the wells are inlet and outlet ports for securing luer locks to then attach media/pump tubing. Four inserts can be used to hang in the remaining wells of the plate. Two pump heads are required per plate, one to push media from the reservoir into the plate, the other to pull media from the plate back to the reservoir. The reservoir is a small (125 mL) media bottle containing 130

mL media per plate, although approximately 30 mL of this is in the plate at any one time. A sterile 0.22 μm filter was used to provide an air release with the atmosphere so that the bottle does not deform under the pump action. Finally, the plate was raised to a similar height of the pump head so that gravity does not severely disrupt the flow (although some gravitational forces are inevitable).

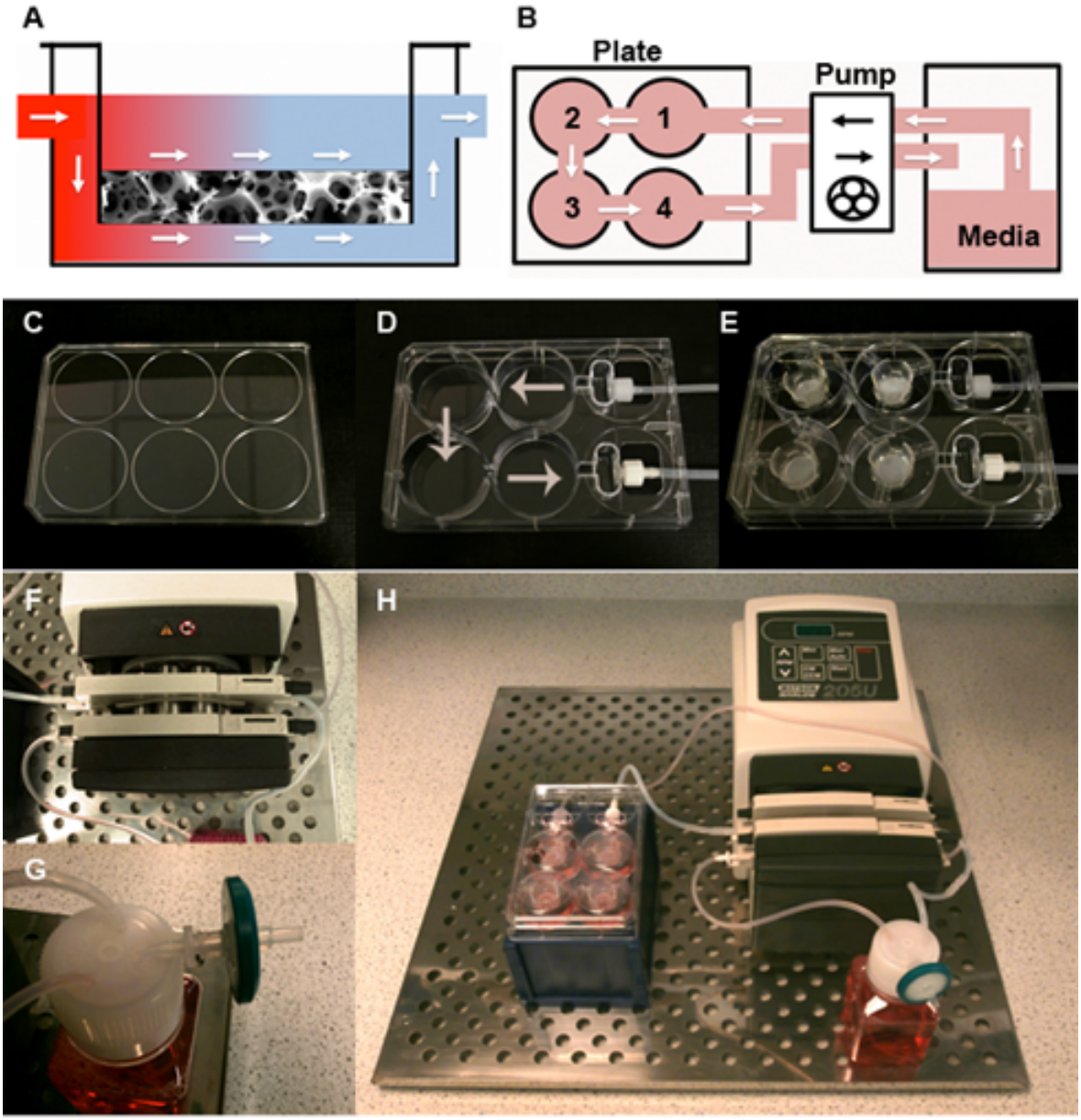

Figure 3.41 Set up for media perfusion through the Alvetex®Scaffold microenvironment using the Reinnervate Perfusion Plate. (A): Schematic of media flow across the scaffold within the perfusion plate. (B): Media circuit using the Reinnervate Perfusion Plate. (C): 6-well plate ringed-lid. (D): Reinnervate Perfusion Plate based on a modified standard 6-well plate. (E): Reinnervate Perfusion Plate housing 4 Alvetex®Scaffold membrane inserts. (F): Pump head cassette with tubing passing through. (G): Media bottle and media cap showing tubing and air vent. (H): Complete set up.

Prior to achieving this set-up for perfusion experiments, several practical problems had to be resolved during development. These are captured in Table 3-6

Table 3-6 Troubleshooting Issues for the Development of the Perfusion System.

Problem	Solution
Leakage of media from in/out ports	Port alteration on plate. Specific luer lock identified.
Overflow issues	Raising plate to pump head height. Ensuring tube distance transferring media to the plate is longer (60 cm) than the tube distance carrying media from the plate (35 cm).
Deformation of media reservoir bottle	Sterile filter valve employed in media reservoir cap to provide an air vent.
Slippage of tubing through the pump head	Use of tube-to-tube connectors to prevent slippage

Previous work within the Przyborski group using the Quasi Vivo (*Kirkstall*) bioreactor identified that a re-circulated flow rate of 200 μL/min was sufficient for hepatocytes (unpublished data). This was therefore employed for this system by setting the pump to 2 rpm (calibration data not shown).

The first experiment employed HepG2 cells to check that cells could survive under the media perfusion conditions employed. Figure 3.42 shows that the total metabolic activity is comparable between static and perfused cultures after 4 and 7 days culture. It is hypothesised that for HepG2 cells, which are already a robust and proliferative cell line, the media conditions employed by the static culture are already sufficient for optimal HepG2 growth in the scaffold. Consequently media perfusion was attempted using the more delicate Upcyte® cells and primary rat hepatocytes. Figure 3.43 compares the total metabolic activity of Upcyte® hepatocytes and primary rat hepatocytes under static and perfused conditions (up to 7 days culture). For Upcyte® cells, after 7 days culture there appears to be an increase in metabolic activity for perfused cells. This could be consistent with better nutrient quality throughout the culture period. For primary rat hepatocytes there is increased metabolic activity for the perfused cells after 3 days culture, however after 5 days the activity of the perfused cells is reduced to be parity with the static cells. This may be explained by a gradual cell loss from the scaffold throughout the perfusion period, given that these cells are extremely delicate and are even more sensitive to physical stress compared to Upcyte® cells.

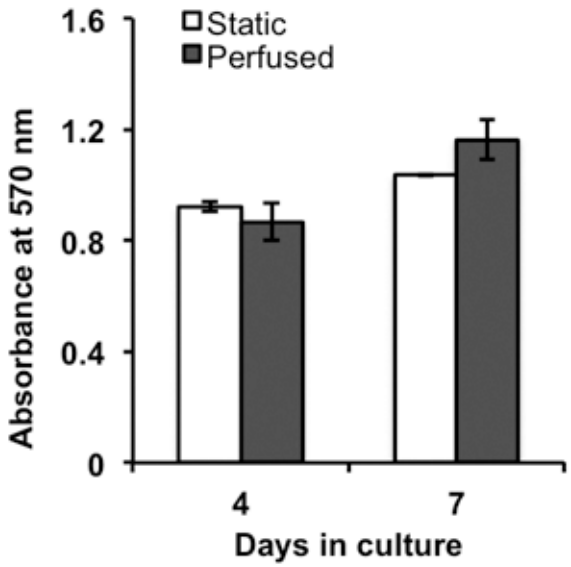

Figure 3.42 Media perfusion of HepG2 cells cultured on Alvetex®Scaffold using the Reinnervate Perfusion Plate. The MTT assay was used to assess total metabolic activity. It is hypothesised that standard static culture conditions are already sufficient for the highly robust and proliferative HepG2 cell line. Data represent mean ± s.e.m (n=2).

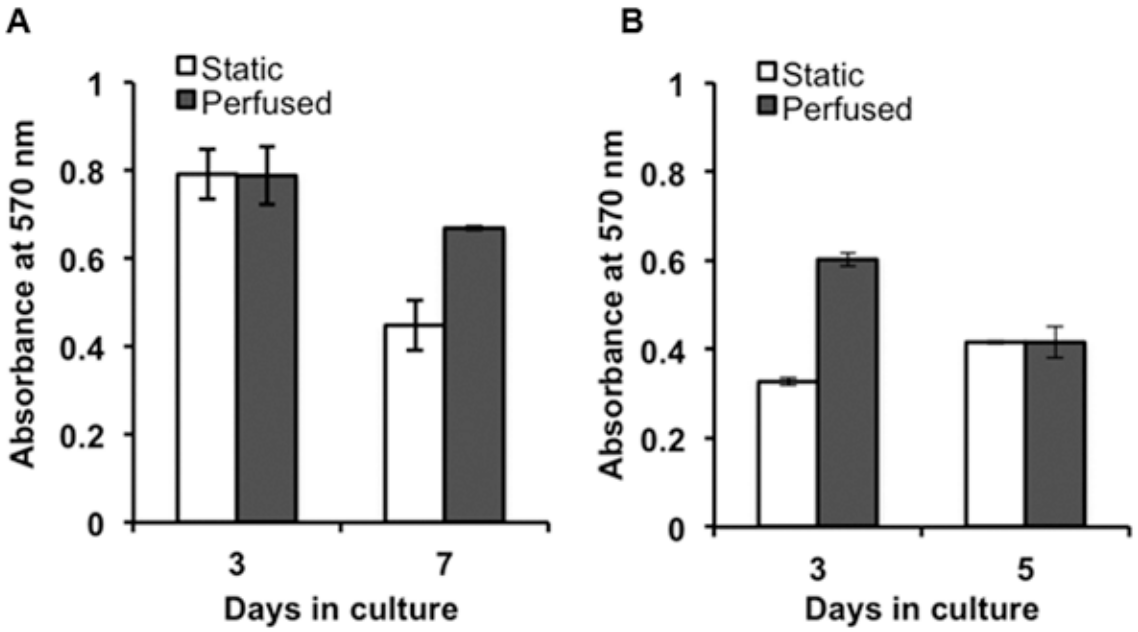

Figure 3.43 Metabolic activity of hepatocytes cultured in the perfusion model compared to static media conditions. (A): Upcyte® cells showing an increase for perfused conditions after 7 days. (B): Primary rat cells showing an increase for perfused conditions after 3 days but not 5 days. Data represent mean ± s.e.m (n=2).

3.3.7 Extracting Intact Hepatocytes from the Scaffold Microenvironment

One of the main advantages of cell growth on Alvetex®Strata is that the cells can potentially be extracted and then used for 3D passaging or subsequent analysis. To assess the feasibility of this, HepG2 cells were first cultured on Alvetex®Strata for 2, 7 and 14 days using the insert/6-well plate/contact format. After each time point, the membranes were removed from their insert housings and placed in a new 6-well plate containing 2 mL of Trypsin-EDTA (Sigma) and then incubated for 15 mins at 37 ^{o}C and 5 % CO_2. After this period, 1 mL of MEM was added and a cell scraper was gently applied to the membrane. The Trypsin-EDTA/MEM solution was then re-suspended in MEM and either analysed using flow cytometry or re-seeded onto fresh Alvetex®Strata membranes for 3D passaging.

Figure 3.44 shows the HepG2 growth on the membrane before and after cell extraction. Encouragingly, nearly all of the cells growing on top of the membrane were extracted at each time point. Some cells that penetrated into the material, particularly after 14 days culture, were not removed and remained in the top portion of the membrane. This is surprising given the small void diameter of Alvetex®Strata, and suggests that HepG2 cells are willing to alter their morphology to move closer towards the media supply in this environment. Note that residual cells left on the membrane means that the extracted cells are not fully representative of the entire cell population. Hence care should be taken when interpreting subsequent analysis data.

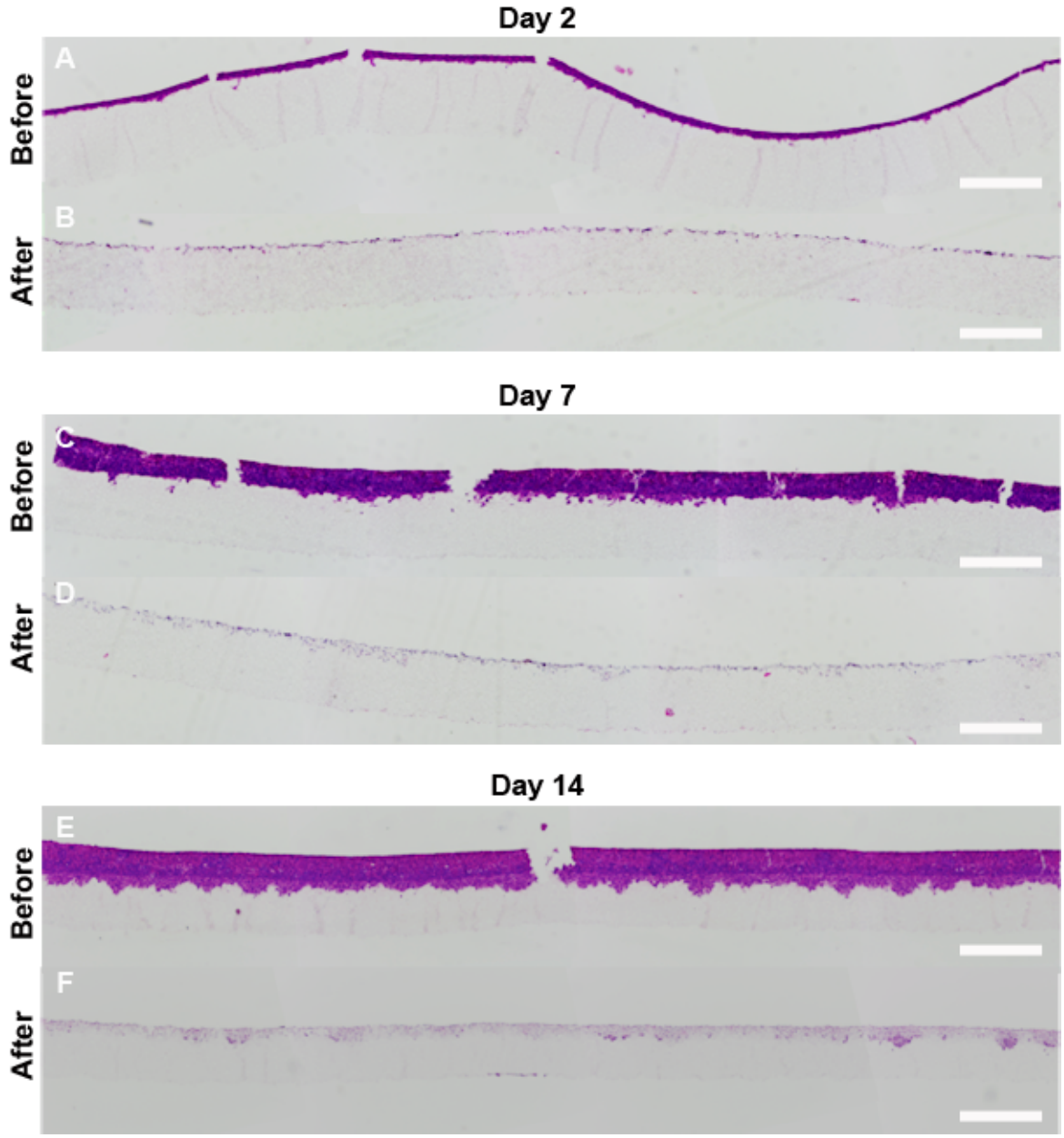

Figure 3.44 Extracting HepG2 cells from Alvetex®Strata. (A,C,E): Before treatment with Trypsin-EDTA and a cell scraper. (B,D,F): After treatment with Trypsin-EDTA and a cell scraper. The extraction process removes the majority of cells, although after 14 days culture those cells that have penetrated into the material are not removed. Scale bars = 400 μm.

Having successfully extracted the majority of cells from Alvetex®Strata, the cells were then analysed using flow cytometry and the Guava Nexin® reagent (Millipore). This is a reagent that detects (1): external Annexin V (a calcium-dependent phospholipid binding protein) as an indicator of early-apoptotic cells and (2): cell membrane integrity using 7-aminoactinomycin D (7-AAD) as an indicator of necrotic/late apoptotic cells. As a result, three cell states can be analysed simultaneously: (1) viable cells being (-) Annexin V and (-) 7-AAD. (2) early apoptotic cells being (+) Annexin V and (-) 7-AAD. (3) Necrotic/late apoptotic cells being (+) Annexin V and (+) 7-AAD. The

(+) Annexin V gate on the flow cytometer was set using HepG2 cultures that were treated with 2 μM staurosporine for 18 hours (an inducer of apoptosis). The (+) 7-AAD gate was set on the flow cytometer using HepG2 cultures that were heated treated at 58 ^{o}C for 20 mins.

Figure 3.45 shows the results of the flow cytometric analysis of the extracted cells using the Guava Nexin® reagent. After 2 days culture on Alvetex®Strata the majority of cells appear to be (-) Annexin V/(-) 7-AAD. This is consistent with H&E staining showing healthy and viable cells. After 7 days culture, a slight shift occurs towards (+) Annexin V/(-) 7-AAD and (+) Annexin V/(+) 7-AAD cells. At day 14, most of the extracted cells are (+) Annexin V/(+) 7-AAD, consistent with the substantial cell necrosis observed in the H&E staining.

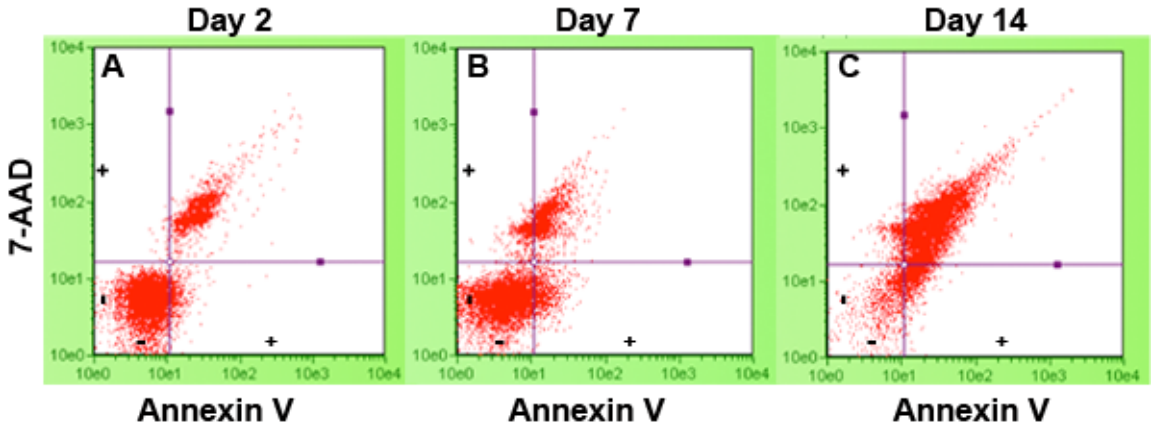

Figure 3.45 Flow cytometric analysis of HepG2 cells extracted from Alvetex®Strata obtained using the Guava Nexin® reagent. (A): Day 2 data showing the majority of cells to be (-) Annexin V and (-) 7-AAD. (B): Day 7 data showing a slight shift towards (+) Annexin V and (+) 7-AAD. (C): Day 14 data showing the majority of cells to be (+) Annexin V and (+) 7-AAD.

Quantification of the flow cytometry data is shown in Figure 3.46. A comparison with extracted cells taken from submerged cultures is made to help normalise the severity of necrosis occurring in contact cultures. As expected, a steep drop in cell viability and increase in necrosis is observed for contact cultures as time progresses. This is consistent with previous histology images. Submerged cultures show less of a decline in cell viability, although this does still drop, with more cells becoming apoptotic or necrotic.

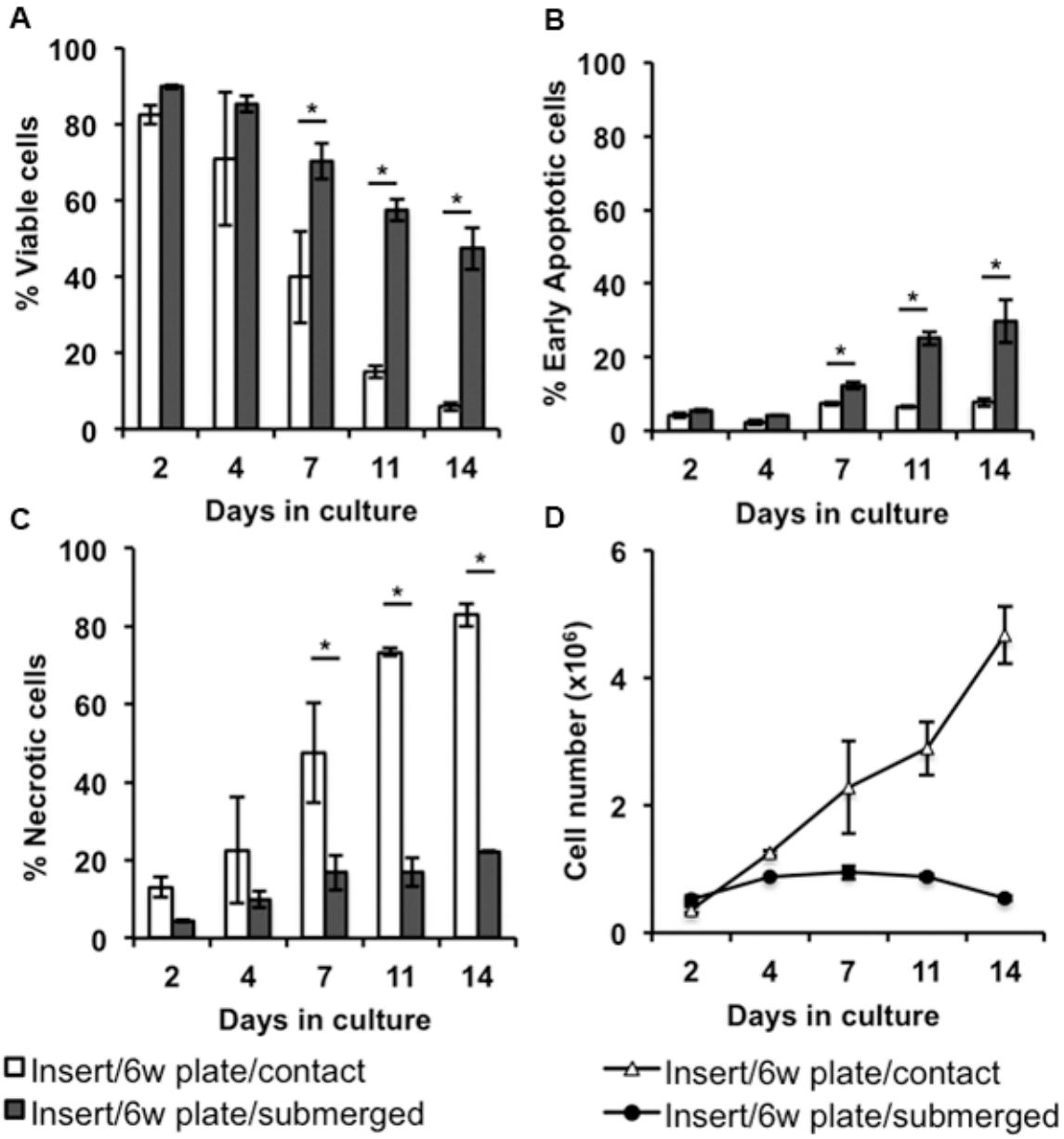

Figure 3.46 Quantifying flow cytometry data for HepG2 cells extracted from Alvetex®Strata and analysed using the Guava Nexin® reagent. (A): % viable cells. A significant decrease in HepG2 viability is observed for contact cultures compared to submerged cultures across the culture period. (B): % early apoptotic cells. Interestingly submerged cultures show an increase in apoptosis as the culture period progress. (C): % necrotic cells. A significant increase in necrotic cells is observed for contact cultures compared to submerged cultures. (D): Number of intact cells extracted from Alvetex®Strata at different time points. Data represent mean ± s.e.m. (n=2-9). * denotes $p<0.005$ as determined by the *Student's t-test*.

In addition to flow cytometric analysis, the extracted cells were also re-seeded on new Alvetex®Strata membranes for subsequent culture (3D passaging). HepG2 cells were first cultured on Alvetex®Strata for 7 days using the insert/6-well plate/contact format. After this period cells

were extracted and re-seeded onto fresh Alvetex®Strata and cultured for an additional 4 days. The growth of these 3D-passaged cells was compared against cells with a 2D pre-culture history, as shown in Figure 3.47. Cells with a 2D history were found to grow in the familiar homogeneous manner to form a tissue-structure near the top portion of the scaffold. Some cells actually penetrated into the material. Conversely those cells with an Alvetex®Strata pre-culture history were found to grow in tightly packed aggregates, with very few cells entering the scaffold. These data suggest that 3D pre-culture may have an important effect on programing cell structure and growth characteristics in subsequent experiments.

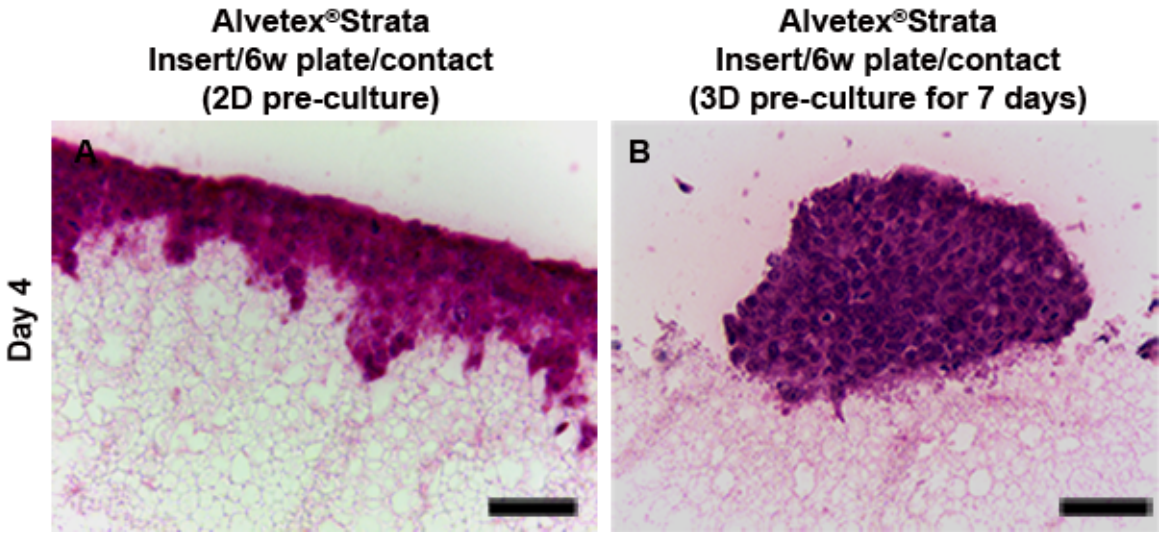

Figure 3.47 The impact of 2D and 3D pre-culture on HepG2 growth on top of Alvetex®Strata. HepG2 cells were either pre-cultured in T75 flasks (2D) or Alvetex®Strata. Cells were then extracted and re-seeded onto new Alvetex®Strata and cultured for 4 days. (A): Growth after 2D pre-culture showing cells growing in a homogeneous manner near the top portion of the membrane, with some cells entering the material. (B): Growth after Alvetex®Strata pre-culture showing cells have aggregated together and not entered the membrane. Scale bars = 50 μm.

In summary, this section has shown that the majority of HepG2 cells growing on top of Alvetex®Strata can be extracted. These cells can be used for subsequent analysis, such as determining cell viability using flow cytometry. Most of the cells extracted are viable up to 7 days culture, whereby a noticeable increase in necrotic cells is observed. In comparison, extracted cells from submerged cultures remain viable for longer. Finally, extracted cells can be re-seeded onto new Alvetex®Strata membranes and used for 3D passaging. The growth profiles of cells coming from a 3D pre-culture history is more aggregated compared to those coming from a 2D pre-culture history.

3.4 Discussion

Replicating native tissue density and architecture *in vitro* is expected to improve the predictive accuracy of *in vitro* models. Consequently many groups are assessing the growth of cells in different 3D technologies in an attempt to re-create *in vivo* growth patterns (see Chapter 1 for a review of different 3D technologies). For example, MacNeil *et al.* have explored electrospun scaffolds to approximate native geometries and cell-cell interactions *in vitro*[103]. Other groups have explored protein hydrogels to mimic native 3D cell-ECM interactions[189]. This study aimed to understand if emulsion templated polystyrene scaffolds could re-create native liver tissue architecture and density by exploring hepatocyte growth under different culture conditions and scaffold presentations. It also aimed to optimise the scaffold microenvironment through ECM coatings and media perfusion, as well as exploring new avenues to extract intact cells for subsequent analysis.

Prior to the growth assessment in polystyrene scaffolds, hepatocytes were first cultured in 2D. Under conventional 2D culture conditions, all three hepatocyte sources employed in this study displayed a severely flattened morphology towards a monolayer, consistent with previous literature reports using 2D substrates[76, 166]. Indeed, the diameter of hepatocytes cultured in 2D was found to be much greater than hepatocytes *in vivo,* supporting existing literature that cells in 2D spread out into unrealistic geometries. Moreover, the majority of the cell surface was found to be in contact with either 2D plastic or the culture media, with only a small portion coming into contact with other cells. As described in Chapter 1, this limited cell-cell contact is far removed from the complex 3D interactions found *in vivo* that govern tissue homeostasis[190]. Indeed, *in vivo* human liver tissue was densely packed with cells with extensive opportunity for cell-cell interaction in multiple directions.

To explore hepatocyte growth in polystyrene scaffolds, Alvetex®Scaffold and Alvetex®Strata were employed. Characterisation of these materials confirmed that Alvetex®Scaffold has an average void diameter of ca. 42 μm, whereas Alvetex®Scaffold has an average void diameter of ca. 12 μm. Both materials display porosities of ca. 90 %.

HepG2 cells entered the top portion of Alvetex®Scaffold and adhered without issue. It is hypothesised that the adherence mechanism is similar to that for 2D polystyrene, where glycoproteins such as fibronectin (from serum or the cells themselves) first adsorb onto the polystyrene to facilitate cell attachment[168]. Once adhered, cells on Alvetex®Scaffold adopted a cell diameter much closer to that of the *in vivo* scenario. This is consistent with previous reports

demonstrating that hepatocytes adopt a more natural 3D morphology in emulsion templated scaffolds compared to 2D substrates[159].

The presentation of Alvetex®Scaffold was found to influence HepG2 growth in the material. Submerged insert cultures encouraged cells to migrate and proliferate into the scaffold to produce multidirectional 3D growth similar to *in vivo*, although dense *in vivo* like packing was not observed. Importantly, no signs of necrosis were observed even after 14 days, suggesting that the porosity of the scaffold can support effective nutrient transfer to cells. This offers an attractive advantage over many other 3D cell culture substrates such as hydrogels, where poor media diffusion can often restrict nutrient supply to cells growing in the centre of the substrate. Conversely, the 24-well plate presentation did not encourage HepG2 migration in Alvetex®Scaffold and the growth profile of cells lacked the high density associated with *in vivo*. It is hypothesised this is due to the lower media supply of a 24-well plate in comparison to the insert presentation. Interestingly, contact insert cultures (air-liquid interface) produced a densely packed 3D cell organisation within the material, almost entirely approximating *in vivo* density and cell-cell interaction. This is consistent with other reports that have employed hepatocyte air-liquid interface cultures and observed a similar tightly clustered 3D cell organisation[191, 192]. Indeed, similar air-liquid interface liver slice cultures have also been proposed as suitable *in vitro* liver models for fibrosis[193]. The precise reason as to why cells pack tightly during contact (air-interface) cultures remains unknown, although it may be due to surface-tension effects pulling cells together and/or reducing cell loss from the insert during turbulent media changes. One advantage of this dense growth behaviour is the opportunity for multicellular contact within the microenvironment, re-creating important cell-cell and cell-ECM communication present *in vivo*. However a major disadvantage of contact cultures is the cell death that occurs for those cells closest to the air interface after prolonged culture periods.

Similar to HepG2 cells, Upcyte® hepatocytes and primary rat hepatocytes also entered the top portion of Alvetex®Scaffold and adhered. They also displayed a similar cell diameter to the *in vivo* dimension. Upcyte® hepatocytes, having some proliferative capacity, seemed to remain viable after 21 days culture and slowly migrated into the material to approximate *in vivo* cell density in the top portion of the scaffold. Primary rat cells, having limited proliferative capacity did not migrate into the material and remained in the top portion of the scaffold. Employing a contact insert presentation formed an impressive densely packed growth profile of these cells, similar to the profile of HepG2 cells.

HepG2 cells adhered on top of Alvetex®Strata and did not initially enter the scaffold. A contact insert scaffold presentation formed a dense tissue structure, consistent with other reports of air-liquid hepatocyte cultures[191, 192]. As the culture period progressed the thickness of the tissue-structure increased, starting at ca. 47 μm (day 2) and moving up to ca. 180 μm (day 14). This is highly advantageous in replicating native liver tissue density and organisation, particularly as this culture condition is essentially scaffold-less. However, a significant amount of cell necrosis was observed in the top portion of the tissue-structure after prolonged culture, likely due to media starvation. Attempts to prevent this cell necrosis were unsuccessful. It was hypothesised that reducing the membrane thickness of the scaffold would increase media access to cells, however significant cell necrosis was still observed even on membranes as thin as 60 μm. Alternatively, employing insert submerged cultures did enable healthy cell growth, but completely prevented the formation of a tissue-structure on top of the membrane. Indeed, after 14 days culture the thickness of the cell population was still only ca. 41 μm, in comparison to ca. 180 μm for contact cultures. It is postulated that submerged cultures lack sufficient surface tension to densely pack the cells and make cells growing on top of the scaffold more susceptible to being washed away during media changes. The ''washing away'' effect was supported by observing significantly more cells outside of the insert for submerged cultures compared to contact cultures.

The hepatic ECM plays a crucial role in maintaining normal hepatocyte survival and function *in vivo*[14]. Extensive reports have therefore employed hepatic ECM components for *in vitro* hepatocyte culture. For example, 2D plastic coated with fibronectin has been shown to increase hepatocyte adhesion and spreading[194, 195]. Sandwich cultures derived from collagen, fibronectin or Matrigel™ have been shown to prolong hepatocyte viability, cytochrome P450 activity and cell polarisation[76, 79, 80]. Similarly there have been numerous reports describing the use of ECM-based hydrogels for 3D hepatocyte culture[91].

In this study, Alvetex®Scaffold was coated with fibronectin and collagen I in an attempt to improve the biological relevance of the scaffold to promote cell adhesion and function via offering native ECM mimics. Fibronectin coatings deposited thin films or spindles of protein on the scaffold. Generally an increase in protein coating concentration resulted in an increase in fibronectin deposition. A solution concentration of 1000 μg/mL was therefore selected as optimum. Conversely collagen I coating solutions deposited more granular-type structures on the walls of the scaffold. Furthermore, increasing the concentration of coating solution did not proportionally increase the amount of collagen I deposited on the scaffold. Consequently a solution of 50 μg/mL was chosen as optimum.

Culturing HepG2 cells on collagen I coated Alvetex®Scaffolds improved migration into the scaffold, suggesting opportunity to form extensive 3D constructs or suitability for liver cancer migration assays. Migration was more profound for insert/submerged cultures compared to insert/contact and 24 welled-plate cultures. On the contrary, fibronectin coatings had only a slight impact on cell migration and proliferation compared to uncoated scaffolds. However, fibronectin did increase the initial total metabolic activity of the cells (day 2), suggesting that fibronectin may be involved in specific functional pathways during the 3D adhesion period.

Media perfusion through an emulsion templated polystyrene scaffold combines a more suitable physical environment with a more representative media supply that potentially mimics aspects of native liver vascularisation. In this study, a media perfusion system was developed for Alvetex®Scaffold using the Reinnervate Perfusion Plate. Several practical challenges were overcome during the development of the perfusion system, including media leakages, flow issues and tubing slippage issues. Once the issues were rectified, the perfusion system showed enhanced metabolic activity of Upcyte® cells after 7 days culture and enhanced metabolic activity of primary rat hepatocytes after 3 days culture compared to static 3D cultures. This is consistent with other perfusion models reported in the literature (see section 3.1.6). In addition, preliminary experiments with Alvetex®Scaffold and the commercial *Quasi-Vivo®* perfusion kit (*Kirkstall*) were performed alongside this study by the *Reinnervate* development team (Dr. Frederique Tholozan) and observed similar results (data not yet published). That study also observed that Upcyte® cells were more viable after 7 days culture in the *Quasi-Vivo®* system compared to static 3D cultures.

One of the limitations of 3D cell culture substrates may be the difficulty in extracting the cells. Cells that are densely packed into a 3D structure will secrete their own ECM to anchor themselves to one another and to the 3D substrate. In addition, most 3D substrates cannot be easily opened or disrupted, especially chemically cross-linked hydrogels, electrospun fibres and polymeric scaffolds. As a result, the short incubation times with proteases such as trypsin-EDTA that were suitable for retrieving cells from 2D cultures are much less effective in 3D.

Whilst full cell retrieval may not be an issue for tissue engineering or regenerative medicine applications, where the biodegradable material is intended to be implanted into the body along with the cells, it does pose an issue for *in vitro* cell culture applications. Not being able to continually passage proliferative cells in 3D is a major challenge, in that cells stocks need to be pre-cultured in 2D before being applied to 3D experiments. Similarly many *in vitro* biological techniques require cells to be extracted from the substrate, including flow cytometry or using transfection kits.

Growing cells on top of Alvetex®Strata was found to be a highly effective route to extracting intact hepatocytes. Applying a Trypsin-EDTA incubation followed by cell scraping was found to retrieve most cells, particularly for up to 7 days culture. Importantly, the extracted cells were viable and could be subsequently cultured on fresh Alvetex®Strata membranes, offering one of the first tools to enable 3D-3D passaging. Once more, extracted cells could also be analysed using flow cytometry. This method allowed confirmation of cell viability differences between contact and submerged cultures using the Guava Nexin® reagent.

3.5 Conclusions

The following conclusions can be made from the results of this Chapter:

- Hepatocytes *in vivo* are densely packed and experience cell-cell contact in multiple directions.

- When grown on 2D plastic, HepG2 cells, Upcyte® hepatocytes and primary rat hepatocytes spread out and flatten, severely deviating from their native geometry and architecture. Note that Chapter 4 probes in more detail into the structural consequences of 2D and 3D cell culture.

- Hepatocytes cultured on emulsion templated polystyrene scaffolds can adhere onto the scaffold and penetrate into the voids of the scaffold to form a 3D cell shape that more closely resembles *in vivo*. Furthermore, hepatocytes can remain viable for prolonged periods and can approximate native liver tissue density and cellular interaction.

- The presentation of Alvetex®Scaffold impacts HepG2 growth characteristics and viability. Scaffold insert cultures encourage cell migration into the scaffold, whereas scaffold plate cultures do not. Submerging scaffold inserts in culture media leads to healthy hepatocyte growth throughout the culture period. Conversely, only supplying culture media from below the insert leads to densely packed cell growth, but with signs of cell necrosis near the air-liquid interface.

- Hepatocytes cultured on Alvetex®Strata have a tendency to grow on top of the scaffold to re-create a thick tissue mass very similar to native liver in terms of cell density and cell-cell contact. Supplying media from underneath Alvetex®Strata inserts lead to thick tissue-like structures that build up on top of the scaffold. However, substantial cell necrosis is observed in this tissue-structure for those cells close to the air-liquid interface. Employing thinner scaffold membranes still encourages tissue-structures to grow on top of the scaffold, but does little to prevent cell necrosis. Employing submerged cultures with Alvetex®Strata does not enable the formation of extensive cell growth on top of the scaffold. It is therefore hypothesised that surface tension and/or a lack of turbulent media supply is required to form thick tissue-like structures on top of Alvetex®Strata.

- Alvetex®Scaffold can be coated with collagen I or fibronectin to increase the biochemical relevance of the scaffold. Collagen I coatings increase HepG2 migration into Alvetex®Scaffold throughout the culture period. Fibronectin coatings do little to help HepG2 migration, however preliminary evidence suggests that fibronectin may help to increase the metabolic activity of the cells during the early stages of the culture period.

- A 3D media perfusion model that re-creates aspects of native liver vascularisation has been developed with polystyrene scaffolds. Preliminary results suggests this perfusion model may hep to enhance viability of Upcyte® cells and primary rat hepatocytes growing in scaffolds.

- Intact healthy hepatocytes can be extracted from Alvetex®Strata. These can be used for subsequent analysis (for example flow cytometry) or even 3D-3D passaging.

Chapter 4: Structure, Function and Gene Expression of Hepatocytes Cultured in Emulsion Templated Polystyrene Scaffolds

4.1 Introduction

4.1.1 Overview

Chapter 3 introduced emulsion templated polystyrene scaffolds and assessed hepatocyte growth in these materials under different culture conditions. This Chapter probes in more detail the structural, functional and genetic consequences of culturing hepatocytes in these scaffolds. A comparison with conventional 2D hepatocyte culture is made, along with an *in vivo* comparison where possible.

4.1.2 Previous Reports on Hepatocyte Structure, Function and Gene Expression in Emulsion Templated Polystyrene Scaffolds

Przyborski and Cameron had previously published two reports on HepG2 structure and function in emulsion templated polystyrene scaffolds[150, 151]. These reports showed that HepG2 cells in scaffolds displayed a higher level of albumin synthesis compared to 2D HepG2 cultures. They also showed that HepG2 cells cultured in scaffolds displayed increased resistance to the drug methotrexate compared to 2D, suggesting a more drug-resistant cancerous cell line is established in the 3D microenvironment. These reports also featured some preliminary ultrastructural images of HepG2 cells in scaffolds; showing the formation of bile canaliculi and the presence of some surface microvilli. However, these reports only provide an initial insight into some of the critical questions regarding HepG2 structure, function and gene expression in polystyrene scaffolds. For example, cell morphology had not been fully compared between 2D and 3D using advanced techniques such as confocal immunofluorescence. Similarly a detailed ultrastructural comparison with 2D cultures and *in vivo* tissue had not been performed. Moreover, the toxicity profiles of other drugs and gene expression differences with 2D had also not been explored for HepG2 cells.

Only one report has described the culture of Upcyte® hepatocytes in polystyrene scaffolds[188]. This report showed that cytochrome P450 activity was enhanced for the cells when cultured in scaffolds compared to 2D. However, no indication of cell morphology, structure and gene expression was described. Similarly, only one reported described the culture of primary rat hepatocytes in polystyrene scaffolds[159]. This report demonstrated that cells in the scaffold adopted a more rounded morphology compared to 2D culture. They also showed increased cytochrome P450 activity and increased sensitivity to the drug acetaminophen (APAP). However, no reports had described primary rat ultrastructure in scaffolds, nor had they investigated typical primary hepatocyte functions such as albumin synthesis or urea conversion. Table 4-1 summarises the known and unknown pieces of data for hepatocytes cultured in polystyrene scaffolds prior to starting this study. Accordingly, this study attempted to address some of these unknown data

points to develop a more comprehensive understanding of how 3D scaffold cultures compare to 2D cultures and *in vivo* liver tissue.

Table 4-1 Summary of Hepatocyte Data Previously Reported for Polystyrene Scaffolds

	HepG2	**Upcyte® Hepatocytes**	**Primary Rat Hepatocytes**
Cell morphology	Unknown	Unknown	Scaffold produces a more rounded cell shape[159]
Cell ultrastructure	Key organelles are present. Some bile canaliculi are observed[150, 151]	Unknown	Unknown
Albumin synthesis	Increased vs. 2D[150, 151]	Unknown	Unknown
Urea synthesis	N/A	Unknown	Unknown
Drug toxicity	Increased resistance to methotrexate vs. 2D[151]	Increased CYP activity vs. 2D[188]	Increased sensitivity to acetaminophen vs. 2D[159] Increased CYP activity vs. 2D[159]
Gene expression	Unknown	Unknown	Increased vs. 2D

4.1.3 Acetaminophen and Gemfibrozil Metabolism

Understanding if hepatocytes cultured in scaffolds display a more realistic metabolism of drugs is a key part of this study. Two model drugs were chosen to probe this; acetaminophen (APAP) and Gemfibrozil. APAP (paracetamol) is a common mild analgesic often used for hepatotoxicity studies. It is metabolised by the UGT and SULT enzyme families into polar, non-toxic compounds that are transported to the kidneys and subsequently excreted from the body. However, APAP is also metabolised by the cytochrome P450 enzymes into a minor but toxic metabolite known as *N*-acetyl-*p*-benzo-quinone imine (NAPQI). Under therapeutic doses of APAP, any NAPQI formed is quickly detoxified by a coupling reaction with glutathione via the GST enzymes. However, with overdose levels of APAP, glutathione stores are eventually depleted allowing a build up of NAPQI and thus cellular toxicity (Figure 4.1). Importantly, many *in vitro* hepatocyte models fail to replicate the suitable enzyme levels required for native (predictive) APAP metabolism.

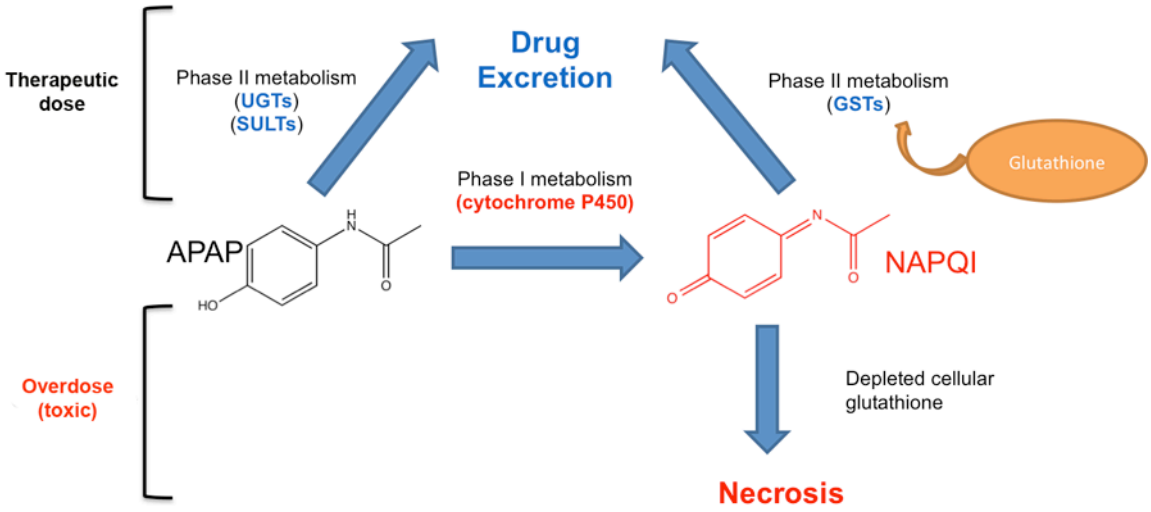

Figure 4.1 APAP metabolism by the hepatic drug metabolising enzymes. APAP is metabolised by the UGT or SULT enzymes into polar non-toxic compounds that are excreted from the body. APAP is also metabolised by the cytochrome P450 enzymes into the toxic intermediate NAPQI. At therapeutic doses of APAP, NAPQI is detoxified by glutathione conjugation. However, once cellular glutathione is depleted (overdose conditions), NAPQI can build up within cells and cause cellular toxicity.

Gemfibrozil is a common lipid-lowering drug and is also metabolised by hepatocytes in the liver. The drug is first metabolised by the UGT enzymes to form Gemfibrozil 1-O-β-glucuronide[196]. This metabolite can then undergo oxidation with the cytochrome P450 enzymes to form hydrodroxylated Gemfibrozil 1-O-β-glucuronide.

4.1.4 Probing Structure, Function and Gene Expression in 3D

Materials that offer a 3D interface for cell growth must still allow researchers to obtain information about the biological status of the cells during and after the growth period. There is little point culturing in 3D if a researcher cannot 'talk' or 'listen' to cells in that environment. Being able to image cells, examine their cell structure, assess function and quantify gene expression are just some of the crucial needs of researchers working in the field of 3D hepatocyte models for drug discovery applications. However, this is not entirely straightforward;

- Imaging cells in 3D is difficult. 3D cultures approximate the complexity and structure of native tissue, creating issues with light scattering and thus preventing clear, crisp cell-imaging. Furthermore, many scaffolds are not transparent, which again limits the use of conventional bright field microscopes for direct live-cell imaging.

- Comparing functional data between 2D and 3D requires some form of normalisation due to differences in cell adhesion, proliferation and viability. Normalisation against cell

number, protein content or DNA then requires extensive method development to ensure all appropriate biological material is extracted from the 3D scaffold to ensure a fair test.

Due to the challenges above, a significant proportion of this thesis involved method/protocol development in order to effectively compare 2D, 3D and *in vivo* hepatocyte behaviour. Outcomes of these method developments formed part of the commercial protocols associated with Alvetrex®Scaffold, currently available on the Reinnervate website (http://reinnervate.com/science-technical-resources/application-notes/).

4.2 Aims and Objectives

The overall aim of this Chapter was to assess the structural, functional and genetic consequences of culturing hepatocytes in emulsion templated polystyrene scaffolds. Chapter 3 showed that hepatocytes in emulsion templated polystyrene scaffolds could approximate native tissue density and cell-cell contact under specific culture conditions and scaffold presentations. This Chapter therefore aimed to understand if the structure-function-genetic relationships of hepatocytes in polystyrene scaffolds are more physiologically relevant.

The main objectives are to:

- Compare the morphology of individual hepatocyte cells cultured in scaffolds *versus* 2D using confocal immunofluorescence microscopy.
- Use SEM to obtain high resolution images of hepatocyte structure in scaffolds *versus* 2D *versus in vivo* mouse tissue.
- Probe hepatocyte ultrastructure (bile canaliculi, surface microvilli, tight junctions) in scaffolds *versus* 2D *versus in vivo* mouse tissue. Use confocal immunofluorescence to target specific bile canaliculi markers.
- Compare hepatocyte function in scaffolds *versus* 2D (under static media conditions). Include specific hepatocyte functional tests (albumin synthesis, urea conversion) as well as preliminary assessments of drug toxicity using APAP and Gemfibrozil.
- Compare hepatocyte function in scaffolds for static *versus* perfused media conditions. Use CYP3A4 activity as a representative measure of drug metabolism capacity.
- Assess the genetic differences between hepatocytes cultured in scaffolds *versus* 2D. Target genes that are associated with hepatic drug metabolism (genes coding for enzymes involved in phase I, phase II and phase III (transporter) drug metabolism).

4.3 Results

4.3.1 Hepatocyte Morphology

Chapter 3 employed ImageJ™ analysis of histology images to show that the XY diameter of hepatocytes cultured in emulsion templated polystyrene scaffolds more closely resembles the XY diameter of hepatocytes found *in vivo.* The same method also showed that hepatocytes cultured in 2D display an unusually large XY diameter as they flatten out across the 2D surface. However, to fully understand hepatocyte morphology in emulsion templated polystyrene scaffolds, laser scanning confocal microscopy was employed. This technique uses optical depth sections (Z-stacks) to obtain cell dimensions in the XYZ plane, as opposed to simply measuring XY diameters.

Hepatocytes were cultured on Alvetex®Scaffold, Alvetex®Strata and 2D glass coverslips for 24 hours. Alvetex®Scaffold was presented in the insert/12-well plate/submerged format, whereas Alvetex®Strata was presented in the insert/12-well plate/contact format. After the culture period cells were fixed and processed for confocal microscopy. Cells were stained for F-actin (cytoskeleton marker) and DAPI (nuclei stain). Imaging of the cells was taken directly on the scaffolds and glass coverslips.

Figure 4.2 shows the XYZ morphology differences of HepG2 cells cultured on Alvetex®Scaffold, Alvetex®Strata and 2D glass coverslips. For 2D culture, the cell nuclei and cytoskeleton flatten out across the plastic, consistent with the ImageJ™ analysis performed in Chapter 3**.** HepG2 cell length (longest distance in XY plane) is 48 μm, however the height (z plane) is only 6 μm**.** Conversely HepG2 cells cultured on Alvetex®Scaffold and Alvetex®Strata are much more rounded, with cell length, width and height being approximately the same. For Alvetex®Scaffold the length of the 3D cell cytoskeleton is 28 μm and the height is 28 μm. Similarly for Alvetex®Strata the length of the 3D cell cytoskeleton is 21 μm and the height is 25 μm. Interestingly, for Alvetex®Strata the F-actin filaments appeared to have localised at the joining membranes of cell-cell junctions, suggesting abundant cell-cell adhesions in this microenvironment. Table 4-2 summarises the HepG2 cell dimensions obtained from the confocal microscopy images.

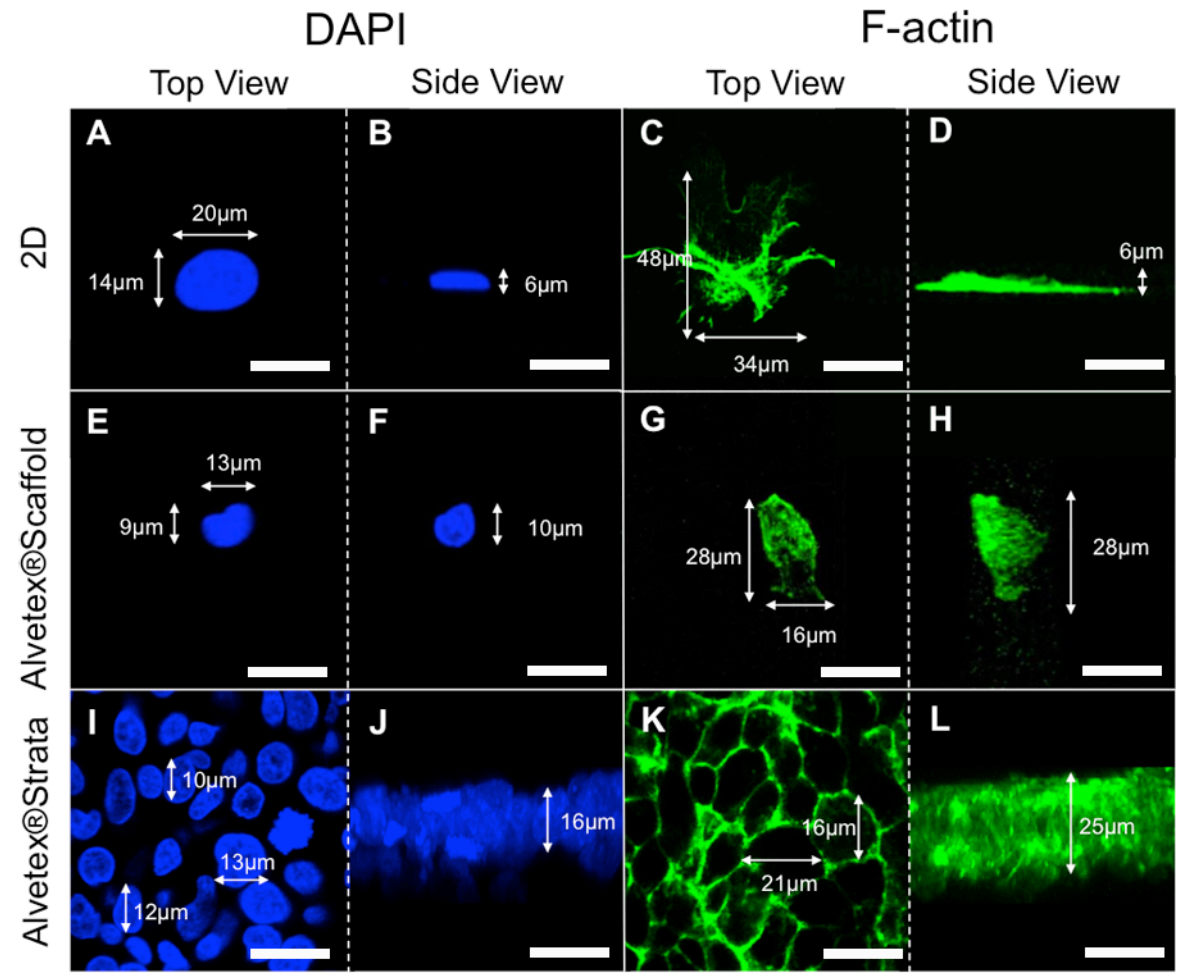

Figure 4.2 HepG2 morphology by F-actin/DAPI staining and imaging using laser-scanning confocal microscopy. (A-D): HepG2 cells grown on 2D glass coverslips. (E-H): HepG2 cells grown on Alvetex®Scaffold. (I-L): HepG2 cells grown on Alvetex®Strata. Cells were cultured for 24 hours and then stained for nuclei (DAPI: *blue*) and F-actin (Phalloidin: *green*). 2D HepG2 cells show a flat morphology with a cell height of only 6 µm. F-actin filaments appeared to have crawled out across the plastic creating a very large, flat cell surface. Cells grown within the Alvetex®Scaffold are more rounded, with the cell height being almost equal to the width and length. Cells grown on top of the Alvetex®Strata also display a more rounded morphology. Furthermore the F-actin staining in Alvetex®Strata shows extensive membrane localisation, demonstrating the formation of cytoskeleton-linked cell junctions. Scale bars = 20 µm.

Table 4-2 Dimensions of HepG2 Cytoskeletons Observed by Confocal Microscopy

	Length (µm)	Width (µm)	Height (µm)
2D	48	34	6
Alvetex®Scaffold	28	16	28
Alvetex®Strata	21	16	25

Figure 4.3 shows the morphology of Upcyte® cells cultured on Alvetex®Scaffold and 2D glass coverslips after 24 hours using confocal microscopy. Alvetex®Scaffold was presented in the

insert/12-well plate/submerged format. Similar to the HepG2 morphology data above, 2D cultures displayed extensive flattening. Actin filaments are visible and are mostly stress fibres. Upcyte® cell length (longest distance in XY plane) is 60 μm, however the height (z plane) is only 5 μm. Conversely, Upcyte® cells cultured on Alvetex®Scaffold display a cell length of 19 μm and a cell height of approximately 16 μm. Table 4-3 summarises the Upcyte® cell dimensions obtained from the confocal microscopy images.

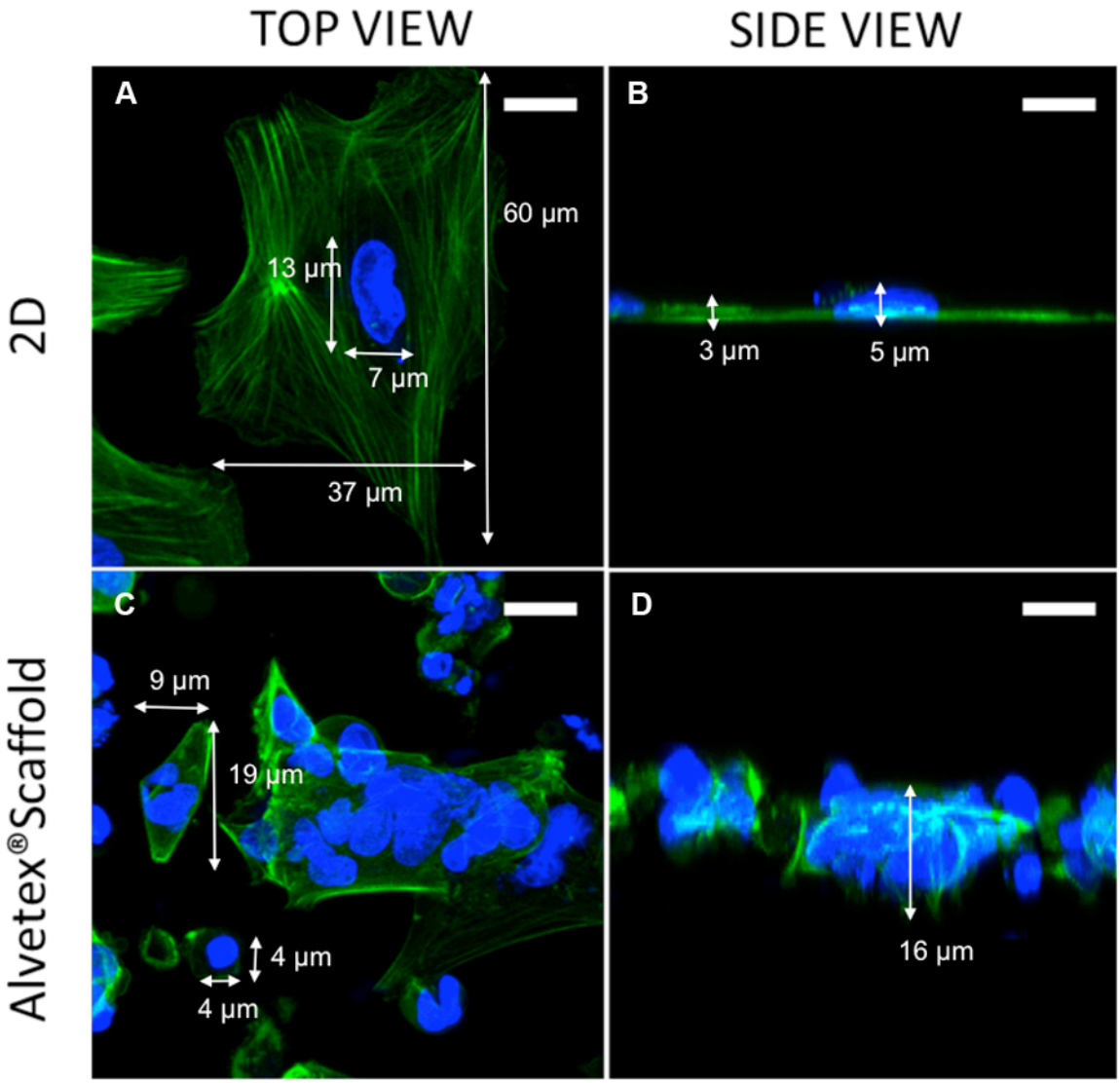

Figure 4.3 Upcyte® morphology by F-actin/DAPI staining and imaging using laser-scanning confocal microscopy. (A,B): Upcyte® cells grown on 2D glass coverslips. (C,D): Upcyte® cells grown on Alvetex®Scaffold. Cells were cultured for 24 hours and then stained for nuclei (DAPI: *blue*) and F-actin (Phalloidin: *green*). 2D Upcyte® cells show a flat morphology with a cell height of only 5 μm. F-actin filaments are visible and appear as stress fibres. Cells grown within the Alvetex®Scaffold are more rounded, with the cell height being almost equal to the width and length. Scale bars = 10 μm.

Table 4-3 Some Typical Dimensions of Upcyte® Cytoskeletons by Confocal Microscopy

	Length (μm)	Width (μm)	Height (μm)
2D	60	37	5
Alvetex®Scaffold	19	9	16

SEM was employed as an additional technique to visualise cell morphology directly on the growth substrate. Figure 4.4 shows SEM micrographs of HepG2 cells cultured on 2D, Alvetex®Scaffold and Alvetex®Strata after 7 days. An SEM image of adult male nude (nu/nu) mouse liver tissue is shown for comparison (tissue kindly donated by Eleanor Knight at Durham University and obtained in accordance with UK Home Office guidelines). Alvetex®Scaffold was presented in the insert/12-well plate/submerged format, whereas Alvetex®Strata was presented in the insert/12-well plate/contact format.

HepG2 cells in 2D are extremely flat, consistent with the histological analysis and confocal microscopy data. At this confluence there are also lots of open gaps where cells are not in contact with their neighbours (white arrows in Figure 4.4A). HepG2 cells in Alvetex®Scaffold have filled up the structure and appear to have adopted a rounded/elliptical morphology (white dotted circles in Figure 4.4B). Some gaps still remain in the structure where cells are not in contact with neighbours (white arrows in Figure 4.4B). For Alvetex®Strata a thick mass of 3D cell tissue is observed on top of the structure. It is difficult to visualise individual cells as the tissue is so densely packed. The mouse tissue is similar to Alvetex®Strata; a thick mass of 3D cells with maximum cell-cell contact.

Upcyte® cells in Alvetex®Scaffold were also imaged using SEM. Cells were grown for 7 days in the insert/12-well plate/submerged format. Figure 4.5 shows that individual Upcyte® cells in Alvetex®Scaffold adopt a round (almost spherical) morphology. Moreover, abundant microvilli can be found on the cell surface (Figure 4.5E-H). This suggests that the cells have retained some polarisation within Alvetex®Scaffold throughout the culture period employed.

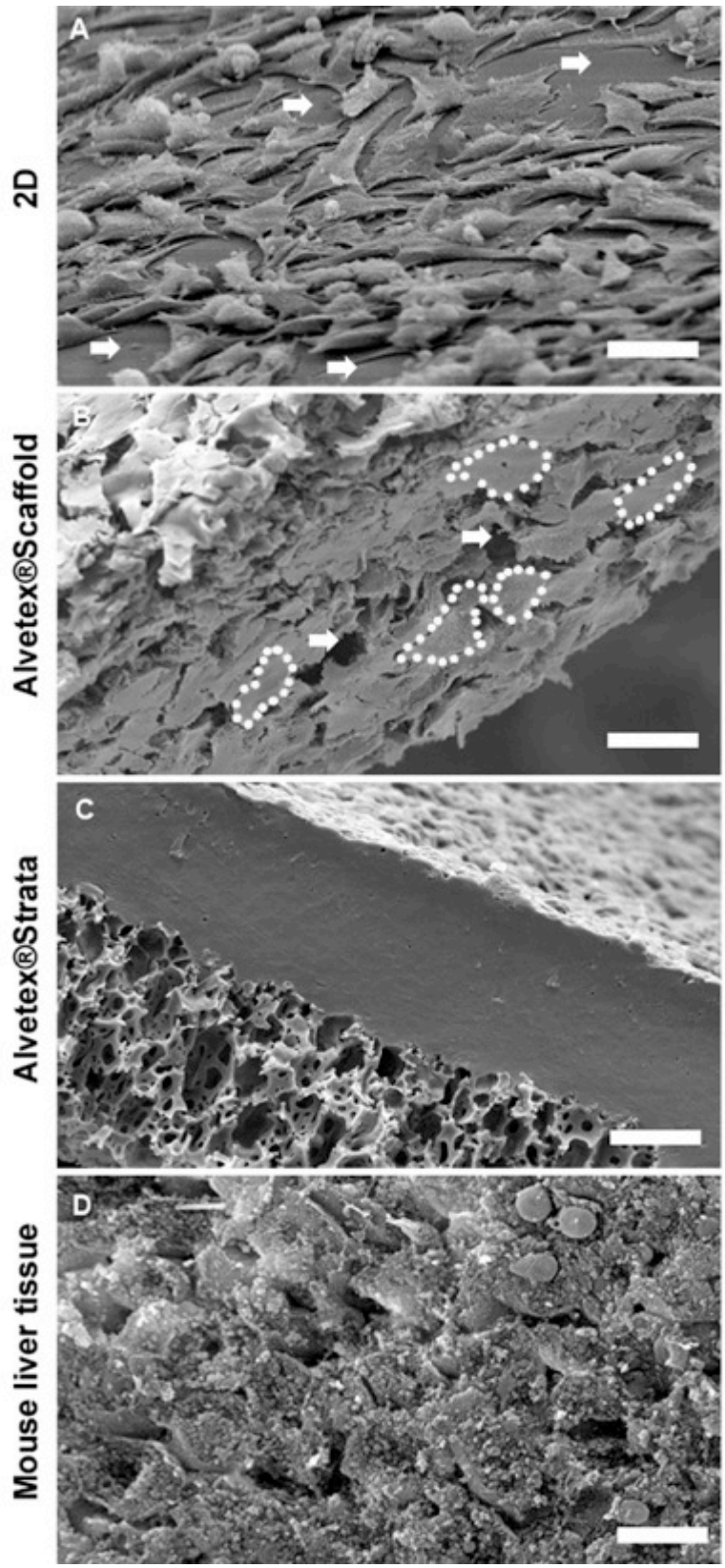

Figure 4.4 SEM images of HepG2 cells cultured in 2D, Alvetex®Scaffold and Alvetex®Strata after 7 days compared to mouse liver tissue. (A): 2D cells. The white arrows show regions lacking cell-cell contact. (B): 3D cells filling Alvetex®Scaffold adopting an elliptical shape (white dotted lines). Some regions still lack cell-cell contact (white arrows). (C): 3D cells on top of Alvetex®Strata forming a dense tissue mass. (D): *In vivo* mouse liver control with maximum cell-cell contact. Scale bars = 50 μm.

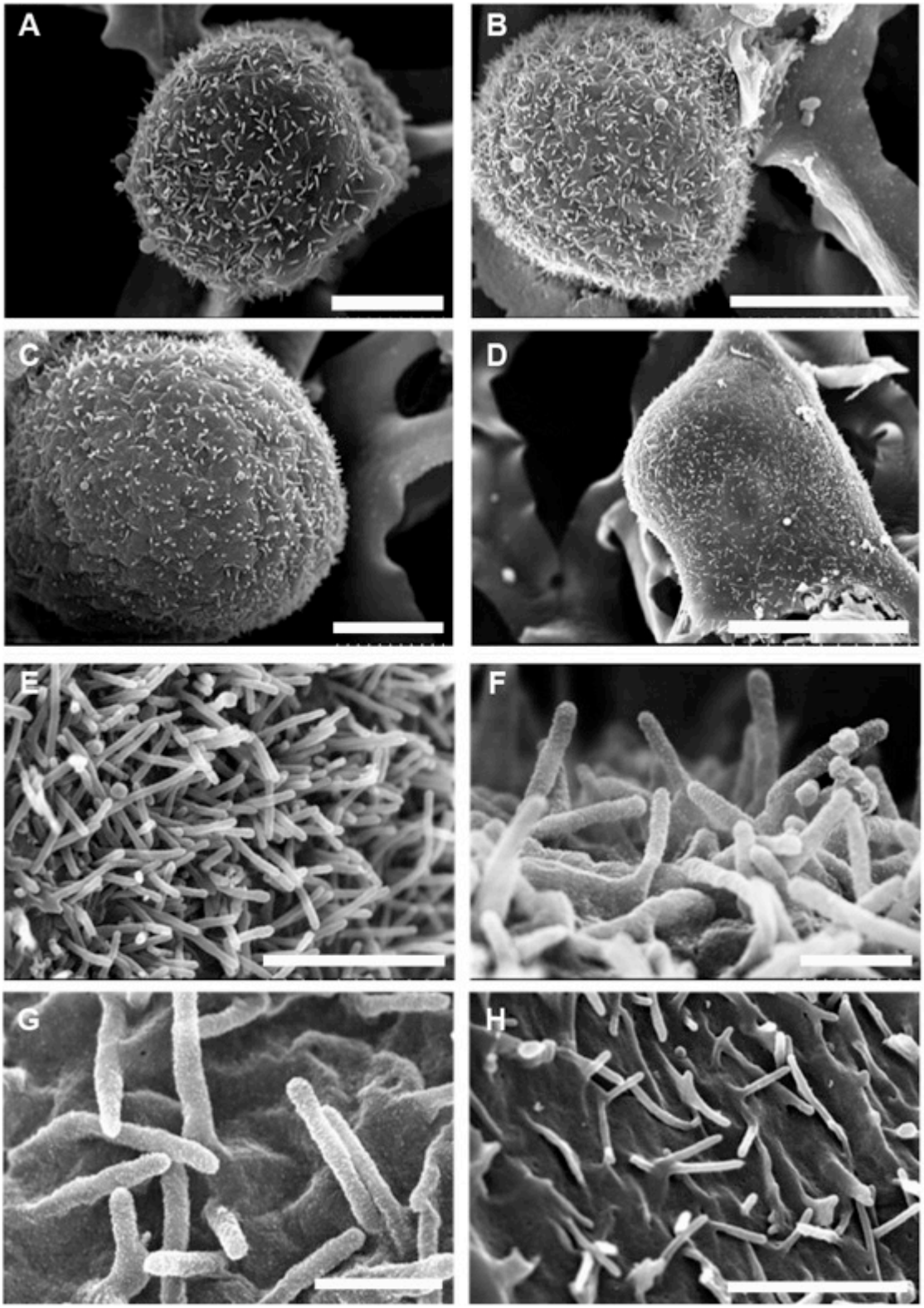

Figure 4.5 SEM images of Upcyte® cells cultured in Alvetex®Scaffold for 7 days. (A-D): Individual cells show a rounded morphology. (E-H): Abundant microvilli are present on the cell surface suggesting maintenance of polarisation throughout the culture period. Scale bars: A = 5 μm, B = 10 μm, C = 5 μm, D = 20 μm, E = 2 μm, F = 500 nm, G = 500 nm, H = 2 μm.

4.3.2 Hepatocyte Ultrastructure

As discussed in Chapter 1, hepatocyte ultrastructure is crucial for function. Sinusoidal microvilli and bile canaliculi are particularly important for drug uptake and elimination. This study assessed the ability of scaffold cultures to form these structures using confocal immunofluorescence and transmission electron microscopy (TEM).

Tight junctions (zonula occludens, Zo) are required for the formation of sinusoidal microvilli as well as bile canaliculi. Furthermore, drug transporter proteins such as MDR1 and MRP2 are localised at the bile canaliculi membranes. Immunofluorescence staining using antibodies for Zo (ZO1, *Life Technologies*), MRP2 (abcam) and MDR1 (abcam) was therefore employed to probe hepatocyte ultrastructure.

HepG2 cells were cultured for 3 days on 2D glass coverslips, Alvetex®Scaffold and Alvetex®Strata and then processed for immunofluorescence. Alvetex®Scaffold was presented in the insert/12-well plate/submerged format, whereas Alvetex®Strata was presented in the insert/12-well plate/contact format. Confocal imaging was performed directly on the growth substrate. Figure 4.6 shows that most positive green staining for ZO1 occurs for HepG2 cells cultured on Alvetex®Strata. This is to be expected and is consistent with the previous histology and SEM data showing maximum cell-cell contact for Alvetex®Strata. Alvetex®Scaffold displays the second most positive green staining for ZO1, whereas 2D cultures show the least. Indeed, the 2D culture shows only faint green staining for ZO1 (white dotted line in Figure 4.6A represents cell boundaries).

HepG2 cells cultured on Alvetex®Strata also showed the most positive staining for MRP2 and MDR1. Alvetex®Scaffold and 2D cultures did show signs of positive MRP2 staining, however this was noticeably less compared to Alvetex®Strata. Very little positive MDR1 staining was observed for Alvetex®Scaffold and 2D.

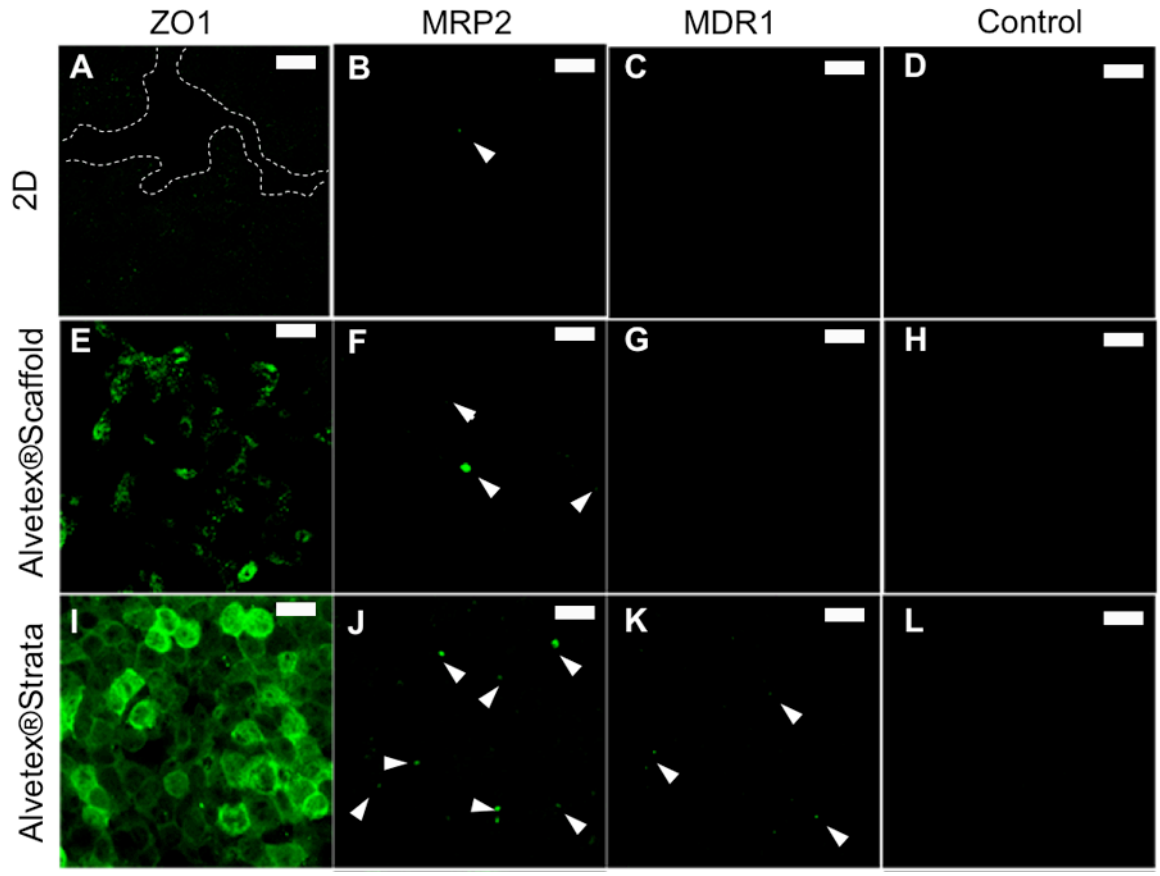

Figure 4.6 Immunofluorescence staining for ZO1, MRP2 and MDR1 for HepG2 cells cultured on 2D glass coverslips, Alvetex®Scaffold and Alvetex®Strata. (A-D): Cells grown on 2D plastic. Only faint green staining is observed. The white dotted line in (A) represents cell boundaries. Very little positive green staining for MRP2 and MDR1 is observed. (E-H): Cells grown on Alvetex®Scaffold. More positive ZO1 staining is observed compared to 2D, however positive green staining for MRP2 and MDR1 is still low. (I-L): Cells grown on Alvetex®Strata. Abundant positive green staining for ZO1 is observed. There is also some staining for MRP2 and MDR1. Cells were cultured for 3 days before processing. The negative control micrographs represent secondary antibody staining only. Scale bar = 20µm.

For TEM analysis, adult male nude (nu/nu) mouse liver tissue was used as an *in vivo* control for the study (tissue kindly donated by Eleanor Knight at Durham University and obtained in accordance with UK Home Office guidelines). Figure 4.7 and Figure 4.8 show the ultrastructure of the mouse liver tissue by TEM. As expected, most key hepatocyte organelles are present including the nucleus (NU), mitochondria (Mt), rough endoplasmic reticulum (RER) and lipid storing droplets (LD) (see Figure 4.7). Cell shape in Figure 4.8A is almost rectangular, translating into an expected cuboidal shape in 3D. Hepatocytes at the sinusoidal interface are observed in Figure 4.8B and Figure 4.8C. Here a Kupffer cell (KC) is in close contact with the hepatocytes, along with liver sinusoidal cells (LSECs) and erythrocyte cells (EC). Abundant microvilli (MV) can be seen protruding into the *Space of Disse* (SoD). Figure 4.8D shows the cell-cell adhesions forming

between two adjacent hepatocytes. Desmosomes (D) are observed by the wide and dense protein shadows in the TEM micrograph. Next to the desmosomes are zonula adherens (Za) and finally zonula occludens (Zo) to form a tight junction (TJ) complex between the two cells. Bile canaliculi can be seen in Figure 4.8E and Figure 4.8F. These form between adjacent hepatocytes, using Zo junctions and are usually filled with MV. The size of the bile canaliculi are approximately 1 μm wide.

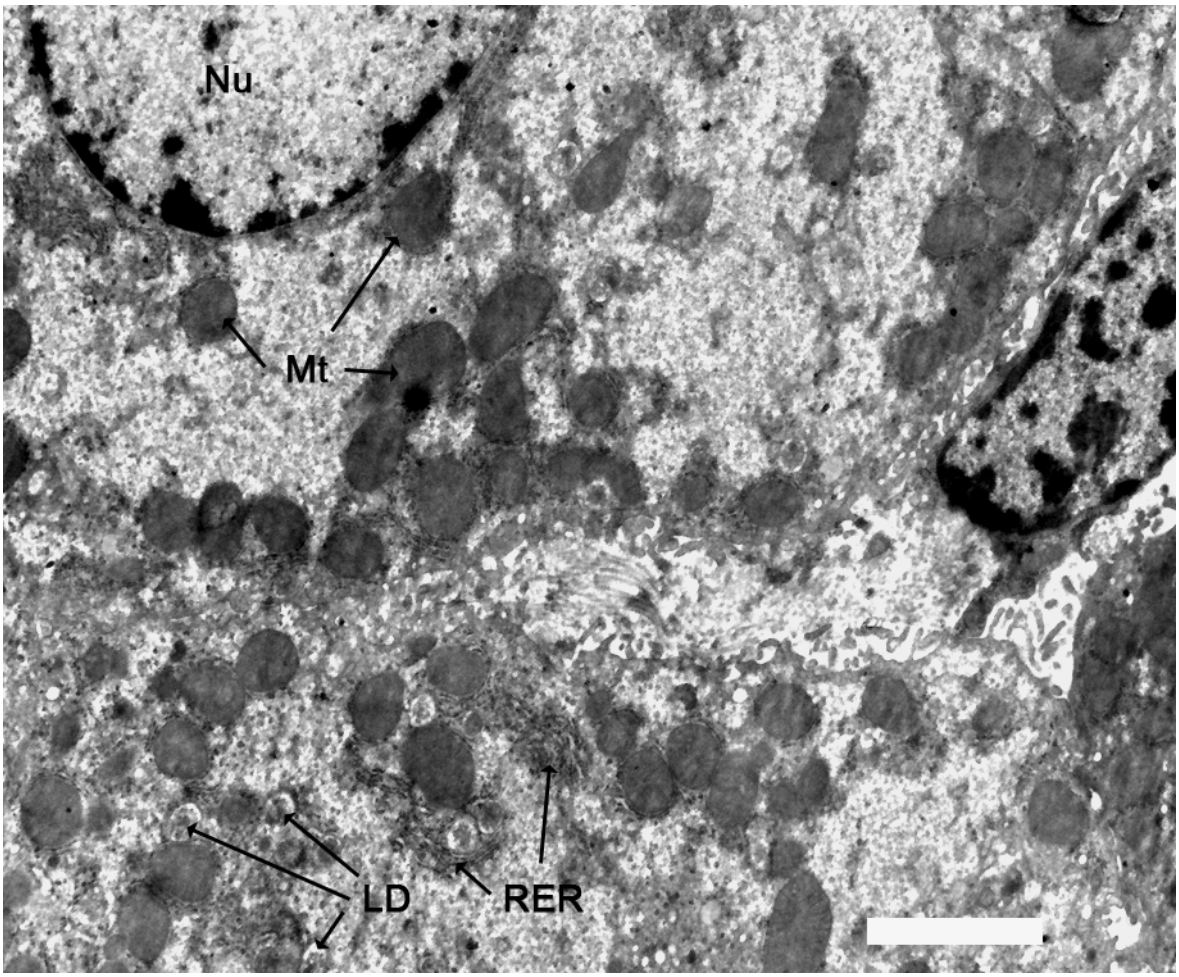

Figure 4.7 TEM analysis of mouse liver tissue extracted from adult male nude (nu/nu) mice. Most key hepatocyte organelles can be seen, including the nucleus (NU), mitochondria (Mt), rough endoplasmic reticulum (RER) and lipid storing droplets (LD). Scale bar = 2 μm. The pre-fixed mouse liver tissue was kindly donated by Eleanor Knight at Durham University and was obtained with guidelines and permission from the UK Home Office.

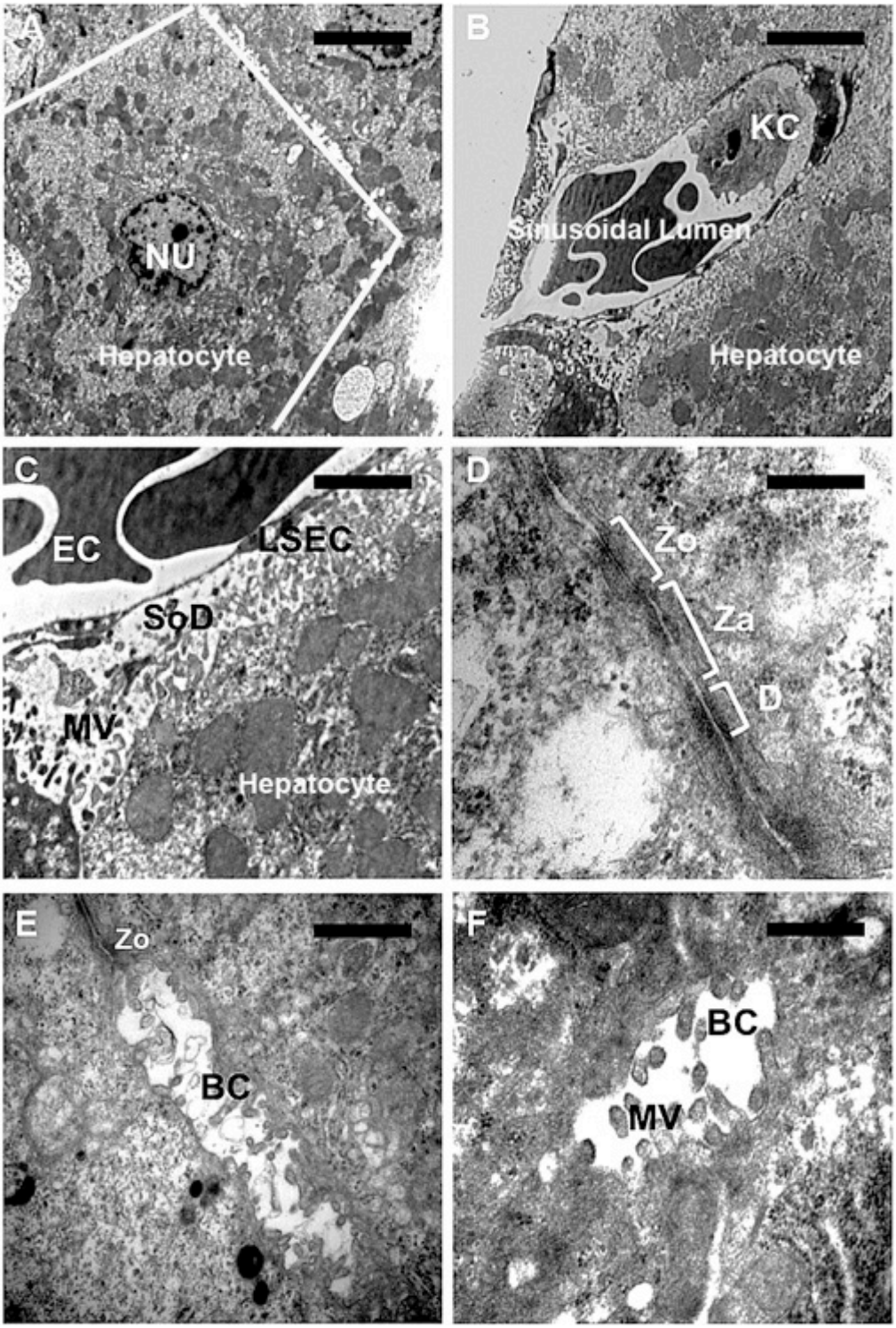

Figure 4.8 TEM analysis of mouse liver tissue extracted from adult male nude (nu/nu) mice. (A): A single hepatocyte adopting an almost rectangular shape. The white lines represent the boundaries between adjacent cells. Scale bar = 5 μm. (B): Hepatocytes at the sinusoidal interface in close contact with a Kupffer cell (KC). Scale bar = 5 μm. (C): Sinusoidal interface of a hepatocyte cell with its microvilli (MV) protruding into the Space of Disse (SoD). Liver sinusoidal endothelial cells (LSECs) and blood erythrocyte cells (EC) are also present. Scale bar = 1 μm (D): Cell-cell junction between two adjacent hepatocytes containing desmosomes (D), zonula adherens (Za) and zonula occludens (Zo). Scale bar = 400 nm (E-F): Bile canaliculi (BC) between adjacent hepatocytes. Scale bar in E = 2 μm. Scale bar in F = 500 nm.

TEM images of HepG2 cells cultured on 2D glass coverslips for 3 days are shown in Figure 4.9. Most key hepatocyte organelles can be seen including the nucleus (NU), mitochondria (Mt), rough endoplasmic reticulum (RER) and lipid storing droplets (LD). Some microvilli (MV) can be seen protruding from the surface of the cells, however these are sparse and quite elongated. All the cells and cell nuclei are extremely flattened, in contrast to the rectangular hepatocyte shapes observed in the mouse tissue TEM images. Furthermore, there is very little opportunity for cell-cell contact, to the extent that hepatocytes appear to be wrapping around one another to maximise cell-cell contact (black arrows in Figure 4.9E). Importantly no advanced bile canaliculi were observed in this experiment (see Figure 4.13).

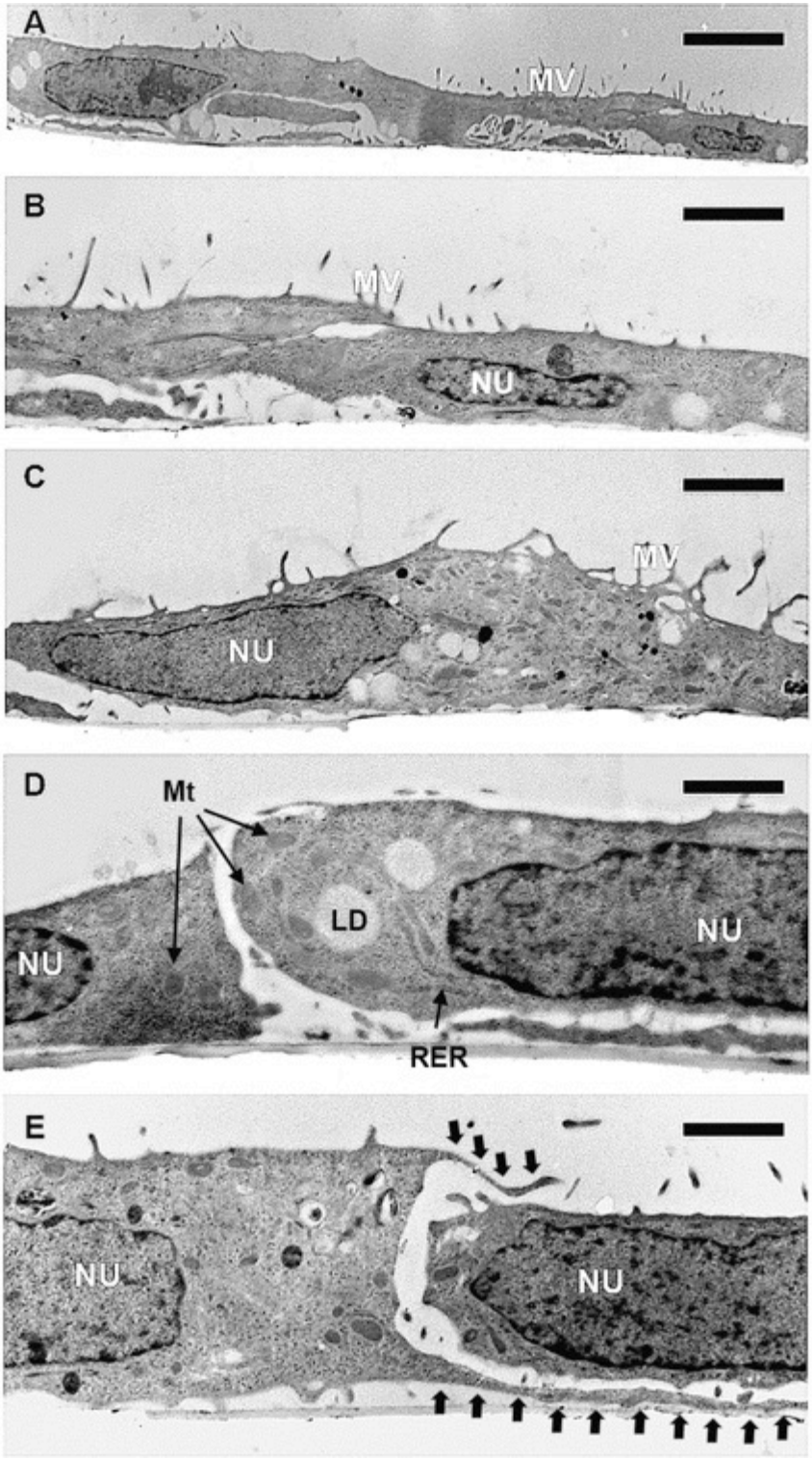

Figure 4.9 TEM analysis of HepG2 ultrastructure when cultured on 2D glass coverslips for 3 days. (A): A severely flattened morphology is observed. Only sparse and elongated microvilli (MV) are present on the cell surface. Scale bar = 8 μm. (B,C): Cell nuclei (NU) are also forced into a flattened shape. Scale bar = 4 μm. (D): Most key hepatocyte organelles are still present in 2D including mitochondria (Mt), rough endoplasmic reticulum (RER) and lipid storing droplets (LD). Scale bar = 2 μm. (E): Cells appear to be wrapping around one another to maximise cell-cell contact (black arrows). Scale bar = 2 μm.

TEM images of HepG2 cells cultured in Alvetex®Scaffold (insert/12-well plate/submerged) for 4 days are shown in Figure 4.10 and Figure 4.11. Most key hepatocyte organelles can be seen including the nucleus (NU), mitochondria (Mt), rough endoplasmic reticulum (RER) and lipid storing droplets (LD). The image in Figure 4.10 further illustrates the round morphology of HepG2 cells cultured in Alvetex®Scaffold, consistent with previous data.

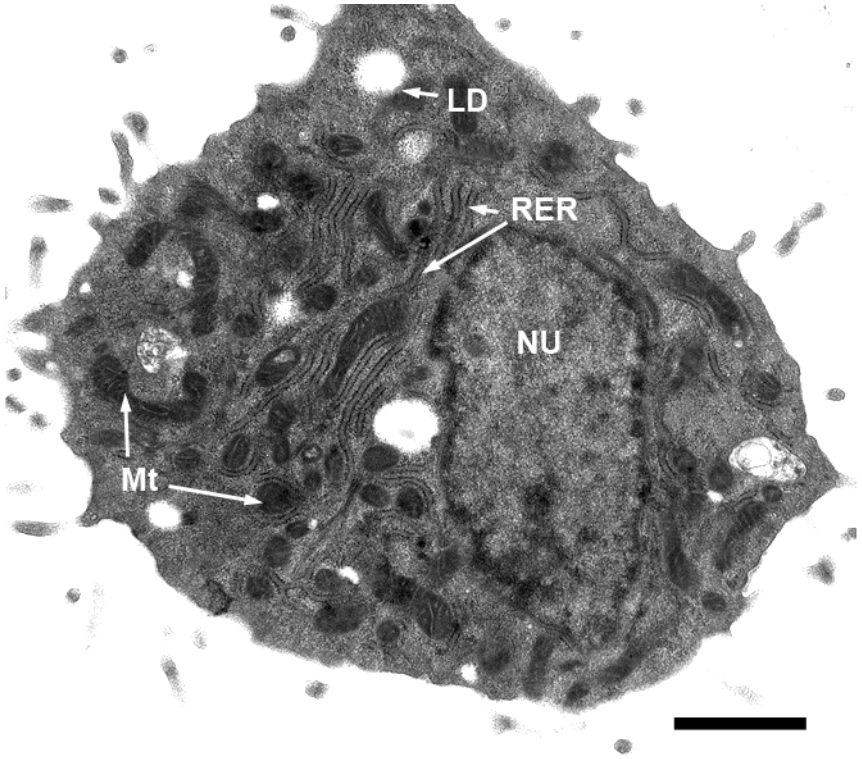

Figure 4.10 TEM analysis of HepG2 ultrastructure when cultured in Alvetex®Scaffold for 4 days using the insert/12-well plate/submerged format. Most key hepatocyte organelles can be seen including the nucleus (NU), mitochondria (Mt), rough endoplasmic reticulum (RER) and lipid storing droplets (LD). Cell shape is round. Scale bar = 1 μm.

Figure 4.11A-E highlights how the scaffold (SC) structure supports cells into a 3D shape. Nearly all cells are encouraged into a round shape by the scaffold walls. Interestingly, the cell in Figure 4.11C seems to be modifying its structure to squeeze through an interconnecting window in the scaffold (white dotted circle). This is consistent with data in Chapter 3 showing that HepG2 cells can migrate through the scaffold structure. From an ultrastructural standpoint, HepG2 cells in Alvetex®Scaffold display abundant microvilli (MV), as shown in Figure 4.11B and Figure 4.11E. There is also evidence of bile canaliculi (see Figure 4.11F and Figure 4.13).

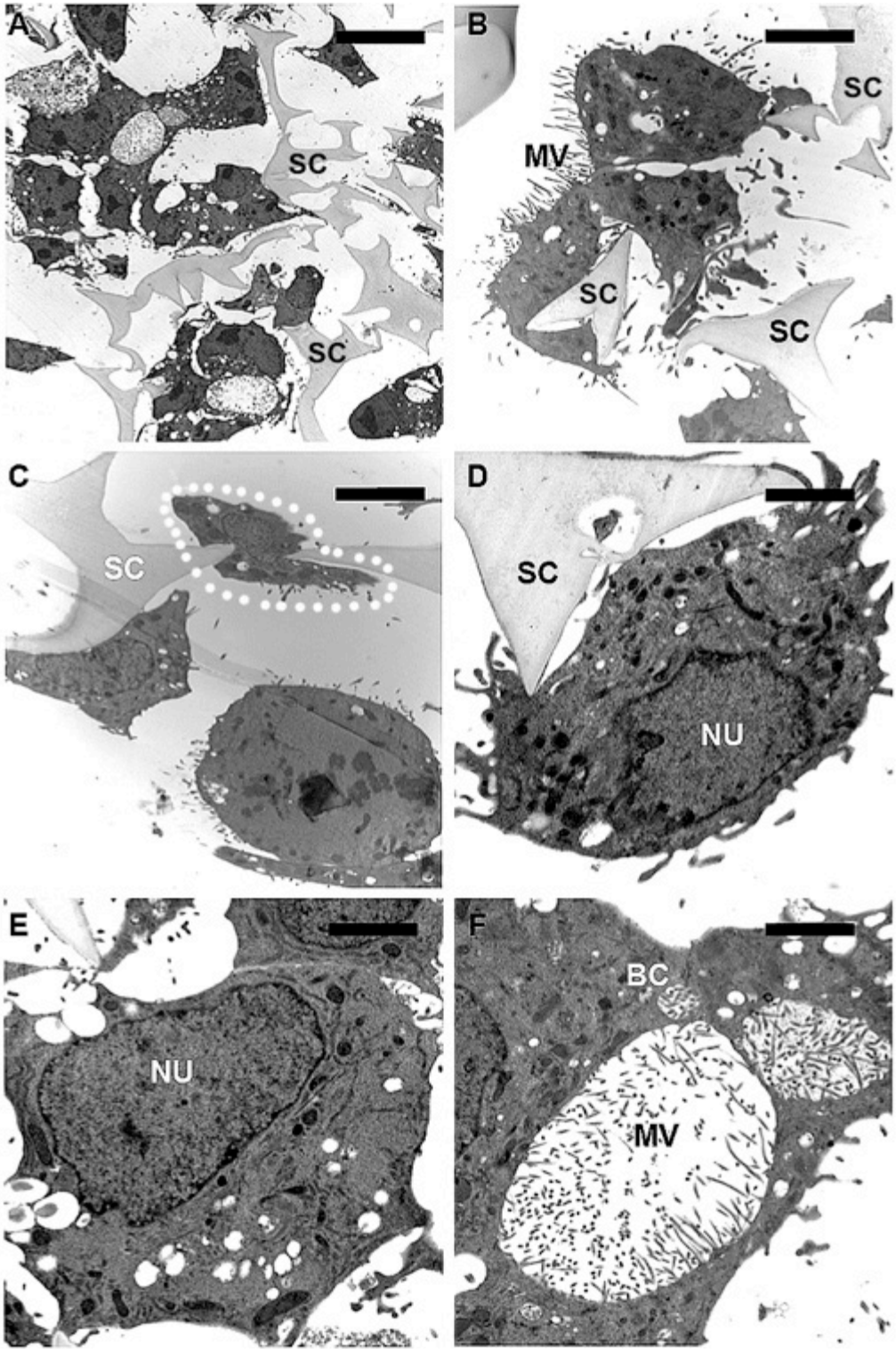

Figure 4.11 TEM analysis of HepG2 ultrastructure when cultured in Alvetex®Scaffold for 4 days using the insert/12-well plate/submerged format. (A-E): Scaffold (SC) walls seem to encourage HepG2 cells into a 3D morphology. One hepatocyte cell appears to be altering its structure to squeeze through an interconnecting window on the scaffold (white dotted circles in C). Abundant microvilli are observed in B and F. A bile canaliculus can also be seen in F. Scale bar A = 8 μm. Scale bars B,C = 5 μm. Scale bars D,E,F = 2 μm.

Figure 4.12 shows the ultrastructure of HepG2 cells cultured on Alvetex®Strata for 4 days using the insert/12-well plate/contact format. As with 2D and Alvetex®Scaffold, HepG2 cells on Alvetex®Strata display most of the key organelles, including the nucleus (NU), mitochondria (Mt), rough endoplasmic reticulum (RER) and lipid storing droplets (LD). Cells are very densely packed and grow in an almost ''scaffold-less'' manner on top of Alvetex®Strata. Some signs of cell necrosis are observed for cells closest to the air-liquid interface, evident by the decaying nuclei and faint cytoplasm in Figure 4.12B. Nonetheless, for healthy cells closer to the media supply there is extensive opportunity for cell-cell contact. These cells also seem to protrude microvilli into a lumen-type structure, suggesting early signs of structural re-organisation towards the native sinusoidal domains (Figure 4.12D).

The formation of bile canaliculi is crucial for normal hepatocyte function. Figure 4.13 shows the features attributable to bile canaliculi formation for HepG2 cells in 2D, Alvetex®Scaffold and Alvetex®Strata by TEM imaging. For 2D, no convincing bile canaliculi features were observed, except for small lumen structures (see Figure 4.13A). However these were often lacking microvilli and/or tight junctions. Conversely Alvetex®Scaffold did show some signs of advanced bile canaliculi with appropriate microvilli and tight junctions, albeit infrequently (see Figure 4.13B). Alvetex®Strata displayed even more evidence of bile canaliculi formation (see Figure 4.13C-E). These features were abundant throughout the healthy tissue mass and always displayed appropriate microvilli and tight junctions.

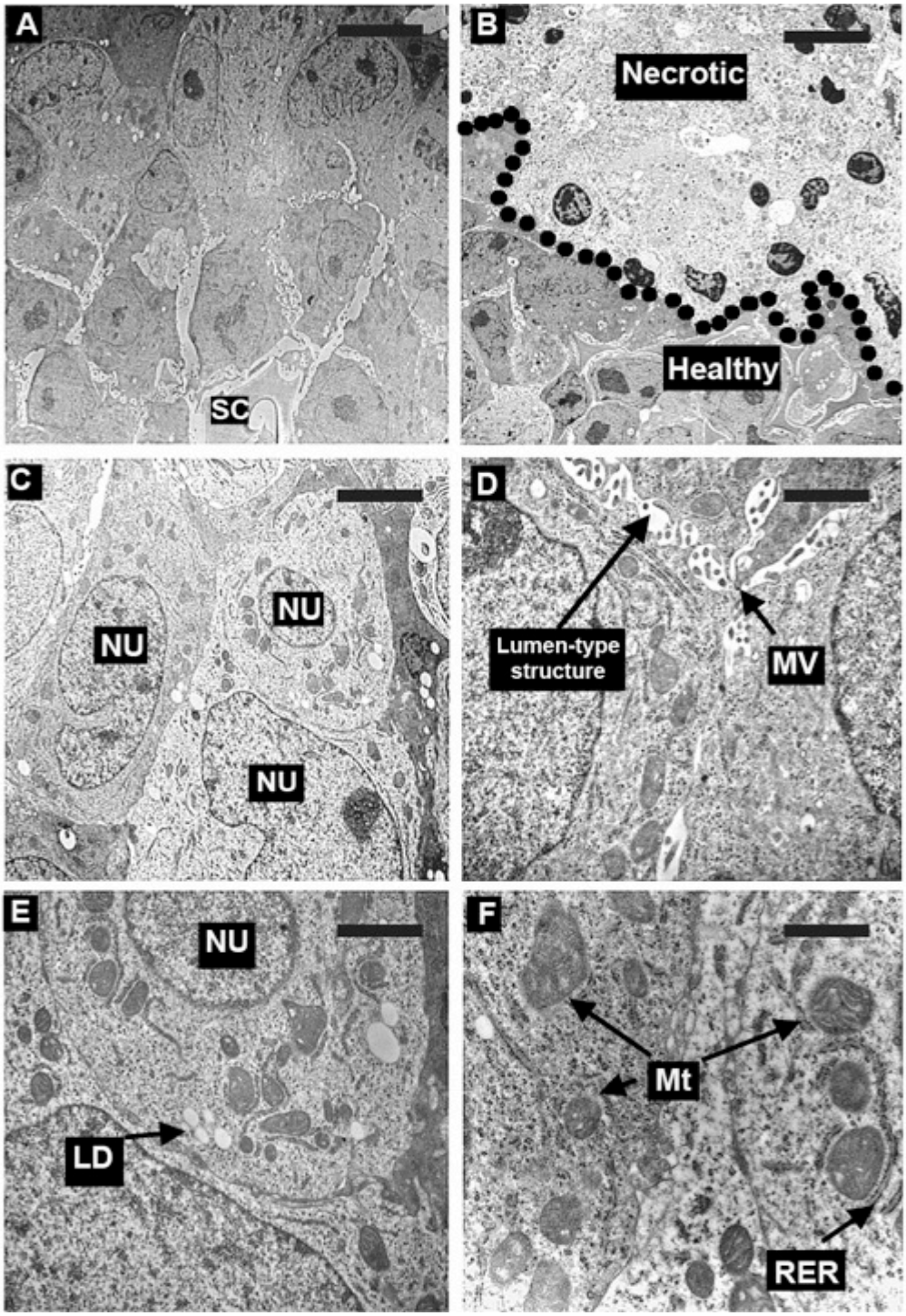

Figure 4.12 TEM analysis of HepG2 ultrastructure when cultured on Alvetex®Strata for 4 days using the insert/12-well plate/contact format. (A): Cell growth is almost ''scaffold-less'', with the scaffold (SC) only visible in the lower portion of the cell mass. (B): Cell necrosis is present near the top portion of the tissue mass even after 4 days, evident by the decaying nuclei and the faint cytoplasms. The black dotted line indicates the boundary between healthy and necrotic cells. (C): Several HepG2 cells in contact with one another demonstrating the significant opportunity for cell-cell contact. (D): Three cells joining together and protruding microvilli (MV) into a lumen-type structure. (E-F): Most of the key hepatocyte organelles are present including the nucleus (NU), mitochondria (Mt), rough endoplasmic reticulum (RER) and lipid storing droplets (LD). Scale bars A,B = 10 μm. Scale bar C = 5 μm. Scale bars D,E = 2 μm. Scale bar F = 1 μm.

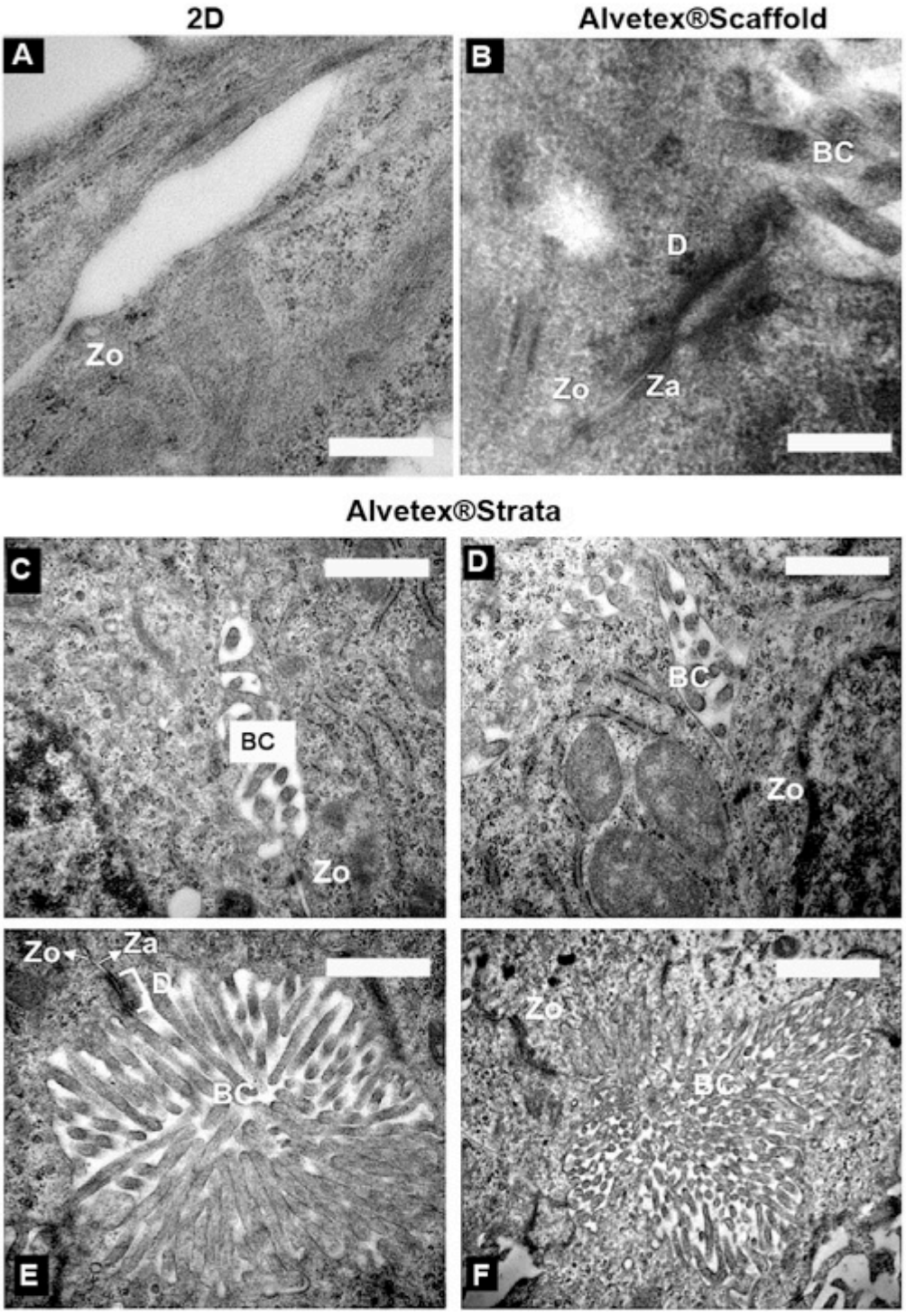

Figure 4.13 Evidence of bile canaliculi formation for HepG2 cells cultured on 2D glass coverslips, Alvetex®Scaffold and Alvetex®Strata. (A): HepG2 cells cultured on 2D show features that could be assumed to be bile canaliculi, however these are not entirely convincing due to a lack of microvilli and/or tight junctions (zonula occludens, Zo). (B): HepG2 cells cultured on Alvetex®Scaffold show promising signs of advanced bile canaliculi formation, albeit infrequently. Evidence of desmosomes (D), zonula adherens (Za) and Zo were present along with microvilli suggesting the features were indeed bile canaliculi (BC). (C-F): An abundance of BC were observed for HepG2 cells cultured on top of Alvetex®Strata. Scale bar A = 500 nm. Scale bar B = 300 nm. Scale bars C, D, E = 1 μm. Scale bar F = 2 μm.

Upcyte® hepatocytes were also investigated by TEM. Prior to this study there had been no ultrastructural assessment of these cells in 2D or 3D culture. Figure 4.14 and Figure 4.15 show the ultrastructure of Upcyte® cells cultured in Alvetex®Scaffold (insert/12-well plate/submerged) for 4 days. Cells appear healthy with most key organelles observable, including the nucleus (NU), mitochondria (Mt), rough endoplasmic reticulum (RER), smooth endoplasmic reticulum (SER) and lipid storing droplets (LD). There is also evidence of surface microvilli (MV). There are also signs of glycogen storage (GLY) within the hepatocytes.

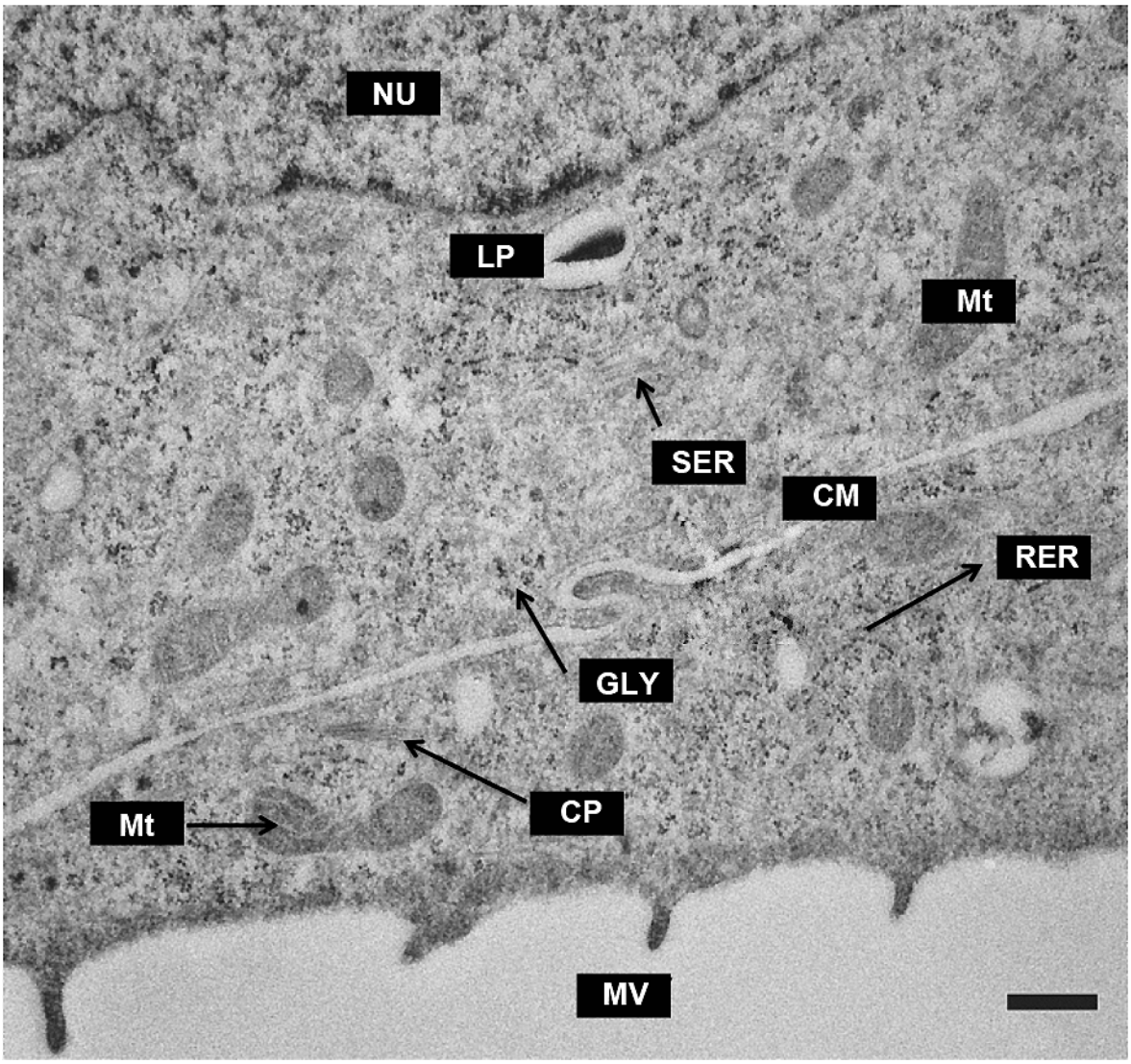

Figure 4.14 Ultrastructural features of Upcyte® cells in Alvetex®Scaffold by TEM (high power). All key organelles appear normal and healthy: nucleus (NU), mitochondria (Mt), rough endoplasmic reticulum (RER), smooth endoplasmic reticulum (SER), lipid droplets (LD) and cytoskeletal proteins (CP). There is also evidence of cell-surface microvilli (MV) and glycogen (GLY). Two cells are separated by a cell membrane (CM). Scale bar = 500 nm.

Importantly the ultrastructural shape of the cells is almost rectangular (Figure 4.15), which would be expected to translate into a cuboidal shape in 3D. As for HepG2 cells, evidence of the scaffold (SC) supporting cell shape is also observed (Figure 4.15B,D).

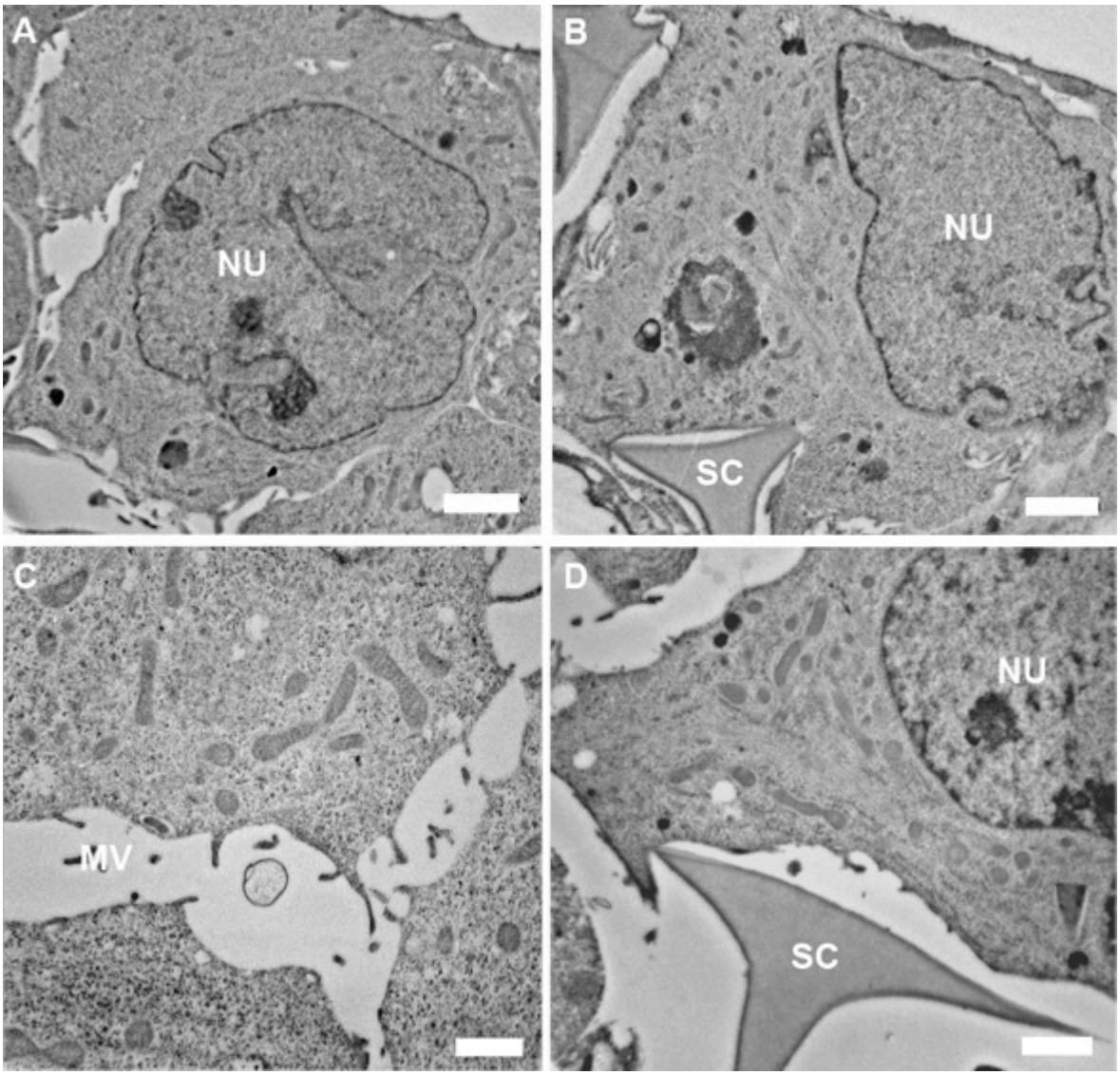

Figure 4.15 Ultrastructural features of Upcyte® cells in Alvetex®Scaffold by TEM (low power). (A,B): A rectangular cell shape is observed for cells in the scaffolds. Scale bars = 2 μm. (C): Cells appear healthy and seem to protrude microvilli from the cell surface. Scale bar 500 nm. (D): The wall of Alvetex®Scaffold (SC) can be seen to be supporting the weight of an Upcyte® cell. Scale bar = 2 μm.

The ultrastructure of Upcyte® cells cultured in 2D is shown in Figure 4.16 and Figure 4.17. Most key organelles can be seen, including the nucleus (NU), mitochondria (Mt), rough endoplasmic reticulum (RER) and lipid storing droplets (LD). However, cells and organelles are extremely flattened. Similar to HepG2 cells, there is very little opportunity for cell-cell contact. Where cell

edges do meet, the cells seem to wrap around one another as much as possible to maximise contact (Figure 4.16B,C).

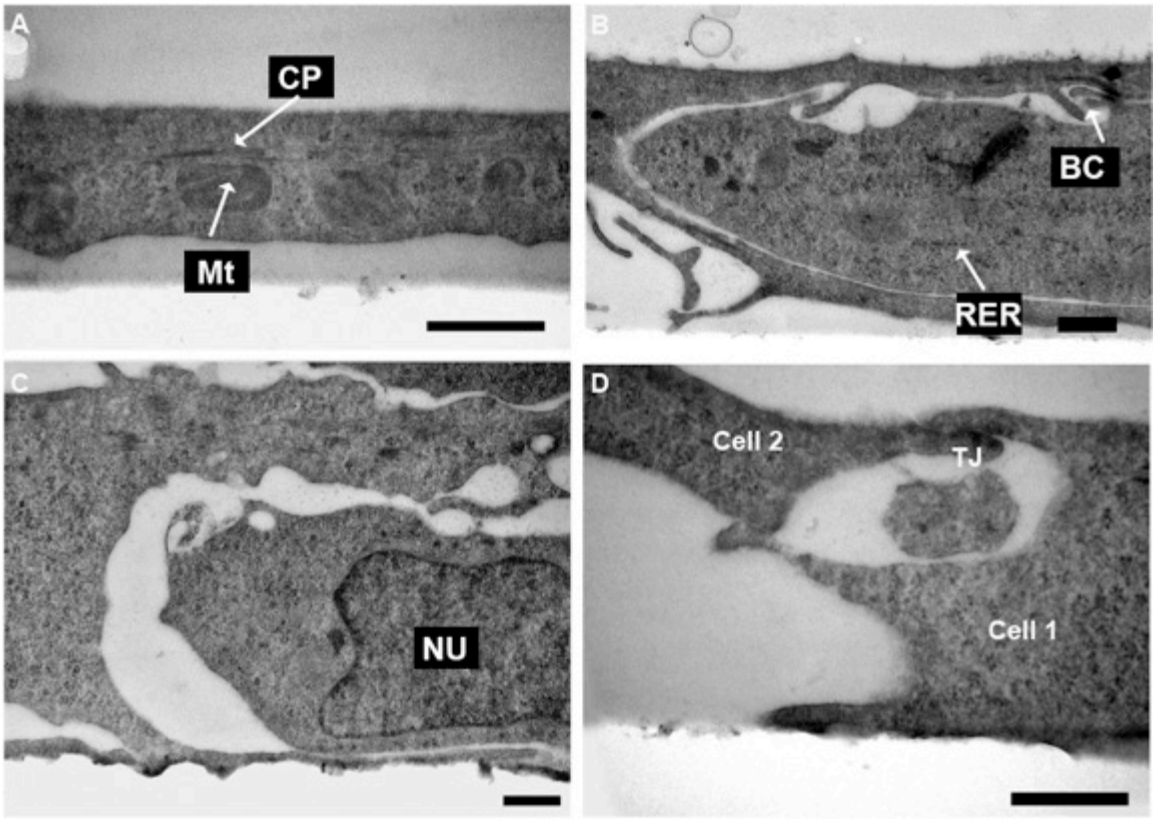

Figure 4.16 Ultrastructural features of Upcyte® cells cultured on 2D glass coverslips (part 1). (A): Cytoskeletal proteins (CP) appear to be stretching horizontally. Some mitochondria (Mt) are present. Scale bar = 2 µm. (B): A cell is wrapping around another to maximise contact. Possible attempts at bile canaliculi (BC) are being made, although there is a noticeable absence of tight junctions between cells. Scale bar = 500 nm. (C): Another example of two cells wrapping around one another to maximize cell-cell contact. Scale bar = 500 nm. (D): Example of limited cell-cell contact between two cells. Some signs of tight junctions (TJ) are observed. Scale bar = 500 nm.

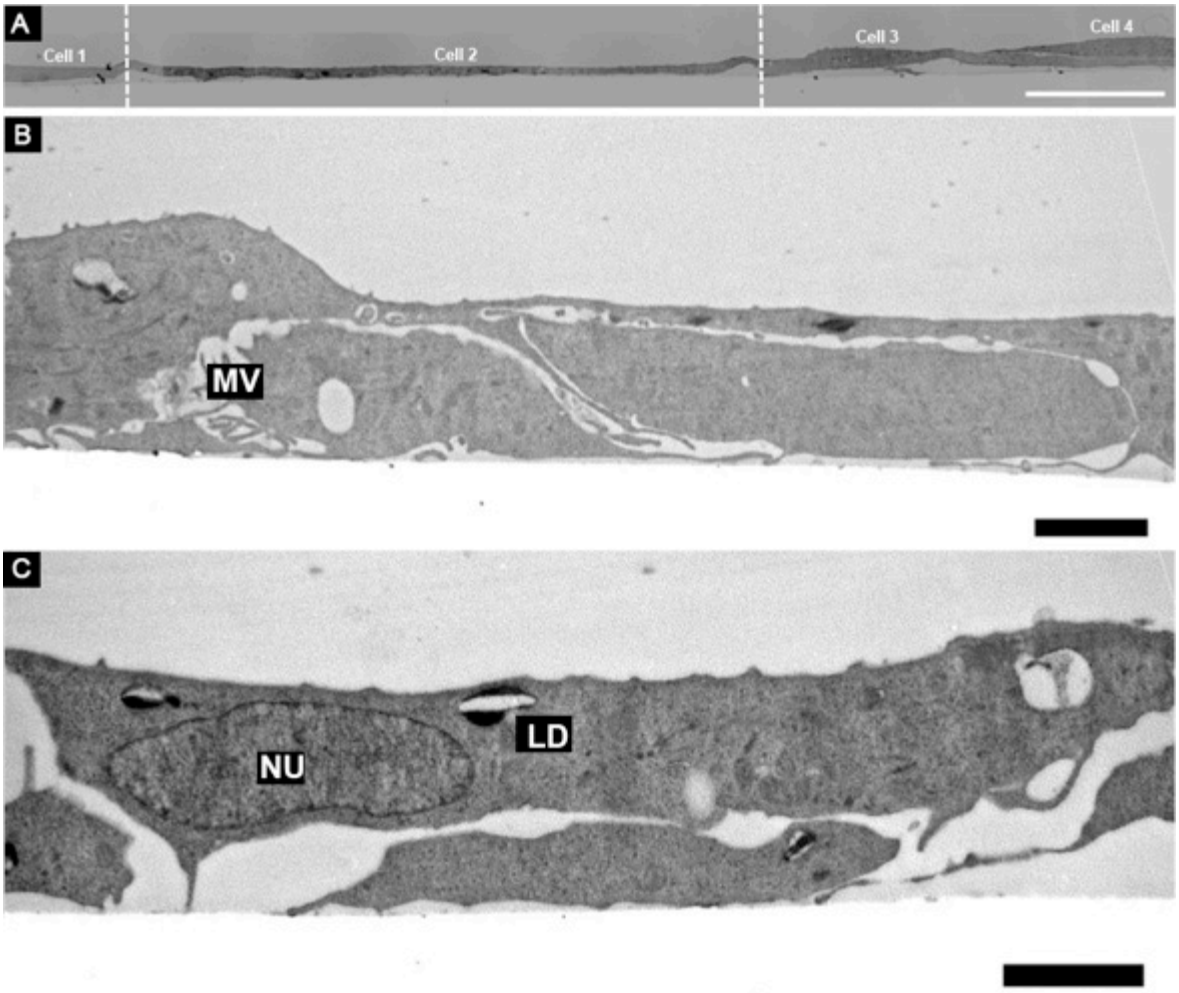

Figure 4.17 Ultrastructural features of Upcyte® cells cultured on 2D glass coverslips (part 2). (A): Low power image of three Upcyte® cells grown on 2D coverslips. Cells appear viable but are extremely flattened. Cells 2 spans approximately 50 µm, with only a tiny portion of its cell surface being in contact with Cell 1 and Cell 3. A noticeable lack of microvilli on the hepatocyte surface is observed. Scale bar = 10 µm. (B,C): Medium power images. Some microvilli (MV) can be seen. Scale bars = 2 µm.

4.3.3 Hepatocyte Function (3D Static *versus* 2D Static)

Hepatocyte function was compared between 2D and 3D cultures under static media conditions to provide a correlation with the above structural differences. Glucose consumption between 2D and 3D cultures was first compared. Primary rat hepatocytes were seeded onto fibronectin coated 12-well plates (2D) and Alvetex®Scaffold (insert/12-well plate/submerged) at a density of 0.2 million cells. Media was brought up to 4 mL and the cells were cultured for 2 days. Media samples were taken throughout the culture period to monitor glucose consumption. Figure 4.18 shows the change in media glucose (per hour) throughout the culture period. A significantly greater consumption of glucose is observed for 3D cultures compared to 2D cultures.

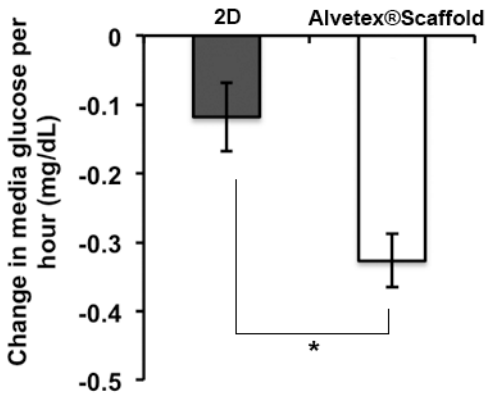

Figure 4.18 Hourly change in media glucose for primary hepatocytes cultured in 2D and 3D. Cells were seeded at equal density between 2D and 3D (0.8 million) and cultured in 4 mL of media for 2 days. A greater consumption of glucose is observed for 3D compared to 2D suggesting that these cells are more metabolically active. Data represents mean ± s.e.m. (n=3). * denotes $p < 0.05$ as determined by the *Student's t-test*.

Drug toxicity is a key functional response for hepatocytes. Indeed, comparing drug metabolism of 3D cultures *versus* 2D cultures is one of the key aims of this project. HepG2 cells were seeded onto fibronectin coated 12-well plates (2D) and Alvetex®Scaffold (insert/12-well plate/submerged) at a density of 0.3 million cells. Cells were cultured for 24 hours in standard culture media before being treated with APAP-containing media for an additional 24 hours. Cell metabolic activity (MTT assay) was assessed for each APAP treatment.

Figure 4.19 shows the results of the MTT assay for the APAP dose response in 2D and 3D. 2D cultures gradually show a decline in metabolic activity as APAP is increased, suggesting that the cells are sensitive to the drug. Conversely, 3D cells in Alvetex®Scaffold appear much more resistant to higher concentrations of the drug, even displaying an enhanced metabolic activity compared to the nil-APAP control. This suggests that the 3D cells are more capable of detoxifying the drug compared to 2D cultures.

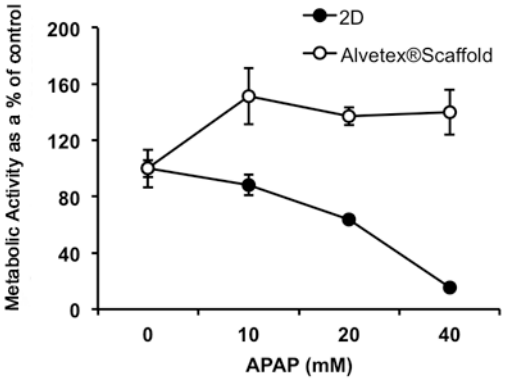

Figure 4.19 HepG2 response to acetaminophen (APAP) in 2D and 3D cultures. The MTT assay was used to determine cell activity/viability under different drug concentrations. 2D cultures (12-well plate) appear more sensitive to the drug, evident by the gradual decrease in viability with increasing APAP concentration. Conversely 3D cultures appear resistant to the drug, with even an increase in activity/viability compared to the nil-APAP control observed. Data represents 24 hours culture in standard culture media followed by 24 hours culture in APAP-containing culture media. Data represents mean ± s.e.m. (n=3).

Gemfibrozil was employed as a second model drug to probe 2D and 3D function. In this experiment HepG2 cells were seeded onto fibronectin coated 12-well plates (2D) and Alvetex®Scaffold (insert/12-well plate/submerged) at a density of 0.25 million cells. Cells were cultured for 2 days in standard culture media before being treated with Gemfibrozil-containing media for an additional 24 hours. Cell metabolic activity (MTT assay) was assessed for each Gemfibrozil treatment. Figure 4.20 shows that 3D cells are generally more resistant to Gemfibrozil compared to 2D cultures, although the differences between the two cultures are much smaller compared to the APAP data above. In the case of Gemfibrozil, both 2D and 3D metabolic activity is gradually reduced upon increasing drug exposure, with the 3D cells only having a slightly higher metabolic activity than 2D at each drug concentration.

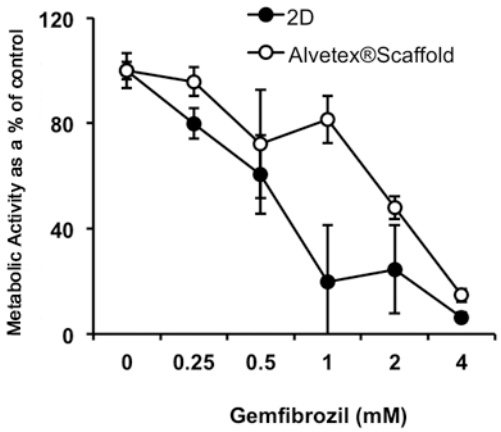

Figure 4.20 HepG2 response to Gemfibrozil in 2D and 3D cultures. The MTT assay was used to determine cell activity/viability under different drug concentrations. 2D cultures (12-well plate) appear slightly more sensitive to the drug, evident by the gradual decrease in viability with increasing Gemfibrozil concentration. Conversely 3D cultures appear more resistant to the drug, but still show a gradual decrease in viability with increasing Gemfibrozil concentration. Data represents 2 days culture in standard culture media followed by 24 hours culture in Gemfibrozil-containing culture media. Data represents mean ± s.e.m. (n=3).

Albumin and urea synthesis were compared for primary rat cells cultured in 2D and 3D. In this experiment primary rat hepatocytes were seeded onto fibronectin coated 12-well plates (2D) and Alvetex®Scaffold (insert/12-well plate/submerged) at a density of 0.3 million cells. Cells were cultured for 2 days in Rat Culture Media. After this period culture media samples were assessed for albumin and urea. Data was normalised against total DNA extracted from the 2D and 3D samples using the PicoGreen® assay. Figure 4.21 shows the albumin production of 2D and 3D primary rat hepatocytes determined by a rat-albumin specific ELISA. A greater production of albumin synthesis for 3D hepatocytes is observed after 2 days culture compared to 2D. Figure 4.22 shows the urea synthesis of 2D and 3D primary rat hepatocytes determined by a colorimetric urea assay. A greater production of urea for 3D hepatocytes is observed after 2 days culture compared to 2D.

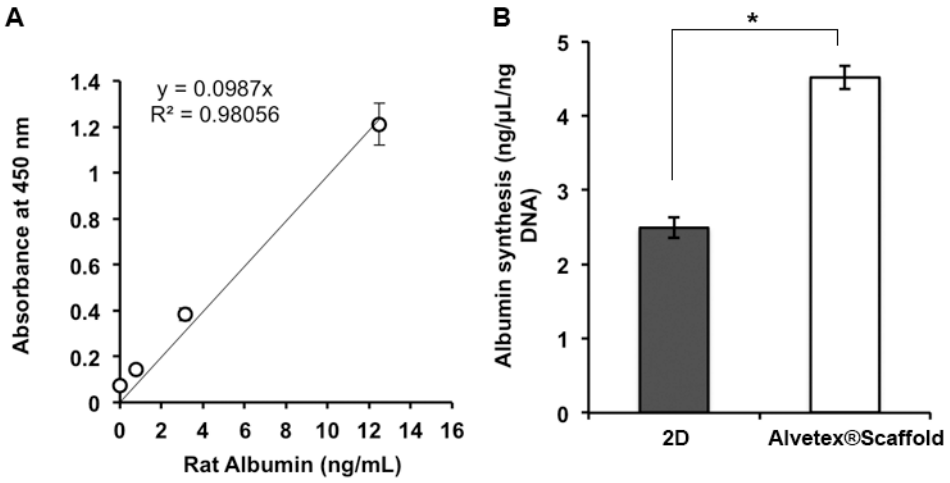

Figure 4.21 Albumin synthesis of primary rat hepatocytes cultured in 2D and 3D determined by a rat-specific albumin ELISA. Cells were cultured for 2 days before analysis. (A): Standard curve using known rat-albumin concentrations used to correlate absorbance with albumin level. (B): Albumin levels for 2D and 3D cultures. Data was normalised against total DNA, quantified using the PicoGreen® assay. A significantly greater amount of albumin was produced for 3D cultures compared to 2D. Data represents mean ± s.e.m. (n=3). * denotes $p < 0.05$ as determined by the *Student's t-test*.

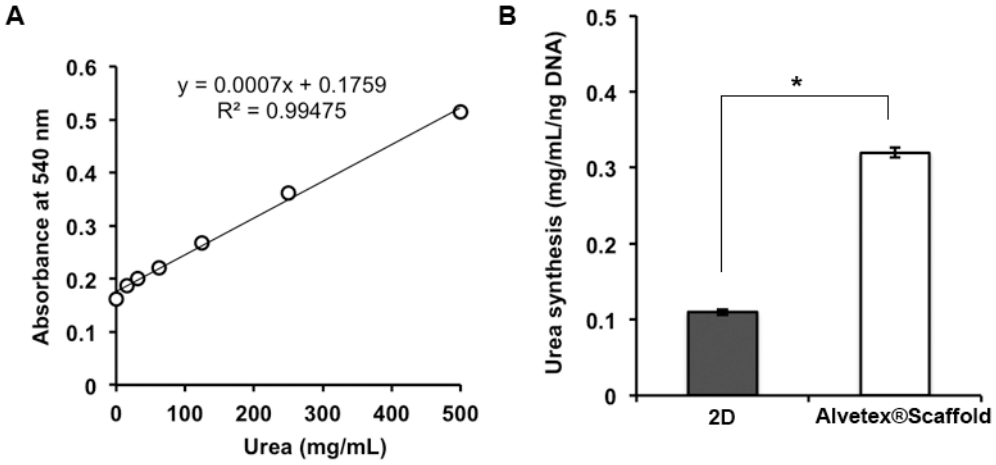

Figure 4.22 Urea synthesis of primary rat hepatocytes cultured in 2D and 3D determined by a urea colorimetric assay. Cells were cultured for 2 days before analysis. (A): Standard curve using known urea concentrations used to correlate absorbance with urea level. (B): Urea levels for 2D and 3D cultures. Data was normalised against total DNA, quantified using the PicoGreen® assay. A significantly greater amount of urea was produced for 3D cultures compared to 2D. Data represents mean ± s.e.m. (n=3). * denotes $p < 0.05$ as determined by the *Student's t-test*.

4.3.4 Hepatocyte Function (3D Static versus 3D Perfused)

Hepatocyte function was also compared between 3D static and 3D perfused media conditions. Upcyte® hepatocytes were seeded onto Alvetex®Scaffold (insert/12-well plate/submerged) at a density of 0.5 million cells and the culture was allowed to establish for 24 hours. Media perfusion was then applied using the Reinnervate Perfusion Plate with a media flow of 200 μL/min. Samples were either treated with 0.1 % DMSO or 0.1 % DMSO + 20 μM rifampicin (an inducer of CYP3A4 activity). Cells were cultured for 7 days under perfused and static conditions. Figure 4.23 shows the difference in glucose consumption across the entire culture period. The greater volume of culture media offered by the perfused conditions compared to the static (120 mL compared to 4 mL) ensures that the hourly change in media glucose is smaller for the perfused system. This suggests that a more steady state glucose environment is offered by the perfused media culture.

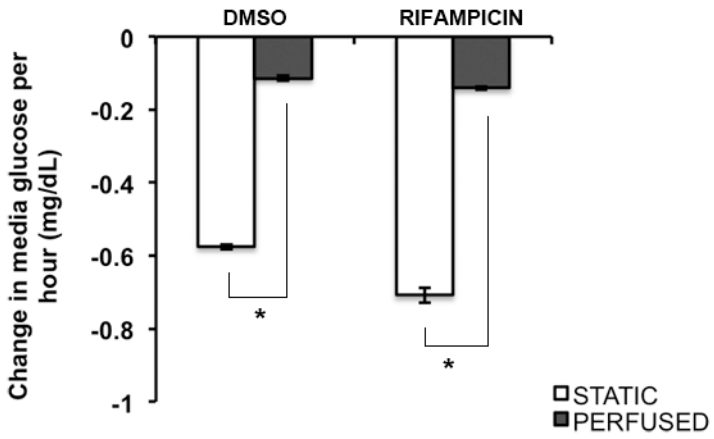

Figure 4.23 Hourly change in media glucose for 3D static and 3D perfused Upcyte® cultures. Cells were cultured for 7 days and the change in glucose consumption monitored. A much greater change in media glucose for the static culture (4 mL media) is observed compared to the perfused culture (120 mL media). This suggests that the perfused conditions offer a more steady state glucose environment for cells compared to static conditions. Data represents mean ± s.e.m. (n=4). * denotes $p < 0.05$ as determined by the *Student's t-test*.

Total protein was compared at the end of the 7 day static and perfused culture period to assess differences in Upcyte® proliferation. Data from the Bradford assay is shown in Figure 4.24. No significant differences were observed between total protein content for static and perfused cultures, suggesting that a 7 day media perfusion does not significantly enhance Upcyte® proliferation.

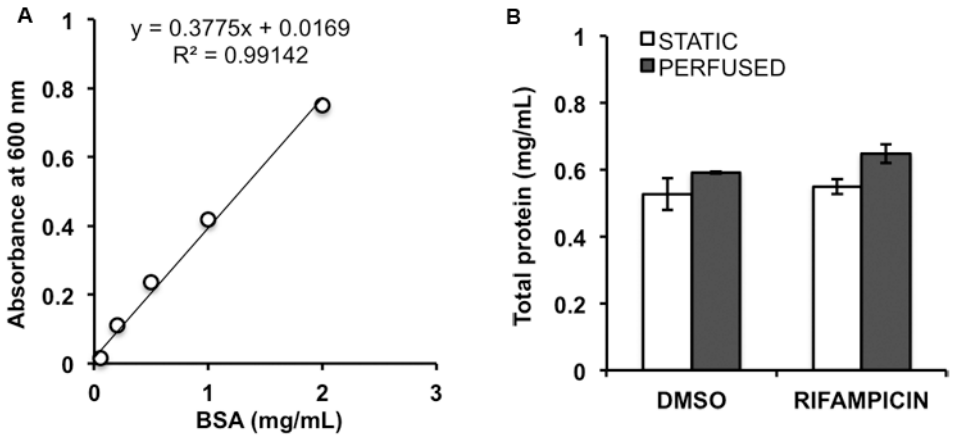

Figure 4.24 Total protein content for 3D Upcyte® cells cultured under static and perfused media conditions on Alvetex®Scaffold for 7 days. (A): Standard curve with known protein (Bovine Serum Albumin, BSA) levels was used to correlate Bradford assay absorbance with protein content. (B): Total protein levels for static and perfused media conditions. Data represents mean ± s.e.m. (n=2).

CYP3A4 activity was also assessed under static and perfused media conditions using the testosterone assay. Cells were cultured for 7 days under static and perfused media conditions and then incubated in 250 μM testosterone for 1 hour. Samples were then frozen and shipped to Medicyte (Germany) for analysis of a testosterone metabolite (6-β-OH-testosterone) via high performance liquid chromatography (HPLC). Figure 4.25 shows a significantly higher CYP3A4 activity compared to static cultures for the DMSO control. This difference is not observed for the induced (rifampicin) treatments, and may be due to rifampicin already pushing CYP3A4 up to maximum activity for 3D *in vitro* cultures.

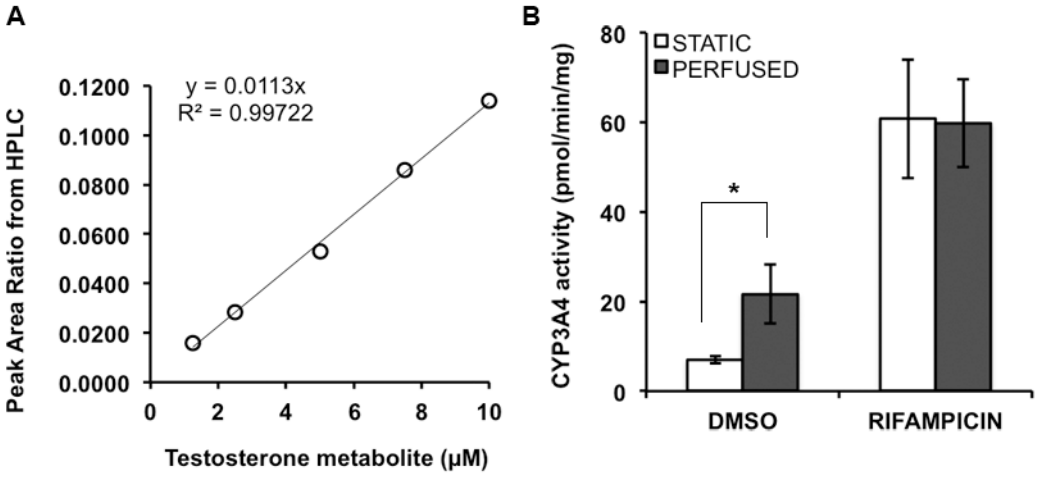

Figure 4.25 CYP3A4 activity of 3D Upcyte® cells cultured under static and perfused media conditions on Alvetex®Scaffold for 7 days. (A): Standard curve with known testosterone metabolite (6-β-OH-testosterone) levels used to correlate HPLC peak-area-ratio with CYP3A4 activity. (B): CYP3A4 activity for static and perfused media conditions. Data represents mean ± s.e.m. (n=4). * denotes $p < 0.05$ as determined by the *Student's t-test*.

4.3.5 Hepatocyte Gene Expression

HepG2 cells were seeded onto fibronectin coated 12-well plates (2D) and Alvetex®Scaffold (insert/12-well plate/submerged) at a density of 0.3 million cells. Cells were cultured for 24 hours in standard culture media before being treated with either nil-APAP media (Basal) or 10 mM APAP media for an additional 24 hours. Cells were then assessed for gene expression using a Qiagen RNA isolation kit and TaqMan® gene expression probes for CYP1A2, CYP2E1, CYP3A4, GSTP1, UGT1A1, ABCB1 and ABCC2. All gene expression data was referenced *versus* the housekeeping gene glyceraldehyde 3-phosphate dehydrogenase (GAPDH).

Figure 4.26 shows the gene expression of CYP1A2, CYP2E1 and CYP3A4. A significant increase in CYP2E1 expression was observed for 3D cells compared to 2D for both basal and 10 mM APAP conditions. However this difference is relatively small (ca. a 2-fold increase). Relatively large error bars were observed for CYP3A4 and CYP1A2, however this could be expected given that the data represent means of three biological (external) repeats.

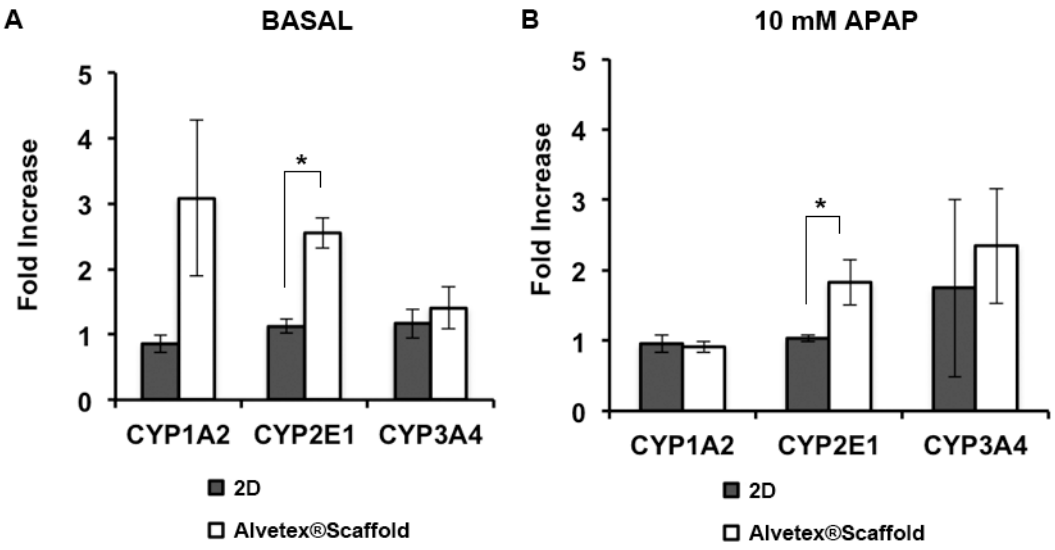

Figure 4.26 HepG2 gene expression for CYP enzymes when cultured under 2D and 3D (Alvetex®Scaffold) conditions. (A): Basal media supply. (B): 10 mM APAP media supply. A significant increase in CYP2E1 gene expression is observed for 3D cultures compared to 2D, however this difference is relatively small (ca. 2-fold). Data represents mean ± s.e.m. (n=3). * denotes $p < 0.05$ as determined by the *Student's t-test*.

Figure 4.27 shows the gene expression of GSTP1 and UGT1A1 for 2D and 3D HepG2 cultures. A significant and substantial increase is observed in GSTP1 for 3D cells compared to 2D (73-fold for basal and 99-fold for 10 mM APAP). Similarly, a significant increase is observed in UGT1A1 for 3D cells compared to 2D (13-fold for basal and 4-fold for 10 mM APAP).

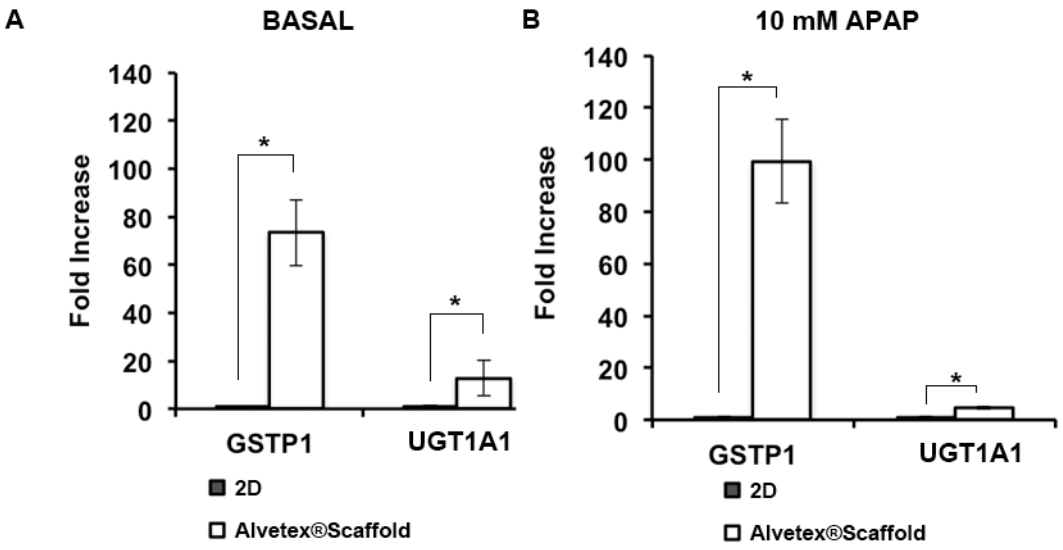

Figure 4.27 HepG2 gene expression for phase II drug metabolising enzymes when cultured under 2D and 3D (Alvetex®Scaffold) conditions. (A): Basal media supply. (B): 10 mM APAP media supply. A significant increase in phase II drug enzyme gene expression is observed for 3D cultures compared to 2D. Data represents mean ± s.e.m. (n=3). * denotes $p < 0.005$ as determined by the *Student's t-test*.

Figure 4.28 shows the gene expression of ABCB1 and ABCC2 for 2D and 3D HepG2 cultures. A significant increase in ABCC2 expression is observed for 3D cells compared to 2D for both basal and 10 mM APAP conditions. However this difference is relatively small (less than 2-fold increase).

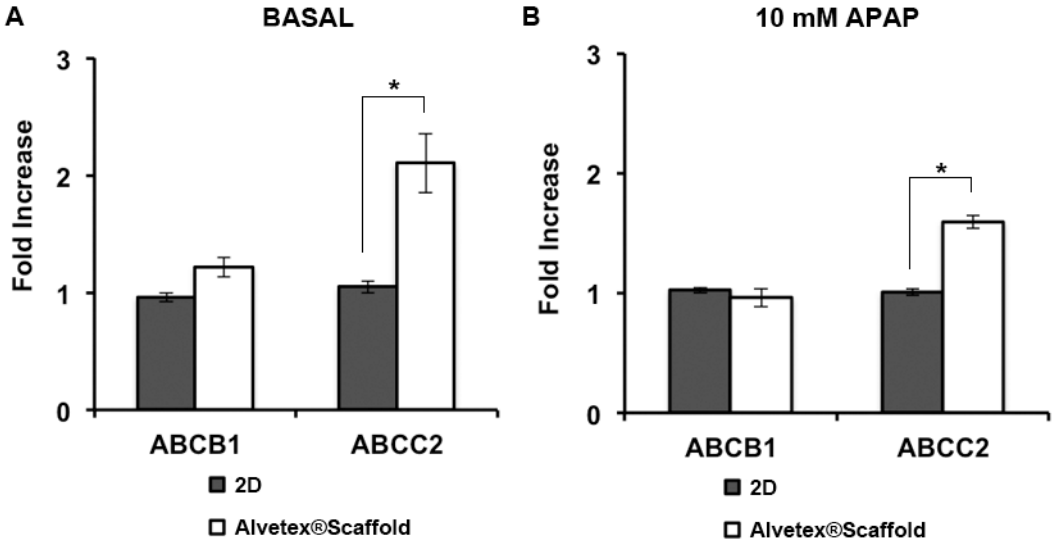

Figure 4.28 HepG2 gene expression for phase III drug transporter proteins when cultured under 2D and 3D (Alvetex®Scaffold) conditions. (A): Basal media supply. (B): 10 mM APAP media supply. A significant but small increase in gene expression is observed for 3D cultures compared to 2D. Data represents mean ± s.e.m. (n=3). * denotes $p < 0.05$ as determined by the *Student's t-test*.

4.4 Discussion

It is known that cell morphology influences gene expression and function[50, 51]. Several groups have demonstrated this for hepatocytes: Mooney *et al.* comprehensively showed that hepatocyte shape alone can influence gene expression and protein secretion, independent of changes to cell-cell contact[197]. Pioneering work from LeCluyse *et al.* and Dunn *et al.* showed that a 3D hepatocyte morphology is crucial for bile canaliculi formation and the maintenance of hepatic function using sandwich culture[76, 176]. Sawamoto *et al.* showed that by reducing hepatocyte spreading across 2D polystyrene it is possible to prolong native hepatic enzyme activity[198]. Similarly, hepatic cell lines grown in hydrogels have also been shown to display more realistic gene expression levels as they adopt a round morphology[199, 200].

This study compared hepatocyte morphology in Alvetex®Scaffold and Alvetex®Strata with 2D cultures. Confocal immunofluorescence microscopy was used to obtain optical Z-stacks to construct cell morphology in each microenvironment. The technique has also been employed by other groups to visualise cell morphology in 3D substrates, such as the 3D shape of adipose stem cells in 3D printed scaffolds[201]. Results from this study showed that those cells in scaffolds were able to adopt a more rounded (cuboidal) shape that is more consistent with those *in vivo*. Cell height was found to be approximately equal to cell length and width. Nuclei were also more rounded in scaffolds compared to 2D. The F-actin filaments for cells in Alvetex®Scaffold were not stretched out and appeared to wrap around the nuclei in a 3D manner. For Alvetex®Strata, where there is an abundance of cell-cell contact, F-actin filaments were also not stretched and were found close to the nuclei, but were also localised at the junctions where cells are in contact with one another. On the contrary, F-actin filaments in 2D cultures were severely stretched out across the XY plane. Very little F-actin staining was present above the nuclei in the Z plane. It is hypothesised this distorted F-actin arrangement in 2D would be inappropriate for hepatocyte polarisation towards surface microvilli at the sinusoidal domain.

The morphology of hepatocytes in scaffolds was also assessed via SEM. Neuhaus *et al.* used SEM to show that hepatocytes adopt a 3D morphology in a multi-compartment system[202]. Similarly Vacanti *et al*. demonstrated that hepatocytes adopt a 3D architecture in biodegradable polymeric scaffolds using SEM[203]. SEM has also been used to show hepatocytes adopt a 3D morphology in electrospun scaffolds[105]. This study used SEM to probe hepatocyte morphology and structure in 2D and polystyrene scaffolds. Hepatocytes grown in 2D severely spread out across the plastic. Hepatocytes in Alvetex®Scaffold seemed to display a more rounded morphology within the voids of the scaffold. For Alvetex®Strata, hepatocytes formed a thick 3D tissue mass on top of the material with optimal cell-cell contact, very similar to what was observed for *in vivo* mouse liver. The formation of a thick tissue mass is not often observed for other 3D technologies. For example,

hepatocytes grown on top of electrospun scaffolds still only managed to form individual pockets of 3D cell growth that lacked extensive 3D organisation[105].

In summary, hepatocytes in Alvetex®Scaffold and Alvetex®Strata adopt a 3D morphology representative of their native environment. As cell morphology is important for normal hepatocyte genotype and phenotype, it is expected that Alvetex®Scaffold and Alvetex®Strata should help to improve the physiological relevance of *in vitro* hepatocyte models used in drug discovery.

Hepatocyte ultrastructure is crucial for function. The formation of bile canaliculi as a result of cell polarisation plays a vital role in the secretion and transport of bile, as well as in drug elimination (see Chapter 1). Failure to form these structures *in vivo* results in cholestasis and liver damage[204]. Accordingly, it is also well known that hepatocytes cultured in 2D fail to mimic these extensive bile canaliculi networks[80]. This is therefore a major limitation in appropriately mimicking native liver function using 2D models. Unsurprisingly, several groups have attempted to use 3D substrates as a tool to encourage bile canaliculi formation *in vitro*. Sandwich cultures are proving very beneficial for studying bile canaliculi formation and regulation[205]. Hydrogels have been shown to encourage bile canaliculi formation for HepG2 cells, with the canaliculi containing specific drug transporter proteins (MDR1 and MRP2)[206]. Interestingly, no reports could be found on the formation of extensive bile canaliculi networks in electrospun scaffolds, probably because 3D cell growth is restricted to where the nodes of the fibres overlap.

This study used TEM to probe for hepatocyte ultrastructure *in vivo* and *in vitro.* As expected, mouse liver appeared healthy with all the appropriate organelles. Sinusoidal microvilli were observed protruding into the sinusoidal lumen. Bile canaliculi were observed containing appropriate tight junction complexes and microvilli. Most of the key organelles appeared round. In contrast, 2D *in vitro* cultures displayed only sparse sinusoidal microvilli. Furthermore, no advanced bile canaliculi were observed. This is supported by the lack of positive MDR1 and MRP2 staining. Some of the organelles, particularly the nucleus and some mitochondria, appeared flattened in comparison to native liver tissue.

Hepatocytes grown on Alvetex®Scaffold showed frequent signs of sinusoidal microvilli. They also showed signs of bile canaliculi, consistent with the positive staining for MRP2 and previous reports of HepG2 growth on polystyrene scaffolds[150]. The morphology of the cells and internal organelles also resembled the round morphology of those found in native mouse liver. It was observed that the scaffold walls were able to support hepatocytes across multiple surfaces to encourage a 3D morphology.

Hepatocytes grown on Alvetex®Strata were also more round in morphology. They appeared to experience extensive cell-cell contact within the tissue mass. Abundant sinusoidal microvilli were observed, as well as the formation of lumen-type structures. This suggests that hepatocytes grown in a 3D scaffold-less manner may be capable of structural re-organisation towards features resembling native liver. Such re-organisation processes towards lumen and/or bile-ductular structures have previously been reported for spheroidal aggregate cultures[82]. Here some of the cells within the aggregates spontaneously re-organised to form lumens. Not only this, cells displayed a different secretion of ECM components depending on whether they were part of the lumen structure or not. Other groups have also reported the formation of lumen-type structures for hepatocytes in Matrigel®[207].

An abundance of advanced bile canaliculi features were observed for hepatocytes in Alvetex®Strata for those cells close to the media supply in the bottom portion of the scaffold. This is consistent with the observed positive staining for MDR1 and MPR2. However, those cells near the top portion of the scaffold showed clear signs of cell necrosis, consistent with the histology and flow cytometry data shown in Chapter 3.

Understanding if the structural differences between 2D and 3D cells *in vitro* are translated into functional and genetic improvements is a key part of *in vitro* model validation. This study first showed that the glucose consumption between 2D and 3D hepatocyte culture is different. Cells in 3D appeared to consume more glucose than their 2D counterparts. This may be attributed to either an increase in respiration (metabolic activity) or an increase in glycogen synthesis. The latter of these has previously been observed in 3D cultures[208]. However, without further experiments it is difficult to determine which mechanism is occurring here.

Albumin synthesis and urea synthesis are key indicators of hepatic function. Several groups have shown that 3D cultures help to increase albumin and urea compared to 2D. For example hepatocytes grown on electrospun scaffolds have shown enhanced albumin and urea[208]. Hepatocytes grown in 3D micro-plates have shown increased albumin[209]. Other groups have explored hydrogels as a means of increasing hepatocyte albumin *in vitro*[210]. In this study we have shown that scaffolds such as the Alvetex®Scaffold also help to increase albumin and urea synthesis over conventional 2D cultures.

HepG2 response to acetaminophen (APAP) is different in scaffolds and 2D. HepG2 cells in 3D appear more resistant to the drug, suggesting an increased elimination/detoxification capacity. Unfortunately there are very limited *in vivo* reports of how hepatocellular carcinoma patients respond to APAP, however some reports have demonstrated increased elimination in the urine

via an up regulation of SULT1A1 activity[211]. Although not directly comparable, this does provide a preliminary indication that 3D HepG2 cultures are at least moving in the right direction for more predictive *in vivo* response. Interestingly, this trend is the reverse to what is observed for healthy primary hepatocytes exposed to APAP in 2D and 3D. Primary hepatocytes cultured in collagen gels are more sensitive to APAP compared to 2D[212]. Indeed, primary hepatocytes cultured in Alvetex®Scaffold are also more sensitive to APAP compared to 2D[159]. The hypothesis as to why HepG2 cells are more resistant to APAP in 3D, whereas primary cells are more sensitive to APAP in 3D may be due to the difference in genotype and phenotype between these two types of cells. It is well known that HepG2 cells have an almost negligible set of cytochrome P450 enzymes, whereas primary cells have a near complete set[187]. Conversely, HepG2 cells have reasonable levels of phase II enzymes, similar to primary cells[213]. It can therefore be hypothesised that 3D HepG2 culture serves to increase the expression and activity of phase II enzymes, leading to an increased drug elimination process compared to 2D. With primary hepatocytes, it is known that 3D culture increases cytochrome P450 activity[32]. Consequently it is expected that primary 3D cultures are more exposed to the formation of toxic NAPQI and are thus more sensitive to the drug.

HepG2 response to Gemfibrozil was also different in scaffolds compared to 2D. Cells in 3D appeared more resistant compared to 2D, consistent with the APAP data. As Gemfibrozil is first metabolised by the UGT family, it is hypothesised that 3D culture helps to increase the activity of the phase II enzymes and thus increase the ability of the cells to detoxify and eliminate the drug.

Gene expression of the drug metabolising enzymes was compared between 2D and 3D cultures for HepG2 cells. Some small increases in cytochrome P450 enzyme expression were observed for 3D cultures compared to 2D. However, given that HepG2 cells already have a very low level of these enzymes to begin with, and that genetic changes do not necessary translate into phenotypic changes, it is not expected that these cytochrome P450 changes would have a profound effect on HepG2 function. In the context of APAP metabolism, it is not expected that these small increases in CYP gene expression would lead to increased NAPQI formation and thus drug toxicity.

Conversely, large increases in phase II enzyme expression was observed for 3D cultures (as much as 100-fold). Such large changes, if translated into enzyme activity, could be sufficient to alter cellular function. In the context of APAP and Gemfibrozil metabolism, it is possible that these increases in gene expression could be sufficient to increase the detoxification and elimination of these drugs, potentially explaining why cells in 3D appeared to be more resistant to these drugs compared to their 2D counterparts. Only small increases were observed in phase III transporter proteins.

This study also compared the function of hepatocytes cultured in scaffolds under static and perfused media conditions. Several groups have explored this using other 3D technologies. Perfusion through 3D-printed scaffolds has been shown to enhance albumin synthesis compared to static media conditions[214]. Increased albumin synthesis has also been observed for 3D perfusion using scaffolds fabricated from gas-foaming[215]. This study demonstrated an increase in CYP3A4 activity for 3D cells cultured in perfused scaffolds compared to static scaffolds.

4.5 Conclusions

The following conclusions can be made from the results of this Chapter:

- Hepatocytes cultured in scaffolds adopt a more rounded, native-like morphology compared to those cultured in 2D. Cell height in 3D culture is approximately equal to cell width and length. Conversely for 2D cell culture, cell height is much smaller than cell width and length as the cell flattens out across the plastic.

- Cell-cell contact increases from cultures in 2D to cultures in Alvetex®Scaffold to cultures in Alvetex®Strata. Those hepatocytes grown on top of Alvetex®Strata display maximum cell-cell contact across all cell surfaces, similar to hepatocytes found in native mouse liver.

- Evidence of drug transporter proteins known to localise at the bile canaliculi membranes were found in 2D cultures, Alvetex®Scaffold and Alvetex®Strata. Alvetex®Strata displayed the most positive staining for the drug transporter proteins.

- TEM analysis of 2D hepatocyte ultrastructure revealed that 2D cultures adopt a flat morphology with distorted organelles. Cells showed only sporadic surface microvilli. There was a noticeable absence of advanced bile canaliculi containing appropriate tight junctions and microvilli. Cell contact was restricted to the edges of the cells to the extent where cells appeared to crawl around one another to improve cell-cell contact.

- TEM analysis of hepatocytes in Alvetex®Scaffold showed that the shape of cells and organelles were representative of *in vivo*. Moreover, this cell shape was supported by the scaffold architecture. Surface microvilli were frequently observed for cells in Alvetex®Scaffold. Advanced bile canaliculi features containing appropriate tight junctions and microvilli were also observed.

- TEM analysis of hepatocytes on Alvetex®Strata also showed that the shape of cells and organelles were representative of *in vivo*. Abundant surface microvilli were observed protruding into lumen-type structures, suggesting some primitive signs of structural reorganisation. Abundant bile canaliculi were observed for hepatocytes in Alvetex®Strata.

- Hepatocyte function is different in scaffolds compared to 2D culture. HepG2 cells are more resistant to acetaminophen and Gemfibrozil in scaffolds compared to 2D. This

correlates to increased gene expression of the phase II drug metabolising enzymes in 3D compared to 2D. It is hypothesised that the increased gene expression translates into increased enzyme activity and thus a greater capacity of the cells to detoxify and eliminate the drug.

- Primary rat cells show increased albumin and urea synthesis in scaffolds compared to 2D. This is consistent with data from other 3D hepatocyte culture systems.

- Hepatocytes cultured in scaffolds under perfused media conditions appear to show increased basal CYP3A4 activity compared to static cultures after 7 days culture. Inducing CYP3A4 activity in the 3D cultures removes any difference between perfused and static cultures with regards to CYP3A4 activity.

Chapter 5: Functionalising Emulsion Templated Polystyrene Scaffolds with Galactose for Enhanced Hepatocyte Adhesion and Function

5.1 Introduction

5.1.1 Overview

One of the potential limitations of emulsion templated polystyrene scaffolds as substrates for 3D cell growth is surface chemistry. Cells *in vivo* are surrounded by a complex ECM that contributes to cell anchorage, survival and function[216]. They also receive a plethora of biochemical cues from molecules such as carbohydrates and proteins that serve to regulate normal cell behaviour. As the surface of synthetic polystyrene is far removed from this, the ability to introduce ECM mimics onto the scaffold surface is therefore an attractive prospect for improving the biochemical relevance of the materials.

In vivo, galactose is often the terminal carbohydrate for many glycoproteins. Hepatocytes specifically recognise galactose via the asialoglycoprotein receptor (ASGP-R)[217], a mechanism used to remove various glycoproteins from circulation. *In vitro*, galactose is often employed as a surface ligand for enhanced hepatocyte adhesion and function with several substrates, including 2D films, electrospun scaffolds and hydrogel sponges. However, there have been no reports on the functionalisation of emulsion templated polystyrene scaffolds with galactose, even though these materials are gaining significant attention as suitable substrates for 3D cell growth.

This Chapter therefore describes the surface-functionalisation of an emulsion templated polystyrene scaffold with galactose to improve the biochemical relevance of the material, as illustrated in Figure 5.1. Two different routes towards galactose functionalisation are described, one employing ester functionalisation of the scaffold and the other acid functionalisation. The ester-functionalised polystyrene scaffold was then reacted with a galactose-amine to render galactose functionality on the scaffold surface. The impact of this galactose functionality on hepatocyte adhesion and function was then explored.

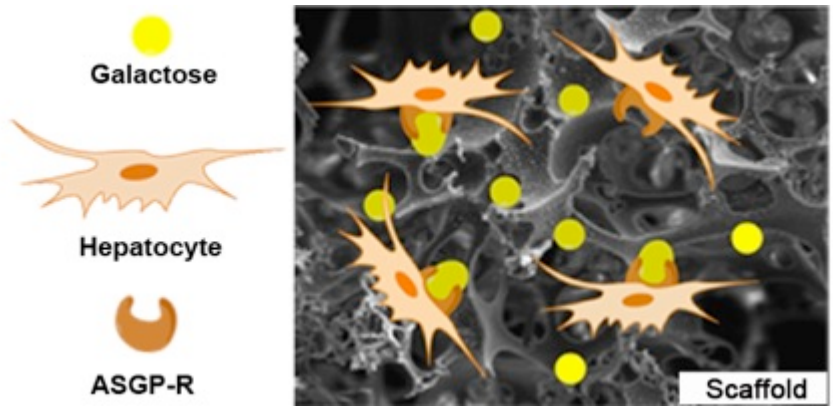

Figure 5.1 Illustration of an emulsion templated polystyrene scaffold functionalised with galactose. Pendent galactose residues (yellow circles) on the scaffold surface were hypothesised to act as a ligand for the hepatocyte ASGP-R, improving the biochemical relevance of the material.

5.1.2 Composition of Emulsion Templated Polystyrene Scaffolds

Emulsion templated polystyrene scaffolds used for 3D cell growth applications are prepared from water-in-oil (w/o) HIPEs. For scaffolds like the Alvetex®Scaffold, three hydrophobic monomers constitute the external oil phase of the HIPE, namely: styrene (STY), divinylbenzene (DVB) and 2-ethylhexyl acrylate (EHA)[164, 165]. STY is the primary monomer, constituting ca. 60 wt% of the total monomer mixture. DVB is present at ca. 10 wt% to offer chemical cross-linking, which increases the mechanical strength of the material. EHA is also present at ca. 30 wt% to increase polymer elasticity by reducing the polymer $T_{g.}$ The non-ionic surfactant Span80™ (Sigma) is often used to form the HIPE as it has low solubility in the aqueous droplet phase and so inhibits emulsion phase separation. Typically, the materials are fabricated with potassium persulfate (KPS) as the free radical initiator, which being water-soluble, favours polymerisation of any monomers found in excess at the interface. However, alternative initiators that reside in the external oil phase of the HIPE are also sometimes employed, such as the hydrophobic initiator azobisisobutyronitrile (AIBN).

5.1.3 Synthetic Strategy

Attaching galactose directly onto the surface of emulsion templated polystyrene scaffolds (post-polymerisation) is challenging due to the relatively inert nature of polystyrene. This study therefore employed an indirect route to galactose functionalisation via first incorporating additional functionality into the pre-polymerised material. Pentafluorophenyl acrylate (PFPA) was incorporated into the HIPE external oil phase to introduce pendent ester functionality on the scaffold surface. Alternatively, acrylic acid (Aa) was incorporated into the HIPE internal aqueous phase to introduce pendent carboxylic acid functionality on the scaffold surface. Attachment of galactose residues was then achieved by a facile coupling reaction between the ester-functionalised scaffold and 2'-aminoethyl-β-D-galactopyranoside, as shown in Figure 5.2. Note that a similar surface reaction with 2'-aminoethyl-β-D-glucopyranoside was also employed to render pendent glucoses to provide a selective control for studies with the hepatocyte ASGP-R.

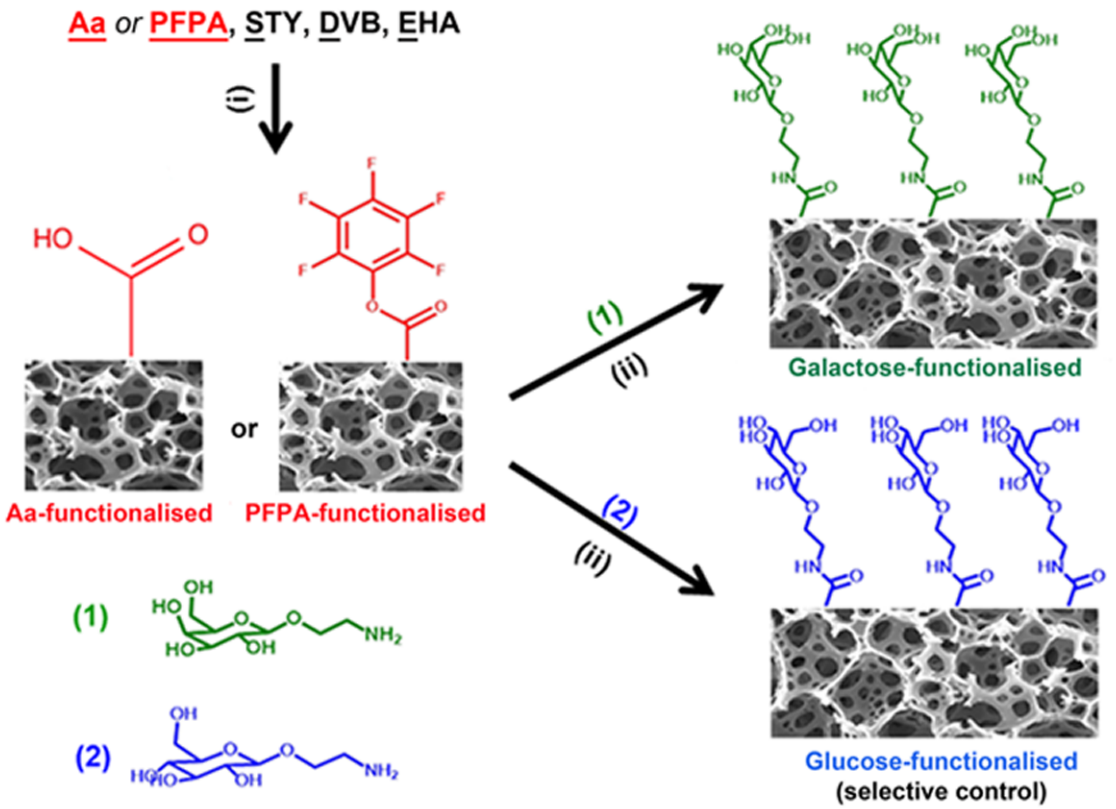

Figure 5.2 Illustration showing the indirect strategy to functionalise a polystyrene scaffold with galactose. Aa or PFPA were incorporated into the styrene (STY) based HIPE prior to polymerisation to leave functional reactive sites on the polymeric scaffold. These reactive sites were then used to undergo a facile coupling reaction with 2'-aminoethyl-β-D-galactopyranoside (1) to render pendent galactose on the surface. A similar reaction with 2'-aminoethyl-β-D-glucopyranoside (2) was used to render pendent glucose on the material to provide a useful selective control for subsequent hepatocyte culture experiments. Reaction conditions (i) and (ii) are described in detail in Chapter 2.

PFPA was chosen as a suitable functional co-monomer to introduce ester reactive sites on the polystyrene surface for three reasons. Firstly, it has a similar hydrophobicity to STY (log P_{PFPA} = 2.55 and log P_{STY} = 2.95) and thus was expected to be sufficiently soluble in the external oil phase of the HIPE, as illustrated in Figure 5.3A. Secondly, PFPA contains 5 fluorine atoms that are conveniently detectable by NMR and x-ray photoelectron spectroscopy (XPS), making surface characterisation experiments easier. Thirdly is that PFPA has been previously reported to undergo facile coupling reactions with amines when incorporated into photopolymerised polyacrylate polyHIPEs[218], as well as when polymerised as a poly(PFPA) homopolymer[219] .

Aa was chosen as a suitable hydrophilic functional co-monomer to introduce acid reactive sites on the polystyrene surface for two reasons. Firstly is that is it completely miscible in water and thus was expected to reside in the internal aqueous phase of the HIPE, as illustrated in Figure 5.3B. This was hypothesised to be particularly beneficial, as the Aa would most likely be polymerised

into the polymer at the emulsion interface and thus localise the carboxylic acid groups on the scaffold surface. Secondly, Aa has been previously reported to undergo facile surface coupling reactions with amines when polymerised as polyacrylic acid[220].

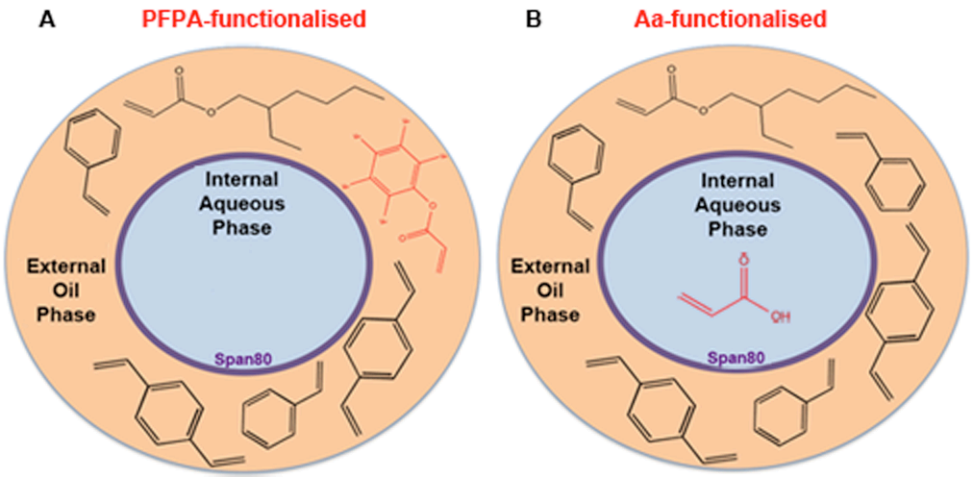

Figure 5.3 Illustration showing the expected location of the PFPA and Aa co-monomers in the STY-DVB-EHA HIPE. (A): PFPA (red molecule) has a similar hydrophobicity to STY and thus was expected to reside in the external oil phase of the emulsion along with the other hydrophobic monomers. (B): Aa (red molecule) is completely miscible in water and thus was expected to reside in the internal aqueous phase of the emulsion.

In this study, 2'-Aminoethyl-β-D-galactopyranoside and 2'-aminoethyl-β-D-glucopyranoside were chosen for reaction with the ester-functionalised scaffold. These aminoethyl glycosides were chosen over galactosamine and glucosamine in order to lock the carbohydrate in the beta conformation after coupling. With galactosamine and glucosamine, the amine group is attached to the 2-carbon leaving the 1-carbon free. This can therefore lead to ring opening of the carbohydrate into the open-chair form and thus the subsequent cyclic rearrangement into alpha, beta and furanoside forms that may jeopardise binding with the ASGP-R.

Span80™ was used as the surfactant throughout the study. KPS and ABIN were investigated as suitable initiators to preserve scaffold morphology.

5.2 Aims and Objectives

The overall aim of this Chapter was to surface functionalise an emulsion templated polystyrene scaffold with galactose whilst still preserving scaffold morphology and porosity. It was hypothesised that the surface galactose would act as a ligand for the hepatocyte ASGP-R, mimicking the glycoprotein-cell interactions found in native liver and thus further improving the biochemical relevance of the scaffold.

The main objectives were to:

- Fabricate a suitable ester-functionalised polystyrene scaffold by adding PFPA as an additional co-monomer into the HIPE external phase
- Characterise the ester-functionalised scaffold and investigate the suitability for 3D hepatocyte growth
- Demonstrate the attachment of pendent galactose residues onto the ester-functionalised scaffold via coupling with 2'-aminoethyl-β-D-galactopyranoside
- Explore the impact of pendent galactose on hepatocyte adhesion and function
- Fabricate a suitable acid-functionalised polystyrene scaffold by adding Aa as a co-monomer in the HIPE internal phase
- Characterise the acid-functionalised scaffold and investigate the suitability for 3D hepatocyte growth

5.3 Results

5.3.1 Sample Naming Protocol

The sample naming protocol for the incorporation of a functional co-monomer is as follows: poly[xC*o-monomer-SDE(initiator*)], where (i) x = wt% co-monomer out of total monomer mixture, (ii) co-monomer = PFPA or Aa, (iii) SDE = **S**TY, **D**VB and **E**HA coming from the parent scaffold formulation and (iv) initiator = KPS or AIBN. For example, poly[26PFPA-SDE(AIBN)] refers to a scaffold prepared using 26 wt% PFPA as a co-monomer and AIBN initiation.

Subsequent attachment of galactose to the appropriate functional scaffold is therefore termed GAL-poly[xC*o-monomer-SDE(initiator*)]. Similarly, attachment of glucose (a control carbohydrate) is termed GLU-poly[xC*o-monomer-SDE(initiator*)].

5.3.2 Incorporating PFPA as a Functional Co-Monomer

Table 5-1 shows the different HIPE formulations used to create the poly[xPFPA-SDE(AIBN)] materials. An oil phase was prepared containing the organic monomers (STY, DVB, EHA, PFPA), AIBN and Span80™. AIBN was employed as the initiator in this case as the interfacial activity of PFPA compared to the other monomers was unknown. Water was added to the oil phase and the mixture stirred vigorously to form a HIPE. A morphological control (a formulation similar to Alvetex®Scaffold) was also included in the study: poly[0PFPA-SDE(KPS)].

Table 5-1 HIPE Formulations used to Prepare Poly[xPFPA-SDE(AIBN)] Materials

	Wt. % in HIPE								% PFPA[b]
	Oil						Aq.		
HIPE formulation	**STY**	**DVB**	**EHA**	**PFPA[a]**	**Span80**	**AIBN**	**H_2O**	**KPS**	
0PFPA-SDE(KPS)	4.1	0.7	2.1	0.0	2.4	0	88.8	1.0	0
10PFPA-SDE(AIBN)	3.9	0.7	2.0	0.7	2.3	0.3	90.1	0.0	9.6
20PFPA-SDE(AIBN)	3.7	0.6	1.8	1.5	2.1	0.3	90.0	0.0	19.7
26PFPA-SDE(AIBN)	3.5	0.6	1.8	2.1	2.1	0.3	89.6	0.0	26.3
33PFPA-SDE(AIBN)	3.3	0.6	1.7	2.8	1.9	0.3	89.4	0.0	33.3
43PFPA-SDE(AIBN)	3.0	0.5	1.5	3.8	1.8	0.3	89.1	0.0	43.2

[a]PFPA was added to a stock SDE mixture. [b]PFPA percentage in total monomer mixture

All formulations formed a stable HIPE with no apparent signs of phase separation. The HIPE mixtures were then thermally polymerised at 60 ^{o}C for 24 hours to form poly[xPFPA-SDE(AIBN)] materials. Each polyHIPE was then soxhlet washed in acetone for 24 hours and then left to dry in

a fume hood. Figure 5.4 is a photograph of the dried polyHIPEs after washing. A stable (non-deformed) monolith was observed for each polyHIPE, suggesting that PFPA does not significantly disrupt scaffold morphology and thus is a potentially suitable functional co-monomer for this study.

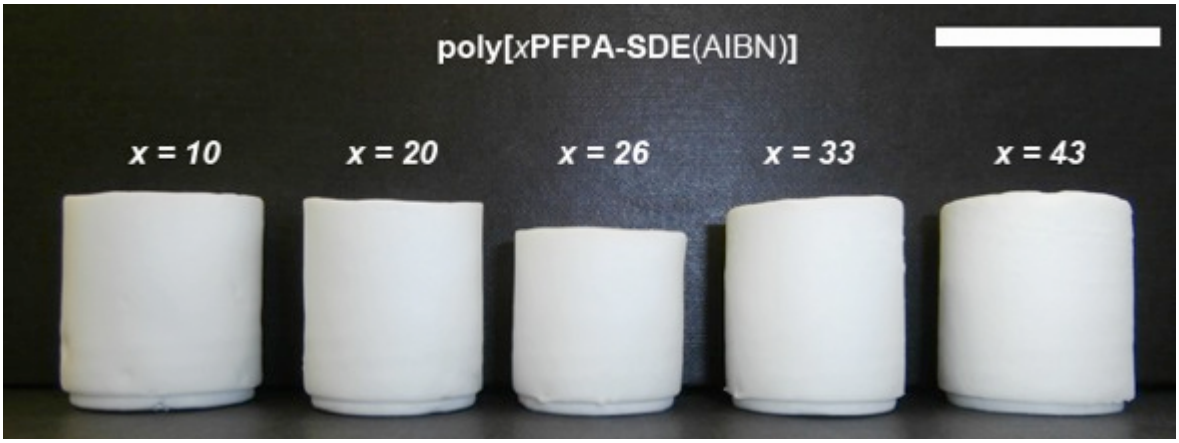

Figure 5.4 Resulting polyHIPE monoliths after polymerising the HIPE formulations shown in Table 5-1. Stable (non-deformed) monoliths were observed for each formulation suggesting that PFPA does not significantly disrupt the HIPE stability. Note that x corresponds to the % PFPA in the total monomer mixture. Scale bar = 4 cm.

The morphologies of the poly[xPFPA-SDE(AIBN)] materials are shown in Figure 5.5. A typical polystyrene scaffold morphology was observed for all poly[xPFPA-SDE(AIBN)] materials except for the poly[43PFPA-SDE(AIBN)] material. The morphology of this material was found to be collapsed and with unidentifiable voids. For the other materials, an overall decrease in void diameter was observed with increasing PFPA concentration (quantified in Table 5-2 by ImageJ™ analysis of the SEM images). This trend towards smaller void sizes suggests an increase in emulsion stability with higher PFPA incorporation, which is likely the result of the higher organic content helping to form wider and more robust continuous phase films around the internal phase droplets. This hypothesis is supported in the case of the poly[43PFPA-SDE(AIBN)], where the strut thickness of the material is visibly larger than those polyHIPEs with lower PFPA content (Figure 5.5 white arrow).

Table 5-2 also shows that the average interconnect diameter decreases with increasing PFPA content, which is to be expected given that void diameter decreases. The degree of interconnectivity (<d>/<D>) increases with increasing PFPA content, which would generally suggest an increase in emulsion stability. Figure 5.6 shows the interconnect diameter distribution for the poly[xPFPA-SDE(AIBN)] materials. Generally, a wider distribution in interconnect diameter was observed with higher levels of PFPA incorporation. The porosities of all materials remained

high (ca. 90 %), although a general decreasing trend was observed with increasing PFPA concentration (Table 5-2), which is to be expected with an increasing organic phase content and therefore a lowered internal phase volume fraction.

Table 5-2 Physical Characteristics of the Poly[xPFPA-SDE(AIBN)] Materials

	<D> (µm)[a]	<d> (µm)[b]	<d>/<D>	Porosity (%)
poly[0PFPA-SDE(KPS)]	69	15	0.21	92
poly[10PFPA-SDE(AIBN)]	46	10	0.22	93
poly[20PFPA-SDE(AIBN)]	37	10	0.27	92
poly[26PFPA-SDE(AIBN)]	33	10	0.30	92
poly[33PFPA-SDE(AIBN)]	28	11	0.39	89
poly[43PFPA-SDE(AIBN)]	/	5	/	85

[a]Average void diameter determined by ImageJ™ analysis of the SEM images. [b]Average interconnect diameter determined by mercury porosimetry. / = data unobtainable due to deformed nature of material.

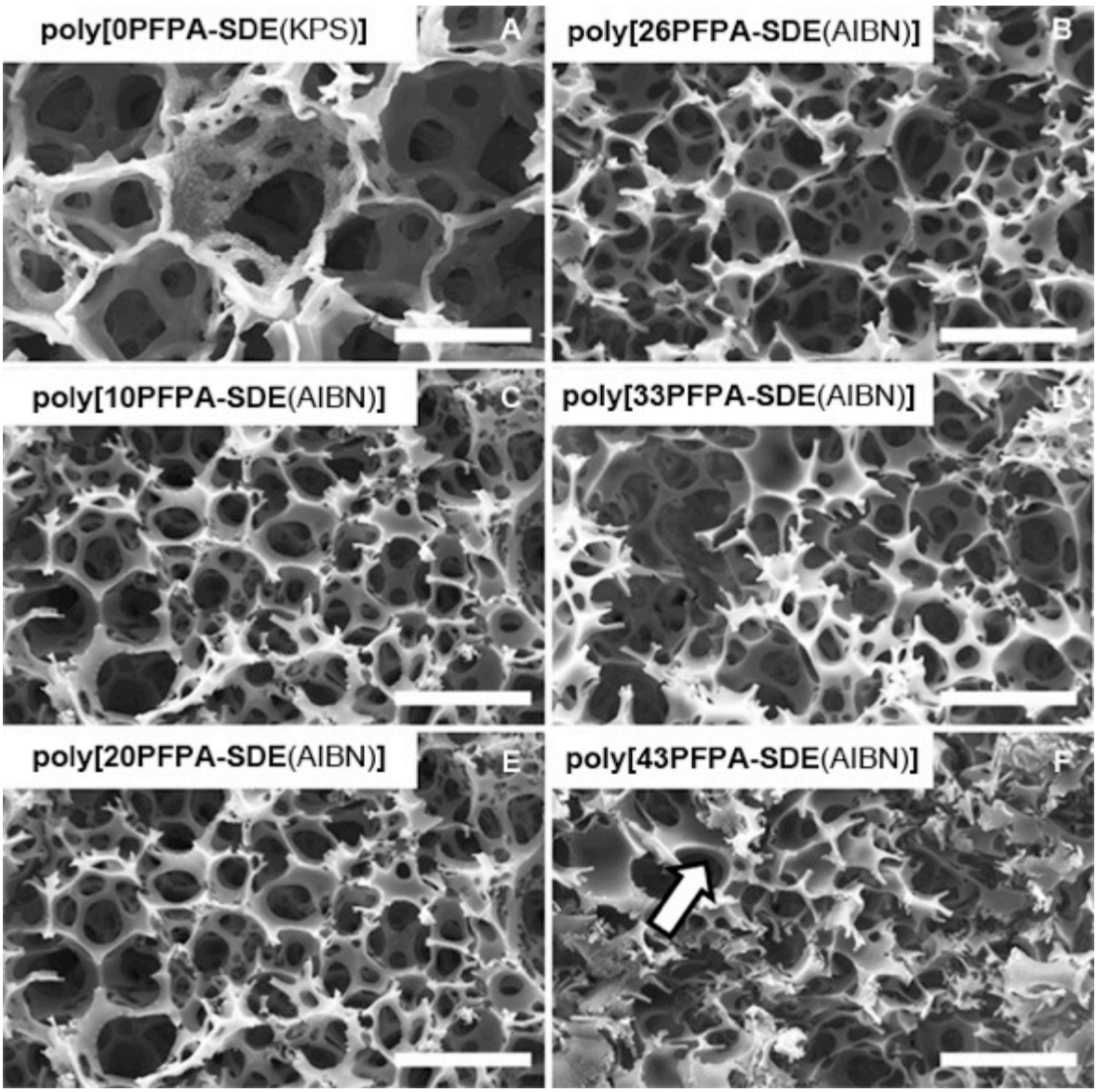

Figure 5.5 Morphology of the poly[xPFPA-SDE(AIBN)] materials by SEM. (A-F): Increasing concentrations of PFPA in the monomer mixture from 0 % control (A) to 43 % (F). All materials resemble a typical polystyrene scaffold morphology with the exception of the poly[43PFPA-SDE(AIBN)] material, which has a slightly deformed structure with unidentifiable voids. The white arrow in F indicates noticeable thicker scaffold walls compared to the other materials. Scale bars = 50 µm.

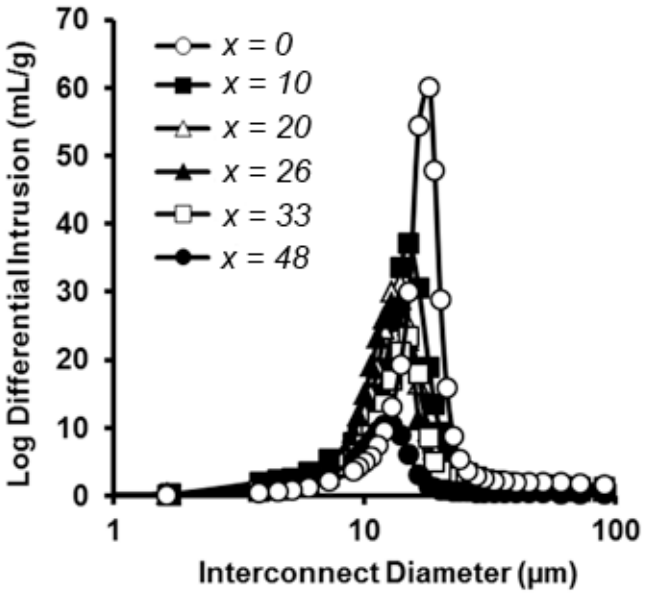

Figure 5.6 Interconnect size distribution for the poly[xPFPA-SDE(AIBN)] materials derived from the HIPE formulations in Table 5-1. Generally a wider distribution is observed with increased PFPA content. Note that x corresponds to the % PFPA in the total monomer mixture. For x = 0 this corresponds to the control poly[0PFPA-SDE(KPS)] formulation.

The poly[26PFPA-SDE(AIBN)] material appeared to display optimum physical characteristics for the maximum theoretical PFPA loading. The material has an average void diameter of 33 μm and an average interconnect diameter of 10 μm, compared to 69 μm and 15 μm respectively in the control poly[PFPA-SDE(KPS)] material (the control being representative of Alvetex®Scaffold). This difference was deemed acceptable, given that many cells have diameters in the region of 15 μm to 25 μm, therefore sufficiently smaller than the 33 μm voids in poly[26PFPA-SDE(AIBN)]. Furthermore, the commercial Alvetex®Scaffold has an average void diameter of 42 μm. To check the suitability of the poly[26PFPA-SDE(AIBN)] material for 3D scaffold applications, HepG2 cells were cultured on the material and the growth characteristics compared against Alvetex®Scaffold.

The poly[26PFPA-SDE(AIBN)] material was sectioned into 200 μm membranes (15 mm in diameter) and housed in the insert/12-well plate/submerged format. Alvetex®Scaffold membranes were housed in the same format for control purposes. Membranes were rendered hydrophilic through immersion in 70 % ethanol and PBS washing. HepG2 cells were then seeded onto the scaffolds at a density of 0.4 million cells in 100 μL and cultured for 5 days at 37 ^{o}C and 5 % CO_2 in 4 mL of MEM. Figure 5.7 shows a histological cross-section of the cells after the growth period. HepG2 cells appeared to have anchored onto the PFPA-functionalised scaffold in a similar manner to Alvetex®Scaffold, and formed a tissue-like layer in the top portion of the membrane. Encouragingly, all cells appear healthy and viable on the poly[26PFPA-SDE(AIBN)] material,

suggesting that the material is not detrimental to cell survival. The penetration of cells into the material was slightly less compared to Alvetex®Scaffold (35 μm compared to 55 μm). This is expected given that Alvetex®Scaffold has a slightly larger average void diameter and thus is more likely to allow cells to migrate into the material. Nonetheless, cells still managed to enter the PFPA-functionalised material after only 5 days culture and adopt a structure almost identical to those cells cultured on Alvetex®Scaffold, evident by the similar cell dimensions shown in Figure 5.7C.

Albumin synthesis was also assessed for HepG2 cells growing on poly[26PFPA-SDE(AIBN)] compared to Alvetex®Scaffold, as shown in Figure 5.8. A very slight decrease in albumin synthesis was observed for the poly[26PFPA-SDE(AIBN)] material after 4 days culture compared to Alvetex®Scaffold. This may be because cells have not penetrated as far into the material and thus are more susceptible to being washed away during media changes. Alternatively it could be that the PFPA functionality does directly reduce albumin synthesis. Nonetheless the decrease in total albumin synthesis is small and so a decision was made to progress this material for subsequent attachment of galactose molecules.

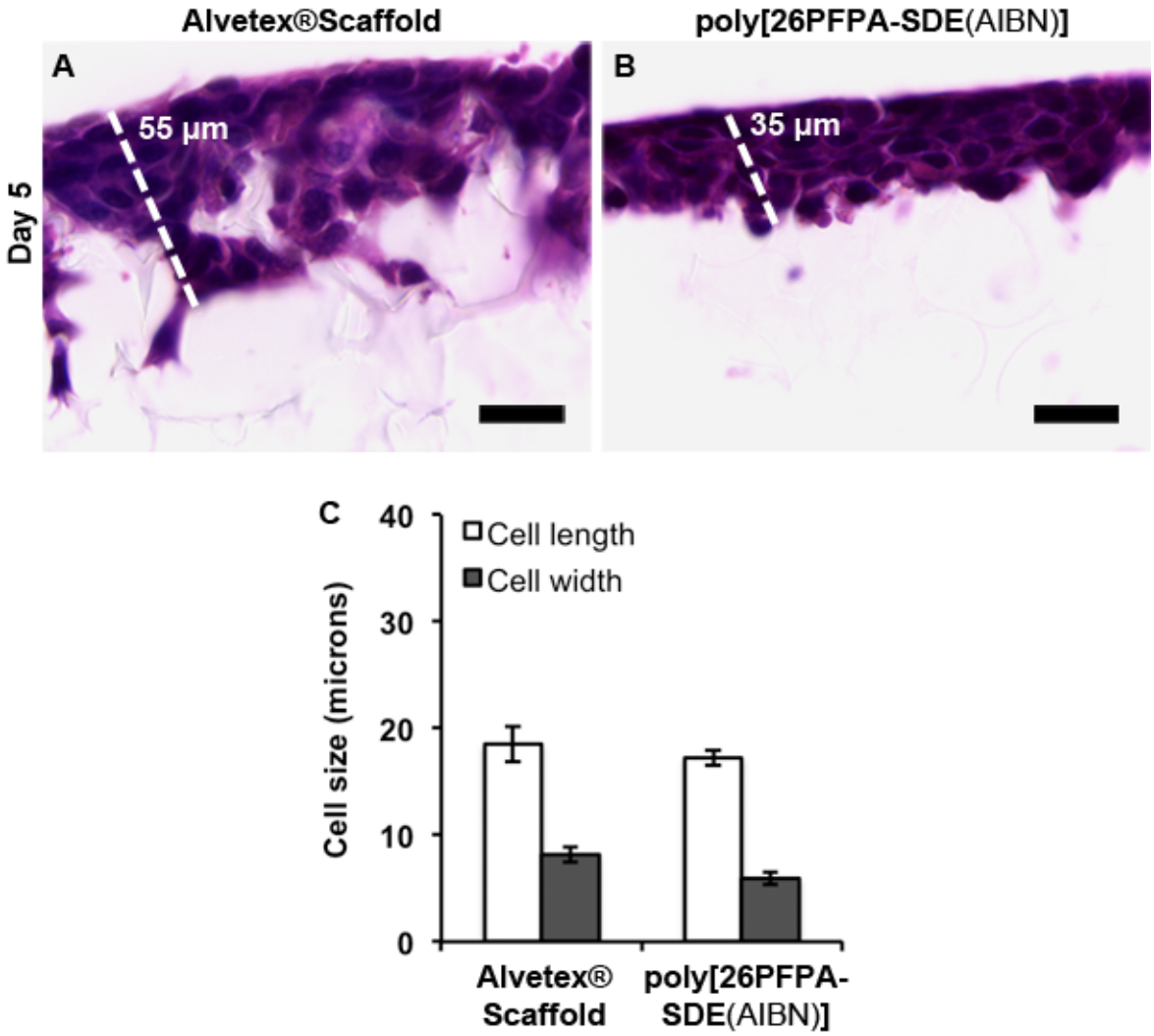

Figure 5.7 Growth of HepG2 cells in poly[26PFPA-SDE(AIBN)] compared to Alvetex®Scaffold. (A,B): H&E staining after 5 days culture. Cells in the poly[26PFPA-SDE(AIBN)] material have adhered well and appear healthy with no signs of necrosis, similar to cells in Alvetex®Scaffold. Cell penetration is slightly lower for the poly[26PFPA-SDE(AIBN)] material compared to Alvetex®Scaffold, which is expected given the smaller void diameter. Scale bars = 20 µm. (C): Quantification of cell structure on the two scaffolds showing very similar cell dimensions. Data represents mean ± s.e.m (n = 15).

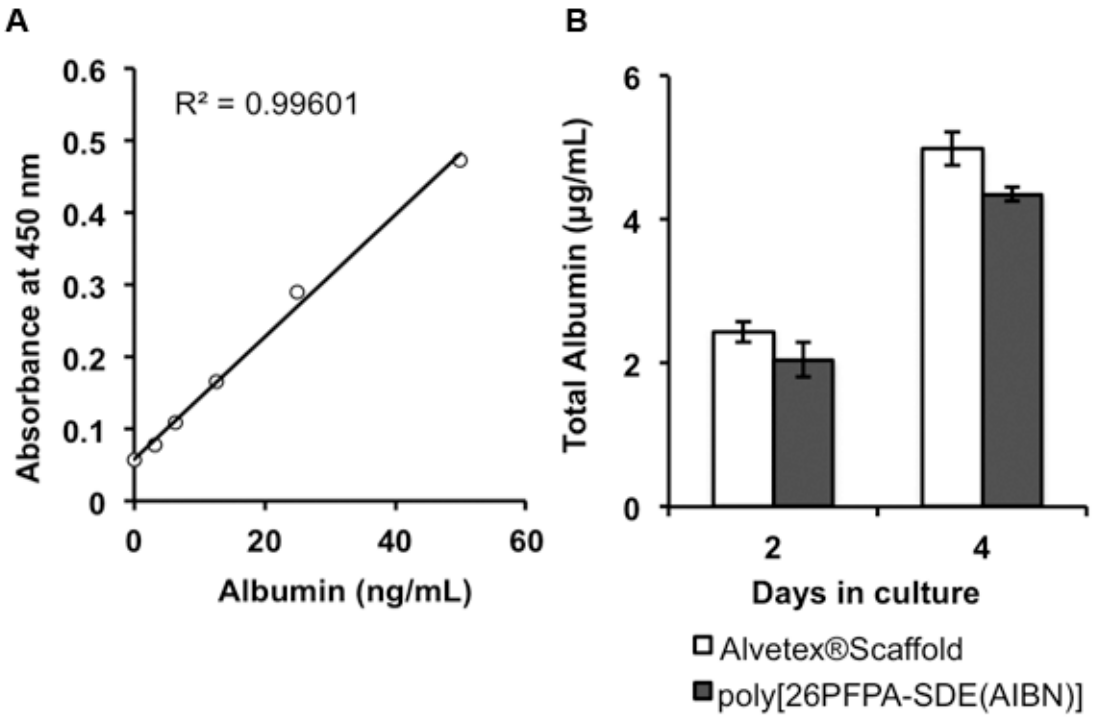

Figure 5.8 Total albumin synthesis of HepG2 cells growing on poly[26PFPA-SDE(AIBN)] compared to Alvetex®Scaffold. (A): Standard curve used to calibrate measured absorbances from the ELISA with known albumin levels. (B): Total HepG2 albumin levels showing only a slight decrease in measured albumin for the poly[26PFPA-SDE(AIBN)] material after 4 days culture. Data represents mean ± s.e.m (n = 3).

5.3.3 Attaching Galactose onto Poly[26PFPA-SDE(AIBN)]

For coupling with 2'-aminoethyl-β-D-galactopyranoside (and the glucose control), the poly[26PFPA-SDE(AIBN)] material was first sectioned into 200 µm membranes and cut into discs of 15 mm in diameter. These discs were then mixed with a solution of the aminoethyl glycoside in dimethylformamide (DMF) for 48 hours at 40 ^{o}C under constant agitation. The resulting materials, termed either GAL-poly[26PFPA-SDE(AIBN)] or GLU-poly[26PFPA-SDE(AIBN)] due to galactose or glucose coupling respectively, were then slowly re-hydrated and washed extensively with MilliQ water before characterisation.

Figure 5.9 shows the ATR-FTIR spectra for poly[26PFPA-SDE(AIBN)] along with GAL-poly[26PFPA-SDE(AIBN)] and GLU-poly[26PFPA-SDE(AIBN)]. All materials contain a peak at 1732 cm^{-1}, which corresponds to the EHA carbonyl group from the parent polystyrene scaffold formulation (EHA ester C=O stretching). The presence of PFPA in the poly[26PFPA-SDE(AIBN)] material is indicated by the peaks at 996 cm^{-1} (C-F stretching), 1520 cm^{-1} (Ar C=C stretching) and 1786 cm^{-1} (PFPA ester C=O stretching). For the carbohydrate-functionalised materials, these three peaks almost

disappear, which is consistent with the loss of pentafluorophenol during nucleophilic substitution. The spectra of the carbohydrate-functionalised materials also have additional peaks at 1658 cm^{-1} (amide C=O stretching) and 3400 cm^{-1} (O-H stretching), suggesting the attachment of carbohydrate.

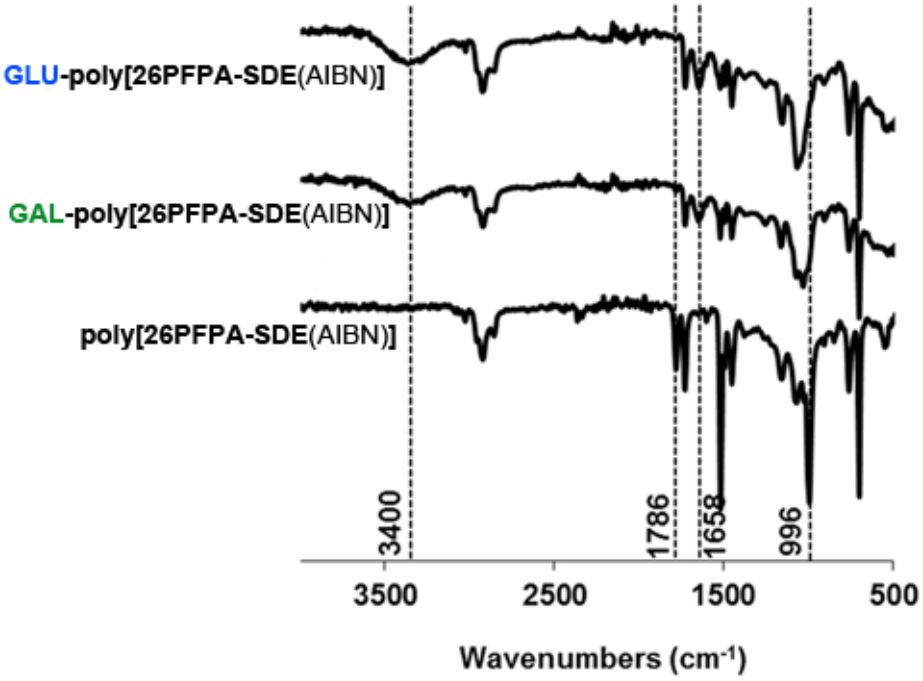

Figure 5.9 ATR-FTIR spectra of poly[26PFPA-SDE(AIBN)], GAL-poly[26PFPA-SDE(AIBN)] and GLU-poly[26PFPA-SDE(AIBN)]. The presence of PFPA in poly[26PFPA-SDE(AIBN)] is indicated by peaks at 996 cm^{-1} (C-F), 1520 cm^{-1} (Ar C=C) and 1786 cm^{-1} (ester C=O). These almost disappear after coupling with carbohydrate and two new peaks are observed that suggest carbohydrate attachment: 1658 cm^{-1} (amide C=O) and 3400 cm^{-1} (O-H).

Figure 5.10 shows the solid state NMR spectra (^{13}C and ^{19}F) for poly[26PFPA-SDE(AIBN)] along with GAL-poly[26PFPA-SDE(AIBN)] and GLU-poly[26PFPA-SDE(AIBN)]. A new carbon peak occurs at ca. 70 ppm in the ^{13}C spectra of the carbohydrate-functionalised materials (C-OH) that is not present in the starting poly[26PFPA-SDE(AIBN)] material. Similarly, a complete disappearance of fluorine peaks is observed in the ^{19}F spectra for both carbohydrate functionalised materials, suggesting a near complete conversion to the amide-carbohydrate.

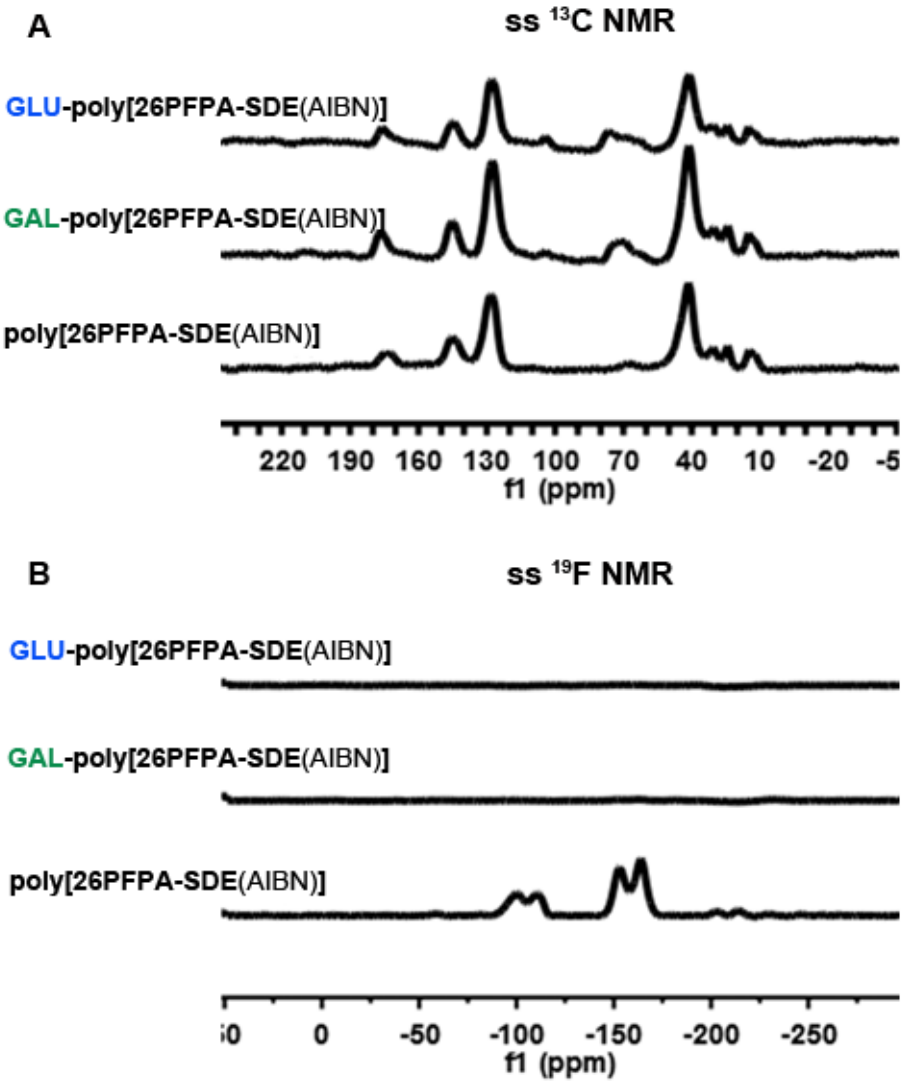

Figure 5.10 Solid-State NMR spectra of poly[26PFPA-SDE(AIBN)], GAL-poly[26PFPA-SDE(AIBN)] and GLU-poly[26PFPA-SDE(AIBN)]. (A): ^{13}C spectra showing the appearance of a new peak at ca. 70 ppm (C-OH) for the carbohydrate-functionalised materials that is absent on poly[26PFPA-SDE(AIBN)]. (B): ^{19}F spectra showing the presence of fluorine in poly[26PFPA-SDE(AIBN)] which is absent on the carbohydrate-functionalised materials.

XPS was used to quantify the amount of PFPA and carbohydrate on the surface of the poly[26PFPA-SDE(AIBN)], GAL-poly[26PFPA-SDE(AIBN)] and GLU-poly[26PFPA-SDE(AIBN)] materials. Table 5-3 shows the surface atomic concentrations (%) obtained from survey spectra for the three materials. The poly[26PFPA-SDE(AIBN)] material surface contains 1.86 % fluorine whereas the carbohydrate-functionalised materials contain only negligible fluorine levels. Moreover, the carbohydrate-functionalised materials contain increased surface oxygen and nitrogen compared to the poly[26PFPA-SDE(AIBN)] material. Note that traces of calcium, silicon and sulphur were also found on the samples that are believed to be from surface contamination.

Table 5-3 Surface Atomic Concentrations (%) Obtained From XPS Survey Spectra For Poly[26PFPA-SDE(AIBN)], GAL-poly[26PFPA-SDE(AIBN)] and GLU-poly[26PFPA-SDE(AIBN)]

	Surface atomic concentration (%)						
	C	F	O	Ca	N	Si	S
poly[26PFPA-SDE(AIBN)]	91.02	1.86	6.83	0.30	0.00	0.00	0.00
GLU-poly[26PFPA-SDE(AIBN)]	89.53	0.00	9.21	0.31	0.62	0.32	0.00
GAL-poly[26PFPA-SDE(AIBN)]	89.36	0.10	8.76	0.65	0.37	0.68	0.09

Figure 5.11 shows the peak-fitted high resolution C1s spectra for the three scaffolds. Peaks were fitted for (a) C-C, C=C at a binding energy (BE) of 285.11 eV, (b) C-OH, C-OC at a BE of 286.00 eV, (c) C-O-C=O at BE's of 286.81 eV and 288.93 eV, (d) C-F at BE of 287.12 eV and (e) O=C-N at BE of 288.13 eV. Noticeably larger peak areas for C-F and C-O-C=O are observed for poly[26PFPA-SDE(AIBN)] material compared to the carbohydrate-functionalised materials. Quantification of peak areas show that the poly[26PFPA-SDE(AIBN)] material contains ca. 9 % PFPA, whereas the GAL-poly[26PFPA-SDE(AIBN)] and GLU-poly[26PFPA-SDE(AIBN)] contain ca. 0 %. Both carbohydrate-functionalised materials display new peak areas for C-OH/C-OC and O=CN that are absent in the poly[26PFPA-SDE(AIBN)] material. Quantification of these peak areas show that the materials contain between ca. 7 % and 9 % carbohydrate, suggesting a near complete conversion from ester to amide under the reaction conditions employed.

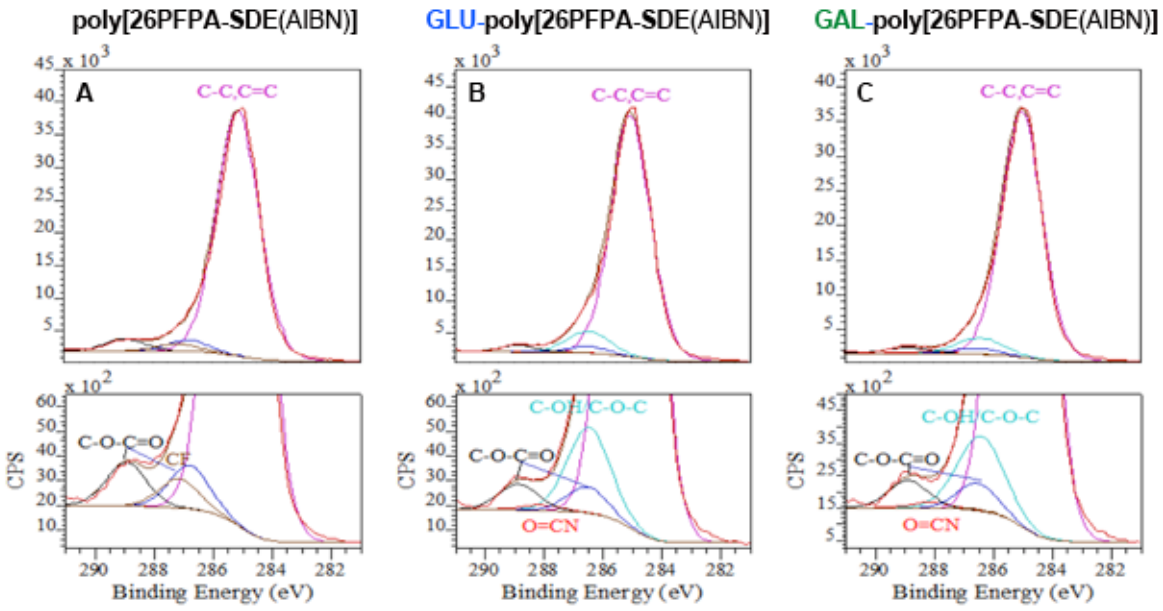

Figure 5.11 High resolution peak-fitted C1s spectra for poly[26PFPA-SDE(AIBN)], GAL-poly[26PFPA-SDE(AIBN)] and GLU-poly[26PFPA-SDE(AIBN)]. (A): Poly[26PFPA-SDE(AIBN)] spectrum showing relatively large peaks for C-F and C-O-C=O corresponding to PFPA on the material surface. (B,C): Carbohydrate-functionalised spectra showing new C-OH/C-O-C and O=CN peaks, as well as a reduction in C-O-C=O peaks corresponding to the attachment of carbohydrate on the material surface.

Figure 5.12 shows the high resolution F1s and N1s spectra for the three scaffolds. Fluorine is present on the poly[26PFPA-SDE(AIBN)] material but not the carbohydrate-functionalised materials. Furthermore, nitrogen is present on the carbohydrate functionalised materials but not the poly[26PFPA-SDE(AIBN)] material.

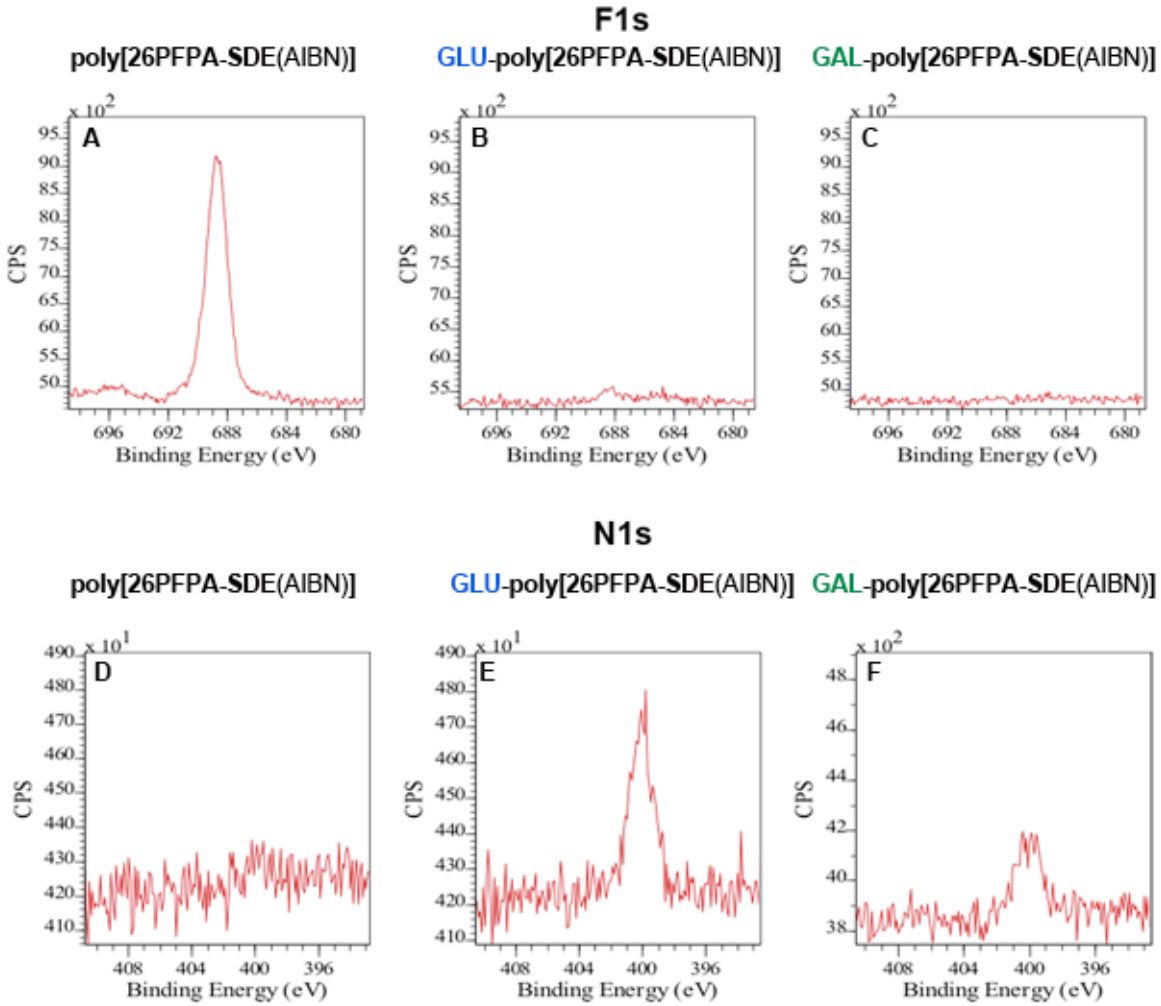

Figure 5.12 High resolution F1s and N1s spectra for poly[26PFPA-SDE(AIBN)], GAL-poly[26PFPA-SDE(AIBN)] and GLU-poly[26PFPA-SDE(AIBN)]. (A,D): Poly[26PFPA-SDE(AIBN)] spectra showing the presence of fluorine but not nitrogen on the material surface. (B,C,E,F): Carbohydrate-functionalised spectra showing the absence of fluorine but the presence of nitrogen.

5.3.4 Assessing Hepatocyte Function on GAL-poly[26PFPA-SDE(AIBN)]

To assess the accessibility and selectivity of the pendent galactose residues on the GAL-poly[26PFPA-SDE(AIBN)] material, primary rat hepatocytes were cultured for up to 24 hours. The poly[26PFPA-SDE(AIBN)] and GLU-poly[26PFPA-SDE(AIBN)] materials were used as controls for the experiment.

The 24-well plate format was used. Scaffold membranes (200 μm thick and 15 mm diameter) were first rendered hydrophilic via immersion in 70 % ethanol and PBS washing. Primary rat hepatocytes were then seeded on the materials via 0.2 million cells in 1 mL of culture media. Note that culture media contained serum proteins which were expected to adsorb non-specifically onto the scaffold surface and thus mask some of the galactose sites. However, completely removing serum proteins from the culture media raised concern over cell survival and so they were not removed.

Figure 5.13 shows the albumin synthesis of the cells during the culture period. A significantly larger amount of albumin was measured for hepatocytes growing on the GAL-poly[26PFPA-SDE(AIBN)] material compared to the poly[26PFPA-SDE(AIBN)] material and GLU-poly[26PFPA-SDE(AIBN)] after 3 hours culture. This suggests that the pendent galactose is accessible and can maintain selectivity with the ASGP-R. However, as the culture period progressed, this enhanced albumin synthesis was lost, potentially due to non-selective hepatocyte adherence onto the scaffold via a serum protein coating.

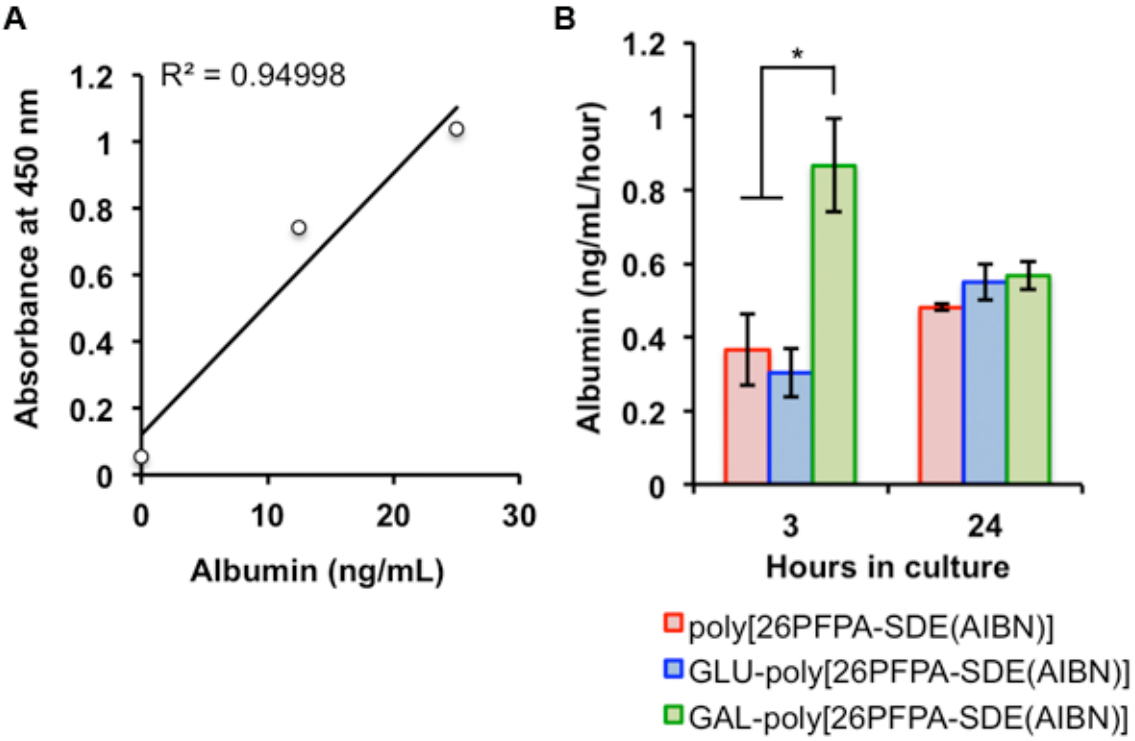

Figure 5.13 Total albumin synthesis of primary rat hepatocytes growing on GAL-poly[26PFPA-SDE(AIBN)] compared to GLU-poly[26PFPA-SDE(AIBN)] and poly[26PFPA-SDE(AIBN)]. (A): Standard curve used to calibrate measured absorbances from the ELISA with known albumin levels. (B): Total primary rat albumin levels showing a significant increase in albumin synthesis for cells on the GAL-poly[26PFPA-SDE(AIBN)] material after 3 hours culture (crucial adhesion period). After 24 hours culture no difference in albumin synthesis is observed. Data represents mean ± s.e.m (n = 3).

5.3.5 Incorporating Aa as a Functional Co-Monomer

Table 5-4 shows the different HIPE formulations used to prepare poly[xAa-SDE(AIBN or KPS)] materials. Note that Aa functionalisations were attempted using both AIBN and KPS as initiators. The [0Aa-SDE(KPS)] formulation represents a typical polystyrene scaffold formulation and therefore serves as a morphological control for the study. The [0Aa-SDE(AIBN)] formulation was used as an additional morphological and chemical control.

Table 5-4 HIPE Formulations used to Prepare Poly[xAa-SDE(AIBN or KPS)] Materials

	Wt. % in HIPE								% Aa[a]
	Oil					Aq.			
HIPE Formulation	**STY[b]**	**DVB[b]**	**EHA[b]**	**Span80**	**AIBN**	**Aa**	**H_2O**	**KPS**	
[0Aa-SDE(KPS)]	4.1	0.7	2.0	2.4	0.0	0.0	89.8	1.0	0
[3Aa-SDE(KPS)]	4.1	0.7	2.0	2.4	0.0	0.2	89.6	1.0	3
[13Aa-SDE(KPS)]	4.1	0.7	2.0	2.4	0.0	1.0	88.8	1.0	13
[0Aa-SDE(AIBN)]	4.1	0.7	2.1	2.4	0.3	0.0	90.4	0.0	0
[13Aa-SDE(AIBN)]	4.1	0.7	2.1	2.4	0.3	1.0	89.4	0.0	13

[a]Weight percentage of total monomer mixture; [b]molar quantities of monomers in oil phase as a percentage of total (oil phase) monomer content: STY – 70.6%; DVB – 9.4%; EHA – 20.0%.

HIPEs were formed by adding an aqueous water phase to the oil phase and then stirring vigorously for 2 minutes. Aa was added to the aqueous phase prior to HIPE formation for the three formulations containing Aa. Stable HIPEs were formed for all formulations with the exception of [13Aa-SDE(KPS)], which phase separated after approximately 1 hour. Encouragingly, the [13Aa-SDE(AIBN)] formulation displayed a typical STY-DVB-EHA HIPE viscosity and appearance. Figure 5.14 shows the appearance of thermally cured HIPEs described in Table 5-4. A typical polystyrene scaffold monolith was produced for the [13Aa-SDE(AIBN)] formulation after curing. On the contrary, both [3Aa-SDE(KPS)] and [13Aa-SDE(KPS)] formulations did not produce a typical scaffold monolith. The poly[3Aa-SDE(KPS)] material displayed large (0.5 mm) heterogeneous holes throughout the structure, whereas the [13Aa-SDE(KPS)] formulation remained as a phase separated liquid. These data suggest that KPS is not a suitable initiator for Aa functionalisations of STY-DVB-EHA scaffolds, and that AIBN appears to be the better choice. It is hypothesised this is because the Aa serves to decrease emulsion stability, and that KPS, which preferentially polymerises monomers in the hydrophilic phase, kinetically cannot polymerise the majority of the organic monomers before phase separation occurs.

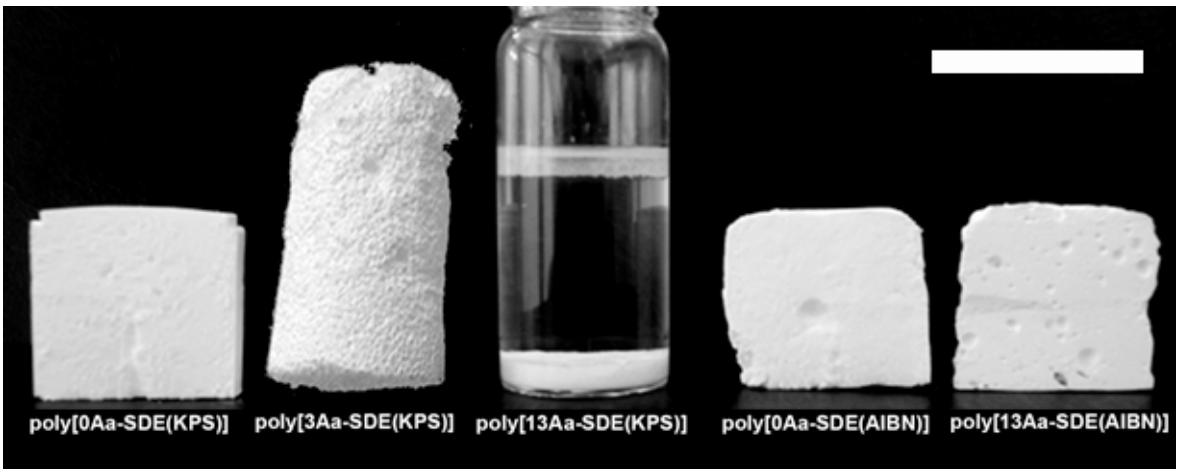

Figure 5.14 Resulting polyHIPE monoliths after polymerising the HIPE formulations shown in Table 5-4. As expected, the control poly[0Aa-SDE(KPS)] material formed a stable (non-deformed) monolith. However the addition of Aa to KPS initiated HIPEs did not produce suitable monoliths: poly[3Aa-SDE(KPS)] displayed huge heterogeneous voids and poly[13Aa-SDE(KPS)] remained as two phase separated liquids. Using AIBN as the HIPE initiator produced stable monoliths, even for the poly[13Aa-SDE(AIBN)] material. Scale bar = 3 cm.

The morphology of each monolith was investigated using SEM, as shown in Figure 5.15. As expected, the morphology of the poly[0Aa-SDE(KPS)] control was typical to that of a polystyrene scaffold used in 3D cell culture applications, with clear open-cell voids and a high degree of interconnectivity. The poly[13Aa-SDE(AIBN)] material also exhibited a typical polyHIPE morphology, indicating the fabrication of a functional material with desirable scaffold characteristics. It is hypothesised that AIBN, a hydrophobic initiator, is able to polymerise the STY-DVB-EHA monomers before phase separation can occur, thus producing a typical polystyrene scaffold morphology. Interestingly, the unfunctionalised AIBN control, poly[0Aa-SDE(AIBN)], showed low interconnectivity, visibly thicker scaffold walls and signs of deformation. Finally the poly[3Aa-SDE(KPS)] material did not display a polyHIPE morphology, with the large voids being filled with a gel-like material that is likely to be a polyacrylic acid hydrogel.

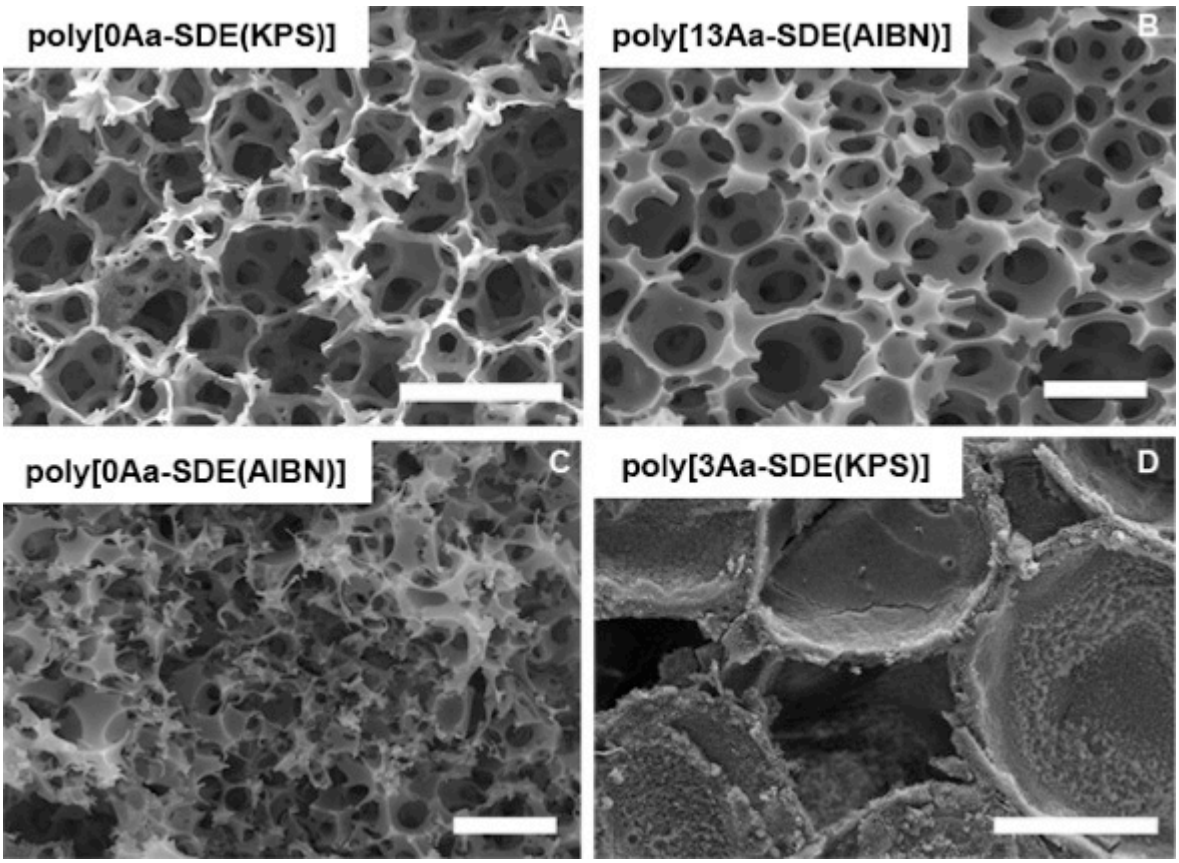

Figure 5.15 Morphology of the poly[xAa-SDE(AIBN or KPS)] materials by SEM. (A): Poly[0Aa-SDE(KPS)] control showing a typical open-cell scaffold morphology. Scale bar = 100 μm. (B): Poly[13Aa-SDE(AIBN)] also showing an open-cell morphology. Scale bar = 20 μm. (C) Poly[0Aa-SDE(AIBN)] showing a deformed and less-open morphology. Scale bar = 20 μm (D): Poly[3Aa-SDE(KPS)] showing extremely large voids filled with a gel-type material that can be assumed to be polyacrylic acid. Scale bar = 500 μm.

The physical characteristics of the poly[13Aa-SDE(AIBN)] material in comparison with the poly[0Aa-SDE(KPS)] control is shown in Table 5-5. The average void diameter of the poly[13Aa-SDE(AIBN)] material was found to be 19 μm, compared to 60 μm for poly[0Aa-SDE(KPS)] control (obtained from ImageJ™ analysis of SEM micrographs).

Mercury intrusion porosimetry showed that the average interconnect diameter for the poly[13Aa-SDE(AIBN)] material was 6 μm, in comparison to 15 μm for poly[0Aa-SDE(KPS)] control. This is expected given the reduction in void diameter. The interconnect diameter distribution was found to be narrow for the poly[13Aa-SDE(AIBN)] material, as shown in Figure 5.16. Encouragingly, the porosity of the poly[13Aa-SDE(AIBN)] material was 89 % porous, in comparison to 92 % porosity for the poly[0Aa-SDE(KPS)] control.

Table 5-5 Physical Characteristics of poly[13Aa-SDE(AIBN)] in comparison to poly[0Aa-SDE(KPS)]

	<D> (µm)[a]	<d> (µm)[b]	<d>/<D>	Porosity (%)
poly[0Aa-SDE(KPS)]	60	15	0.25	92
poly[13Aa-SDE(AIBN)]	19	6	0.32	89

[a]Average void diameter from ImageJ™ analysis of SEM images. [b]Average interconnect diameter from mercury intrusion porosimetry.

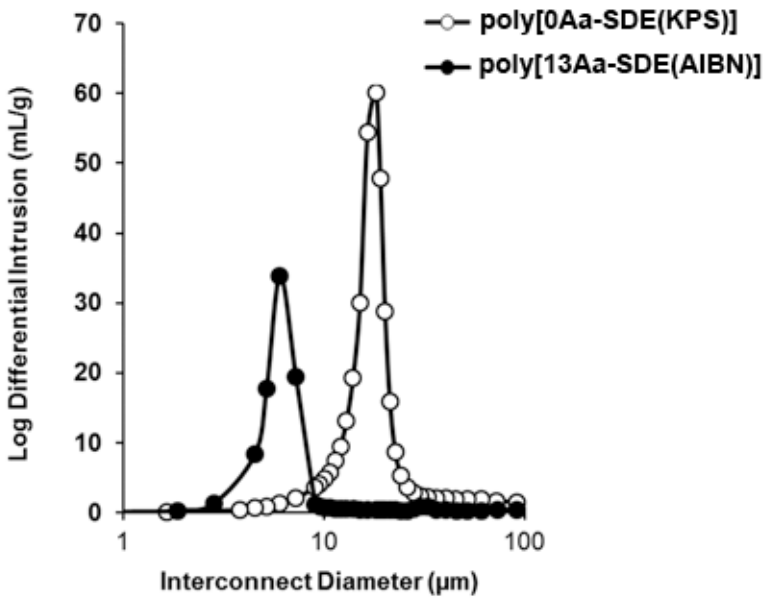

Figure 5.16 Interconnect diameter distribution for the poly[13Aa-SDE(AIBN)] in comparison to poly[0Aa-SDE(KPS)]. A narrow distribution is observed even though the average void diameter is lower for the poly[13Aa-SDE(AIBN)] material.

The initial detection of surface carboxylic acid groups on the poly[13Aa-SDE(AIBN)] material was performed by Toluidine Blue O (TBO) staining. TBO is a basic blue dye often used to detect carboxylic acid functionality[221]. Scaffolds were immersed in a TBO solution (0.1 mg/mL) for 2 minutes and then washed extensively with distilled water. Figure 5.17 shows a significantly greater uptake of the basic dye for the poly[13Aa-SDE(AIBN)] material compared to the unfunctionalised poly[0Aa-SDE(AIBN)] control, indicating the presence of acid functionality from Aa incorporation at the polymerising interface.

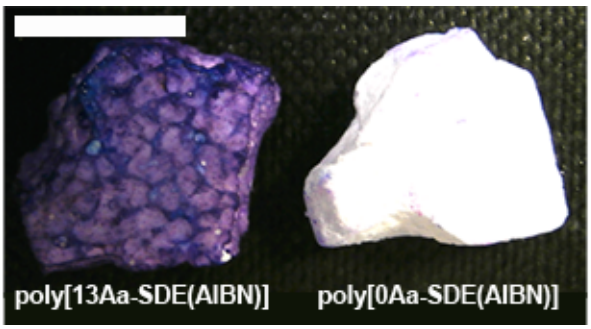

Figure 5.17 Detection of surface carboxylic acid groups on the poly[13Aa-SDE(AIBN)] material using the basic TBO stain. A significant uptake of the blue TBO stain is observed for the poly[13Aa-SDE(AIBN)] material, whereas no staining is observed for the poly[0Aa-SDE(AIBN)] control. Scale bar = 3 cm.

To further demonstrate the presence of surface carboxylic acid groups on the poly[13Aa-SDE(AIBN)] scaffold wettability by water was assessed. After fully submerging the material in water for 5 seconds and then re-applying a water droplet, the poly[13Aa-SDE(AIBN)] scaffold was found to be wettable. On the contrary, the poly[0Aa-SDE(AIBN)] control remained non-wettable after pre-submerging in water (Figure 5.18).

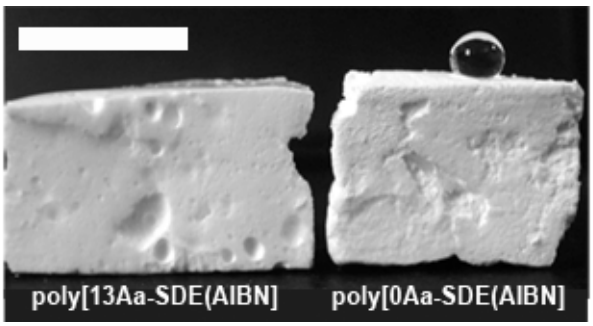

Figure 5.18 Wettability by water of the poly[13Aa-SDE(AIBN)] material. After submerging the material in water the material became wettable by water. On the contrary the poly[0Aa-SDE(AIBN)] material remained non-wettable by water. Scale bar = 3 cm.

Attempts at quantifying the amount of carboxylic acid on the poly[13Aa-SDE(AIBN)] scaffold was first performed using an acid-base back titration. The scaffold was ground into a powder and then treated with 0.2 M NaOH solution for 24 hours. This NaOH solution was then filtered and titrated against 0.2 M HCl solution to determine original acid concentration on the scaffold. The same treatment was applied to the poly[0Aa-SDE(AIBN)] control. Figure 5.19 shows that a lower volume of HCl was required to neutralise the NaOH solution pre-exposed to the poly[13Aa-SDE(AIBN)] polyHIPE compared to the unfunctionalised poly[0Aa-SDE(AIBN)] control, indicating the presence of acid in the original scaffold. However, issues such as poor scaffold-NaOH mixing, potential EHA

hydrolysis (disrupting acid concentrations) and sample loss during filtration unfortunately prevented accurate carboxylic acid quantification using this method. As a result XPS was used to quantify surface carboxylic acid groups.

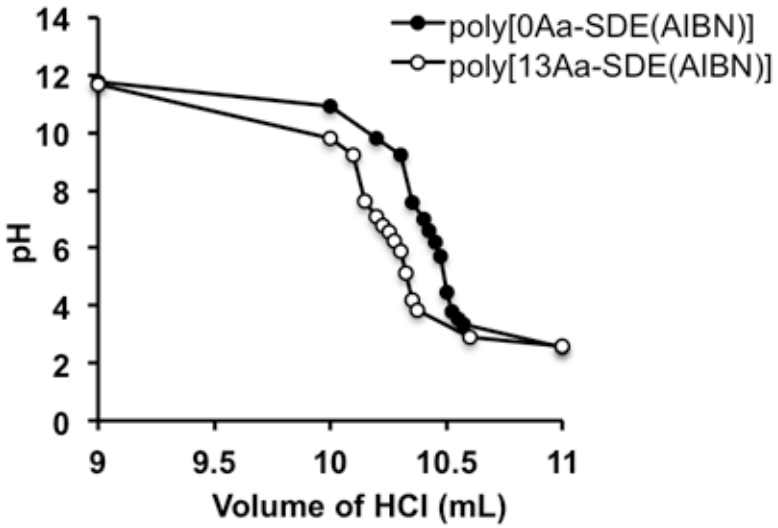

Figure 5.19 Acid-base back titration of an NaOH solution pre-exposed to poly[13Aa-SDE(AIBN)] and poly[0Aa-SDE(AIBN)]. The NaOH solution pre-exposed to poly[13Aa-SDE(AIBN)] (white dots) required less acid for neutralisation compared to the NaOH solution pre-exposed to poly[0Aa-SDE(AIBN)] (black dots). This indicates the presence of acid on poly[13Aa-SDE(AIBN)], however quantification was not applied due to several practical issues.

XPS was used to quantify the amount of surface carboxylic acid functionality on the poly[13Aa-SDE(AIBN)] material compared to the poly[0Aa-SDE(AIBN)] control. Table 5-6 shows the surface atomic concentrations (%) obtained from survey spectra for the two materials. A noticeable decrease in carbon concentration and increase in oxygen concentration is observed for poly[13Aa-SDE(AIBN)] compared to poly[0Aa-SDE(AIBN)], suggesting a displacement of organic monomers with Aa at the polymerising interface for the functionalised material. Small quantities of Ca, Si and S were found on both materials and are likely from surface contamination.

Table 5-6 Surface Atomic Concentrations (%) Obtained From XPS Survey Spectra For Poly[13Aa-SDE(AIBN)] And Poly[0A-SDE(AIBN)] Materials.

	Surface atomic concentration (%)				
	C	**O**	**Ca**	**Si**	**S**
poly[0Aa-SDE(AIBN)]	89.6	8.4	0.5	1.3	0.2
poly[13Aa-SDE(AIBN)]	79.2	19.6	0.1	1.1	0.0

Figure 5.20 shows the high resolution C1s spectra for poly[13Aa-SDE(AIBN)] and poly[0Aa-SDE(AIBN)] with peak fitting. Both spectra were fitted with three components: (i) C-C, C=C at a binding energy (BE) of 285.0 eV, (ii) C-O at a BE of 286.3 eV and (iii) COOH at a BE of 289.2 eV. The peak area for the carboxylic acid functional group (289.2 eV) is 7.5 % for poly[13Aa-SDE(AIBN)]. The same area for poly[0Aa-SDE(AIBN)] is 0.0%. We can therefore conclude that approximately half of the original 13 % Aa monomer was incorporated into the scaffold surface. Note that the peak area of the C-O functional group (286.3 eV) is 19.2 % for poly[0Aa-SDE(AIBN)] and 19.4 % for poly[13Aa-SDE(AIBN)]. It is hypothesised that this comes from residual Span80 left on each scaffold after washing.

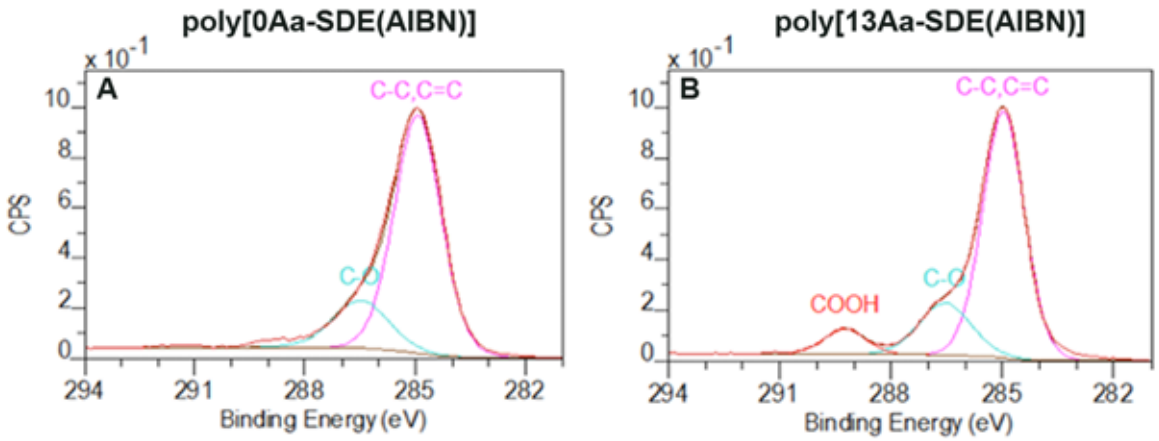

Figure 5.20 High resolution peak-fitted C1s spectra for poly[0Aa-SDE(AIBN)] and poly[13Aa-SDE(AIBN)]. (A): Poly[0Aa-SDE(AIBN)] spectrum showing an absence of a COOH peak. (B): Poly[13Aa-SDE(AIBN)] spectrum showing a COOH peak and thus confirming the presence of Aa in the material.

As with the PFPA-functionalised scaffold, it was hypothesised that the carboxylic acid functionality on the surface of the poly[13Aa-SDE(AIBN)] material could provide a useful reactive site for subsequent galactose attachment using galactose-amines. A preliminary assessment of the biocompatibility of this precursor material for 3D cell growth was therefore performed using Upcyte® cells and assessing adhesion on the material after 2 hours culture. Figure 5.21 shows adhered cells (green dots) on poly[13Aa-SDE(AIBN)] and Alvetex®Scaffold after seeding the same cell number. No significant difference was observed for the number of cells adhered to the poly[13Aa-SDE(AIBN)] material compared to Alvetex®Scaffold. These preliminary data indicate that the precursor scaffold may provide a suitable environment for the attachment of human hepatocytes and indicates its suitability as a precursor scaffold for subsequent galactose attachment by reaction with galactose-amines.

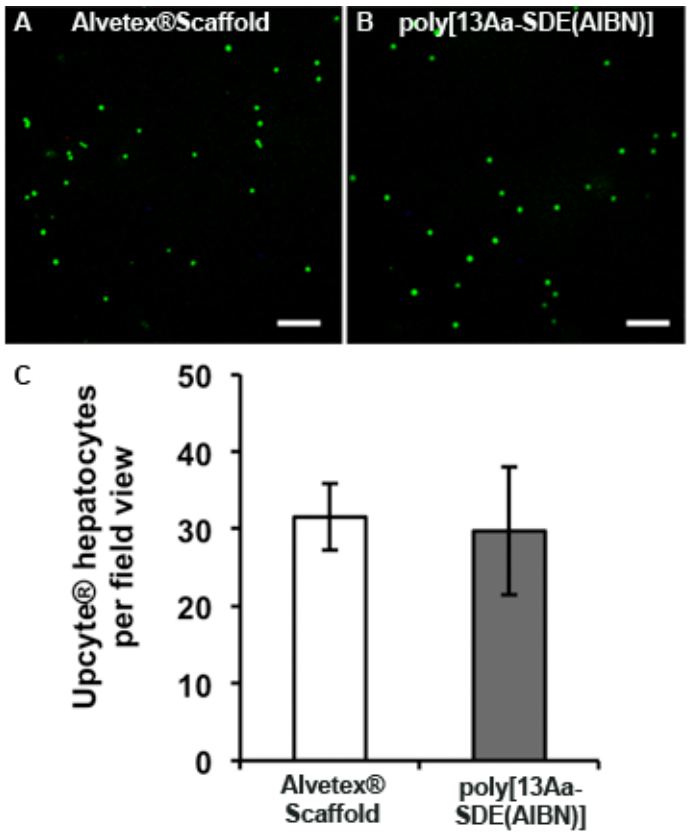

Figure 5.21 Adhesion of Upcyte® hepatocytes onto poly[13Aa-SDE(AIBN)] compared to Alvetex®Scaffold. (A,B): Staining cells with phalloidin (green dots) and imaging using a fluorescence microscope. Scale bars = 200 μm. (C): Quantification of adherent cells per field of view showing no difference between the number of cells on poly[13Aa-SDE(AIBN)] and Alvetex®Scaffold. Data represent mean ± s.e.m (5 fields per replicate, n = 3).

5.3.6 Additional Attempts at Incorporating Aa using KPS Initiation

The previous data indicated that KPS is not a suitable initiator for incorporating Aa into an emulsion templated polystyrene scaffold. To further investigate this, additional Aa concentrations were explored for completion. Figure 5.22 shows the resulting materials for Aa incorporation when $x \leq 3$ using KPS as the initiator. As shown previously, when $x = 3$ large heterogeneous holes are visible in the monolith. However, even when $x < 3$ the monoliths have deformed, further supporting that KPS is an unsuitable initiator for Aa incorporation.

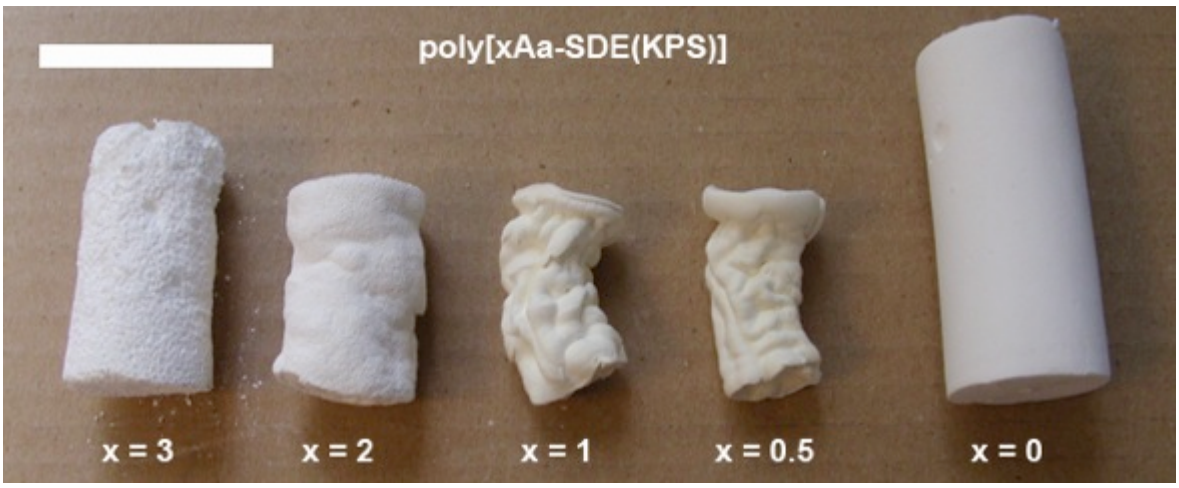

Figure 5.22 Resulting monoliths for low levels of Aa incorporation into polystyrene scaffolds using KPS as the initiator. Even when x < 3 monoliths deform, further demonstrating the unsuitability of KPS as an initiator for Aa incorporation. Scale bar = 4 cm.

Figure 5.23 shows the resulting materials for Aa incorporation when x ≥ 13 using KPS as the initiator. As shown previously, when x = 13 the HIPE phase separates and remains as two liquids after polymerisation. This is also the case when x = 22. Interestingly, when x ≥ 33 a gel is formed, as shown in Figure 5.23B,C. This demonstrates the unsuitability of KPS as an initiator for Aa incorporation in polystyrene scaffolds.

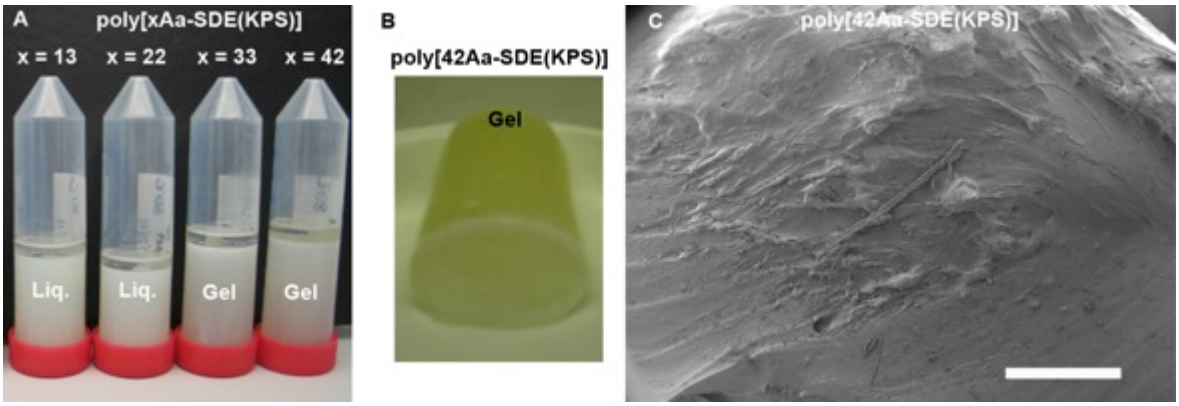

Figure 5.23 Resulting materials for high levels of Aa incorporation into polystyrene scaffolds using KPS as the initiator. (A): When x ≥ 13 the resulting materials are either phase separated liquids or gels post-polymerisation. (B): Photograph confirming that when x = 42 a gel is formed. (C): SEM image confirming that when x = 42 a gel is formed. Scale bar = 1 mm.

5.4 Discussion

For a cell to successfully attach and survive on a synthetic scaffold there usually needs to be the appropriate biochemical ligands present on the material surface for integrin-mediated recognition and binding. That is, the synthetic scaffold needs to be rendered biochemically relevant. Often this is achieved through proteins such as fibronectin present in the serum or secreted by the cells themselves pre-adsorbing onto the substrate prior to cell attachment. However, this process can often be non-specific and dependent on the scaffolds affinity for protein deposition.

Scaffold surface modification through atmospheric plasma treatment to introduce hydrophilic functionality is one method of aiding cell attachment and function *in vitro*[222]. Indeed, reports have shown that plasma treated surfaces can either directly accommodate cell adhesion without serum[223] or facilitate serum protein deposition to aid in cell attachment[224]. However, one major limitation of plasma treatment is that the effect is temporary, such that the modified surface slowly reverts back to the original state over time. Another limitation is that plasma treatment does not always deliver a uniform surface modification, particularly for 3D scaffolds. Consequently, many researchers have found that covalently immobilising specific biomolecules present *in vivo* onto the scaffold surface is a very effective approach to improving selective cell adhesion and overall function *in vitro*[225-227]. For example, scaffolds modified with specific peptide motifs have been shown to greatly enhance cell attachment[228, 229]. Immobilising specific growth factors onto scaffolds has been shown to influence stem cell differentiation[230, 231]. Electrospun scaffolds surface-modified with gelatin improved cell adhesion and viability[232]. Recognising these benefits researchers are now striving towards 3D scaffolds that present appropriate biochemical ligands to re-create native cell-ECM interactions *in vitro*.

Several groups have utilised galactose as a surface ligand to improve hepatocyte adhesion and function *in vitro*, given the specificity with the hepatic ASGP-R. For example, 2D poly(ethylene terephthalate) (PET) films have been functionalised with galactose and found to increase hepatocyte adhesion and function compared to unfunctionalised films[220, 233]. Chan *et al.* demonstrated that galactose immobilised onto 2D coverslips could be used to control hepatocyte spreading and adhesion dynamics on a 2D surface[234]. Galactose-functionalised 3D substrates have also recently gained significant attention and review[235, 236]. Park *et al*. galactose-functionalised a gas-foamed PLGA scaffold and found that hepatocyte adhesion and albumin synthesis was greatly enhanced[215]. Mao *et al*. galactose-functionalised an electrospun scaffold derived from poly(caprolactone-co-ethyl ethylene phosphate) (PCLEEP) and subsequently demonstrated its suitability for primary rat hepatocyte culture[105]. Similarly, Börner *et al*. recently prepared a galactose-functionalised electrospun scaffold composed of poly(pentafluorophenyl methacrylate)

(PPfpMA) and PCL[237]. Gu *et al*. showed that galactosylated chitosan could be electrospun into 3D scaffolds that were found to increase hepatocyte albumin synthesis, urea synthesis and cytrochrome P450 activity compared to chitosan scaffolds[106]. Moreover, Yu *et al*. developed a hydrogel-based soft sponge conjugated with galactose that was found to enhance hepatocyte adhesion and function over conventional collagen I sandwich cultures[238].

Despite the extensive reports described above, prior to this study there had been no developments on the functionalisation of emulsion templated polystyrene scaffolds with galactose. One potential reason for this is that polystyrene is relatively inert, making any surface modifications challenging. Indeed, most polystyrene functionalisations first require the incorporation of additional functional groups (e.g. acids, esters, amines, alkyl halides) onto the surface to act as reactive sites for subsequent modifications. One route to adding new functional groups onto polystyrene is post-polymerisation modification. For example, Deleuze *et al.* described several routes to additional functionality using the pendent vinyl groups in the polymer via reactions such as bromination or hydroboration[239]. Similarly Sherrington *et al.* reported successful electrophilic aromatic substitutions of the free benzene rings with reactions such as sulfonation, nitration and bromination reactions[240]. However, nearly all of these post-polymerisation modifications reactions employ harsh reaction conditions with multiple synthesis and washing steps. A more attractive route to adding functionality onto polystyrene scaffolds is to include a functional co-monomer into the initial HIPE mixture as a means of providing a reactive site for subsequent galactose attachment post-polymerisation.

In this study, PFPA was added to the HIPE external phase to form a scaffold with pendent ester functionality. Suitable open-cell scaffolds were formed with up to 33 wt% PFPA in the monomer mixture, however concentrations higher then this seemed to cause scaffold deformation and a less open-cell morphology. In this study, 26 wt% PFPA in the monomer mixture seemed to offer the optimal scaffold characteristics for maximum PFPA loading. The scaffold displayed an average void diameter of 33 μm and a porosity of 92 %, both highly suitable characteristics for 3D cell culture applications. Indeed, the material supported the 3D growth of HepG2 cells in a similar manner to Alvetex®Scaffold. XPS analysis revealed that ca. 9 % of the scaffold surface could be attributed to the PFPA ester reactive site. This loss of PFPA compared to the original 26 wt% in the initial emulsion has also been observed in other polyHIPE systems[218], and may be attributed to either partial PFPA solubility in the aqueous phase, hydrolysis of the pentafluorophenyl ester or incomplete PFPA polymerisation.

The incorporation of PFPA into an emulsion templated polystyrene scaffold is consistent with other literature reports employing similar hydrophobic functional co-monomers into the pre-polymerised HIPE. For example, Heise *et al.* incorporated amino functionality via adding 4-vinylbenzylphthalimide into the external oil phase[241]. Furthermore the resulting polyHIPE was then used to subsequently attach peptide brushes for bioseparation applications[242]. Krajnc *et al*. demonstrated that methacrylic acid could be incorporated, again adding the co-monomer via the oil phase[243]. Other groups have also added 4-vinylbenzyl chloride (VBC) into the oil phase to deliver pendent benzyl chloride functionality [244-246].

The pendent PFPA ester groups on the poly[26PFPA-SDE(AIBN)] material were reacted with 2'-aminoethyl-β-D-galactopyranoside to attach pendent galactose residues, similar to the strategy described by Boyer and Davis for solution-based glycopolymer synthesis[247-249]. XPS revealed that ca. 7 – 9 % of the surface could be attributed to carbohydrate. However, it is hypothesised that this could be significantly increased if amines carrying multiple galactose residues were employed. The accessibility and selectivity of the pendent galactose residues on the poly[26PFPA-SDE(AIBN)] material was assessed via primary rat hepatocyte culture. During the crucial adhesion period, a significant increase in albumin synthesis was observed for the galactose-functionalised scaffold, consistent with the reports described above for other 2D and 3D galactose-functionalised *in vitro* substrates. However, as the culture period progressed the albumin increase diminished. It is hypothesised that the serum proteins are able to deposit onto the scaffold and offer non-selective binding of hepatocytes onto the scaffold.

Aa was also incorporated into an emulsion templated polystyrene scaffold via addition into the HIPE aqueous droplet phase. With this approach, a suitable scaffold morphology was observed using 13 wt% Aa and AIBN as the initiator. The material displayed an average void diameter of 19 μm and a porosity of 89 %. XPS analysis of the poly[13Aa-SDE(AIBN)] scaffold showed that ca. 7.5 % of the material surface could be attributed to acrylic acid, approximately half of what was added to the HIPE mixture. Interestingly, using KPS as the initiator was not suitable for Aa functionalisation of polystyrene scaffolds. This is entirely consistent with the literature. Silverstein *et al.* demonstrated that acrylamide added via the aqueous phase and using KPS as the initiator produced non-polyHIPE morphologies (such as bicontinuous hydrophilic-hydrophobic polymers suitable for drug loading and release)[250]. The same report also showed that hydrophobic initiators such as benzoyl peroxide (BPO) did produce typical polyHIPE morphologies, consistent with the findings from this study employing AIBN.

5.5 Conclusions

The following conclusions can be made from the results of this Chapter:

- Galactose can be incorporated onto the surface of an emulsion templated polystyrene scaffold, potentially improving the biochemical relevance of these materials for *in vitro* hepatocyte culture.

- Functionalisation was achieved by adding 26 wt% PFPA into the HIPE external oil phase and polymerising using AIBN as the initiator. The resulting scaffold displayed a typical emulsion templated polystyrene scaffold morphology and porosity and also supported the 3D growth of hepatocyte cells.

- XPS analysis revealed that the ester-functionalised scaffold surface contained ca. 9% ester, which could be converted into pendent galactose functionality via a facile coupling reaction with 2'-aminoethyl-β-D-galactopyranoside.

- The pendent galactose on the scaffold surface was found to be accessible and selective to hepatocytes growing on the material and actually enhanced albumin synthesis during the crucial adhesion period.

- This study also showed that Aa could also be incorporated into an emulsion templated polystyrene scaffold as an alternative route towards surface galactose functionalisation. By adding 13 wt% Aa into the HIPE aqueous internal phase and using AIBN as the initiator, a typical emulsion templated polystyrene scaffold morphology was produced.

- XPS analysis revealed that this acid-functionalised scaffold contained ca. 7 % carboxylic acid functionality, which could potentially offer useful reactive sites for subsequent reactions with galactose-amines (similar to the strategy employed with the PFPA scaffold). This acid functionality did not disrupt the initial adhesion of Upcyte® hepatocytes onto the material.

- Finally, the choice of initiator is crucial for functionalisations involving Aa. A more hydrophobic initiator such as AIBN can deliver the required scaffold morphology, whereas hydrophilic initiators such as KPS either lead to phase separation or deformed monoliths.

Chapter 6: Concluding Remarks and Future Work

6.1 Concluding Remarks

6.1.1 Recap of Research Field and Project Aim

Hepatocytes are the main functional cells of the liver and play a crucial role in drug detoxification and metabolism[32, 33]. *In vivo*, hepatocytes adopt specific 3D cell geometries and tissue architectures as part of the lobule unit. Moreover, within the 3D hepatic plate hepatocytes experience extensive cell-cell contact with adjacent hepatocytes to form specialised sinusoidal and bile canaliculi domains that are crucial for normal function. Hepatocytes also receive anchorage and biochemical cues from a surrounding ECM that serves to regulate normal behaviour. In short, hepatocyte function *in vivo* is highly dependent on a 3D cell geometry, tissue architecture and physical interaction.

In vitro hepatocyte models are a key component of drug discovery in predicting toxicity profiles prior to *in vivo* trials. However, in order for *in vitro* models to be predictive of *in vivo* they need to be physiologically relevant and thus suitably mimic the native growth environment. Traditionally, plastic Petri dishes and welled plates have been used as the artificial growth environment for most *in vitro* hepatocyte models. Whilst this approach has proved an extremely practical and accessible method of cell growth in the past, it is now regarded as highly unrealistic. Hepatocytes in 2D are forced into a flattened geometry. Crucially, cell geometry influences cell genotype and function. Hence failing to mimic the native cuboidal shape can lead to deviations in normal hepatic function and hence a loss of predictive accuracy in the model. Furthermore, 2D models severely limit cell-cell contact between adjacent hepatocytes, which in turn can reduce polarisation and the formation of important structural features such as sinusoidal and bile canaliculi domains[76]. Unsurprisingly, most 2D hepatocyte models cause a rapid deviation in cell genotype and phenotype and thus deliver a poor prediction of a drug's toxicity profile.

Recognising the limitations of 2D culture substrates there is now a strong demand for materials that can offer hepatocytes a 3D interface for growth[57]. By adding the third dimension to the growth substrate, cells can more readily approximate their native 3D geometry and tissue architecture. This in turn encourages cell-cell interactions to preserve key hepatic features such as sinusoidal and bile canaliculi domains. It is therefore hypothesised that 3D hepatocyte models will promote a more realistic hepatocyte genotype and phenotype and thus produce more accurate predictions of a drug's toxicity profile.

There are many technologies being developed for 3D cell culture. Sandwiching cells between layers of ECM proteins helps to preserve hepatocyte geometry and the formation of bile canaliculi domains. However, this approach fails to mimic extensive 3D organisation. Spheroid cultures and hydrogels promote 3D aggregates, although they pose issues with mass transfer of nutrients and batch-to-batch consistency. Electrospun scaffolds are versatile and commercially available, however they often have poor mechanical strength properties and only really encourage 'pockets' of 3D cell growth where fibres overlap. Rapid prototyping is showing great promise for obtaining reproducible and chemically inert *in vitro* scaffolds, although they are currently far too expensive for broad application such as drug discovery. Porous polymers derived from conventional techniques such as particle leaching, gas foaming or phase separation are also potential candidates for 3D scaffolds, although they carry issues with reproducibility and residual contaminants that have severely limited their commercialisation for routine 3D cell culture.

Polystyrene scaffolds derived from emulsion templating are attractive materials as substrates for 3D hepatocyte growth for several reasons. They are essentially just an alternative geometric version of the well-known Petri dish. They are highly uniform and reproducible, enabled by the strict control of processing parameters. They are highly porous, ensuring effective mass transfer of nutrients throughout the 3D cell mass. They are chemically inert, allowing them to be storable products with sufficient robustness to typical laboratory processing chemicals. They have suitable mechanical strength properties to support the weight of large cell numbers. They are also already commercially available and can be supplied in typical welled-plate formats.

However, prior to this thesis the suitability of polystyrene scaffolds for 3D hepatocyte culture had not been fully determined. Little was known about the optimum culture conditions for approximating native hepatocyte growth in these materials. Hepatocyte geometry and ultrastructure were not fully characterised. Hepatocyte function and gene expression in polystyrene scaffolds was also poorly understood. There was also the question of improving the biochemical relevance of the polystyrene surface, and if this could be modified with ligands such as galactose to further improve hepatocyte adhesion and function. This thesis therefore set out to:

- Explore hepatocyte growth in polystyrene scaffolds under different culture conditions to re-create native liver tissue architecture *in vitro*.
- Compare structure, function and gene expression of hepatocytes cultured in polystyrene scaffolds with to 2D cultures and *in vivo*. The broad aim here was to determine if

polystyrene scaffolds enable the preservation of key structure-function-genetic relationships *in vitro*.

- Surface modify polystyrene scaffolds with galactose for further enhanced biochemical relevance.

6.1.2 Summary of Thesis Conclusions

The following conclusions that can be drawn from the study:

- Emulsion templated polystyrene scaffolds can support the 3D growth of hepatocytes *in vitro* to approximate native liver tissue density and growth. Three different hepatocyte sources were used to demonstrate this; HepG2 cells, Upcyte® cells and primary rat hepatocytes. All three hepatocyte sources adhered and remained viable on the scaffolds. Scaffolds with larger voids (Alvetex®Scaffold) encouraged cell growth within the membrane whereas scaffolds with smaller voids (Alvetex®Strata) encouraged cell growth on top of the membrane. Manipulation of culture conditions was found to alter the growth characteristics of the cells on the scaffolds, with contact cultures encouraging growth profiles very similar in cell density to *in vivo*. Furthermore, conventional culture optimisations such as ECM protein coatings and media perfusions were also found to be suitable for polystyrene scaffolds to replicate native cell-ECM interactions and steady-state nutrient conditions.

- Hepatocytes cultured in polystyrene scaffolds are more physiologically relevant compared to 2D hepatocyte models. Hepatocytes in scaffolds displayed a more representative 3D morphology compared to those cultured in 2D. This was demonstrated by several techniques, including histological diameter analysis, confocal immunofluorescence, SEM and TEM. Hepatocyte ultrastructure in scaffolds was also more comparable to *in vivo*, unlike 2D culture; hepatocytes in scaffolds showed signs of microvilli, bile canaliculi and tight junction complexes that are present *in vivo* but almost absent in 2D culture. Indeed, when culturing hepatocytes on top of small-void polystyrene scaffolds, extensive bile canaliculi were observed. There were even signs of structural re-organisation towards lumen-type features comparable to the sinusoidal lumens found in native liver. Importantly, these structural differences between 3D and 2D hepatocyte cultures translated into functional and genetic differences. Hepatocytes cultured in 3D showed enhanced albumin synthesis, urea synthesis and a different response to toxicological challenge. They also showed a shift towards more representative gene expression

profiles. Indications of even more enhanced function were observed for 3D perfused systems, evident by the increased in CY3A4 activity over static 3D cultures.

- Emulsion templated polystyrene scaffolds can be made more biochemically relevant by surface modification with galactose, a ligand that can selectively bind to hepatocytes via the ASGP-R. Two new functional polystyrene-based scaffolds were developed in the galactose-attachment process; one carrying pendent ester functionality and the other acid functionality. These scaffolds had physical properties typical to that of the commercial Alvetex®Scaffold. The ester-containing scaffold was then easily modified via coupling with a galactose-amine to attach pendent galactose. This pendent galactose on the scaffold surface was found to enhance hepatocyte albumin synthesis during the crucial adhesion period.

6.2 Future work

A 3D hepatocyte model using polystyrene scaffolds is now in place that approximates native liver tissue density and architecture. Within this 3D model hepatocyte structure function and gene expression are more physiologically relevant compared to 2D. Moreover, there is also potential for these polystyrene scaffolds to be made more biochemically relevant via the attachment of galactose onto the surface.

However, significant work still remains in this area. The following points are regarded as the key next steps in the project:

- Expanding and validating drug toxicity profiles in polystyrene scaffolds. This thesis has shown that there is a different functional response to drug exposure in 3D compare to 2D. The next step is now to use primary hepatocyte cultures to expand the range of drugs to build a more comprehensive understanding of model predictive accuracy. A variety of different drugs should be explored with different metabolism profiles. Hepatocytes should then be assessed for viability, enzyme induction, metabolite formation and necrosis/apoptosis during drug exposure. Crucially, the data should be compared with known *in vivo* toxicity profiles (LD50 values) for the appropriate species to understand if 3D models are indeed more predictive.

- Microarray analysis of RNA expression in polystyrene scaffolds. This study showed that RNA expression is different in 2D and 3D. This needs to be expanded further to explore the broader genotype and then compared with *in vivo*. Microarray analysis (high-throughout genetic analysis) should be used for this and then subsequently validated using real-time quantitative PCR.

- Proteomic studies. Whilst this study indicated differences in hepatic specific protein synthesis (albumin), there is also a need to compare the wider proteome in scaffolds *versus in vivo.*

- Long-term hepatocyte culture using the perfusion model. This study introduced a media perfusion model for 3D hepatocyte culture in polystyrene scaffolds. This perfusion system now needs to be developed for optimum flow rate, cell seeding density and scaffold presentation to enable long-term hepatocyte viability (post 3 weeks). Furthermore, an extensive characterisation of hepatocyte gene expression and function needs to be

performed for perfusion cultures. Long-term perfusion cultures should then be used for prolonged drug exposure studies.

- Development of a 3D co-culture model. This study only investigated hepatocytes. However, the native liver has many other cells types that contribute to normal hepatocyte function and drug metabolism. Co-culture involving liver non-parenchymal cells and hepatocytes could therefore further enhance the physiological relevance of the model and improve predictive accuracy. One method of co-culture could be to simply mix the different cell types and allow them to grow in the scaffold. Alternatively, some cells could be seeded into the scaffold whilst other cell types could be grown as 2D monolayers below the scaffold inserts.

- Culture of hepatic progenitor cells. Freshly isolated primary human hepatocytes are limited in supply. Using hepatocyte progenitor cells as a potentially limitless supply of mature hepatocytes could therefore have huge implications for drug toxicity studies as a readily available and relevant hepatocyte source. Understanding if polystyrene scaffolds can provide the appropriate stem-cell niche to encourage hepatic progenitor cells into a differentiated hepatocyte lineage could have important implications for managing the supply of primary hepatocytes and thus reducing the need for animal sacrifice.

- Further surface modifications with galactose. This study provided proof-of-principle that emulsion templated polystyrene scaffolds could be surface functionalised with galactose for enhanced hepatocyte function during adhesion. A key next step is to increase the amount of galactose on the material by coupling the PFPA-containing scaffold with amines containing multiple galactose residues. There is also the potential to provide a spacer/linker to separate the galactose from the scaffold and so potentially render the carbohydrate more accessible to the cells. A better understanding of the impact of galactose-functionalised scaffolds on hepatocyte structure and function also needs to be determined.

- Towards an optimum 3D hepatocyte model. The impact of using galactose-functionalised scaffolds combined with media perfusion and co-culture with non-parenchymal cells should be explored. It is hypothesised that this model provides the relevant physical environment (scaffold), surface chemistry (galactose), mass transfer (perfusion) and

cellular interaction (co-culture) for more appropriately mimicking the native liver scenario.

- Comparing polystyrene scaffold cultures with other 3D models. Throughout this thesis several other 3D substrates have been discussed for 3D hepatocyte growth, including hydrogels, electrospun scaffolds, rapid prototyping scaffolds and sandwich cultures. Consistent with results from this thesis, many of these other 3D technologies have demonstrated improvements in cell geometry, genotype and phenotype compared to conventional 2D cultures. However, a direct comparison between these different 3D technologies is yet to be made. Performing this comparison will give researchers an informed choice on the suitability of each technology for their specific experimental needs.

Chapter 7: References

(1) Underhill, G. H.; Khetani, S. R.; Chen, A. A.; Bhatia, S. N., Tissue engineering of the liver. In *The Liver*, John Wiley & Sons, Ltd: 2009; 933-953.
(2) Molina, D. K.; Dimaio, V. J. M., Normal organ weights in men: Part II-The brain, lungs, liver, spleen, and kidneys. *American Journal Of Forensic Medicine And Pathology* **2012,** 33, 368-372.
(3) Bioulac-Sage, P.; Le Bail, B.; Balabaud, C., Liver and biliary tract histology. In *Textbook Of Hepatology*, Blackwell Publishing Ltd: 2008; 9-19.
(4) Ross, M. H.; Pawlina, W., *Histology: A Text And Atlas*. Fifth Ed.; Lippincott Williams And Wilkins: 2006.
(5) Braiterman, L. T.; Hubbard, A. L., Hepatocyte surface polarity: Its dynamic maintenance and establishment. In *The Liver*, John Wiley & Sons, Ltd: 2009; 73-105.
(6) Alrefai, W. A.; Gill, R. K., Bile acid transporters: Structure, function, regulation and pathophysiological implications. *Pharmaceutical Research* **2007,** 24, 1803-1823.
(7) Klaassen, C. D.; Watkins, J. B., Mechanisms of bile formation, hepatic-uptake, and biliary-excretion. *Pharmacol. Rev.* **1984,** 36, 1-67.
(8) Fladmark, K. E.; Gjertsen, B. T.; Molven, A.; Mellgren, G.; Vintermyr, O. K.; Doskeland, S. O., Gap junctions and growth control in liver regeneration and in isolated rat hepatocytes. *Hepatology* **1997,** 25, 847-855.
(9) Leibold, E.; Schwarz, L. R., Intercellular communication in primary cultures of putative preneoplastic and normal hepatocytes. *Carcinogenesis* **1993,** 14, 2127-2129.
(10) Hamilton, G. A.; Jolley, S. L.; Gilbert, D.; Coon, D. J.; Barros, S.; Lecluyse, E. L., Regulation of cell morphology and cytochrome P450 expression in human hepatocytes by extracellular matrix and cell-cell interactions. *Cell Tissue Res.* **2001,** 306, 85-99.
(11) Khan, Z.; Crawford, J. M.; Stolz, D. B., Ultrastructure of the hepatocyte. In *Textbook Of Hepatology*, Blackwell Publishing Ltd: 2008; 20-28.
(12) Martinezhernandez, A.; Amenta, P. S., The hepatic extracellular-matrix .1. Components and distribution in normal liver. *Virchows Arch. A-Pathol. Anat. Histopathol.* **1993,** 423, 1-11.
(13) Bissell, D. M.; Caron, J. M.; Babiss, L. E.; Friedman, J. M., Transcriptional Regulation of the albumin gene in cultured rat hepatocytes - Role of basement-membrane matrix. *Molecular Biology & Medicine* **1990,** 7, 187-197.
(14) Bucher, N. L. R.; Robinson, G. S.; Farmer, S. R., Effects of extracellular-matrix on hepatocyte growth and gene-expression - Implications for hepatic regeneration and the repair of liver-injury. *Seminars In Liver Disease* **1990,** 10, 11-19.
(15) Martinez-Hernandez, A.; Amenta, P., The extracellular matrix in hepatic regeneration. *The FASEB Journal* **1995,** 9, 1401-1410.
(16) Nagaki, M.; Shidoji, Y.; Yamada, Y.; Sugiyama, A.; Tanaka, M.; Akaike, T.; Ohnishi, H.; Moriwaki, H.; Muto, Y., Regulation of hepatic genes and liver transcription factors in rat hepatocytes by extracellular-matrix. *Biochemical And Biophysical Research Communications* **1995,** 210, 38-43.
(17) Rana, B.; Mischoulon, D.; Xie, Y. H.; Bucher, N. L. R.; Farmer, S. R., Cell-extracellular matrix interactions can regulate the switch between growth and differentiation in rat hepatocytes - Reciprocal expression of C/EBP-Alpha and immediate-early growth-response transcription factors. *Molecular And Cellular Biology* **1994,** 14, 5858-5869.
(18) Wells, R. G., The role of matrix stiffness in regulating cell behavior. *Hepatology* **2008,** 47, 1394-1400.

(19) Schuppan, D.; Ruehl, M.; Somasundaram, R.; Hahn, E. G., Matrix as a modulator of hepatic fibrogenesis. *Seminars In Liver Disease* **2001,** 21, 351-372.
(20) Wells, R. G., Cellular sources of extracellular matrix in hepatic fibrosis. *Clinics In Liver Disease* **2008,** 12, 759-768.
(21) Braet, F.; Wisse, E., Structural and functional aspects of liver sinusoidal endothelial cell fenestrae: A review. *Comp Hepatol* **2002,** 1, 1-17.
(22) Xie, G.; Wang, L.; Wang, X.; Wang, L.; Deleve, L. D., Isolation of periportal, midlobular, and centrilobular rat liver sinusoidal endothelial cells enables study of zonated drug toxicity. *American Journal Of Physiology-Gastrointestinal And Liver Physiology* **2010,** 299, 1204-1210.
(23) Friedman, S. L., Hepatic stellate cells: Protean, multifunctional, and enigmatic cells of the liver. *Physiological Reviews* **2008,** 88, 125-172.
(24) Kordes, C.; Sawitza, I.; Haeussinger, D., Hepatic and pancreatic stellate cells in focus. *Biological Chemistry* **2009,** 390, 1003-1012.
(25) Atzori, L.; Poli, G.; Perra, A., Hepatic stellate cell: A star cell in the liver. *International Journal Of Biochemistry & Cell Biology* **2009,** 41, 1639-1642.
(26) Jaeschke, H., Kupffer cells. In *Textbook Of Hepatology*, Blackwell Publishing Ltd: 2008; 36-42.
(27) Hoebe, K. H. N.; Witkamp, R. F.; Fink-Gremmels, J.; Van Miert, A.; Monshouwer, M., Direct cell-to-cell contact between kupffer cells and hepatocytes augments endotoxin-induced hepatic injury. *American Journal Of Physiology-Gastrointestinal And Liver Physiology* **2001,** 280, 720-728.
(28) Jungermann, K.; Kietzmann, T., Zonation of parenchymal and nonparenchymal metabolism in liver. *Annual Review Of Nutrition* **1996,** 16, 179-203.
(29) Kietzmann, T.; Jungermann, K., Modulation by oxygen of zonal gene expression in liver studied in primary rat hepatocyte cultures. *Cell Biol. Toxicol.* **1997,** 13, 243-255.
(30) Gaudio, E.; Carpino, G.; Cardinale, V.; Franchitto, A.; Onori, P.; Alvaro, D., New insights into liver stem cells. *Digestive And Liver Disease* **2009,** 41, 455-462.
(31) Turner, R.; Lozoya, O.; Wang, Y.; Cardinale, V.; Gaudio, E.; Alpini, G.; Mendel, G.; Wauthier, E.; Barbier, C.; Alvaro, D.; Reid, L. M., Human hepatic stem cell and maturational liver lineage biology. *Hepatology* **2011,** 53, 1035-1045.
(32) Godoy, P.; Hewitt, N. J.; Albrecht, U.; Andersen, M. E.; Ansari, N.; Bhattacharya, S.; Bode, J. G.; Bolleyn, J.; Borner, C.; Bottger, J.; Braeuning, A.; Budinsky, R. A.; Burkhardt, B.; Cameron, N. R.; Camussi, G.; Cho, C. S.; Choi, Y. J.; Rowlands, J. C.; Dahmen, U.; Damm, G.; Dirsch, O.; Donato, M. T.; Dong, J.; Dooley, S.; Drasdo, D.; Eakins, R.; Ferreira, K. S.; Fonsato, V.; Fraczek, J.; Gebhardt, R.; Gibson, A.; Glanemann, M.; Goldring, C. E. P.; Gomez-Lechon, M. J.; Groothuis, G. M. M.; Gustavsson, L.; Guyot, C.; Hallifax, D.; Hammad, S.; Hayward, A.; Haussinger, D.; Hellerbrand, C.; Hewitt, P.; Hoehme, S.; Holzhutter, H. G.; Houston, J. B.; Hrach, J.; Ito, K.; Jaeschke, H.; Keitel, V.; Kelm, J. M.; Park, B. K.; Kordes, C.; Kullak-Ublick, G. A.; Lecluyse, E. L.; Lu, P.; Luebke-Wheeler, J.; Lutz, A.; Maltman, D. J.; Matz-Soja, M.; Mcmullen, P.; Merfort, I.; Messner, S.; Meyer, C.; Mwinyi, J.; Naisbitt, D. J.; Nussler, A. K.; Olinga, P.; Pampaloni, F.; Pi, J. B.; Pluta, L.; Przyborski, S. A.; Ramachandran, A.; Rogiers, V.; Rowe, C.; Schelcher, C.; Schmich, K.; Schwarz, M.; Singh, B.; Stelzer, E. H. K.; Stieger, B.; Stober, R.; Sugiyama, Y.; Tetta, C.; Thasler, W. E.; Vanhaecke, T.; Vinken, M.; Weiss, T. S.; Widera, A.; Woods, C. G.; Xu, J. J.; Yarborough, K. M.; Hengstler, J. G., Recent advances in 2D and 3D in vitro systems using primary hepatocytes, alternative hepatocyte sources and non-parenchymal liver cells and their use in investigating mechanisms of hepatotoxicity, cell signaling and ADME. *Arch. Toxicol.* **2013,** 87, 1315-1530.

(33) Hewitt, N. J.; Lechon, M. J. G.; Houston, J. B.; Hallifax, D.; Brown, H. S.; Maurel, P.; Kenna, J. G.; Gustavsson, L.; Lohmann, C.; Skonberg, C.; Guillouzo, A.; Tuschl, G.; Li, A. P.; Lecluyse, E.; Groothuis, G. M. M.; Hengstler, J. G., Primary hepatocytes: Current understanding of the regulation of metabolic enzymes and transporter proteins, and pharmaceutical practice for the use of hepatocytes in metabolism, enzyme induction, transporter, clearance, and hepatotoxicity studies. *Drug Metab. Rev.* **2007,** 39, 159-234.

(34) Chandra, P.; Brouwer, K., The complexities of hepatic drug transport: Current knowledge and emerging concepts. *Pharmaceutical Research* **2004,** 21, 719-735.

(35) Kalliokoski, A.; Niemi, M., Impact of OATP transporters on pharmacokinetics. *British Journal Of Pharmacology* **2009,** 158, 693-705.

(36) Burckhardt, G.; Burckhardt, B. C., In Vitro and in vivo evidence of the importance of organic anion transporters (OATs) in drug therapy. In *Drug Transporters*, Fromm, M. F.; Kim, R. B., Eds. 2011; Vol. 201, 29-104.

(37) Nies, A. T.; Koepsell, H.; Damme, K.; Schwab, M., Organic cation transporters (OCTs, MATEs), In vitro and in vivo evidence for the importance in drug therapy. In *Drug Transporters*, Fromm, M. F.; Kim, R. B., Eds. 2011; Vol. 201, 105-167.

(38) Schinkel, A. H.; Jonker, J. W., Mammalian drug efflux transporters of the ATP binding cassette (ABC) family: An overview. *Advanced Drug Delivery Reviews* **2003,** 55, 3-29.

(39) Polgar, O.; Robey, R. W.; Bares, S. E., ABCG2: Structure, function and role in drug response. *Expert Opinion On Drug Metabolism & Toxicology* **2008,** 4, 1-15.

(40) Zelcer, N.; Van De Wetering, K.; Hillebrand, M.; Sarton, E.; Kuil, A.; Wielinga, P. R.; Tephly, T.; Dahan, A.; Beijnen, J. H.; Borst, P., Mice lacking multidrug resistance protein 3 show altered morphine pharmacokinetics and morphine-6-glucuronide antinociception. *Proceedings Of The National Academy Of Sciences Of The United States Of America* **2005,** 102, 7274-7279.

(41) Keppler, D., Multidrug resistance proteins (MRPs, ABCCs): Importance for pathophysiology and drug therapy. In *Drug Transporters*, Fromm, M. F.; Kim, R. B., Eds. 2011; Vol. 201, 299-323.

(42) Borst, P.; Evers, R.; Kool, M.; Wijnholds, J., A family of drug transporters: The multidrug resistance-associated proteins. *Journal Of The National Cancer Institute* **2000,** 92, 1295-1302.

(43) Derelanko, M. J., Hollinger, M.A., Metabolism and toxicokinetics of xenobiotic*s In: Handbook Of Toxicology*. 1st Ed.; CRC Press, New York: 1995.

(44) Wrighton, S. A.; Stevens, J. C., The human hepatic cytochromes-P450 involved in drug-metabolism. *Critical Reviews In Toxicology* **1992,** 22, 1-21.

(45) Guengerich, F. P., Common and uncommon cytochrome P450 reactions related to metabolism and chemical toxicity. *Chemical Research In Toxicology* **2001,** 14, 611-650.

(46) Cashman, J. R., Role of flavin-containing monooxgenase in drug development. *Expert Opinion On Drug Metabolism & Toxicology* **2008,** 4, 1507-1521.

(47) Tephly, T. R.; Burchell, B., UDP-Glucuronosyltransferases: A family of detoxifying enzymes. *Trends In Pharmacological Sciences* **1990,** 11, 276-279.

(48) Bissell, M. J.; Barcellos-Hoff, M. H., The influence of extracellular matrix on gene expression: Is structure the message? *Journal Of Cell Science. Supplement* **1987,** 8, 327-343.

(49) Bissell, M. J.; Hall, H. G.; Parry, G., How does the extracellular-matrix direct gene-expression. *J. Theor. Biol.* **1982,** 99, 31-68.

(50) Mcbeath, R.; Pirone, D. M.; Nelson, C. M.; Bhadriraju, K.; Chen, C. S., Cell shape, cytoskeletal tension, and RhoA regulate stem cell lineage commitment. *Developmental Cell* **2004,** 6, 483-495.

(51) Chen, C. S.; Mrksich, M.; Huang, S.; Whitesides, G. M.; Ingber, D. E., Micropatterned surfaces for control of cell shape, position, and function. *Biotechnology Progress* **1998,** 14, 356-363.
(52) Zegers, M. M. P.; O'brien, L. E.; Yu, W.; Datta, A.; Mostov, K. E., Epithelial polarity and tubulogenesis in vitro. *Trends Cell Biol.* **2003,** 13, 169-176.
(53) Bissell, M. J.; Rizki, A.; Mian, I. S., Tissue architecture: The ultimate regulator of breast epithelial function. *Curr. Opin. Cell Biol.* **2003,** 15, 753-762.
(54) Yamada, K. M.; Cukierman, E., Modeling tissue morphogenesis and cancer in 3D. *Cell* **2007,** 130, 601-610.
(55) Baker, B. M.; Chen, C. S., Deconstructing the third dimension - How 3D culture microenvironments alter cellular cues. *J. Cell Sci.* **2012,** 125, 3015-3024.
(56) Smalley, K. S. M.; Lioni, M.; Herlyn, M., Life isn't flat: Taking cancer biology to the next dimension. *In Vitro Cellular & Developmental Biology-Animal* **2006,** 42, 242-247.
(57) Maltman, D. J.; Przyborski, S. A., Developments in three-dimensional cell culture technology aimed at improving the accuracy of in vitro analyses. *Biochemical Society Transactions* **2010,** 38, 1072-1075.
(58) Pampaloni, F.; Reynaud, E. G.; Stelzer, E. H. K., The third dimension bridges the gap between cell culture and live tissue. *Nat. Rev. Mol. Cell Biol.* **2007,** 8, 839-845.
(59) Abbott, A., Cell culture: Biology's new dimension. *Nature* **2003,** 424, 870-872.
(60) Griffith, L. G.; Swartz, M. A., Capturing complex 3D tissue physiology in vitro. *Nat. Rev. Mol. Cell Biol.* **2006,** 7, 211-224.
(61) Weaver, V. M.; Petersen, O. W.; Wang, F.; Larabell, C. A.; Briand, P.; Damsky, C.; Bissell, M. J., Reversion of the malignant phenotype of human breast cells in three-dimensional culture and in vivo by integrin blocking antibodies. *Journal Of Cell Biology* **1997,** 137, 231-245.
(62) Roskelley, C. D.; Desprez, P. Y.; Bissell, M. J., Extracellular matrix-dependent tissue-specific gene-expression in mammary epithelial-cells requires both physical and biochemical signal-transduction. *Proceedings Of The National Academy Of Sciences Of The United States Of America* **1994,** 91, 12378-12382.
(63) Levenberg, S.; Huang, N. F.; Lavik, E.; Rogers, A. B.; Itskovitz-Eldor, J.; Langer, R., Differentiation of human embryonic stem cells on three-dimensional polymer scaffolds. *Proceedings Of The National Academy Of Sciences Of The United States Of America* **2003,** 100, 12741-12746.
(64) Cao, Y.; Croll, T. I.; Lees, J. G.; Tuch, B. E.; Cooper-White, J. J., Scaffolds, stem cells, and tissue engineering: A potent combination! *Australian Journal Of Chemistry* **2005,** 58, 691-703.
(65) Kimlin, L. C.; Casagrande, G.; Virador, V. M., In Vitro Three-Dimensional (3D) models in cancer research: An update. *Molecular Carcinogenesis* **2013,** 52, 167-182.
(66) Lutolf, M. P.; Hubbell, J. A., Synthetic biomaterials as instructive extracellular microenvironments for morphogenesis in tissue engineering. *Nature Biotechnology* **2005,** 23, 47-55.
(67) Pashuck, E. T.; Stevens, M. M., Designing regenerative biomaterial therapies for the clinic. *Science Translational Medicine* **2012,** 4, 160sr164.
(68) Lysaght, M. J.; Hazlehurst, A. L., Tissue engineering: The end of the beginning. *Tissue Eng.* **2004,** 10, 309-320.
(69) Gómez-Lechón, M. J.; Jover, R.; Donato, T.; Ponsoda, X.; Rodriguez, C.; Stenzel, K. G.; Klocke, R.; Paul, D.; Guillén, I.; Bort, R.; Castell, J. V., Long-term expression of differentiated functions in hepatocytes cultured in three-dimensional collagen matrix. *Journal Of Cellular Physiology* **1998,** 177, 553-562.

(70) Hallen, S.; Clapham, J. C., Cell based in vitro and ex vivo models in metabolic disease drug discovery: Nice to have or critical path? *Expert Opinion On Drug Discovery* **2009,** 4, 417-428.
(71) Caldwell, G. W.; Ritchie, D. M.; Masucci, J. A.; Hageman, W.; Yan, Z., The new pre-preclinical paradigm: Compound optimization in early and late phase drug discovery. *Current Topics In Medicinal Chemistry* **2001,** 1, 353-366.
(72) Kola, I.; Landis, J., Can the pharmaceutical industry reduce attrition rates? *Nature Reviews Drug Discovery* **2004,** 3, 711-715.
(73) Bhadriraju, K.; Chen, C. S., Engineering cellular microenvironments to improve cell-based drug testing. *Drug Discovery Today* **2002,** 7, 612-620.
(74) Kunz-Schughart, L. A.; Freyer, J. P.; Hofstaedter, F.; Ebner, R., The use of 3-D cultures for high-throughput screening: The multicellular spheroid model. *Journal Of Biomolecular Screening* **2004,** 9, 273-285.
(75) Pampaloni, F.; Stelzer, E. H. K.; Masotti, A., Three-dimensional tissue models for drug discovery and toxicology. *Recent Patents On Biotechnology* **2009,** 3, 103-117.
(76) Dunn, J. C. Y.; Tompkins, R. G.; Yarmush, M. L., Long-term in vitro function of adult hepatocytes in a collagen sandwich configuration. *Biotechnology Progress* **1991,** 7, 237-245.
(77) Dunn, J. C. Y.; Yarmush, M. L.; Koebe, H. G.; Tompkins, R. G., Hepatocyte function and extracellular-matrix geometry - Long-term culture in a sandwich configuration. *FASEB Journal* **1989,** 3, 174-177.
(78) Dunn, J.; Yarmush, M.; Koebe, H.; Tompkins, R., Hepatocyte function and extracellular matrix geometry: Long-term culture in a sandwich configuration. *The FASEB Journal* **1989,** 3, 174-177.
(79) Kern, A.; Bader, A.; Pichlmayr, R.; Sewing, K. F., Drug metabolism in hepatocyte sandwich cultures of rats and humans. *Biochemical Pharmacology* **1997,** 54, 761-772.
(80) Lecluyse, E. L.; Audus, K. L.; Hochman, J. H., Formation of extensive canalicular networks by rat hepatocytes cultured in collagen-sandwich configuration. *American Journal Of Physiology - Cell Physiology* **1994,** 266, 1764-1774.
(81) Swift, B.; Pfeifer, N. D.; Brouwer, K. L. R., Sandwich-cultured hepatocytes: An in vitro model to evaluate hepatobiliary transporter-based drug interactions and hepatotoxicity. *Drug Metab. Rev.* **2010,** 42, 446-471.
(82) Landry, J.; Bernier, D.; Ouellet, C.; Goyette, R.; Marceau, N., Spheroidal aggregate culture of rat-liver cells - Histotypic reorganization, biomatrix deposition, and maintenance of functional activities. *Journal Of Cell Biology* **1985,** 101, 914-923.
(83) Li, A. P.; Colburn, S. M.; Beck, D. J., A simplified method for the culturing of primary adult-rat and human hepatocytes as multicellular spheroids. *In Vitro Cellular & Developmental Biology-Animal* **1992,** 28a, 673-677.
(84) Takabatake, H.; Koide, N.; Tsuji, T., Encapsulated multicellular spheroids of rat hepatocytes produce albumin and urea in a spouted bed circulating culture system. *Artificial Organs* **1991,** 15, 474-480.
(85) Yuasa, C.; Tomita, Y.; Shono, M.; Ishimura, K.; Ichihara, A., Importance of cell-aggregation for expression of liver functions and regeneration demonstrated with primary cultured-hepatocytes. *Journal Of Cellular Physiology* **1993,** 156, 522-530.
(86) Sakai, Y.; Yamagami, S.; Nakazawa, K., Comparative analysis of gene expression in rat liver tissue and monolayer- and spheroid-cultured hepatocytes. *Cells Tissues Organs* **2010,** 191, 281-288.

(87) Tostoes, R. M.; Leite, S. B.; Serra, M.; Jensen, J.; Bjorquist, P.; Carrondo, M. J. T.; Brito, C.; Alves, P. M., Human liver cell spheroids in extended perfusion bioreactor culture for repeated-dose drug testing. *Hepatology* **2012,** 55, 1227-1236.

(88) Tong, J. Z.; Delagausie, P.; Furlan, V.; Cresteil, T.; Bernard, O.; Alvarez, F., Long-term culture of adult-rat hepatocyte spheroids. *Exp. Cell Res.* **1992,** 200, 326-332.

(89) Flouriot, G.; Vaillant, C.; Salbert, G.; Pelissero, C.; Guiraud, J. M.; Valotaire, Y., Monolayer And Aggregate Cultures Of Rainbow-Trout Hepatocytes - Long-term and stable liver-specific expression in aggregates. *J. Cell Sci.* **1993,** 105, 407-416.

(90) Drury, J. L.; Mooney, D. J., Hydrogels for tissue engineering: scaffold design variables and applications. *Biomaterials* **2003,** 24, 4337-4351.

(91) Lee, K. Y.; Mooney, D. J., Hydrogels for tissue engineering. *Chemical Reviews* **2001,** 101, 1869-1879.

(92) Wang, F.; Weaver, V. M.; Petersen, O. W.; Larabell, C. A.; Dedhar, S.; Briand, P.; Lupu, R.; Bissell, M. J., reciprocal interactions between beta 1-integrin and epidermal growth factor receptor in three-dimensional basement membrane breast cultures: A different perspective in epithelial biology. *Proceedings Of The National Academy Of Sciences Of The United States Of America* **1998,** 95, 14821-14826.

(93) Kleinman, H. K.; Mcgarvey, M. L.; Hassell, J. R.; Star, V. L.; Cannon, F. B.; Laurie, G. W.; Martin, G. R., Basement membrane complexes with biological activity. *Biochemistry* **1986,** 25, 312-318.

(94) Kleinman, H. K.; Mcgarvey, M. L.; Liotta, L. A.; Robey, P. G.; Tryggvason, K.; Martin, G. R., Isolation and characterization of type-IV procollagen, laminin, and heparan-sulfate proteoglycan from the EHS sarcoma. *Biochemistry* **1982,** 21, 6188-6193.

(95) Kleinman, H. K.; Martin, G. R., Matrigel: Basement membrane matrix with biological activity. *Seminars In Cancer Biology* **2005,** 15, 378-386.

(96) Moghe, P. V.; Coger, R. N.; Toner, M.; Yarmush, M. L., Cell-cell interactions are essential for maintenance of hepatocyte function in collagen gel but not on Matrigel. *Biotechnology And Bioengineering* **1997,** 56, 706-711.

(97) Molina-Jimenez, F.; Benedicto, I.; Viet Loan Dao, T.; Gondar, V.; Lavillette, D.; Marin, J. J.; Briz, O.; Moreno-Otero, R.; Aldabe, R.; Baumert, T. F.; Cosset, F.-L.; Lopez-Cabrera, M.; Majano, P. L., Matrigel-embedded 3D culture of Huh-7 cells as a hepatocyte-like polarized system to study hepatitis C virus cycle. *Virology* **2012,** 425, 31-39.

(98) Prestwich, G. D.; Liu, Y.; Yu, B.; Shu, X. Z.; Scott, A., 3-D culture in synthetic extracellular matrices: New tissue models for drug toxicology and cancer drug discovery. *Advances In Enzyme Regulation* **2007,** 47, 196-207.

(99) Semino, C. E.; Merok, J. R.; Crane, G. G.; Panagiotakos, G.; Zhang, S., Functional differentiation of hepatocyte-like spheroid structures from putative liver progenitor cells in three-dimensional peptide scaffolds. *Differentiation* **2003,** 71, 262-270.

(100) Paszek, M. J.; Zahir, N.; Johnson, K. R.; Lakins, J. N.; Rozenberg, G. I.; Gefen, A.; Reinhart-King, C. A.; Margulies, S. S.; Dembo, M.; Boettiger, D.; Hammer, D. A.; Weaver, V. M., Tensional homeostasis and the malignant phenotype. *Cancer Cell* **2005,** 8, 241-254.

(101) Lutolf, M. P.; Lauer-Fields, J. L.; Schmoekel, H. G.; Metters, A. T.; Weber, F. E.; Fields, G. B.; Hubbell, J. A., Synthetic matrix metalloproteinase-sensitive hydrogels for the conduction of tissue regeneration: Engineering cell-invasion characteristics. *Proceedings Of The National Academy Of Sciences Of The United States Of America* **2003,** 100, 5413-5418.

(102) Sill, T. J.; Von Recum, H. A., Electro spinning: Applications in drug delivery and tissue engineering. *Biomaterials* **2008,** 29, 1989-2006.

(103) Sun, T.; Norton, D.; Mckean, R. J.; Haycock, J. W.; Ryan, A. J.; Macneil, S., Development of a 3D cell culture system for investigating cell interactions with electrospun fibers. *Biotechnology And Bioengineering* **2007,** 97, 1318-1328.

(104) Sun, T.; Jackson, S.; Haycock, J. W.; Macneil, S., Culture of skin cells in 3D rather than 2D improves their ability to survive exposure to cytotoxic agents. *Journal Of Biotechnology* **2006,** 122, 372-381.

(105) Chua, K. N.; Lim, W. S.; Zhang, P. C.; Lu, H. F.; Wen, J.; Ramakrishna, S.; Leong, K. W.; Mao, H. Q., Stable immobilization of rat hepatocyte spheroids on galactosylated nanofiber scaffold. *Biomaterials* **2005,** 26, 2537-2547.

(106) Feng, Z. Q.; Chu, X. H.; Huang, N. P.; Wang, T.; Wang, Y. C.; Shi, X. L.; Ding, Y. T.; Gu, Z. Z., The effect of nanofibrous galactosylated chitosan scaffolds on the formation of rat primary hepatocyte aggregates and the maintenance of liver function. *Biomaterials* **2009,** 30, 2753-2763.

(107) Ghaedi, M.; Soleimani, M.; Shabani, I.; Duan, Y. Y.; Lotfi, A. S., Hepatic differentiation from human mesenchymal stem cells on a novel nanofiber scaffold. *Cell. Mol. Biol. Lett.* **2012,** 17, 89-106.

(108) Yang, F.; Murugan, R.; Wang, S.; Ramakrishna, S., Electrospinning of nano/micro scale poly(L-lactic acid) aligned fibers and their potential in neural tissue engineering. *Biomaterials* **2005,** 26, 2603-2610.

(109) Yeong, W. Y.; Chua, C. K.; Leong, K. F.; Chandrasekaran, M., Rapid prototyping in tissue engineering: challenges and potential. *Trends In Biotechnology* **2004,** 22, 643-652.

(110) Seitz, H.; Rieder, W.; Irsen, S.; Leukers, B.; Tille, C., Three-dimensional printing of porous ceramic scaffolds for bone tissue engineering. *Journal Of Biomedical Materials Research Part B-Applied Biomaterials* **2005,** 74b, 782-788.

(111) Lin, C. Y.; Kikuchi, N.; Hollister, S. J., A novel method for biomaterial scaffold internal architecture design to match bone elastic properties with desired porosity. *J. Biomech.* **2004,** 37, 623-636.

(112) Mikos, A. G.; Temenoff, J. S., Formation of highly porous biodegradable scaffolds for tissue engineering. *Ejb Electronic Journal Of Biotechnology* **2000,** 3, 1-12.

(113) Freed, L. E.; Marquis, J. C.; Nohria, A.; Emmanual, J.; Mikos, A. G.; Langer, R., Neocartilage formation invitro and invivo using cells cultured on synthetic biodegradable polymers. *Journal Of Biomedical Materials Research* **1993,** 27, 11-23.

(114) Mikos, A. G.; Bao, Y.; Cima, L. G.; Ingber, D. E.; Vacanti, J. P.; Langer, R., Preparation of poly(glycolic acid) bonded fiber structures for cell attachment and transplantation. *Journal Of Biomedical Materials Research* **1993,** 27, 183-189.

(115) Mikos, A. G.; Thorsen, A. J.; Czerwonka, L. A.; Bao, Y.; Langer, R.; Winslow, D. N.; Vacanti, J. P., Preparation and characterization of poly(L-lactic acid) foams. *Polymer* **1994,** 35, 1068-1077.

(116) Mikos, A. G.; Sarakinos, G.; Leite, S. M.; Vacanti, J. P.; Langer, R., Laminated 3-Dimensional biodegradable foams for use in tissue engineering. *Biomaterials* **1993,** 14, 323-330.

(117) Mooney, D. J.; Park, S.; Kaufmann, P. M.; Sano, K.; Mcnamara, K.; Vacanti, J. P.; Langer, R., Biodegradable sponges for hepatocyte transplantation. *Journal Of Biomedical Materials Research* **1995,** 29, 959-965.

(118) Kaufmann, P. M.; Heimrath, S.; Kim, B. S.; Mooney, D. J., Highly porous polymer matrices as a three-dimensional culture system for hepatocytes. *Cell Transplant.* **1997,** 6, 463-468.

(119) Mooney, D. J.; Baldwin, D. F.; Suh, N. P.; Vacanti, L. P.; Langer, R., Novel approach to fabricate porous sponges of poly(D,L-lactic-co-glycolic acid) without the use of organic solvents. *Biomaterials* **1996,** 17, 1417-1422.

(120) Salerno, A.; Oliviero, M.; Di Maio, E.; Iannace, S.; Netti, P. A., Design of porous polymeric scaffolds by gas foaming of heterogeneous blends. *Journal Of Materials Science-Materials In Medicine* **2009,** 20, 2043-2051.

(121) Nam, Y. S.; Yoon, J. J.; Park, T. G., A Novel Fabrication method of macroporous biodegradable polymer scaffolds using gas foaming salt as a porogen additive. *Journal Of Biomedical Materials Research* **2000,** 53, 1-7.

(122) Lo, H.; Kadiyala, S.; Guggino, S. E.; Leong, K. W., Poly(L-lactic acid) foams with cell seeding and controlled-release capacity. *Journal Of Biomedical Materials Research* **1996,** 30, 475-484.

(123) Lo, H.; Ponticiello, M. S.; Leong, K. W., Fabrication of controlled release biodegradable foams by phase separation. *Tissue Eng.* **1995,** 1, 15-28.

(124) Nam, Y. S.; Park, T. G., Porous biodegradable polymeric scaffolds prepared by thermally induced phase separation. *Journal Of Biomedical Materials Research* **1999,** 47, 8-17.

(125) Nam, Y. S.; Park, T. G., Biodegradable polymeric microcellular foams by modified thermally induced phase separation method. *Biomaterials* **1999,** 20, 1783-1790.

(126) Whang, K.; Thomas, C. H.; Healy, K. E.; Nuber, G., A novel method to fabricate bioabsorbable scaffolds. *Polymer* **1995,** 36, 837-842.

(127) Hasirci, V.; Berthiaume, F.; Bondre, S. P.; Gresser, J. D.; Trantolo, D. J.; Toner, M.; Wise, D. L., Expression of liver-specific functions by rat hepatocytes seeded in treated poly(lactic-co-glycolic) acid biodegradable foams. *Tissue Eng.* **2001,** 7, 385-394.

(128) Shapiro, L.; Cohen, S., Novel alginate sponges for cell culture and transplantation. *Biomaterials* **1997,** 18, 583-590.

(129) Glicklis, R.; Shapiro, L.; Agbaria, R.; Merchuk, J. C.; Cohen, S., hepatocyte behavior within three-dimensional porous alginate scaffolds. *Biotechnology And Bioengineering* **2000,** 67, 344-353.

(130) Dvir-Ginzberg, M.; Elkayam, T.; Cohen, S., Induced differentiation and maturation of newborn liver cells into functional hepatic tissue in macroporous alginate scaffolds. *FASEB Journal* **2008,** 22, 1440-1449.

(131) Godugu, C.; Patel, A. R.; Desai, U.; Andey, T.; Sams, A.; Singh, M., Algimatrix™ based 3D cell culture system as an in-vitro tumor model for anticancer studies. *PLoS One* **2013,** 8.

(132) Bartl, H.; Vonbonin, W., Uber die polymerisation in umgekehrter emulsion. *Makromolekulare Chemie* **1962,** 57, 74-95.

(133) Barby, D.; Haq, Z. Low density porous cross-linked polymeric materials and their preparation. EP060138, 1982.

(134) Cameron, N. R.; Sherrington, D. C., High internal phase emulsions (HIPEs) - Structure, properties and use in polymer preparation. *Biopolymers Liquid Crystalline Polymers Phase Emulsion* **1996,** 126, 163-214.

(135) Cameron, N. R.; Sherrington, D. C.; Albiston, L.; Gregory, D. P., Study of the formation of the open cellular morphology of poly(styrene/divinylbenzene) polyHIPE materials by cryo-SEM. *Colloid And Polymer Science* **1996,** 274, 592-595.

(136) Stefanec, D.; Krajnc, P., 4-Vinylbenzyl chloride based porous spherical polymer supports derived from water-in-oil-in-water emulsions. *React. Funct. Polym.* **2005,** 65, 37-45.

(137) Johnson, D. W.; Sherborne, C.; Didsbury, M. P.; Pateman, C.; Cameron, N. R.; Claeyssens, F., Micro-stereolithography: Macrostructuring Of emulsion-templated porous polymers by 3D laser patterning. *Advanced Materials* **2013,** 25, 3177-3177.

(138) Pulko, I.; Krajnc, P., High internal phase emulsion templating - A path to hierarchically porous functional polymers. *Macromolecular Rapid Communications* **2012,** 33, 1731-1746.

(139) Rajagopalan, V.; Solans, C.; Kunieda, H., ESR study on the stability of w/o gel-emulsions. *Colloid And Polymer Science* **1994,** 272, 1166-1173.

(140) Kimmins, S. D.; Cameron, N. R., Functional porous polymers by emulsion templating: Recent advances. *Advanced Functional Materials* **2011,** 21, 211-225.

(141) Zhang, H.; Cooper, A. I., Synthesis and applications of emulsion-templated porous materials. *Soft Matter* **2005,** 1, 107-113.

(142) Carnachan, R. J.; Bokhari, M.; Przyborski, S. A.; Cameron, N. R., Tailoring the morphology of emulsion-templated porous polymers. *Soft Matter* **2006,** 2, 608-616.

(143) Akay, G.; Birch, M. A.; Bokhari, M. A., Microcellular PolyHIPE polymer supports osteoblast growth and bone formation in vitro. *Biomaterials* **2004,** 25, 3991-4000.

(144) Bokhari, M. A.; Akay, G.; Zhang, S. G.; Birch, M. A., Enhancement Of osteoblast growth and differentiation in vitro on a peptide hydrogel - polyHIPE polymer hybrid material. *Biomaterials* **2005,** 26, 5198-5208.

(145) Moglia, R. S.; Holm, J. L.; Sears, N. A.; Wilson, C. J.; Harrison, D. M.; Cosgriff-Hernandez, E., Injectable polyHIPEs as high-porosity bone grafts. *Biomacromolecules* **2011,** 12, 3621-3628.

(146) Barbetta, A.; Dentini, M.; De Vecchis, M. S.; Filippini, P.; Formisano, G.; Caiazza, S., Scaffolds based on biopolymeric foams. *Advanced Functional Materials* **2005,** 15, 118-124.

(147) Barbetta, A.; Massimi, M.; Devirgiliis, L. C.; Dentini, M., Enzymatic Cross-Linking Versus Radical Polymerization In The Preparation Of Gelatin PolyHIPEs and their performance as scaffolds in the culture of hepatocytes. *Biomacromolecules* **2006,** 7, 3059-3068.

(148) Lumelsky, Y.; Zoldan, J.; Levenberg, S.; Silverstein, M. S., Porous polycaprolactone-polystyrene semi-interpenetrating polymer networks synthesized within high internal phase emulsions. *Macromolecules* **2008,** 41, 1469-1474.

(149) Lumelsky, Y.; Lalush-Michael, I.; Levenberg, S.; Silverstein, M. S., A degradable, porous, emulsion-templated polyacrylate. *Journal Of Polymer Science Part A-Polymer Chemistry* **2009,** 47, 7043-7053.

(150) Bokhari, M.; Carnachan, R. J.; Cameron, N. R.; Przyborski, S. A., Novel cell culture device enabling three-dimensional cell growth and improved cell function. *Biochemical And Biophysical Research Communications* **2007,** 354, 1095-1100.

(151) Bokhari, M.; Carnachan, R. J.; Cameron, N. R.; Przyborski, S. A., Culture Of HepG2 liver cells on three dimensional polystyrene scaffolds enhances cell structure and function during toxicological challenge. *Journal Of Anatomy* **2007,** 211, 567-576.

(152) Hayman, M. W.; Smith, K. H.; Cameron, N. R.; Przyborski, S. A., Enhanced neurite outgrowth by human neurons grown on solid three-dimensional scaffolds. *Biochemical And Biophysical Research Communications* **2004,** 314, 483-488.

(153) Hayman, M. W.; Smith, K. H.; Cameron, N. R.; Przyborski, S. A., Growth of human stem cell-derived neurons on solid three-dimensional polymers. *Journal Of Biochemical And Biophysical Methods* **2005,** 62, 231-240.

(154) Knight, E.; Murray, B.; Carnachan, R.; Przyborski, S., Alvetex®: Polystyrene scaffold technology for routine three dimensional cell culture. In *3D Cell Culture: Methods And Protocols*, Haycock, J. W., Ed. 2011; Vol. 695, 323-340.

(155) Sharma, R.; Barakzai, S. Z.; Taylor, S. E.; Donadeu, F. X., Epidermal-like architecture obtained from equine keratinocytes in three-dimensional cultures. *Journal Of Tissue Engineering And Regenerative Medicine* **2013**.

(156) Stiles, J. M.; Amaya, C.; Rains, S.; Diaz, D.; Pham, R.; Battiste, J.; Modiano, J. F.; Kokta, V.; Boucheron, L. E.; Mitchell, D. C.; Bryan, B. A., Targeting of beta adrenergic receptors results in therapeutic efficacy against models of hemangioendothelioma and angiosarcoma. *PLOS One* **2013,** 8.

(157) Neofytou, E. A.; Chang, E.; Patlola, B.; Joubert, L. M.; Rajadas, J.; Gambhir, S. S.; Cheng, Z.; Robbins, R. C.; Beygui, R. E., Adipose tissue-derived stem cells display a proangiogenic phenotype on 3D scaffolds. *Journal Of Biomedical Materials Research. Part A* **2011,** 98, 383-393.

(158) Rajan, N.; Elliott, R.; Clewes, O.; Mackay, A.; Reis-Filho, J. S.; Burn, J.; Langtry, J.; Sieber-Blum, M.; Lord, C. J.; Ashworth, A., Dysregulated TRK signalling is a therapeutic target in CYLD defective tumours. *Oncogene* **2011,** 30, 4243-4260.

(159) Schutte, M.; Fox, B.; Baradez, M.-O.; Devonshire, A.; Minguez, J.; Bokhari, M.; Przyborski, S.; Marshall, D., Rat primary hepatocytes show enhanced performance and sensitivity to acetaminophen during three-dimensional culture on a polystyrene scaffold designed for routine use. *Assay And Drug Development Technologies* **2011,** 9, 475-486.

(160) Wang, I. K.; Chang, K. M.; Ho, L., Glucose measurement for cell culture - Gluccell, A modified blood glucose meter. *Genet. Eng. News* **2006,** 26, 40.

(161) Busby, W.; Cameron, N. R.; Jahoda, A. B. C., Tissue engineering matrixes by emulsion templating. *Polymer International* **2002,** 51, 871-881.

(162) Alayoubi, A.; Alqahtani, S.; Kaddoumi, A.; Nazzal, S., Effect of PEG surface conformation on anticancer activity and blood circulation of nanoemulsions loaded with tocotrienol-rich fraction of palm oil. *Aaps J* **2013,** 15, 1168-1179.

(163) Koehler, B. C.; Scherr, A.-L.; Lorenz, S.; Urbanik, T.; Kautz, N.; Elssner, C.; Welte, S.; Bermejo, J. L.; Jager, D.; Schulze-Bergkamen, H., Beyond cell death - Antiapoptotic BCL-2 proteins regulate migration and invasion of colorectal cancer cells in vitro. *PLOS One* **2013,** 8, 76446-76446.

(164) Barbetta, A.; Carnachan, R. J.; Smith, K. H.; Zhao, C. T.; Cameron, N. R.; Kataky, R.; Hayman, M.; Przyborski, S. A.; Swan, M., Porous polymers by emulsion templating. *Macromolecular Symposia* **2005,** 226, 203-211.

(165) Bokhari, M.; Carnachan, R. J.; Przyborski, S. A.; Cameron, N. R., Emulsion-Templated Porous Polymers As Scaffolds For Three Dimensional Cell Culture: Effect of synthesis parameters on scaffold formation and homogeneity. *Journal Of Materials Chemistry* **2007,** 17, 4088-4094.

(166) Berthiaume, F.; Moghe, P. V.; Toner, M.; Yarmush, M. L., Effect of extracellular matrix topology on cell structure, function, and physiological responsiveness: Hepatocytes cultured in a sandwich configuration. *FASEB Journal* **1996,** 10, 1471-1484.

(167) Kleinman, H. K.; Luckenbilledds, L.; Cannon, F. W.; Sephel, G. C., Use of extracellular-matrix components for cell-culture. *Analytical Biochemistry* **1987,** 166, 1-13.

(168) Kleinman, H. K.; Klebe, R. J.; Martin, G. R., Role of collagenous matrices in the adhesion and growth of cells. *Journal Of Cell Biology* **1981,** 88, 473-485.

(169) Martinezhernandez, A., The hepatic extracellular-matrix .1. Electron Immunohistochemical studies in normal rat-liver. *Laboratory Investigation* **1984,** 51, 57-74.

(170) Gebhardt, R.; Mecke, D., Perifused monolayer-cultures of rat hepatocytes as an improved invitro system for studies on ureogenesis. *Exp. Cell Res.* **1979,** 124, 349-359.

(171) Gebhardt, R.; Wegner, H.; Alber, J., Perifusion of co-cultured hepatocytes: Optimization of studies on drug metabolism and cytotoxicity in vitro. *Cell Biol. Toxicol.* **1996,** 12, 57-68.

(172) Vinci, B.; Duret, C.; Klieber, S.; Gerbal-Chaloin, S.; Sa-Cunha, A.; Laporte, S.; Suc, B.; Maurel, P.; Ahluwalia, A.; Daujat-Chavanieu, M., Modular bioreactor for primary human hepatocyte culture: Medium flow stimulates expression and activity of detoxification genes. *Biotechnol. J.* **2011,** 6, 554-564.

(173) Guzzardi, M. A.; Vozzi, F.; Ahluwalia, A. D., Study of the crosstalk between hepatocytes and endothelial cells using a novel multicompartmental bioreactor: A comparison between connected cultures and cocultures. *Tissue Engineering Part A* **2009,** 15, 3635-3644.

(174) Lee, P. J.; Hung, P. J.; Lee, L. P., An artificial liver sinusoid with a microfluidic endothelial-like barrier for primary hepatocyte culture. *Biotechnology And Bioengineering* **2007,** 97, 1340-1346.

(175) Lecluyse, E. L.; Witek, R. P.; Andersen, M. E.; Powers, M. J., Organotypic liver culture models: Meeting current challenges in toxicity testing. *Critical Reviews In Toxicology* **2012,** 42, 501-548.

(176) Lecluyse, E. L.; Bullock, P. L.; Parkinson, A., Strategies for restoration and maintenance of normal hepatic structure and function in long-term cultures of rat hepatocytes. *Advanced Drug Delivery Reviews* **1996,** 22, 133-186.

(177) Kocarek, T. A.; Schuetz, E. G.; Strom, S. C.; Fisher, R. A.; Guzelian, P. S., Comparative-analysis of cytochrome P4503A induction in primary cultures of rat, rabbit, and human hepatocytes. *Drug Metabolism And Disposition* **1995,** 23, 415-421.

(178) Vantklooster, G. A. E.; Woutersenvannijnanten, F. M. A.; Blaauboer, B. J.; Noordhoek, J.; Vanmiert, A., Applicability of cultured-hepatocytes derived from goat, sheep and cattle in comparative drug-metabolism studies. *Xenobiotica* **1994,** 24, 417-428.

(179) Li, A. P.; Lu, C.; Brent, J. A.; Pham, C.; Fackett, A.; Ruegg, C. E.; Silber, P. M., Cryopreserved human hepatocytes: Characterization of drug-metabolizing enzyme activities and applications in higher throughput screening assays for hepatotoxicity, metabolic stability, and drug-drug interaction potential. *Chemico-Biological Interactions* **1999,** 121, 17-35.

(180) Li, A. P., Evaluation of drug metabolism, drug-drug interactions, and in vitro hepatotoxicity with cryopreserved human hepatocytes. In *Hepatocytes: Methods And Protocols*, Maurel, P., Ed. 2010; Vol. 640, 281-294.

(181) Mcginnity, D. F.; Soars, M. G.; Urbanowicz, R. A.; Riley, R. J., Evaluation of fresh and cryopreserved hepatocytes as in vitro drug metabolism tools for the prediction of metabolic clearance. *Drug Metabolism And Disposition* **2004,** 32, 1247-1253.

(182) Castell, J. V.; Jover, R.; Martinez-Jimenez, C. P.; Gomez-Lechon, M. J., Hepatocyte cell lines: Their use, scope and limitations in drug metabolism studies. *Expert Opinion On Drug Metabolism & Toxicology* **2006,** 2, 183-212.

(183) Bouma, M.-E.; Rogier, E.; Verthier, N.; Labarre, C.; Feldmann, G., Further cellular investigation of the human hepatoblastoma-derived cell line HepG2: Morphology and immunocytochemical studies of hepatic-secreted proteins. *In Vitro Cellular & Developmental Biology - Plant* **1989,** 25, 267-275.

(184) Everson, G. T.; Polokoff, M. A., HepG2. A human hepatoblastoma cell line exhibiting defects in bile acid synthesis and conjugation. *Journal Of Biological Chemistry* **1986,** 261, 2197-2201.

(185) Ciechanover, A.; Schwartz, A. L.; Lodish, H. F., The asialoglycoprotein receptor internalizes and recycles independently of the transferrin and insulin-receptors. *Cell* **1983,** 32, 267-275.

(186) Wilkening, S.; Stahl, F.; Bader, A., Comparison of primary human hepatocytes and hepatoma cell line HepG2 With regard to their biotransformation properties. *Drug Metabolism And Disposition* **2003,** 31, 1035-1042.

(187) Westerink, W. M. A.; Schoonen, W. G. E. J., Cytochrome P450 enzyme levels in HepG2 cells and cryopreserved primary human hepatocytes and their induction in HepG2 cells. *Toxicology In Vitro* **2007,** 21, 1581-1591.

(188) Burkard, A.; Dahn, C.; Heinz, S.; Zutavern, A.; Sonntag-Buck, V.; Maltman, D.; Przyborski, S.; Hewitt, N. J.; Braspenning, J., Generation of proliferating human hepatocytes using Upcyte® technology: Characterisation and applications in induction and cytotoxicity assays. *Xenobiotica* **2012,** 42, 939-956.

(189) Jongpaiboonkit, L.; King, W. J.; Murphy, W. L., Screening for 3D environments that support human mesenchymal stem cell viability using hydrogel arrays. *Tissue Engineering Part A* **2009,** 15, 343-353.

(190) Kleinman, H. K.; Philp, D.; Hoffman, M. P., Role of the extracellular matrix in morphogenesis. *Curr. Opin. Biotechnol.* **2003,** 14, 526-532.

(191) Rowe, C.; Gerrard, D. T.; Jenkins, R.; Berry, A.; Durkin, K.; Sundstrom, L.; Goldring, C. E.; Park, B. K.; Kitteringham, N. R.; Hanley, K. P.; Hanley, N. A., Proteome-wide analyses of human hepatocytes during differentiation and dedifferentiation. *Hepatology* **2013,** 58, 799-809.

(192) Clayton, R. F.; Rinaldi, A.; Kandyba, E. E.; Edward, M.; Willberg, C.; Klenerman, P.; Patel, A. H., Liver cell lines for the study of hepatocyte functions and immunological response. *Liver Int.* **2005,** 25, 389-402.

(193) Verrill, C.; Davies, J.; Millward-Sadler, H.; Sundstrom, L.; Sheron, N., Organotypic liver culture in a fluid-air interface using slices of neonatal rat and adult human tissue - A model of fibrosis in vitro. *Journal Of Pharmacological And Toxicological Methods* **2002,** 48, 103-110.

(194) Sanchez, A.; Alvarez, A. M.; Pagan, R.; Roncero, C.; Vilaro, S.; Benito, M.; Fabregat, I., Fibronectin regulates morphology, cell organization and gene expression of rat fetal hepatocytes in primary culture. *J Hepatol* **2000,** 32, 242-250.

(195) Hodgkinson, C. P.; Wright, M. C.; Paine, A. J., Fibronectin-mediated hepatocyte shape change reprograms cytochrome P450 2C11 gene expression via an integrin-signaled induction of ribonuclease activity. *Molecular Pharmacology* **2000,** 58, 976-981.

(196) Ogilvie, B. W.; Zhang, D. L.; Li, W. Y.; Rodrigues, A. D.; Gipson, A. E.; Holsapple, J.; Toren, P.; Parkinson, A., Glucuronidation converts gemfibrozil to a potent, metabolism-dependent inhibitor of CYP2C8: Implications for drug-drug interactions. *Drug Metabolism And Disposition* **2006,** 34, 191-197.

(197) Mooney, D.; Hansen, L.; Vacanti, J.; Langer, R.; Farmer, S.; Ingber, D., Switching from differentiation to growth in hepatocytes - Control by extracellular-matrix. *Journal Of Cellular Physiology* **1992,** 151, 497-505.

(198) Sawamoto, K.; Takahashi, N., Modulation of hepatocyte function by changing the cell shape in primary culture. *In Vitro Cellular & Developmental Biology-Animal* **1997,** 33, 569-574.

(199) Laurent, T.; Kataoka, Y.; Kobayashi, S.; Ando, M.; Nagamori, S.; Oda, H., Spherical cell shape of FLC-4 Cell, a human hepatoma cell, enhances hepatocyte-specific function and

suppresses tumor phenotype through the integration of mRNA-microRNA interaction. *Biology Open* **2012,** 1, 958-964.

(200) Laurent, T.; Murase, D.; Tsukioka, S.; Matsuura, T.; Nagamori, S.; Oda, H., A novel human hepatoma cell line, FLC-4, exhibits highly enhanced liver differentiation functions through the three-dimensional cell shape. *Journal Of Cellular Physiology* **2012,** 227, 2898-2906.

(201) Kapyla, E.; Aydogan, D. B.; Virjula, S.; Vanhatupa, S.; Miettinen, S.; Hyttinen, J.; Kellomaki, M., Direct laser writing and geometrical analysis of scaffolds with designed pore architecture for three-dimensional cell culturing. *Journal Of Micromechanics And Microengineering* **2012,** 22.

(202) Gerlach, J. C.; Schnoy, N.; Encke, J.; Smith, M. D.; Muller, C.; Neuhaus, P., Improved hepatocyte in-vitro maintenance in a culture model with woven multicompartment capillary systems - Electron-microscopy studies. *Hepatology* **1995,** 22, 546-552.

(203) Kim, S. S.; Sundback, C. A.; Kaihara, S.; Benvenuto, M. S.; Kim, B. S.; Mooney, D. J.; Vacanti, J. P., Dynamic seeding and in vitro culture of hepatocytes in a flow perfusion system. *Tissue Eng.* **2000,** 6, 39-44.

(204) Arias, I. M.; Che, M. X.; Gatmaitan, Z.; Leveille, C.; Nishida, T.; Stpierre, M., The biology of the bile canaliculus, 1993. *Hepatology* **1993,** 17, 318-329.

(205) Fu, D.; Wakabayashi, Y.; Ido, Y.; Lippincott-Schwartz, J.; Arias, I. M., Regulation of bile canalicular network formation and maintenance by AMP-activated protein kinase and LKB1. *J. Cell Sci.* **2010,** 123, 3294-3302.

(206) Malinen, M. M.; Palokangas, H.; Yliperttula, M.; Urtti, A., Peptide nanofiber hydrogel induces formation of bile canaliculi structures in three-dimensional hepatic cell culture. *Tissue Engineering Part A* **2012,** 18, 2418-2425.

(207) Coger, R.; Toner, M.; Moghe, P.; Ezzell, R. M.; Yarmush, M. L., Hepatocyte aggregation and reorganization of EHS matrix gel. *Tissue Eng.* **1997,** 3, 375-390.

(208) Chu, X. H.; Shi, X. L.; Feng, Z. Q.; Gu, Z. Z.; Ding, Y. T., Chitosan nanofiber scaffold enhances hepatocyte adhesion and function. *Biotechnol. Lett.* **2009,** 31, 347-352.

(209) Nishimura, M.; Hagi, M.; Ejiri, Y.; Kishimoto, S.; Horie, T.; Narimatsu, S.; Naito, S., Secretion of albumin and induction of CYP1A2 and CYP3A4 in novel three-dimensional culture system for human hepatocytes using micro-space plate. *Drug Metabolism And Pharmacokinetics* **2010,** 25, 236-242.

(210) Underhill, G. H.; Chen, A. A.; Albrecht, D. R.; Bhatia, S. N., Assessment of hepatocellular function within PEG hydrogels. *Biomaterials* **2007,** 28, 256-270.

(211) Wang, X.-R.; Qu, Z.-Q.; Li, X.-D.; Liu, H.-L.; He, P.; Fang, B.-X.; Xiao, J.; Huang, W.; Wu, M.-C., Activity of sulfotransferase 1A1 is dramatically upregulated in patients with hepatocellular carcinoma secondary to chronic hepatitis B virus infection. *Cancer Science* **2010,** 101, 412-415.

(212) Schyschka, L.; Martinez Sanchez, J. J.; Wang, Z.; Burkhardt, B.; Mueller-Vieira, U.; Zeilinger, K.; Bachmann, A.; Nadalin, S.; Damm, G.; Nussler, A. K., Hepatic 3D cultures but not 2D Cultures preserve specific transporter activity for acetaminophen-induced hepatotoxicity. *Arch. Toxicol.* **2013,** 87, 1581-1593.

(213) Westerink, W. M. A.; Schoonen, W. G. E. J., Phase II enzyme levels in HepG2 cells and cryopreserved primary human hepatocytes and their induction in HepG2 cells. *Toxicology In Vitro* **2007,** 21, 1592-1602.

(214) Kim, S. S.; Utsunomiya, H.; Koski, J. A.; Wu, B. M.; Cima, M. J.; Sohn, J.; Mukai, K.; Griffith, L. G.; Vacanti, J. P., Survival and function of hepatocytes on a novel three-dimensional

synthetic biodegradable polymer scaffold with an intrinsic network of channels. *Annals Of Surgery* **1998,** 228, 8-13.

(215) Park, T. G., Perfusion culture of hepatocytes within galactose-derivatized biodegradable poly(lactide-co-glycolide) scaffolds prepared by gas foaming of effervescent salts. *Journal Of Biomedical Materials Research* **2002,** 59, 127-135.

(216) Geiger, B.; Bershadsky, A.; Pankov, R.; Yamada, K. M., Transmembrane extracellular matrix-cytoskeleton crosstalk. *Nat. Rev. Mol. Cell Biol.* **2001,** 2, 793-805.

(217) Ashwell, G.; Morell, A. G., Role of surface carbohydrates in hepatic recognition and transport of circulating glycoproteins. *Advances In Enzymology And Related Areas Of Molecular Biology* **1974,** 41, 99-128.

(218) Kircher, L.; Theato, P.; Cameron, N. R., Reactive thiol-ene emulsion-templated porous polymers incorporating pentafluorophenyl acrylate. *Polymer* **2013,** 54, 1755-1761.

(219) Jochum, F. D.; Theato, P., Temperature and light sensitive copolymers containing azobenzene moieties prepared via a polymer analogous reaction. *Polymer* **2009,** 50, 3079-3085.

(220) Ying, L.; Yin, C.; Zhuo, R. X.; Leong, K. W.; Mao, H. Q.; Kang, E. T.; Neoh, K. G., Immobilization of galactose ligands on acrylic acid graft-copolymerized poly(ethylene terephthalate) film and its application to hepatocyte culture. *Biomacromolecules* **2003,** 4, 157-165.

(221) Sano, S.; Kato, K.; Ikada, Y., Introduction of functional-groups onto the surface of polyethylene for protein immobilization. *Biomaterials* **1993,** 14, 817-822.

(222) Mitchell, S. A.; Davidson, M. R.; Emmison, N.; Bradley, R. H., Isopropyl alcohol plasma modification of polystyrene surfaces to influence cell attachment behaviour. *Surface Science* **2004,** 561, 110-120.

(223) Wende, K.; Schroeder, K.; Lindequist, U.; Ohl, A., Plasma-based modification of polystyrene surfaces for serum-free culture of osteoblastic cell lines. *Plasma Processes And Polymers* **2006,** 3, 524-531.

(224) Lopez-Perez, P. M.; Da Silva, R. M. P.; Sousa, R. A.; Pashkuleva, I.; Reis, R. L., Plasma-induced polymerization as a tool for surface functionalization of polymer scaffolds for bone tissue engineering: An in vitro study. *Acta Biomater.* **2010,** 6, 3704-3712.

(225) Yang, K.; Lee, J. S.; Kim, J.; Lee, Y. B.; Shin, H.; Um, S. H.; Kim, J. B.; Park, K. I.; Lee, H.; Cho, S.-W., Polydopamine-mediated surface modification of scaffold materials for human neural stem cell engineering. *Biomaterials* **2012,** 33, 6952-6964.

(226) Goddard, J. M.; Hotchkiss, J. H., Polymer surface modification for the attachment of bioactive compounds. *Progress In Polymer Science* **2007,** 32, 698-725.

(227) Ma, Z.; Mao, Z.; Gao, C., Surface modification and property analysis of biomedical polymers used for tissue engineering. *Colloids And Surfaces B-Biointerfaces* **2007,** 60, 137-157.

(228) Hsu, S. H.; Whu, S. W.; Hsieh, S. C.; Tsai, C. L.; Chen, D. C.; Tan, T. S., Evaluation of chitosan-alginate-hyaluronate complexes modified by an RGD-containing protein as tissue-engineering scaffolds for cartilage regeneration. *Artificial Organs* **2004,** 28, 693-703.

(229) Jeschke, B.; Meyer, J.; Jonczyk, A.; Kessler, H.; Adamietz, P.; Meenen, N. M.; Kantlehner, M.; Goepfert, C.; Nies, B., RGD-peptides for tissue engineering of articular cartilage. *Biomaterials* **2002,** 23, 3455-3463.

(230) Leipzig, N. D.; Wylie, R. G.; Kim, H.; Shoichet, M. S., Differentiation of neural stem cells in three-dimensional growth factor-immobilized chitosan hydrogel scaffolds. *Biomaterials* **2011,** 32, 57-64.

(231) Nakaji-Hirabayashi, T.; Kato, K.; Arima, Y.; Iwata, H., Oriented immobilization of epidermal growth factor onto culture substrates for the selective expansion of neural stem cells. *Biomaterials* **2007,** 28, 3517-3529.

(232) Hoveizi, E.; Nabiuni, M.; Parivar, K.; Rajabi-Zeleti, S.; Tavakol, S., Functionalisation and surface modification of electrospun polylactic acid scaffold for tissue engineering. *Cell Biology International* **2014,** 38, 41-49.

(233) Du, Y. N.; Chia, S. M.; Han, R. B.; Chang, S.; Tang, H. H.; Yu, H., 3D Hepatocyte monolayer on hybrid RGD/galactose substratum. *Biomaterials* **2006,** 27, 5669-5680.

(234) Yin, C.; Liao, K.; Mao, H.-Q.; Leong, K. W.; Zhuo, R.-X.; Chan, V., Adhesion contact dynamics of HepG2 cells on galactose-immobilized substrates. *Biomaterials* **2003,** 24, 837-850.

(235) Cho, C. S.; Seo, S. J.; Park, I. K.; Kim, S. H.; Kim, T. H.; Hoshiba, T.; Harada, I.; Akaike, T., Galactose-carrying polymers as extracellular matrices for liver tissue engineering. *Biomaterials* **2006,** 27, 576-585.

(236) Cho, C. S.; Hoshiba, T.; Harada, I.; Akaike, T., Regulation of hepatocyte behaviors by galactose-carrying polymers through receptor-mediated mechanism. *React. Funct. Polym.* **2007,** 67, 1301-1310.

(237) Gentsch, R.; Pippig, F.; Nilles, K.; Theato, P.; Kikkeri, R.; Maglinao, M.; Lepenies, B.; Seeberger, P. H.; Borner, H. G., Modular approach toward bioactive fiber meshes carrying oligosaccharides. *Macromolecules* **2010,** 43, 9239-9247.

(238) Nugraha, B.; Hong, X.; Mo, X. J.; Tan, L. O. L.; Zhang, W. X.; Chan, P. M.; Kang, C. H.; Wang, Y.; Beng, L. T.; Sun, W. X.; Choudhury, D.; Robens, J. M.; Mcmillian, M.; Silva, J.; Dallas, S.; Tan, C. H.; Yue, Z. L.; Yu, H., Galactosylated cellulosic sponge for multi-well drug safety testing. *Biomaterials* **2011,** 32, 6982-6994.

(239) Mercier, A.; Deleuze, H.; Mondain-Monval, O., preparation and functionalization of (vinyl)polystyrene polyHIPE.: Short routes to binding functional groups through a dimethylene spacer. *Reactive And Functional Polymers* **2000,** 46, 67-79.

(240) Cameron, N. R.; Sherrington, D. C.; Ando, I.; Kurosu, H., Chemical modification of monolithic poly(styrene-divinylbenzene) polyHIPE materials. *Journal Of Materials Chemistry* **1996,** 6, 719-726.

(241) Audouin, F.; Fox, M.; Larragy, R.; Clarke, P.; Huang, J.; O'connor, B.; Heise, A., Polypeptide-grafted macroporous polyHIPE by surface-initiated N-carboxyanhydride (NCA) polymerization as a platform for bioconjugation. *Macromolecules* **2012,** 45, 6127-6135.

(242) Audouin, F.; Larragy, R.; Fox, M.; O'connor, B.; Heise, A., Protein immobilization onto poly(acrylic acid) functional macroporous polyHIPE obtained by surface-initiated ARGET ATRP. *Biomacromolecules* **2012,** 13, 3787-3794.

(243) Sevsek, U.; Krajnc, P., Methacrylic acid microcellular highly porous monoliths: Preparation and functionalisation. *React. Funct. Polym.* **2012,** 72, 221-226.

(244) Benicewicz, B. C.; Jarvinen, G. D.; Kathios, D. J.; Jorgensen, B. S., Open-celled polymeric foam monoliths for heavy metal separations study. *Journal Of Radioanalytical And Nuclear Chemistry* **1998,** 235, 31-35.

(245) Alexandratos, S. D.; Beauvais, R.; Duke, J. R.; Jorgensen, B. S., Functionalized polymer foams as metal ion chelating agents with rapid complexation kinetics. *Journal Of Applied Polymer Science* **1998,** 68, 1911-1916.

(246) Barbetta, A.; Cameron, N. R.; Cooper, S. J., High internal phase emulsions (HIPEs) containing divinylbenzene and 4-vinylbenzyl chloride and the morphology of the resulting polyHIPE materials. *Chemical Communications* **2000**, 221-222.

(247) Boyer, C.; Davis, T. P., One-Pot synthesis and biofunctionalization of glycopolymers via raft polymerization and thiol-ene reactions. *Chemical Communications* **2009**, 6029-6031.

(248) Beija, M.; Li, Y.; Lowe, A. B.; Davis, T. P.; Boyer, C., Factors influencing the synthesis and the post-modification of PEGylated pentafluorophenyl acrylate containing copolymers. *European Polymer Journal* **2013,** 49, 3060-3071.

(249) Li, Y.; Duong, H. T. T.; Jones, M. W.; Basuki, J. S.; Hu, J.; Boyer, C.; Davis, T. P., Selective postmodification of copolymer backbones bearing different activated esters with disparate reactivities. *Acs Macro Letters* **2013,** 2, 912-917.

(250) Gitli, T.; Silverstein, M. S., Bicontinuous hydrogel-hydrophobic polymer systems through emulsion templated simultaneous polymerizations. *Soft Matter* **2008,** 4, 2475-2485.